

# Battery Management System for Electric Vehicle

Ph.D. Thesis

VENU SANGWAN

ID No. 2014REE9041



DEPARTMENT OF ELECTRICAL ENGINEERING  
MALAVIYA NATIONAL INSTITUTE OF TECHNOLOGY JAIPUR

July 2019



# Battery Management System for Electric Vehicle

*Submitted in*  
*fulfillment of the requirements for the degree of*  
***Doctor of Philosophy***

*by*

Venu Sangwan

ID: 2014REE9041

Under the Supervision of  
**Prof. Rajesh Kumar**  
**Dr. Akshay Kumar Rathore**



DEPARTMENT OF ELECTRICAL ENGINEERING  
MALAVIYA NATIONAL INSTITUTE OF TECHNOLOGY JAIPUR

July 2019

© Malaviya National Institute of Technology Jaipur - 302017

All Rights Reserved

# DECLARATION

I, Venu Sangwan, declare that this thesis titled, “Battery Management System for Electric Vehicles” and the work presented in it are my own. I confirm that:

- This work was done wholly or mainly while in candidature for a research degree at this university.
- Where any part of this thesis has previously been submitted for a degree or any other qualification at this university or any other institution, this has been clearly stated.
- Where I have consulted the published work of others, this is always clearly attributed.
- Where I have quoted from the work of others, the source is always given. With the exception of such quotations, this thesis is entirely my own work.
- I have acknowledged all main sources of help.
- Where the thesis is based on work done by myself, jointly with others, I have made clear exactly what was done by others and what I have contributed myself.

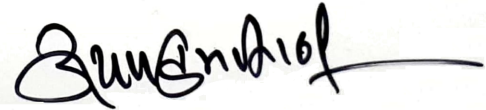
Date:

Venu Sangwan  
(2014REE9041)



# CERTIFICATE

This is to certify that the thesis entitled “**Battery Management System for Electric Vehicle**” being submitted by **Venu Sangwan (ID: 2014REE9041)** is a bonafide research work carried out under my supervision and guidance in fulfillment of the requirement for the award of the degree of **Doctor of Philosophy** in the Department of Electrical Engineering, Malaviya National Institute of Technology, Jaipur India. The matter embodied in this thesis is original and has not been submitted to any other University of Institute for the award of any other degree.



**Prof. Rajesh Kumar**

(Supervisor)

Professor

Department of Electrical Engineering

MNIT, Jaipur

India

**Dr. Akshay Kumar Rathore**

(External Joint-Supervisor)

Associate Professor

Electrical and Computer Engineering

Concordia University, Montreal,

Canada

Place: Jaipur

Date: 11-July-2019





*The thesis is dedicated to*  
*My beloved and caring parents*



# ACKNOWLEDGEMENTS

It gives me immense pleasure to express gratitude and regards to all those people who supported me during the course of this doctoral research work at MNIT Jaipur. I acknowledge the involvement and contribution of each one of them

First of all, I would like to express my sincere thanks and deepest gratitude to my supervisor, **Prof. Rajesh Kumar** (Professor, Department of Electrical Engineering, Malaviya National Institute of Technology, Jaipur, India), for his guidance, technical discussion, and constructive criticism throughout my research work. With his kind cooperation and support and motivation the completion of this thesis became an easy process. I equally thank my external supervisor, **Dr. Akshay Kumar Rathore** (Associate Professor, Department of Electrical and Computer Engineering, Concordia University, Canada) for his valuable suggestions.

I express my sincere gratitude and respect to **Dr. Harpal Tiwari**, (DPGC Convenor, Department of Electrical Engineering, Malaviya National Institute of Technology, Jaipur) for engaging in rounds of beneficial discussion and letting me avail all the facilities to pursue this work. I would like to give special thanks to the members of my Doctoral Research Evaluation Committee (DREC): **Prof. Manoj Fozdar**, **Prof. Harpal Tiwari** and **Dr. Kusum Verma** for providing invaluable suggestions. I am also grateful to all other faculty members of the department for their inspiration and support at various stages. I am also thankful to the staff members of the department for their kind help in official work.

Let me express special thanks to the Head of the Department, **Prof. Rajesh Kumar**, for support and consistent encouragement in our academic activities. I am sincerely thankful to **Prof. Udaykumar R. Yaragatti**, Director, MNIT Jaipur for providing me infrastructural facilities to work, without which this work would not have been possible.

Special regards to my colleagues and friends at **RAMAN Lab** Family, MNIT namely **Dr. Akanksha Shukla**, **Dr. Sujil A**, **Dr. Shashank Vyas**, **Dr. Chandra Prakash**, **Ms. Vishu Gupta**, **Dr. Shalini Pal**, **Dr. Om Ji Shukla** and **Mr. Rahul Singal**, **Mrs. Shivali Maam** and lovely **Aarohi** for their constant support, warmth and affection. Thanks to all members of the robotics group **ZINE** for being a source of inspiration. Special thanks to **Mr. Avinash Sharma** and **Ms. Priyanka Jangir**. With great pleasure, I would like to thank my friends at MNIT, **Dr. Pradeep Singh**, **Dr. Ajeet Kumar Singh**, **Dr. Abhilash Kumar Gupta**, **Mr. Rayees Ahmad Thokar** and

other fellow researchers for their valuable help. I want to express by heartiest thanks to **Dr. Ajeet Kumar Singh** for his valuable comments, motivation and support in shaping my research work. Special thanks to **Dr. Akanksha Shukla** and **Dr. Pradeep Singh** for supporting me in all ups and down phase during my research work.

I feel a deep sense of gratitude to my beloved parents **Smt. Santosh Devi** and **Sub/Clk Suresh Sangwan**, my brother **Major Maneesh Sangwan**, sister-in-law **Dr. Kanta Maan** and sister **Ms. Nisha Jakhar**, who formed part of my vision and taught me good things that matter in life. Their love and support have always been my strength. Their patience and sacrifice will remain my inspiration throughout my life.

I acknowledge several friends and well-wishers, whom I haven't mentioned above and whose best wishes always encouraged me. Above all, I thanked the almighty god who is being with me and showers his blessing and benevolence towards me in all phases of my life.

Finally, I gratefully, acknowledge one and all who are directly or indirectly involved to shape this research work.

(Venu Sangwan)

# ABSTRACT

The use of clean energy in the transportation industry has gained substantial attention in the last two decades with the increase in fuel price and harmful gases emitted by burning fossil fuels in conventional vehicles. Electrical Vehicles (EVs) emit no greenhouse gas, and hence they are a potential alternative to internal combustion engine (ICEs) automobiles. However, the automobile industry had been limited to EVs with short range because of less battery capacity, long charging time, and lack of charging infrastructure. Nowadays, the advent of Li-ion batteries has reinforced the automobile sector to develop long-range BEVs.

These batteries have superior performance concerning specific energy, energy density, cycle lifespan, low self-discharge, and are environment-friendly. However, these batteries can be dangerous if they are not operated within their safety operation window. Therefore, an effective battery management system is indispensable for ensuring the safety of passengers. In this thesis, a battery management system has been developed for EVs to ensure reliable, efficient and consistent operation of batteries under different environmental and driving conditions. Firstly, for the development of battery management system a high fidelity battery model dependent on different operating conditions is developed. Then battery model parameters are identified using manufacturer data sheet without conducting expensive and time-consuming experiments. Secondly, this research work focuses on the estimation of internal states of batteries such as the State of Charge, State of Health and Remaining Useful Life. Determination of internal states of batteries helps in maintaining battery operation in safe operating window.

Automobile industry presently designs and produces single large pack EVs which offers an extended range on the cost of a heavyweight vehicle with a high price. The researchers have suggested EV having two different size batteries. The overall weight of the vehicle is decreased for short-range travel by using smaller size fixed battery. The larger size battery is swappable and is used for longer distances. As it is seldom used, it has longer lifetime and its cost is distributed over the lifetime of the vehicle. In this research work, a power management system is developed to effectively utilize power from both the batteries to supply energy demanded by drivetrain of EVs.



# Contents

<b>Certificate</b>	<b>v</b>
<b>Acknowledgements</b>	<b>ix</b>
<b>Abstract</b>	<b>xi</b>
<b>Contents</b>	<b>xii</b>
<b>List of Tables</b>	<b>xvii</b>
<b>List of Figures</b>	<b>xix</b>
<b>Abbreviations</b>	<b>xxi</b>
<b>Symbols</b>	<b>xxv</b>
<b>1 Introduction</b>	<b>1</b>
1.1 Motivation for the Present Work . . . . .	1
1.2 Literature review . . . . .	4
1.2.1 Lithium Ion Battery . . . . .	4
1.2.2 Battery Management System . . . . .	10
1.2.3 Battery Modeling . . . . .	12
1.2.3.1 Electrochemical models . . . . .	13
1.2.3.2 Data Driven Models . . . . .	14
1.2.3.3 Equivalent circuit-based models . . . . .	14
1.2.4 Battery Model Parameters Identification . . . . .	20
1.2.5 Battery Internal States Estimation . . . . .	22
1.2.5.1 Conventional Mechanism Analysis Methods . . . . .	25
1.2.5.2 Data-driven estimation methods . . . . .	27
1.2.5.3 Model Based Methods . . . . .	29
1.2.6 Power Management Strategies . . . . .	34
1.3 Research gaps . . . . .	37

1.4	Research Objectives . . . . .	40
1.5	Organization of the thesis . . . . .	40
<b>2</b>	<b>Modeling and Parameter Estimation of Battery</b>	<b>45</b>
2.1	Introduction . . . . .	45
2.2	Equivalent circuit model of Li-ion batteries . . . . .	46
2.3	Objective function for optimization process . . . . .	51
2.4	Meta-heuristic optimization algorithms for battery modeling . . . . .	52
2.4.1	Genetic Algorithm (GA) . . . . .	53
2.4.2	Particle Swarm Optimization (PSO) Algorithm . . . . .	54
2.4.3	Differential Evolution (DE) Algorithm . . . . .	55
2.4.4	Teaching Learning Based Optimization (TLBO) Algorithm . . . . .	56
2.4.5	Grey Wolf Optimization (GWO) Algorithm . . . . .	57
2.4.6	Ageist Spider Monkey Optimization (ASMO) Algorithm . . . . .	58
2.5	Results and Discussion . . . . .	59
2.5.1	Estimated Parameters of the Battery Using Proposed Approach . . . . .	60
2.5.2	Validation of estimated battery parameters . . . . .	64
2.5.3	Performance analysis of various optimization algorithms . . . . .	69
2.6	Chapter Summary . . . . .	73
<b>3</b>	<b>Online Assessment of Battery Performance</b>	<b>75</b>
3.1	Introduction . . . . .	75
3.2	Problem Formulation for Estimation of Battery Internal States . . . . .	77
3.2.1	SOC estimation model . . . . .	78
3.2.2	Capacity degradation model . . . . .	78
3.3	Estimation Techniques . . . . .	83
3.3.1	Extended Kalman filter (EKF) . . . . .	84
3.3.2	Sigma Points Kalman filter (SPKF) . . . . .	85
3.3.3	Particle Filter (PF) . . . . .	87
3.4	Results and discussions . . . . .	88
3.4.1	SOC estimation . . . . .	88
3.4.2	SOH estimation . . . . .	97
3.5	Chapter Summary . . . . .	103
<b>4</b>	<b>Power management for EV Powered by Dual Battery System</b>	<b>107</b>
4.1	Introduction . . . . .	107
4.2	Test bed system modeling . . . . .	108
4.2.1	Drivetrain modeling . . . . .	109
4.2.2	Driving cycle . . . . .	113
4.3	Power management system architecture . . . . .	114
4.3.1	Problem formulation . . . . .	114
4.3.2	Strategy Level . . . . .	116
4.3.3	Action Planning Level . . . . .	119
4.3.4	Operation Level . . . . .	119
4.4	Results and Discussion . . . . .	120



---

4.5 Chapter Summary . . . . .	128
<b>5 Conclusions and Future Scope</b>	<b>129</b>
5.1 Major Contributions of this Study . . . . .	129
5.2 Suggestions for Future Works in this Research Domain . . . . .	130
<b>A Data Specification</b>	<b>133</b>
<b>Bibliography</b>	<b>135</b>
<b>Publications</b>	<b>153</b>
<b>Brief bio-data of the Author</b>	<b>155</b>



# List of Tables

1.1	EVs in 2015 and targets committed to achieve by 2020 . . . . .	2
1.2	Main characteristics of popular battery types used in EVs . . . . .	5
1.3	Characteristics of different types of Li-ion battery . . . . .	7
1.4	Comparison of various equivalent circuit based models . . . . .	18
1.5	Detail description of important characteristics of different types of battery model . . . . .	19
1.6	Comparison of Internal States Estimation Techniques . . . . .	32
1.7	Comparative study of different energy management schemes. . . . .	36
2.1	PC's $a_1$ to $a_{34}$ for charging and discharging . . . . .	61
2.2	Error comparison for charge and discharge Model . . . . .	70
2.3	T-test for charging scenario . . . . .	71
2.4	T-test for discharging scenario . . . . .	71
2.5	Wilcoxon-test for charging scenario . . . . .	72
2.6	Wilcoxon-test for discharging scenario . . . . .	72
3.1	Goodness-of-fit for polynomial and exponential model . . . . .	81
3.2	Parameters values for polynomial and exponential model . . . . .	82
3.3	Parameters values for different SPKF filters . . . . .	87
3.4	Prediction error statistics at different temperature assuming correct initial SOC value . . . . .	93
3.5	Execution time analysis (in secs) assuming correct initial SOC value . . . . .	93
3.6	Prediction error statistics at different temperature assuming incorrect initial SOC value . . . . .	96
3.7	Execution time analysis (in secs) assuming incorrect initial SOC value . . . . .	97
3.8	Performance comparison for RUL prediction using defined estimation methods	102
4.1	Driving cycles main parameters . . . . .	113



# List of Figures

1.1	Li-ion battery operation window . . . . .	9
1.2	A typical information flow within battery monitoring System . . . . .	11
1.3	Simple battery model . . . . .	15
1.4	(a) 2 <sup>nd</sup> order Randles circuit (b) Impedance measurement using AC response . . . . .	16
1.5	Thevenin battery model . . . . .	17
1.6	Runtime-based battery model . . . . .	18
1.7	Combined Equivalent Circuit Battery Model . . . . .	19
1.8	Classification of battery internal states estimation methods . . . . .	25
1.9	Model based internal states estimation . . . . .	30
1.10	Block diagram of thesis organization . . . . .	43
2.1	Voltage response part of the combined equivalent circuit based battery model with 1 RC network . . . . .	47
2.2	Battery Model with 1 RC network represented in s-domain . . . . .	49
2.3	Predicted Characteristic Curve (a) For Charging (b) For Discharging (c) Error for Charging at 25°C (b) Error for Discharging at 25°C . . . . .	60
2.4	Predicted Characteristic Curve Error For charging at (a) 0°C (b) 25°C (c) 45°C . . . . .	62
2.5	Predicted Characteristic Curve Error For discharging at (a) 0°C (b) 25°C (c) 45°C . . . . .	63
2.6	Voltage and current profile for Pulse Charge-Discharge Test at 25°C . . . . .	65
2.7	Voltage response to the pulse current . . . . .	65
2.8	Plots for parameters estimated using proposed model and PCDT For Charging (a) $V_{oc}$ (b) $R_0$ (c) $R_1$ (d) $C_1$ . . . . .	66
2.9	Plots for parameters estimated using proposed model and PCDT For Discharging (a) $V_{oc}$ (b) $R_0$ (c) $R_1$ (d) $C_1$ . . . . .	67
2.10	Plots for the PCDT voltages and calculated voltage from the extracted parameters For charging (a) Terminal voltage (b) Prediction error; For discharging (a) Terminal voltage (b) Prediction error . . . . .	68
2.11	Convergence curves for (a) Charging (b) Discharging . . . . .	70
3.1	Capacity data set . . . . .	79
3.2	Curve fitting based on polynomial and exponential model. . . . .	80
3.3	EKF algorithm based SOC estimation approach . . . . .	85
3.4	SPKF algorithm based SOC estimation approach . . . . .	86

3.5	Voltage and current profile for DST driving cycles . . . . .	89
3.6	Estimation results of different adaptive KF assuming correct initial SOC value (a) $-10^{\circ}C$ (b) $0^{\circ}C$ (c) $10^{\circ}C$ (d) $20^{\circ}C$ . . . . .	90
3.7	Estimation results of different adaptive KF assuming correct initial SOC value (a) $25^{\circ}C$ (b) $30^{\circ}C$ (c) $40^{\circ}C$ (d) $50^{\circ}C$ . . . . .	91
3.8	Estimation results of different adaptive KF assuming incorrect initial SOC value (a) $-10^{\circ}C$ (b) $0^{\circ}C$ (c) $10^{\circ}C$ (d) $20^{\circ}C$ . . . . .	94
3.9	Estimation results of different adaptive KF assuming incorrect initial SOC value (a) $25^{\circ}C$ (b) $30^{\circ}C$ (c) $40^{\circ}C$ (d) $50^{\circ}C$ . . . . .	95
3.10	Comparison of RUL prediction results under different prediction point . . .	98
3.11	Comparison of RUL prediction results under different prediction point . . .	99
3.12	Comparison of RUL prediction results under different prediction point . . .	100
3.13	Comparison of RUL prediction results under different prediction point . . .	101
4.1	Architecture of the power management system for a dual battery powered EV platform . . . . .	109
4.2	The resistive forces applied on a EV moving along a slope . . . . .	110
4.3	The speed and power demand for EV for ECE 15 . . . . .	113
4.4	Rules for strategy planning level . . . . .	117
4.5	Controlling strategies for DC-DC converter (a) Fixed battery (b) Swappable battery . . . . .	120
4.6	Dual battery powered EV in MATLAB/Simulink . . . . .	122
4.7	ECE 15 driving cycles results for initial SOC values $SOC_{SB} = 60\%$ and $SOC_{FB} = 60\%$ . . . . .	125
4.8	ECE 15 driving cycles results for initial SOC values $SOC_{SB} = 80\%$ and $SOC_{FB} = 30\%$ . . . . .	126
4.9	ECE 15 driving cycles results for initial SOC values $SOC_{SB} = 30\%$ and $SOC_{FB} = 80\%$ . . . . .	127

# Abbreviations

ANN	Artificial Neural Network
ASMO	Ageist Spider Monkey Optimization
BEV	Battery Powered Electric Vehicles
C-rate	Charging Rate
CALCE	Center for Advanced Life Cycle Engineering
CC-CV	Constant-Current Constant-Voltage
CDKF	Central Difference Kalman Filter
DE	Different Evolution
DOD	Depth of Discharge
DST	Dynamic Stress Test
ECMS	Equivalent Consumption Minimization Strategy
EIS	Electrochemical Impedance Spectroscopy
EKF	Extended Kalman Filter
EUL	End-of-useful Life
EV	Electric Vehicle
FL	Fuzzy Logic
GA	Genetic Algorithm
GHG	Green House Gas
GL	Global Leader
GWO	Grey Wolf Optimization
IEA	International Energy Agency
ICE	Internal Combustion Engine
KF	Kalman Filter

---

LCO	Lithium Cobalt Oxide
LFP	Lithium Iron Phosphate
LL	Local Leader
LMO	Lithium-Manganese Oxide
LTO	Lithium Titanate
LTV	Linear Time-Varying
MAE	Mean Absolute error
MPC	Model Predictive Control
NCA	Lithium Nickel Cobalt Aluminum Oxide
NFL	No Free Lunch theorem
NEMMP	National Electric Mobility Mission Plan
NLLS	Non-Linear Least Square
NMC	Lithium Nickel Manganese Cobalt Oxide
NMEM	National Mission on Electric Mobility
OCV	Open-circuit voltage
PF	Particle Filter
PIO	Proper Integral Observer
PCDT	Pulse-Current Charge-Discharge Test
PSO	Particle Swarm Optimization
SEI	Solid-Electrolyte Interphase layer
SMO	Slide Mode Observer
SOC	State-of-Charge
SOH	State-of-Health
SPKF	Sigma-Point Kalman Filter
SVM	Support Vector Machine
RLS	Recursive Least Square
RMSE	Root-Mean-Square Error
RUL	Remaining Useful Life
UKF	Unscented Kalman Filter
USABC	US Advanced Battery Consortium
UT	Unscented Transformation



TLBO Teaching Learning Based Optimization

WRLS Weighted Recursive Least Square



# Symbols

Subscript $\hat{\phantom{x}}$	Estimated and predicated quantity
Subscript $-\phantom{x}$	Prior predicted quantity based on past measurements
$\alpha_j$	Power assignment factor
$\alpha_{gra}$	Road gradient
$\Delta t$	Sampling time
$\eta_c$	Coulombic efficiency
$\eta_g$	Efficiency of the gear system
$\eta_m$	Efficiency of the propulsion motor
$\eta_{VFD}$	Efficiency of the inverter
$\eta_{con}$	Efficiency of the DC-DC converter
$\gamma$	Scalar scaling factor
$\chi$	Sigma points
$\mu_{rr}$	Tire rolling resistance coefficient
$\nu_{EV}$	Speed of EV
$\rho_{air}$	Density of the air
$\omega_{wh}$	Angular speed of the wheel
$\omega_{sh}$	Shaft angular velocity
$\tau_{st}$	Torque at shaft of the propulsion motor
$\tau_{te}$	Traction torque at the wheel
$\tau_{SOC_{FB}}^m$ <i>in</i>	Minimum SOC threshold value for FB
$\tau_{SOC_{SB}}^m$ <i>in</i>	Minimum SOC threshold value for SB
$\tau_{SOC_{FB}}^m$ <i>ax</i>	Maximum SOC threshold value for FB
$\tau_{SOC_{SB}}^m$ <i>in</i>	Maximum SOC threshold value for SB

---

$\hat{A}_k$	System matrix
$\hat{B}_k$	Input matrix
$\hat{C}_k$	Output matrix
$\hat{D}_k$	Feed-forward matrix
$a_d$	Polynomial coefficients where $d=1,2,\dots,34$
$d_j$	Duty cycle for converters for battery $j=SB, FB$
$e_j$	Coefficient of polynomial capacity degradation model where $j=1,2,3$
$p_j$	Coefficient of exponential capacity degradation model where $j=1,2,3,4$
$r_j$	Random number where $j=1,2,3,4$
$i$	$i^{th}$ Particle
$c_1$ and $c_2$	Acceleration constants for PSO
$f(\cdot)$	State function
$g$	Standard gravity constant
$gb$	Global best position in PSO
$h(\cdot)$	Measurement function
$k$	Sampling step
$k_c$	Cycle number
$l_{bd}$	Lower bound
$maxiter$	Maximum iteration
$n$	Number RC networks in the battery model
$pb_p$	Personal best position found by the $p^{th}$ solution
$pr$	perturbation rate in ASMO
$r_c$	Random number for between 0 and 1 crossover process
$r_m$	Random number for between 0 and 1 mutation process
$r_{wh}$	The radius of EV wheels
$u$	Trail vector in DE
$u_{bd}$	Upper bound
$u_k$	Input vector of the system
$v_d$	Donor vector in DE
$v_k \sim \mathcal{N}(\bar{v}, \sum_v)$	Gaussian measurement noise with mean zero and covariance $\sum_v$ .
$v_p$	Velocity of $p^{th}$ solution

---

$w$	Interia weight factor
$w_k \sim \mathcal{N}(\bar{w}, \Sigma_w)$	Gaussian process noise with mean zero and covariance $\Sigma_w$ .
$x$	System state vector with mean $\bar{x}$ and covariance $\Sigma_x$ .
$x_p$	Population set
$y_k$	System measurement vector at time $k$ .
$A$	Coefficient vector for GWO
$A_{front}$	Vehicle frontal area
$C$	Coefficient factor for GWO
$CR$	Crossover constant in DE
$C_1$	Electrochemical diffusion capacitance
$C_{dl}$	Double layer capacitance
$C_{drag}$	Aerodynamic drag coefficient
$C_{prob}$	Crossover probability
$C_r$	Current rate for charge process
$C_{sei}$	Surface film layer electrodes capacitance
$C_v$	Control variable in GWO
$D$	Number of parameters coefficient
$D_r$	Current rate for discharge process
$DOD$	Depth of discharge
$F_{ad}$	Aerodynamic drag force
$F_{he}$	Hill climbing force
$F_{la}$	Linear acceleration force
$F_{rr}$	Rolling resistance force
$F_{te}$	Tractive force on the vehicle
$F_{wa}$	Rotational acceleration force
$G$	Gear ratio of the transmission system
$J$	Propulsion motor rotor inertia
$I_{BL}$	Battery load current with a positive value at discharging ( $I_{BL,d}$ ) and a negative value at charging ( $I_{BL,c}$ )
$I_{RC}$	Current through the RC network.
$KG$	Kalman gain

---

$M_{ev}$	EV mass
$M$	Mutation factor for DE
$M_s$	Mean solution in TLBO
$M_{prob}$	Mutation probability for GA
$N_{eff}$	Effective sample size
$N_{th}$	Threshold value for resampling
$N_x$	Number of system states
$N_u$	Number of input to system
$N_v$	Number of process noise
$N_w$	Number of measurement noise
$N_P$	Number of particles
$P$	Number of population
$P_s$	Number of optimal solution for GA
$P_m$	Motor power
$P_{te}$	Traction power
$P_{dem}$	Power demanded by the drivetrain of the EV
$P_j$	The power to be supplied by each of the battery $j= SB, FB$
$P^{max}$	Maximum power of the battery
$P^{min}$	Minimum power of the battery
$Q(0)$	Initial charge stored in the capacitor.
$Q_{pkc}$	Battery capacity degradation representation by polynomial model
$Q_{nom}$	Nominal capacity of the battery
$Q_{max}$	Maximum available capacity
$Q_{max_{unused}}$	Maximum available capacity of unused battery
$Q_{pkc}$	Battery capacity degradation representation by polynomial model
$Q_{rated}$	Rated capacity of the battery
$R_0$	Battery internal ohmic resistance
$R_1$	Electrochemical diffusion resistance
$R_{ct}$	Charge transfer resistance
$R_{bk}$	Battery bulk resistance
$R_{sei}$	Surface film layer electrode resistance

---

$SOC_k^M$	Measured SOC from Coulomb Counting method
$SOC_k^M$	Estimated SOC
$SOC_{FB}$	SOC value for FB
$SOC_{SB}$	SOC value for SB
$T_0$	The instantaneous temperature of the battery
$T_r$	The reference temperature of the battery i.e. $25 \text{ }^\circ\text{C}$ .
$T_F$	Teaching factor in TLBO
$V_{oc}$	Battery open-circuit voltage
$V_{oc}(SOC)$	Battery open-circuit voltage dependent of SOC
$V_{Bt}^M$	Battery terminal voltage value measured from the battery model
$V_{Bt}^C$	Catalog battery terminal voltage value provided by the manufacture
$V_{DC}$	DC link voltage
$V_{DC}^{REF}$	Reference value of DC link voltage
$V_{RC}$	Voltage across the RC network
$Z_W$	Warburg impedance





# Chapter 1

## Introduction

### 1.1 Motivation for the Present Work

The present world energy economy is at serious risk with the substantial depletion of fossil fuels, rapid increase in the energy prices, effect on the environment with the emission of Green House Gases (GHG) and the dependency on politically unstable fuel producing countries [1]. Therefore, investments in the development of the exploitation of clean energy resources are increasing worldwide. As per the report of the International Energy Agency (IEA), approximately 14% of total energy-related  $CO_2$  emission (the primary cause of the greenhouse effect) occurs from automobile industry [2]. The urgency for clean energy has raised concern among government, automobile manufacturers and researchers. To promote electrification of transportation, Electric Vehicles (EVs) are a potential alternative to the internal combustion engine (ICEs) automobiles. In 2013, Indian government released National Electric Mobility Mission Plan (NEMMP) 2020, to set guidelines for deploying EVs in the country. According to the NEMMP, India aims to deploy 400,000 passenger EVs by 2020 [3]. Effectively accomplishing this target can abstain India from bringing in 120 million barrels of oil and prevent 4 million tons of  $CO_2$  outflows by 2020 [4]. Moreover, EVs will be a boon to plan a modern transport foundation in India for meeting the needs of the nation's tremendous and diversified population.

EVs, as the name suggest, are propelled by electric motor powered by electrical energy source such as rechargeable batteries. Historically, the first EV came in the automobile market in the mid-19<sup>th</sup> century. However, EVs witnessed declining popularity in the automobile market during the first half of the 20<sup>th</sup> century due to technical limitations of battery, lack of proper charging infrastructure and transistor-based electric technology [5].

In the last decade, with the advancement of technology and policy support, EVs have gained renewed attention in the automobile market. Table 1.1 shows the number of EVs in 14 different countries in 2015 and targets committed to be achieved by 2020 [6]. The number of EVs on the road in 2015 was extremely low (0.1%) compared with existing passengers vehicle around the world [6]. Even achieving the committed target would lead to EVs share increased to 3% only by 2020.

TABLE 1.1: EVs in 2015 and targets committed to achieve by 2020

<b>Countries</b>	<b>EVs in 2015 (thousand)</b>	<b>EVs target by 2020 (million)</b>	<b>EV share by 2020 in the market</b>
Austria	5.3	0.2	4%
China	312.3	4.6	3%
Denmark	8.1	0.2	9%
France	54.3	2.0	6%
Germany	49.2	1.0	2%
India	6.0	0.3	1%
Ireland	2.0	0.1	3%
Japan	126.4	1.0	2%
Netherlands	87.5	0.3	4%
Portugal	2.0	0.2	5%
South Korea	4.3	0.2	1%
Spain	6.0	0.2	1%
United Kingdom	49.7	1.6	5%
United States	101.0	1.2	2%
Total	814.1	12.9	3%

The technological readiness of energy storage system, i.e., batteries, was the crucial problem in mass production and penetration of EVs in the automobile market [7]. Thus, to realize an EVs paradigm shift, it is necessary to investigate the improvement and development of the battery technologies. The popular battery technologies used in EVs till dates are lead-acid, nickel-cadmium, nickel metal hydride, and Lithium-ion (Li-ion) battery [8]. Li-ion battery technology is considered superior to all other battery technologies because of their high operating voltage levels, high energy and power density, wide range of operating temperature, long service life, least self-discharge rate, and absence of the memory effect [9]. Hence, over the last few years, automobile industries have driven the development of EVs with Li-ion battery. However, the Li-ion battery cost and lifetime is the primary concern and challenge in the fast-evolving and promising uptake of EVs in the automobile markets. Top concerns for the potential battery-powered EV customers are safety and reliability of the battery [10]. Improper operations such as over-voltage, over-current and overcharging/over-discharging will cause the battery to combust due to

volatility, flammability, and entropy change. These changes will cause noticeable acceleration in the aging of battery and significant safety issues which can lead to fire or explosion in EVs [11]. Hence for practical implementation in EVs, the battery must not only demonstrate favorable performance and reliable characteristics, but they must also be accurately monitored in situ to facilitate maintenance and operational decisions. An effective battery management system is crucial for the safe, reliable, efficient and consistent operation of the battery under different environmental and driving conditions.

Battery management system is a monitoring and control framework that maintains the operation of the battery in the specified constraints, as well as performs the appropriate safety steps in case of hazardous situations [12]. It utilizes a suitable battery model to describe the dynamic behavior of the battery under different operating conditions. This battery model also helps in the investigation of battery performance, lifetime and driving range of the vehicle. Consequently, the derived model for battery management system should be sufficiently simple but still capable of capturing the critical characteristics of the battery. Moreover, if any abnormal situation such as over-voltage, over-current, and overcharging/over-discharging are detected during the operation of EVs, battery management system should notify to execute preset correction procedure [13]. For these safety issues, battery management system requires accurate determination of various internal states of the battery (such as State-of-Charge (SOC) and State-of-Health (SOH)) and its Remaining Useful Life (RUL). Accurate estimation of internal states is also utilized as the key decision factor for power distribution and energy management system of the EVs. Development of effective battery management system requires a suitable battery model and accurate estimation of internal battery states. This leads to the growing interest of researchers to develop advanced battery management system with accurate battery model and precise online estimation of internal battery states for the application in EVs.

Nowadays, automobile industries design and produce EVs with a single large-size battery pack which offer extended range and high performance. However, these EVs are still in the luxury segment with cost ( $> 40kUS$  \$) out of which price of the battery represents a significant share. In [14], the authors suggested the concept of dual-battery powered EVs having two different size batteries. Small size battery pack was fixed, and big size battery pack can be swapped according to the requirement. For short range, fixed small size battery has been used which will reduce the mass of the EV and improve the energy consumption per unit distance. For more extended range, both small and large size battery packs are utilized simultaneously to power the drivetrain in the EV. The authors have also analyzed the performance of the proposed dual-battery powered EV concept in comparison

with single larger pack EVs and proved that there is a significant improvement in energy consumption (up to 17 %), and economic benefits are achievable by distributing the cost of the large battery pack over the lifetime of the vehicle. Benefits of using dual-battery powered EVs will encourage further studies in the field of power management strategies between different size batteries and development for battery swapping centers for the further popularization of EVs in the automobile market.

## **1.2 Literature review**

Design of battery management system for estimation of internal states of battery and power management for the dual-battery powered EVs underpin the aims of this research work. A summary of recent work has been provided through a comparative analysis of the different estimation techniques for internal states identification and power management methods used. This section begins with a description of the various battery technologies used for EVs and their characteristics. The affect of operating voltage, and temperature variation on the performance of the battery have been analyzed for determining the requirements of an effective battery management system. To understand the significance of the battery management system in detail, a dedicated section on its functioning has been included. The next section provides a thorough review of the recently developed battery models for reflecting the behavior of the battery under different operating conditions and briefly explains their advantages and shortcoming. Battery models have parameters that have to be identified either using experimental tests or with varying techniques of identification. Various techniques for evaluation of the battery model parameters reported in the literature have been discussed. A discussion on different estimation methods used to determine the internal states of battery has been included and the emphasis has been given to model-based estimation methodologies that are deployed for the estimation of internal states. A comprehensive review in the domain of power management of EVs has been presented, and finally, the research objectives to be achieved in this thesis based on research issues identified in the literature are presented.

### **1.2.1 Lithium Ion Battery**

During initial years of development of EVs, their penetration in the automobile market had been bottlenecked by their inefficient energy storage system. Popular types of batteries used for energy storage in EVs include lead-acid, nickel-cadmium, nickel-metal hydride and

Li-ion battery [15]. Indispensably required critical parameters for a comparison of different battery technology are the power density, the energy density, service life, energy efficiency, self-discharge, cost, and safety level [16]. Table 1.2 illustrates critical parameters and their values for these popular battery types. It can be observed that each battery technology dramatically differs from one to another [17,18].

TABLE 1.2: Main characteristics of popular battery types used in EVs

Battery	Lead-Acid	Nickel Cadmium	Nickel Metal Hydride	Lithium-ion
Nominal Voltage [V]	2.1	1.25	1.25	3.6
Power Density [W/Kg]	180	150	1000	1800
Energy Density [Wh/kg]	30-50	50-80	60-120	100-270
Self-discharge/month [% ]	3	20	30	10
Charging Temperature [ $^{\circ}C$ ]	-35 to 40	0 to 45	0 to 45	0 to 45
Discharging Temperature [ $^{\circ}C$ ]	-20 to 60	-20 to 60	-40 to 60	-20 to 60
Service life [cycle]	<350	1500	300-600	500-3000
Typical Battery cost [\$]	25	50	60	100
Energy Efficiency [%]	75-85	60-80	65	85-97
Maintenance [months]	3 to 6	1 to 2	2 to 3	not req.

The lead-acid battery is a popular and well-developed battery technology. The main advantages of the lead-acid battery are low self-discharge rate, high energy efficiency, and economical pricing [19]. They are more economical for large power applications where weight is of less concern, such as backup power system and engine starting [7]. Nonetheless, they are not preferred for EVs because of some obvious technical drawbacks, including low energy density, less service life, heavyweight and risk of toxic chemical leakage. The lead used as the active material is toxic to both human bodies and environment [20]. The requirement of a lighter, smaller and long cycle-life battery has grown significantly in the automobile industry which demands development in the battery technology. To achieve these requirements automobile industry moved towards the usage of the nickel-cadmium battery. The nickel-cadmium is one of most rugged battery type which provides a large number of charge/discharge cycle in economic pricing and can be charged with a higher rate in a shorter time. These batteries are even small and light in weight [15]. But the requirement of periodic maintenance prevents the large-scale application of this battery. Moreover, they have a relatively low energy density, high self-discharge and memory effects that reduces the usable capacity of the battery during its lifespan. The active material "cadmium" is expensive and toxic which make them environmentally unfriendly. Hence, the battery manufacturers of EVs diverted from nickel-cadmium to newer technologies [17]. In the 1990s, nickel-metal hydride battery was designed to substitute the nickel-cadmium battery. Nickel-metal hydride battery has good power/energy density, and is less prone to

memory effect compared to its counterpart nickel-cadmium. This battery type is considered environmental-friendly because it uses a hydrogen absorbing alloy as cathode instead of cadmium. Because of these advantages they have been used in Hybrid EVs such as Toyota Prius, and Chevrolet Malibu, as well as in Plug-in EVs such as General Motors' EV1, Ford's Ranger EV, and Honda's EV Plus. These batteries are small in size, but they require an improvement in their energy density and cell voltage. They also suffer from several technical drawbacks such as a limited service life, higher self-discharge rate, high cost, and low energy efficiency [7]. Moreover, it generates a massive amount of heat during fast charging leading to considerable battery capacity degradation. Li-ion battery is significantly better than preceding battery types, especially in terms of high voltage, high energy/power, higher energy efficiency, more service life, and low self-discharge [21]. Moreover, they require low maintenance and are composed of environmental-friendly metals. Therefore, next generation EVs are adopting Li-ion battery as the most promising energy source.

The significant development in material science motivates the researchers to seek advanced Li-ion battery technologies. Specifications of the battery are dramatically influenced by the material used for the composition of the electrodes. Li-ion battery contains a positive electrode composed of either lithium metal oxides such as cobalt (LCO) and manganese (LMO) or compounds such as nickel manganese cobalt (NMC) or nickel cobalt aluminum (NCA) and iron phosphate (LFP). Carbon and lithium titanate (LTO) are used as the negative electrode. Summarized battery specifications for different types of Li-ion battery have been provided in Table 1.3. From the table, it is concluded that each kind of Li-ion battery has its advantages and disadvantages [22]. For the selection of the battery type for particular applications demands trade-off between the properties of the battery types and preference of the manufacturer. LCO is often found in hand-held electronic equipments such as cell phones and laptop due to its higher specific energy ( $110 - 190 \text{ Wh/Kg}$ ) and low discharge rate. LCO battery types are not preferred in the EVs because of less specific power, low thermal stability, and less service life. Fast charging (applying high C-rate) causes overheating inside the battery. Also, Cobalt metal is scarce and expensive. NCA and NMA also have approximately same specific energy as LCO, but they have higher capacity and high power, thus they can be used for longer driving range. But in these batteries, the exothermic reaction will take place at the higher temperature which leads to the thermal runaway. The use of cobalt and nickel in these battery types leads to an increase in the cost of the battery. Hence, high cost and marginal safety prevent uses of these batteries in the EVs. LMO and LFP are more beneficial and better choice for the application of EVs as they are free from nickel and cobalt. High thermal stability

TABLE 1.3: Characteristics of different types of Li-ion battery

Chemical Name	Lithium Cobalt Oxide	Lithium Nickel Cobalt Aluminum Oxide	Lithium Nickel Manganese Cobalt Oxide	Lithium-Manganese Oxide	Lithium Iron Phosphate	Lithium Titanate
<b>Specifications</b>	LCO	NCA	NMC	LMO	LFP	LTO
<b>Formula</b>	$LiCoO_2$	$LiNi_xCo_yAl_zO_2$	$LiNi_xMn_yCo_zO_2$	$LiMn_2O_4$	$LiFePO_4$	$Li_4Ti_5O_{12}$
<b>Typical Cell Voltage Range</b>	3.0-4.2	3.0-4.2	3.0-4.2	3.0-4.2	2.5-4.2	1.8-2.9
<b>Typical Temperature range (<math>^{\circ}C</math>)</b>	Discharge: -20 to 55 1Charging: 0 to 45					
<b>Thermal Runaway</b>	150	160	210	265	310	safest
<b>Deep-cycle life</b>	500-1000	500	1000-2000	300-700	1000-2000	3000-7000
<b>Specific power Wh/kg</b>	150-190	200-260	150-220	100-150	90-120	50-80
<b>Safety</b>	++	++	+++	+++	++++	++
<b>Specific energy</b>	++++	++++	++++	+++	++	++
<b>Specific Power</b>	++	+++	+++	+++	++++	+++
<b>Lifespan</b>	++	+++	+++	++	++++	++++
<b>Performance at high/low temperature</b>	++	+++	+++	++	+++	++++
<b>Cost</b>	+++	++	+++	+++	+++	+
<b>Automotive usage</b>	Tesla Model S		VW eUP, eGold, BMW i3,Daimler, Fiat 500, Smart	Chevy Volt, Nissan leaf, Renault, Fluence, Zoe	Chevy Spark EV, Coda EV, BYD E6, eBuses	Mitsubishi i-MiEV, Honda Fit eBuses, ECVs
<b>Manufacturers</b>	Panasonic		Kokam, Samsanug, Li-Tee, EIG	AFSC, EnerDel, Toshiba,Hitachi, LG Chem, LiEnergy Japan, GS Yuasa	A123, ATL, Calb, BYD, Lishem, Tianjin, Valence	Altairnano, Toshiba, Tiankang

and enhanced safety are the main benefits of these batteries. LMO batteries suffer from drawbacks such as low calendar life and less capacity. Whereas, LFP have the long service life and low resistance which offers fast charging and maximum discharge rate ability [23]. Nowadays LTO batteries are developed to improve the durability and performance of the battery during the fast charging process due to the wide working temperature range and long cycle life. However, LTO in EVs remains limited because they have low energy density and highly expensive [9]. By comparing different types of Li-ion batteries, it has been concluded that LFP battery will provide superior performance compared to other types of Li-ion battery in the application of EV because of its lowest cost, high power capability, long lifespan and high thermal capability.

The performance of Li-ion battery is influenced by operating voltage and temperature. The operating voltage and temperature should be carefully controlled because excessively high or low voltage as well as temperature can damage the battery. Figure 1.1 defines the operating region for Li-ion battery, and the green box indicates the safe operation window [13]. Safe operation window defines the values of voltage and temperature for reliable operation of the battery. The operation of the battery outside the safe operating window can permanently damage the battery. Voltage related damages could be categories as high voltage impact (overcharging) and low voltage impact (over-discharging) [8]. During the charging process, if the terminal voltage exceeds the recommended upper voltage limit, then excessive current flow results in overheating, increase in temperature and lithium plating. Lithium plating is the deposition of metallic lithium around the positive electrode of Li-ion battery. Lithium plating results in irreversible capacity loss and reduction in free Li-ions [13]. Dendrite formation of plating leads to an internal short circuit which will damage the battery. On the other hand, over-discharging results in the progressive breakdown of the negative electrode material. Breakdown of carbon will increase the self-discharge rate of the battery [24]. When the battery is recharged, then copper ions precipitate as metallic copper which leads to an internal short circuit.

Damage due to variation in temperature can be categories as follow: effect of low-temperature ; effect of high temperature and thermal runaway. According to Arrhenius law, battery operation at the low-temperature results in the reduction in chemical reaction rate at which the active chemical is transformed in the battery [25]. Reduction in chemical reaction rate influences power handling capacity as well as it prevents the adoption of aggressive regenerative braking strategy because it can cause lithium plating. At high-temperature, due to Arrhenius effect high power is demanded from the battery because of increasing the reaction rate. But excessive current results in higher  $I^2R$  heat dissipation [25]. Excessive



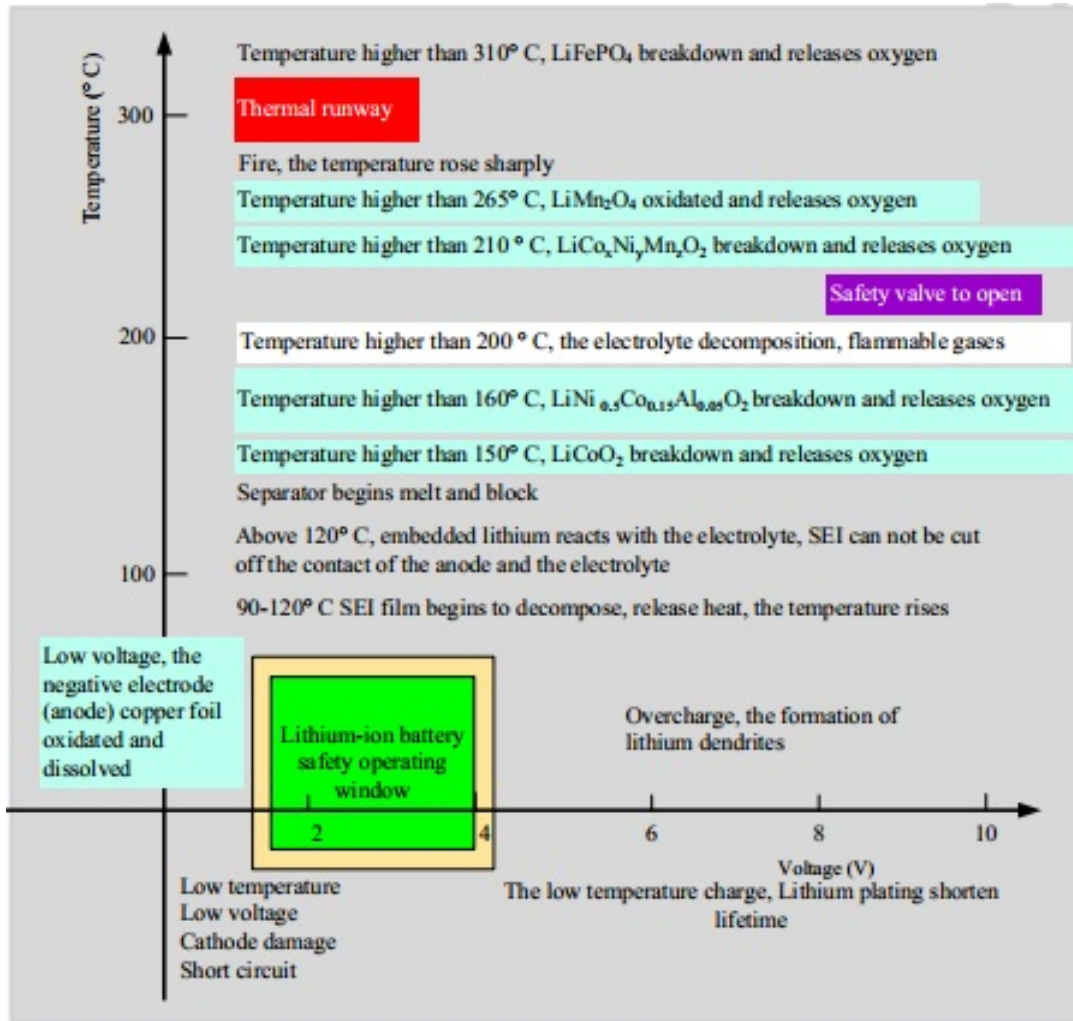


FIGURE 1.1: Li-ion battery operation window

current and high temperature initialize the overheating process which will break down the Solid-Electrolyte Interphase (SEI) layer on the negative electrode. Positive temperature feedback will raise the temperature rapidly unless heat is removed at the faster rate than it is generated. As indicated in Figure 1.1, when the temperature 90 – 120°C, the SEI film will start the exothermic reaction [26]. When the temperature exceeds 120°C, heat dissipation causes breakdown of organic solvents which will release combustible gases but no oxygen [27]. At 130°C, the separator will start melting which leads to an internal short circuit. When the temperature rises beyond 150°C, the decomposition of positive electrode material releases oxygen which causes burning of present combustible gases in the battery. Breakdown of the positive electrode is an exothermic reaction which will increase the temperature even higher. When the temperature is above 200°C, battery starts to catch fire due to exothermic electrolyte oxidation which results in a dangerous

thermal runaway [28].

By analyzing the safe operation window of a Li-ion battery, it has been concluded that exposure to overcharging, over-discharging, and temperature variation results in catastrophic hazards, dramatic degradation in battery service life, loss in battery capacity and premature failure such as the thermal runaway. Notwithstanding significant progress in battery composition and chemical kinetics, an effective battery management system is still required to ensure proper estimation of internal states, maintain the battery reliability and safety, cell balancing and controlled charging/discharging [29]. It is believed that the battery management system can significantly improve the efficiency of EVs by extending service life as well as by reducing the operational cost of the battery. Next section will discuss the significance of the battery management system and its function during the operation of EVs.

### 1.2.2 Battery Management System

For electrification of the automobile, battery refers to core component for energy supply which requires real-time supervisory monitoring and control system for reliable and safe operations [30]. Battery management system is an electronic device that monitors and controls the operation of the battery in the specified constraints as well as perform the appropriate safety steps in case of catastrophic hazardous situations [13]. The battery management system is the brain of the EVs which takes information from the various sensors within the battery as well as external sensors available in the automobile [31]. And then transmit this information to the controllers for issuing control commands as well as decision factors for the power management system. The main function performed by the battery management system is [18, 32]:

- Data acquisition: To measure operation parameters such as battery voltage, current, and temperature, etc.
- State estimation: Monitoring the amount of charge stored (SOC), health condition (SOH) and power capability.
- Safety Protection: Protection of the battery from out-of-tolerance conditions such as overcharging over-discharging, thermal stress and thermal runaway, i.e., Maintain battery operation within their operational limits to prolong its service life.
- Cell balancing: Using passive and active balancing techniques

- Control charge/discharge: Ability to control the charging/discharging conditions of the battery.

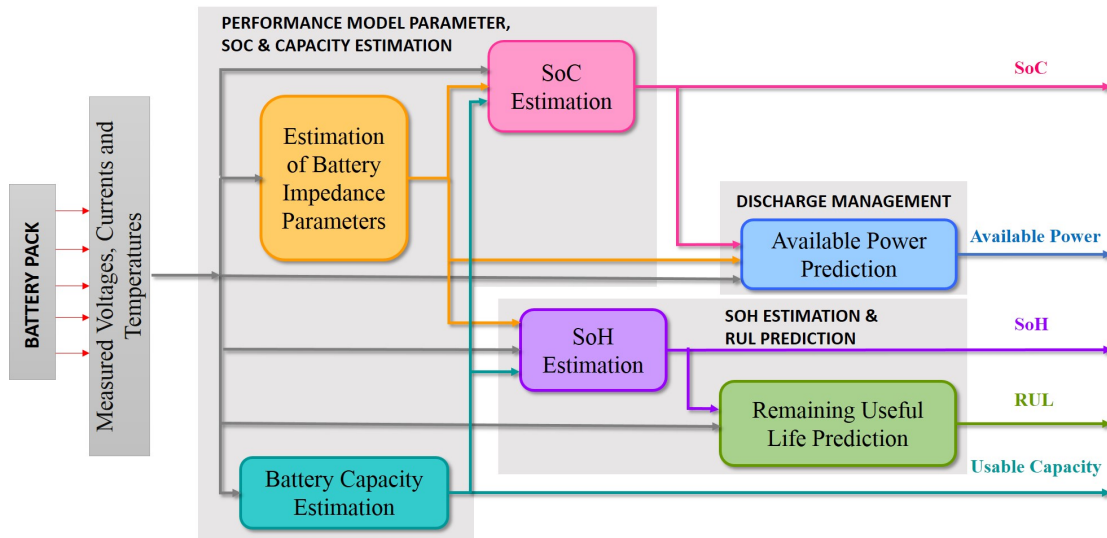


FIGURE 1.2: A typical information flow within battery monitoring System

Developing an effective battery management system has always been a big concern for all the battery drive automobile manufacturers. Battery management system is responsible for accurately monitoring of parameters and internal states of the battery for safe and reliable operation of EVs. Battery parameters term refers to the system characteristics quantities including electric quantities (resistance, capacitance) and chemical quantities (diffusion coefficients, solid phase conductivity, etc.) while the states of the battery are the variables related to system evolution (such as SOC, SOH, RUL, and available power) [12]. Basically, states provide knowledge about system history of usage. Different cells in the battery pack are likely to have different capacity due to manufacture variations, degradation, and natural aging, etc. These variations in the cell capacity result cell unbalancing which leads to overcharging, over discharging and overheating in a particular cell [33]. Therefore, accurate estimation of internal states is the vital function of a battery management system for critical onboard controls to maintain cell balancing, control charging/discharging and safety measures. Hence, efficient battery management system enables the enhancement in the reliability of the energy storage device as well as maximization of the battery service life.

The battery is the complex electrochemical device with distinct nonlinear behavior which significantly depends on the various internal and external conditions and almost all battery characteristics change considerably over the battery service life due to the aging effect [32].

Hence, during the operation of the battery, continuous determination of its dynamic behavior with the variation of internal states is considered a foremost and critical function of the battery management system [12]. Typical information flow within the battery monitoring system has been shown in Figure 1.2 [34]. The critical technologies including battery modeling and state estimation are required for designing an effective battery monitoring system [35]. Firstly, the monitoring system requires a data acquisition unit for observing measurable quantities such as battery current, voltage, and temperature for designing a battery model for the dynamic behavior of the battery [31]. These measurable quantities can be detected using the onboard current sensor, the voltage sensor, and thermocouple conveniently. All these measurable quantities are then used to identify battery model parameters as well as to estimate the internal battery states in later stages [35]. Battery parameters and states are influenced by the variation of temperature, discharge rate, and operating cycles [36]. Therefore, the management system has an embedded battery model that takes into account the effect of different factors on the dynamics of the battery. Battery models are essential for both designs as well as runtime operation. During the designing stage, the battery model helps battery technology specialist to develop robust and reliable battery system whereas, during the runtime phase, accurate battery models help in delivering information about internal battery states. Building the battery model required accurate identification of its parameters which represent electrochemical mechanism inside the battery. The different relevant internal battery states could be estimated by using developed the battery model and their parameters values. These states values are essential to provide information about present charging and discharging level to safety protection circuit as well as for the development of an efficient power management system for the EVs with different energy sources. If any of the parameters exceeds the safe operational window or hazardous situation arises protection devices will perform. The power management system will control the power-sharing between different sources based on power demanded by EVs. This research work focuses on the development of efficient battery management system as well as a power management system for dual battery-powered EVs.

### 1.2.3 Battery Modeling

A high-fidelity battery model is a prerequisite for the development of efficient battery management system, to reflect and predict the performance of battery under varying load and environmental conditions. While operation of EVs, main purpose of the battery model is to reliably simulate the behaviour of the battery behaviour and estimate the

internal states using battery management system. The main aspects to be considered while choosing the appropriate battery model is that it should be accurate and precisely reflect the characteristics and dynamic behavior of battery under different operation conditions [37]. Another aspect is that it should be computationally easy and efficient to implement in battery management system for estimating internal states of the battery. Throughout the years, the researchers have numerous kinds of battery models consisting of different accuracy level and competition complexity for describing the behaviour of the battery [38–40]. These models have been primarily categorized as the electrochemical model, data-driven and equivalent circuit model. This section outlines the state-of-the-art of battery modeling and explains the advantages and disadvantages of different types of battery model.

### 1.2.3.1 Electrochemical models

**Electrochemical models** simulate the electrochemical mechanism of the battery dealing with concentration, movement of active material and the chemical reaction which take place inside the battery [41,42]. These models are structured based models that describe the internal electrochemical process and physical construction of the battery by time-varying spatial partial differential equations [43]. These models could be established by using the macroscopic quantities such as local distributions, battery voltage and current with microscopic parameters for the battery such as concentration distribution, current, voltage, and temperature [44]. Depending upon desired accuracy and aim of battery model different approximation methods are applied for the simplification of equations and their solutions. The widely used electrochemical models are the one-dimension (1D) model [45,46], the pseudo two-dimensional (P2D) model [47], the quasi-three-dimensional full order physical model and the first principle model. The main advantages of these model are that they describe the electrochemical process within the battery more accurately [48]. Set of time-varying spatial partial differential equations used to describe the electrochemical process inside the battery are complex and needed large computational power and memory for solving them. Hence, for modeling purpose explicit recognition of the electrochemical mechanism of the battery requires in-depth knowledge of the chemical process. These models provide high analytical insight about the battery which might interest material scientist or battery technology specialist [49]. However, for electrical engineering such in-depth insight of battery mechanism is not necessary. Hence, these models has been predominantly followed by battery manufacturers and researchers in the chemistry field.

### 1.2.3.2 Data Driven Models

The battery has the complicated internal electrochemical process and uncertain external conditions which make battery modeling as a challenging task for the developer of battery management system. To avoid the need for complex and nonlinear battery modeling, data-driven battery models are developed by researchers [50]. For nonlinear and complex system these model develop transfer functions with the help input-output experimental training data [51]. Parameters of these models do not have any physical significance. Data-driven battery model with generalization ability and acceptance accuracy demand large experimental data [52]. Battery characteristic depends on varies internal and external factors, hence, experimental data should cover enough battery operating conditions [53]. Generations of such as large amount experimental data for training is very time consuming and tedious procedure. This battery model requires high computational power for real-time application. However, once the training phase is completed, these model incur a much lower computational power can achieve comparable accuracy [54].

### 1.2.3.3 Equivalent circuit-based models

**Equivalent circuit-based models** conceptualize the electrochemical mechanism of the battery utilize passive linear elements such as resistance and capacitance, active elements as the voltage source and non-linear elements as the Warburg impedance and diode that strive to approximate the electrochemical behavior of the battery. The battery model structure depends on the desired accuracy, the aim of battery modeling and method used to determine the battery parameters such as Electrochemical Impedance Spectroscopy (EIS) or pulse current charge-discharge behavior. Key features of equivalent circuit based battery models are that they can be more intuitive in circuit simulation, provide real-time implementation, robust in nature with different operating conditions and enable modeling of battery nonlinearities using various circuit parameters [55]. Simple model structure and relatively small number of model parameters are key features are much reason for the wide adoption of equivalent circuit models by system integrators and electrical engineers. These model can be further classified into simple models, Thevenin-based models, impedance-based models, runtime-based models, and combined electrical circuit-based models [56].

**Simple battery models** are composed of the ideal voltage source (open circuit voltage (OCV))  $V_{oc}$  connected in series with the constant internal resistance  $R_0$  as shown in Figure 1.3. Simple battery model parameters are constant and do not depend on the SOC [57]. This model is not capable of describing the voltage profile for the charging and discharging

process [58]. Hence, this model work appropriate when the dependency on SOC is not essential energy released from the battery is supposed to be infinite [59]. In practical conditions, internal resistance changes concerning the change in load. The advanced simple

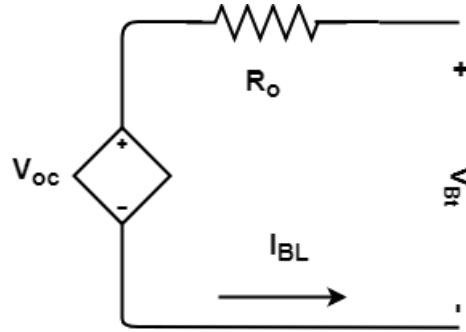


FIGURE 1.3: Simple battery model

battery model is obtained by adding dependency of internal resistance on the SOC and temperature [33, 59–61]. These models represent the static behavior of the battery. Many researchers have utilized this model for monitoring of battery, but this model did not explain the capacitance effect for representing transient current conditions. Modeling of the lead-acid battery used in various application such as uninterpretable power supply is performed by using this battery model [62].

**Impedance-based battery models** is another equivalent circuit based model also known as  $2^{nd}$  order Randles circuit as shown in Figure. 1.4 (a) [63]. Internal impedance calculated using EIS measurements to achieve the AC response of the battery at certain frequency span [64]. EIS is performed by implementing a small amplitude sinusoidal current or voltage signal to the system for different frequencies. Hence, in these models, small-signal excitation allows for direct measurement of system response at any point of the operation [65]. Results are depicted on the chart named Nyquist diagram as shown in Figure 1.4 (b) in which the real axis represents the resistance, and the imaginary axis represents reactance of the battery [63, 66]. Each point on the graph represents the impedance response at a specific frequency. Impedance variation from high frequency to low frequency is represented from the left side of the plot to right side. Parameters of the impedance-based models have the substantial meaning related to the electrochemical process.

Here, bulk resistance is represented by  $R_b$  describes the electric conductivity of the separator, electrodes, and the electrolyte. Surface film layer electrode resistance is represented by  $R_{sei}$  and surface film layer electrodes capacitance is represented by  $C_{sei}$  corresponding to high-frequency impedances. The charges transfer and capacitance between electrode and electrolyte are represented by charge transfer resistance  $R_{ct}$  and double layer capacitance

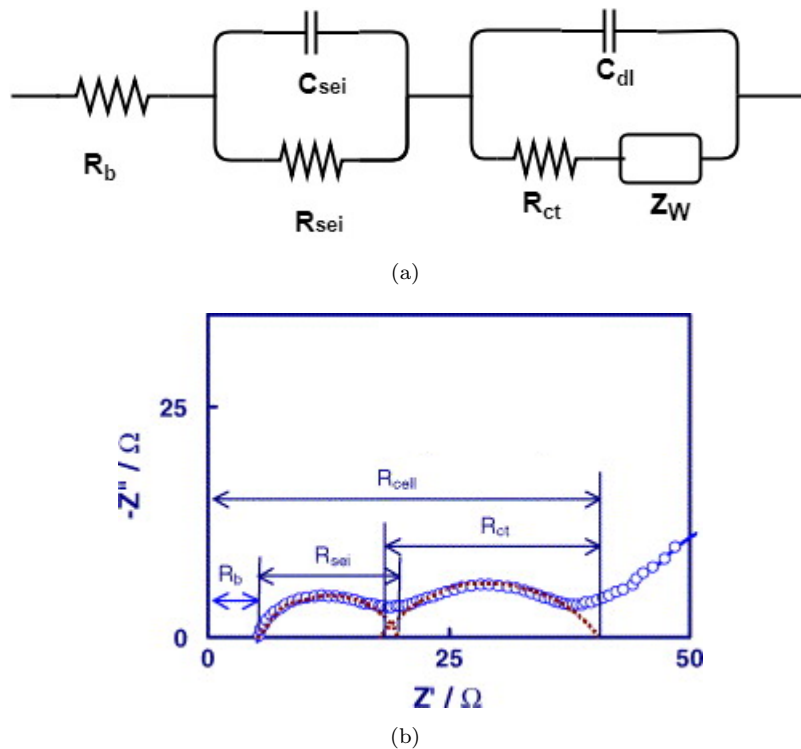


FIGURE 1.4: (a)  $2^{nd}$  order Randles circuit (b) Impedance measurement using AC response

$C_{dl}$  respectively.  $R_{ct}$  and  $C_{dl}$  demonstrate the medium frequency response. Diffusion phenomena between the active material and electrolyte corresponding to the low-frequency response are designated by Warburg impedance  $Z_W$ . In some case, positive reactance response at high frequencies is explained by adding inductance in series. The identification of parameters of the battery model is made by fitting impedance spectra which is the complex, difficult and nonintuitive process. The reason for using this method is to keep the system in the linear region, i.e., the linear battery model is developed. Moreover, the battery model exhibit performs of battery at constant SOC and temperature hence impedance battery model cannot predict the dc response and battery runtime.

**Thevenin battery model** is another commonly used model which was designed to account for the transient behavior of the battery [67]. Thevenin battery model is composed of an ideal voltage source  $V_{oc}$ , an internal series resistance  $R_0$  for the instantaneous voltage drop, the various number of parallel resistance-capacitance (RC) network as shown in Figure 1.5. All the parameters of the Thevenin battery model are considered to be constant which is significant drawbacks of this model as battery behaviors depend on internal and external operating conditions. Thevenin battery model captures transient response but unable to achieve the steady state voltage variation as well as runtime information.



Researchers have gained improvement in the derived models by adding additional components to predict either runtime or dc response, but not both. In the research literature, different forms of Thevenin based equivalent circuit models depending on the number of RC network and considering dependency of battery parameters on the internal states of battery, adding the effect of hysteresis and impact of aging, have been developed by researchers [56,68]. Accuracy and computational effort of Thevenin battery model depend upon the number of parallels connected RC networks. The higher number of RC networks increase the efficiency of the battery model, but at the same time, computational power requirement also increases. Hence, to represent the battery model trade-off must be made between accuracy and complexity [69,70]. Identification of the battery model is performed by using a pulse charge-discharge technique or parameter estimation techniques.

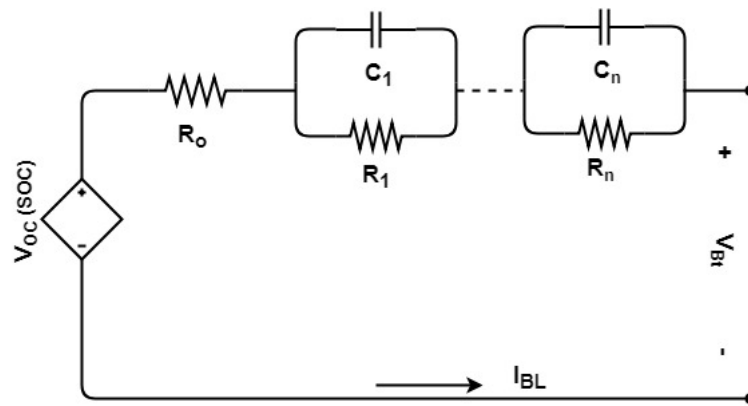


FIGURE 1.5: Thevenin battery model

**Runtime-based battery model** is an equivalent circuit based model for simulating the battery dc response and runtime for a constant discharge current [71]. This battery model consists of three different circuits. The leftmost circuit indicates the dependency of total charge quantity on the battery discharge current rate. It consists of transient elements  $R_{trans}$  and  $C_{trans}$  referring to charge storage resistance and capacitance respectively and battery discharge rate using  $V_{c-rate}$ . The middle part of the circuit indicates the battery behavior dependency on SOC and battery self-discharge rate. It consists of  $C_{use}$  representing battery capacity,  $R_{s,dis}$  representing battery self-discharge due to the loss in energy after long storage,  $V_{Lost}$  to representing the loss due to self-discharge. Battery SOC initialization can be represented by an initial value of  $V_{SOC}$ . Battery SOC 100% corresponds to  $V_{SOC}$  as 1V for fully charged battery and 0% corresponds to  $V_{SOC}$  as 0V for fully discharged. Hence voltage across capacitor  $C_{use}$  represents the battery SOC and  $I_{BL}$  is used to charge and discharge capacitor corresponding to the charging and discharging process respectively. Finally, the right circuit indicates the property of the simple battery model.

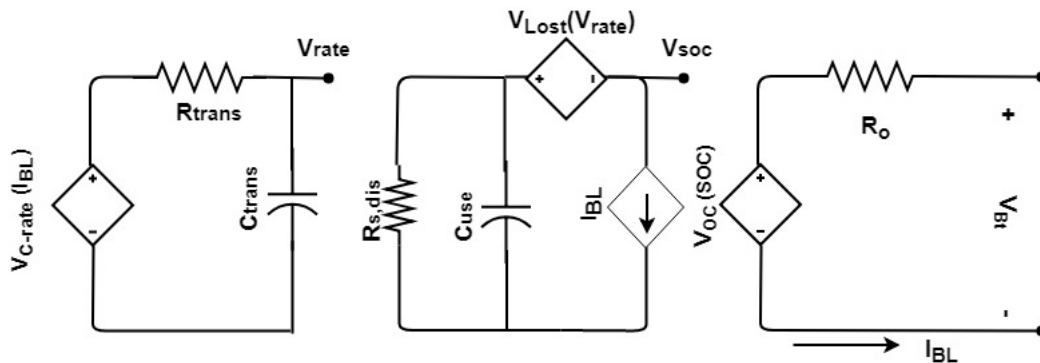


FIGURE 1.6: Runtime-based battery model

A brief comparison and relevant characteristics of the different battery models developed by the researcher are summarized in Table 1.4 [68, 72]. From the table, the conclusion can be drawn that none of the above-defined equivalent circuit based battery models can predict both V-I performance and runtime behavior of the battery. Hence a comprehensive battery model combining Thevenin battery models transient capabilities, impedance-based battery models ac features and prediction of runtime information using runtime-based models is desired for system integration, design, and optimization.

TABLE 1.4: Comparison of various equivalent circuit based models

Model Type	DC	AC	Transient Effects	Runtime
Thevenin	No	Limited	Yes	No
Impedance-Based	No	Yes	Limited	No
Runtime-based	Yes	No	Limited	Yes

**Combined equivalent circuit-based model** is proposed by Chen and Rincon-Mora [72], which combines Thevenin, impedance-based model and runtime-based battery models. A schematic for the combined equivalent circuit-based model is shown in the figure 1.7. This circuit is composed energy balance circuit and voltage response circuit. The elements of voltage response circuit of the battery model vary vigorously over the runtime time of the battery and dependent upon many operating conditions such as SOC, C-rate (capacity normalized current), temperature, number of cycle and hysteresis effect [73]. The voltage response circuit is similar to Thevenin based to simulate the transient response of the battery. Energy balance circuit inherited from runtime based model consists of capacitor  $C_{use}$ , resistance  $R_{dis}$  and current-controlled current source  $I_{BL}$  for modeling battery runtime and DC response.  $C_{use}$  is not an actual capacitance and just used to indicates battery capacity. Battery self discharge is modeled by using resistance  $R_{s,dis}$ . The voltage  $V_{SOC}$  depends on the variation of charging and discharging current. Mapping of SOC and OCV is the bridge between two circuits using a voltage-controlled voltage source

$V_{oc}(V_{SOC})$ . The value of  $V_{SOC}$  varies between 0 and 1 which indicates battery SOC. This battery model can be utilized for modeling the transient behavior of the battery using a voltage balance circuit as well as prediction of battery SOC, and battery capacity are performed by utilizing the energy balance circuit.

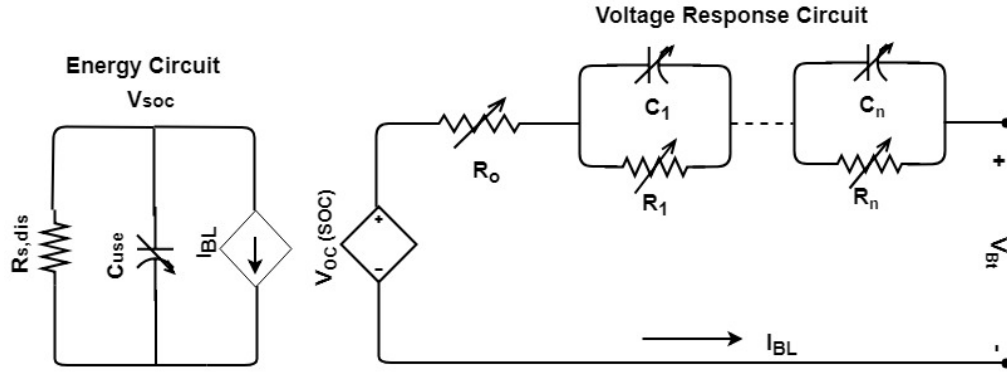


FIGURE 1.7: Combined Equivalent Circuit Battery Model

This review of related works in the battery model focus on three families of battery model types: electrochemical models, data-driven models, and equivalent circuit based models. A summary of different kinds of battery models developed by the researchers is summarized in Table 1.5. From the table, it could be concluded that the suitability of the equivalent circuit-based battery model is high in capturing the dynamic behavior of the battery with medium complexity. The equivalent circuit based models are also capable of achieving the non-linear and transient effect of the battery by predicting V-I performance This review of related works. These models vary in complexity from simple battery model with voltage source plus resistance as circuit elements to battery models with multiple dynamic elements. Combined equivalent battery model that could model transient, DC response and runtime behavior is considered to represent the dynamics of the battery model in this research work.

TABLE 1.5: Detail description of important characteristics of different types of battery model

Model Type	Dynamics	Nonlinear Effects	Transient Effects	I-V Characteristics	Design Difficulty
Electrochemical	Yes	Yes	Yes	No	High
Data-driven	No	Yes	Yes	No	High
Equivalent circuit	Yes	Yes	Yes	Yes	Medium

### 1.2.4 Battery Model Parameters Identification

Battery model parameters including electric (resistance, capacitance) and chemical (diffusion coefficients, solid phase conductivity, etc.) quantities describes the characteristics of the battery. Parameters selection depends upon the type and topology of chosen battery model [74]. A challenging task in battery modeling is how to obtain the value of model parameters as for most of the parameters no sensors are available to measure them directly. Over the years, researchers have developed different methods for identification of parameters values using different measurable qualities (such as terminal voltage, current, and temperature) [75–77]. Human effort to set up necessary test and performing calculations as well as the requirement of hardware to implement the computation is the main factor affecting the identification of the parameters. Hence, different parameter identification methods proposed for optimizing different aspects (such as reliability, robustness, simplicity, accuracy, and speed) have been discussed [78]. The review works in this section discusses different techniques utilized for battery model parameter identification in the literature [79]. Parameter identification techniques for equivalent circuit-based battery models can be categorized as follows: off-line and on-line (recursive) identification methods.

The majority of researchers proposed parameter identification as off-line procedure based on different experimental tests. The main concept of off-line identification methods is to measure the quantities (i.e. current and voltage) over a specified period [80]. Then, store these measurable quantities data in the memory for identification of battery parameters and apply error minimization algorithms to fit with the measured data. The procedure complexity depends upon experimental test process. The battery parameter identification can be performed either using frequency-domain or time-domain parameter extraction experiments [81]. For the frequency-domain parameter identification, EIS test process is commonly used [82]. As discussed earlier, the EIS method identifies parameters by analyzing the AC frequency response of the battery. The EIS techniques are designed to understand the electrochemical impedance characteristic of a battery. Impedance spectroscopy process is performed in the laboratory utilizing the specialized electronic equipment [83]. This method provides more accurate results, but the determination of impedance using systematic incidence of frequency is the primary challenge for this method. This method could not consider dependency of the battery parameters on the current as the amplitude of excitation current is low. Moreover, for charging and discharging process EIS measurement methods require various AC responses of the battery at a specific frequency depending

upon different operating condition. Parameter identification in time-domain is usually obtained through fitting voltage response from either constant current charge-discharge test or Pulse Current Charge-Discharge test (PCDT) [84] with polynomial-exponential based function. PCDT involves alternate cycles of constant current charging and discharging with rest periods [85]. Battery model parameters depend on the C-rate and temperature, hence, repeated experimental tests were performed at different C-rate and temperature. Experiment was performed for both charge and discharge condition due to the presence of some hysteresis effect in the behavior of the battery. The drawback of this method is ignorance of dynamic inputs in tests, hence results in large voltage errors when dynamic inputs are applied. The benefit of off-line non-recursive identification methods is that battery model can be fractional as well as highly non-linear. As parameters are searched in the batch of experimental data which provides high stability and accuracy to the identification process. However, performing these experiments in the laboratory is time-consuming and demands expertise. And data analysis requires high computation power and memory for iterative search.

In recent years, some researchers considered battery parameters identification as a recursive process. Hence, several on-line parameter identification techniques have been proposed [86]. These identification techniques can be categorized as least square method [87, 88], adaptive filters based method [89–91], Artificial Neural Networks (ANN) [92] and optimization techniques. Least square methods have been applied to identify the unknown battery model parameters by minimizing the sum of squared residuals. The employed variants of the least square filters include Recursive Least Squares (RLS) filter and weighted RLS filter (WRLS) [93, 94]. The RLS is an adaptive filter which recursively updates system parameters by incorporating the information at each sample interval. To improve the performance of these filters, each time-varying parameter is assigned with one individual optimized forgetting factor with Newton's method [95]. Hence, RLS filter tune parameters of the time-varying system with a forgetting factor. Asymptotic memory length decides the tuning speed for parameters identification [96]. Asymptote memory length is the time constant for the sample time interval which provides information preserved in the memory. Infinite asymptotic memory length refers that all information is preserved in the memory. The advantage of this approach is the significantly lower computation power demand. These method are affected by significant divergence problems when the battery model inaccurately reproduces the behavior of the battery. In [86], a moving window least-square approach was adopted to improve the convergence of the filter for battery model parameters identification. This was achieved at the expense of more consumption of memory for storage of battery data corresponding to a certain number of past steps

(window). Implementation of KF based adaptive filter for parameter identification is more accurate but computationally expensive process [90]. The KF-based adaptive filters are recursive filters which combine analytical and probabilistic Bayesian models. The battery parameters have identified using measurable quantities which may have measurement noise due to calibration of measuring device. KF-based adaptive filter identification methods have been utilized to eliminate these noise in measurement during identification of parameters [91]. The battery parameter identification is a high dimensional non-linear problem, and the KF-based identification methods assume the model equations to be linear or slightly non-linear. Thus, the high degree of non-linearity in the battery parameter model leads to a lot of approximation errors while using these methods. Even these methods depend on system noise predetermined variable such as mean and covariance matrix. Improper setting of these variables results in divergence and error. Although, the required computational cost has to be significantly higher due to evaluation of inverse matrix which may lead to numerical instability. Hence, these battery parameters values result in significant discrepancy on the accuracy of the battery model. On the other hand, the machine learning algorithms are more accurate than KF-based adaptive filter based identification methods, they require large amount of data and high computational power to properly estimate the model parameters [97]. Intensive computation requires high quality processors which are too expensive to be used in battery management system. These algorithm also depend upon the quantity and quality of the training data, which make these methods computationally more expensive [98].

### 1.2.5 Battery Internal States Estimation

#### State-of-Charge (SOC)

Energy storage, i.e., the battery in EVs is equivalent to the fuel tanks in conventional internal combustion engine automobiles. Imagine vehicle without fuel gauge on the dashboard, how inconvenient it would be for the driver that he doesn't have the precise indicator of how long the vehicle can still travel [99]. In vehicular analogy, SOC estimation of the battery is similar to having dashboard for fuel gauge that shows the absolute level of fuel remaining in the tank. Battery SOC corresponds to the amount of energy left inside a battery to power the EVs [100]. As inaccurate estimation of SOC leads to overcharge and discharge of battery which can damage or even causes explosion of the battery [101].

The battery SOC is defined as the ratio of remaining capacity over the maximum available capacity of a battery when it has been fully charged. With a given starting point  $SOC(t_0)$

and the battery maximum available capacity  $Q_{max}$ , it is relatively straightforward to calculate the SOC using [102]:

$$SOC(t) = SOC(t_0) - \frac{1}{Q_{max}} \int_{t_0}^{t_f} I_{BL,C} dt \quad (1.1)$$

Here,  $SOC(t)$  represents battery SOC at each sample time  $t$ ;  $t_0$  represents the initial value of time;  $I_{BL}$  represents the instantaneous battery terminal current which is positive for discharging and negative for charging process. If a battery is fully discharged then the value of its SOC is 0% and if it is fully charged, its SOC value is 100%. In literature for calculation of SOC of battery capacity has been defined as the rated/nominal capacity [35, 103]. Battery capacity is not constant and affected by the operation conditions and aging status. Hence, the maximum available capacity of the battery is considered for calculation of battery SOC.

The Depth of Discharge (DOD) is the alternative method of indicating the remaining internal charges in the battery. The DOD represents the battery capacity percentage that has been already discharges i.e.  $DOD = 1 - SOC$ . The DOD can be expressed as [104]:

$$DOD(t) = DOD(t_0) + \frac{1}{Q_{max}} \int_{t_0}^t I_{BL,D} dt \quad (1.2)$$

Here SOC and  $DOD$  are utilized to keep track of internal charges of the battery in case of charging and discharging respectively.

### **State-of-Health (SOH)**

Battery aging leads to gradually deteriorates in battery performance due to irreversible chemical changes with load variations [105]. Battery aging is an irreversible process and eventually causes battery End-of-useful life (EUL) or battery failure. For battery degradation analysis, battery EUL is usually considered to occur when battery maximum available capacity has reduced to 80% of maximum capacity for the fresh battery [44]. When internal battery states reach the specified threshold (i.e. EUL point) battery capacity degraded exponentially leading to insulation damage and the partial short circuit which will cause the explosion and spontaneous combustion [106]. Identification of battery states helps the customer to maintain and replace batteries in advance to prevent the loss caused by the unexpected failure of these batteries and help in reducing maintenance cost.

SOH is battery parameters that indicates extent of aging in the battery system compared to a unused battery. Battery aging can be characterized in term of internal states such as degradation in capacity and rises in internal resistance [103]. As battery degradation cannot be measured directly hence battery capacity and internal resistance are widely used as an indicator of the battery health status. The SOH is estimated as the ratio of the maximum capacity of battery i.e.  $Q_{i,max}$  to the capacity of unused battery  $Q_{i,max\_unused}$ . Battery SOH can be express as follow [105]:

$$SOH(k) = \frac{Q_{i,max}}{Q_{i,max\_unused}} \quad (1.3)$$

RUL can be described as a difference in the number of the cycle between the observation cycle and cycle at which battery EUL will occur [107]. Catastrophic failures can be avoided by prediction of battery RUL and prognostic of battery health. Hence, determination of battery degradation is crucial for safety, accurate prediction of battery RUL and improvement in battery performance [108].

## **Background**

Battery is complex electrochemical device, and its performance high depends upon internal and external conditions such as temperature variations, charge-discharge cycles and aging effects, which makes the battery internal states estimation task very complicated and challenging [109]. As well as no sensor is developed for direct measurement of the battery internal states [34]. However battery voltage, current and temperature can be measured directly using specified sensors. Thus, there is a requirement to develop an efficient and robust method that can accurately estimate internal states of the battery in real time applications by utilizing measurable quantities [110]. With the popularization of the EVs, there is a growing demand for a software or hardware to estimate the remaining effective capacity and loss in the maximum capacity of the battery. Hence precise estimation of the battery internal states is the indispensable task for the safe and healthy operation of the battery [65]. Early from the 1960s, the researchers have performed extensive research and proposed numerous methods for accurate determination of the internal states for different types of batteries. The response time required by estimation techniques is the only difference between SOC and SOH estimation. SOC estimation requires fast response time where as battery aging effect is slow process [34]. Similar estimation methods can be utilized for estimation of battery SOC and SOH. This review presents the classification of Li-ion battery internal states estimation methodologies as well as briefly elaborated



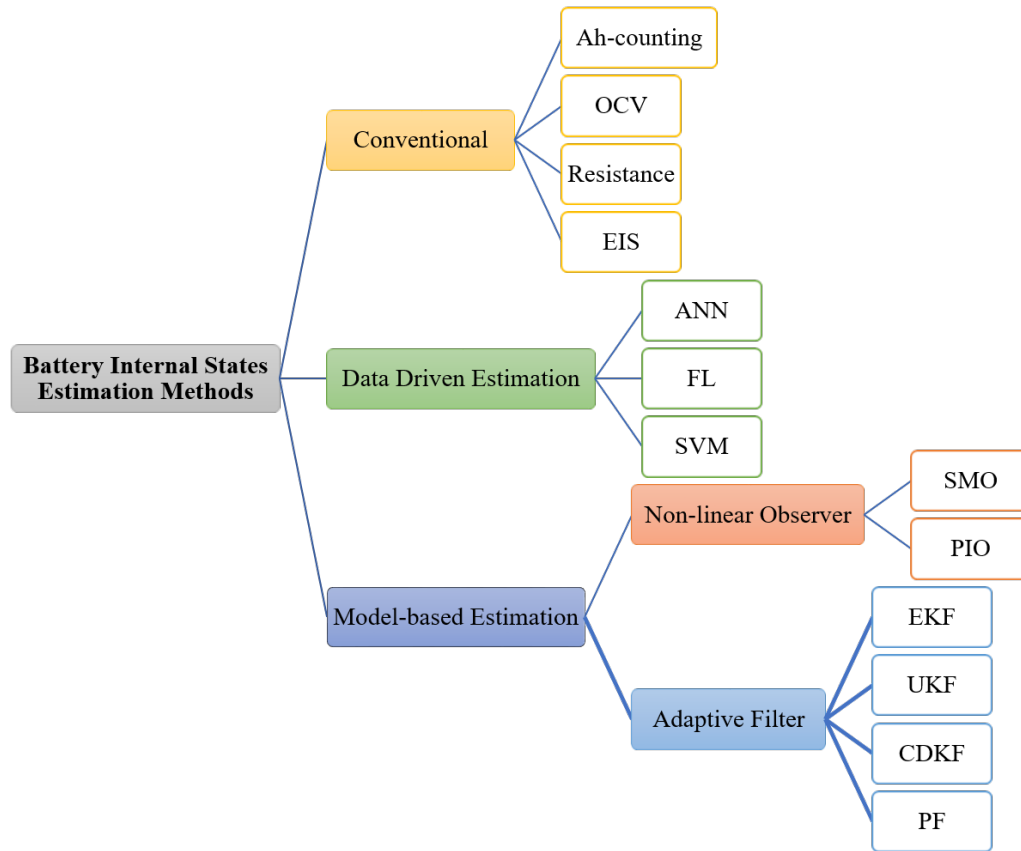


FIGURE 1.8: Classification of battery internal states estimation methods

benefits and drawbacks of all estimation methods [34, 40, 65, 109, 111]. The classification of existing methods has been illustrated in Figure 1.8 [65].

### 1.2.5.1 Conventional Mechanism Analysis Methods

The conventional mechanism analysis methods are based on physical signification and concepts which involves a lot of parameters and complex calculation for accurate estimation of SOC and SOH prognostics. These direct methods require controlled current discharge which is not possible in the application of EVs [112]. In consequence, these methods are useful in theoretical research and battery designation than in practical engineering [113]. Conventional estimation methods refer to direct identification of internal battery states using some physical parameters such as battery terminal current, OCV, resistance, and battery capacity.

**The Ampere-hour (Ah) method** also known as coulomb counting method determines battery SOC by integrating the current entering during charge and leaving during the

discharge process [114]. Ampere-hour method performance is highly reliant on the accurate calibrations of the initial value of battery SOC. If initial SOC estimated inaccurately, then all subsequent estimated values would be inaccurate. Thus precise estimation of initial SOC demands high precision of current sensors [101]. And the capacity of the battery varies with operating conditions and aging levels of the battery. Thus regular recalibration of measurements and battery capacity is needed from time to time. The ampere-hour counting has also used for estimation of the battery SOH [115]. By tracking counts of the amount of ampere-hour transferred and remaining capacity during charge and discharge process track for battery, SOH has also maintained. The drawback for estimation of SOH is that tracking process requires high storage capacity as well as sometimes it is highly time-consuming [116]. Also, ampere-hour method is open loop estimator, hence, it suffers from an accumulation of measurement errors in the battery current measurement due to integration term with the presence of random disturbances such as noise and temperature drift. Indeed Ampere-hour method is the most simple, straightforward and convenient method for internal state estimation if the accuracy of current measurement is maintained and sufficient recalibration points are available [99].

Another way of determining the battery SOC is the **OCV-SOC mapping**. The OCV-SOC mapping method determines battery SOC directly using the monotonous one-to-one relationship between OCV and SOC under specified conditions [117,118]. Hence by measuring battery OCV, the inference of battery SOC can be performed by using lookup table having a relationship between OCV and SOC. The value of OCV has been calculated by determining the true value of the voltage across the battery terminal after long resting time till battery reached equilibrium [110]. For Li-ion batteries, this resting duration is around two hours under low-temperature condition. EVs work continuously their is a very short interval between consecutive use hence resting time become significant limitation for using OCV-SOC estimation method. Further, sensitive of OCV-SOC mapping relationship with uncertain aging status, operating temperatures condition and material characteristics also reduce feasibility and the inference accuracy of the OCV-SOC method [100]. Specifically, for LFP Li-ion battery type this OCV-SOC relationship curve is flat in between 20% to 80% SOC, hence, it is complicated to utilize OCV-SOC mapping for estimation of battery SOC. Even with the presence of hysteresis effect, there are different OCV value for charge and discharge process corresponding to single battery SOC value. This estimation method has been specifically performed in the laboratory environment by using lookup table methods [119]. Battery SOH is independent of OCV hence determination of SOH is not possible from OCV of the battery.

Accordingly, battery capacity and internal resistance determine by applying standard capacity test or pulse current charge-discharge test [120]. Battery aging mechanism is determined by calculating capacity fading and increment of its internal resistance. Hence several researchers have made their research in order to determine the **internal resistance** of the battery [121]. And then these internal resistance value utilized to evaluate battery aging effect [122]. The battery internal resistance has been calculated by applying pulse current and recording voltage variations across the battery. By following the Ohm's law [123]:

$$R_i = \frac{\Delta I}{\Delta V} \quad (1.4)$$

Where  $\Delta V$  represents voltage variation corresponding to applied pulse current. This way internal resistance depending on the SOC and temperature is computed. The internal resistance method requires a test component or circuit comprising high resolution measuring equipment to ensure accurate measurement, which makes this method both cumbersome and costly [124]. In addition, the method is applicable only to unused batteries, which again prevents real-time measurement.

Another way for determining internal states of the battery is measuring battery impedances using **EIS**. EIS diagnosis battery internal impedance as the function of frequency. The battery impedance varies with battery aging and different dynamic conditions which tends to affect EIS measurements at different frequency range [125]. With the variation of high frequency to low frequency, battery impedance changes from inductive to resistive then become capacitive at the lower frequency [83]. EIS methods determine the impedance of battery by measuring the voltage responses of the when a small AC has applied on the battery. This method can provide accurate for identical operating conditions [126]. However, these methods are not suitable for EVs having the different C-rate operation. Even this method demands some specific measurement which needs complicated experiments to be performed [127].

### 1.2.5.2 Data-driven estimation methods

Data-driven estimation methods utilize data-driven battery models which have the ability to model a non-linear system through establishing a relationship between the input-output data. The main benefits of these methods do not require complex battery models for estimation of the battery internal states. Moreover, these have several benefits such as the parallel distribution of processing, high computational rates and highly adaptive to deal with complicated problems [98]. However, data collection for all possible operation

conditions is very tedious, and time-consuming task even uncertainty in datasets affect the robustness of the system model. Hence, data-driven methods are time-consuming, high computation complexity, need an enormous amount of the samples. The standard data-driven methods used for estimation purpose are the neural network [128], fuzzy controller [129] and the support vector machine [130].

Artificial Neural Network (ANN) is a technique that tries to imitate the neural network of the human brain. A typical ANN is composed of three different layers: an input layer, a hidden layer, and an output layer [92]. Hidden layer has been formed of neurons that are interconnected together to control the flow of the information between the network's input and the output layer [131]. The principal functions between different layers have simulated with weights. Various techniques have been developed for training the ANN to determine the appropriate values for these weights. ANN has an excellent capability to learn and recognize patterns from experimental datasets [128]. ANN is often adopted to estimate internal states of the battery due to its superior nonlinear approximation ability for the complex nonlinear system. Its become popular tool for modeling to the complex system because of its ability to handle a large amount of data with nonlinear dependencies [132]. Even ANN has universality properties as it not required to take into to consideration all details about the battery while modeling. The biggest hinder in the implementation of ANN techniques for estimation of internal states in the battery management system is the requirement of a large amount of data and high computational power as well as more number of neurons to increase the accuracy [133]. ANN technique does provide uncertainty in the measurement results if trained ANN for one specific application is utilized for other applications [134]. Hence, ANN is not effective in extrapolation. For EV applications ANN is not considered suitable due to its length learning process and intensive computation.

Fuzzy-Logic (FL) is another powerful technique that presents the modeling of nonlinear and complex systems with the help of training dataset by applying subjective rules of the fuzzy logic theory [135]. The measured data can be categories by fuzzy or crisp sets. Fuzzy sets have uncertainty in the data while crisp sets categories data with certainty. The subsets classify under fuzzy sets are defined by their membership function [136]. The degree of membership function linked with each fuzzy sets indicates the degree of belonging among different subsets. Data fuzzification process determines the appropriate values of the real-valued data [130]. The implementation of FL has four conceptual components which include the rule-based relationship between input-output, membership function based on data for defining the relationship, reasoning mechanism which performs inference procedure and defuzzification process which transform output sets to crisps value [137]. Fuzzy

rules and membership function are usually derived experience and intuition of human being thus effectiveness of control decreases [138]. Though FL is a powerful method to predict the non-linear model but it demands expertise in the field for describing the rule sets and membership function [129]. FL methods demands large amount datasets and complex computation which requires costly processing unit with large memory.

The Support Vector Machine (SVM) is the machine learning algorithm to predict the model based on the statistical decision theory [139]. The basic idea to utilizes SVM to transform the data into input space and then project data using the non-linear transfer function to higher dimensional feature space [140]. Also, fit the sample data using the linear function in feature space. For discrete-valued data, it represents a parametric classifier that finds an optimally separating hyperplane to divide the training data into different classes [141]. The optimal hyperplane can then categorize unseen data points into one of the possible classes [130]. For non-linearly separable training data, an SVM classifier uses a kernel function that relates a subset of training data vectors to the testing data vectors [142].

### 1.2.5.3 Model Based Methods

Model-based estimation methods utilize for estimation of dynamic system states by using generic battery model. Thus, the accuracy of these estimation approaches largely depends upon the accuracy of the battery model. As discussed in battery modeling section that several battery models have been developed by researchers with the development of battery technologies to mimic the dynamic behavior of the battery. Existing battery management systems have limited computation power which increases the demand for accurate and straightforward equivalent circuit based battery model for estimation purpose. These methods infer internal states of battery with relatively moderate computational effort and simple measurement of battery terminal current and voltage [143]. The general flowchart of the model-based internal states estimation method is shown in Figure 1.9 [65]. Model-based estimation methods enhance the estimation process through the utilization state space battery model for dynamic representation behavior as well as the aging effect of the battery. Input/output measurements are used to measure the internal states of the battery. The procedure has been performed by multiplying system gain with the error between measured and estimated output.

In the case of SOC estimation, inaccurate estimation of battery SOC using ampere hour methods develop error in the battery OCV measurement and than OCV error increases the battery terminal voltage prediction error. Therefore, accurate estimation of battery SOC

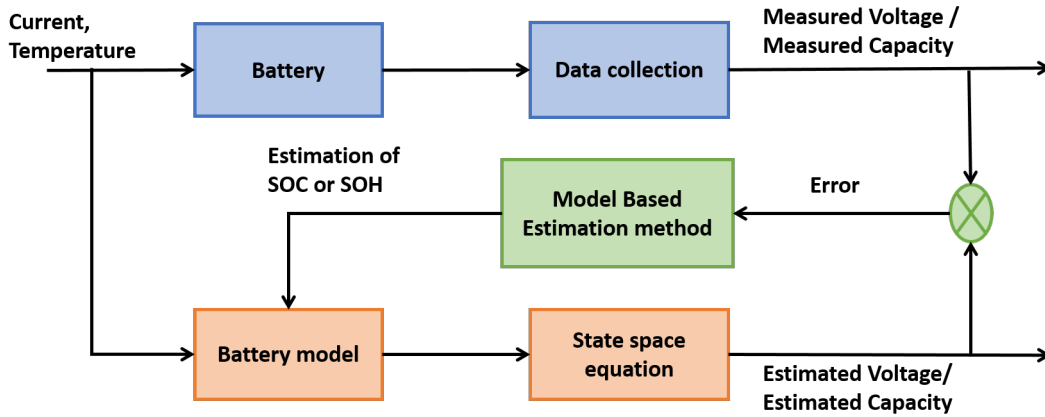


FIGURE 1.9: Model based internal states estimation

minimizes prediction error of the battery terminal voltage. The feedback compensation for estimation of SOC is the battery terminal voltage prediction error. Hence, the method is required to obtain the value of the feedback gain for compensating the uncertainty in battery SOC estimation. Similarly in case of capacity degradation estimation feedback gain is obtained through comparison of measured and estimated battery capacity.

In the literature, different adaptive filters such as Kalman Filter (KF) , Unscented Kalman Filter (UKF) [144], Sigma-Point Kalman Filter (SPKF) and Particle Filter (PF) [145] and nonlinear observers such as Luenberger Observer (LO) [146], Proportional Integral Observer (PIO) [147],  $H_\infty$  , Slide Mode Observer (SMO) [148,149] were utilized to obtain the value of feedback gain of the system. These model-based estimation methods have high accuracy, self-corrective ability, closed-loop evaluation by providing measured voltage signals as feedback, and good adaptability.

### Non-linear Observer

Battery internal states estimation could be performed using different types of observers including linear and non-linear [150]. Commonly linear observers are utilized. Nevertheless, they will increase the internal states estimation error [149]. Hence, nonlinear observers are recommending for linear systems with non-linear observation equations [146]. Exhaustive understanding of battery dynamics is required for the appropriate selection of the gains [113]. Proper gain affects the accuracy of estimation and convergence rate of the observer. However, finding a proper gain matrix to reduce the error is a difficult task [151].

**Sliding Mode Observer (SMO)** work effectively for the system with non-linearity as well as guarantee robustness and stability against external disturbances including model uncertainty [148, 152]. A feedback switching gain is designed to control sliding regime to guarantee the robustness characteristics. The major drawback of SMO is chattering problem which effects the stability of system and sensors [153]. A compromised solution for reducing chattering magnitude is to increase the switching gain of the observer at the cost of slow convergence [154].

**Proportional-integral Observer (PIO)** provides the solution to the problem utilizing proportional-integral structure to replace the feedback system's constant gain [155]. The gain of the feedback system is mainly obtained through trial-and-error, and improper gain settings may lead to system instability [147]. The advantages of this observers are to estimation internal states of battery with less computation time. Also, this observer also behaves robustly against the model uncertainty [156].

### **Adaptive Filter Algorithms**

The adaptive filter algorithms estimate the needed state  $x_{k+1}$  based on the observations  $y_{0:k+1} = [y_1, y_2 \dots y_k]$  under the rule of minimizing mean squared error between observation and estimated output. The current state  $x_{k+1}$  recursively updates through predicted value of the previous state  $x_k$  and current value of the measured input  $u_{k+1}$ . Hence, adaptive filters considered states of systems as the dynamic variable which recursively updates and its evolution is governed by dynamic equations of the systems perturbed by process noise [49]. The basic idea of the adaptive filter based techniques is to compute the filter gain by recursive computation according to statistical properties [157]. **Kalman Filter (KF)** was the first adaptive filter developed by Rudolf E. Kalman in 1960, to provides the effective method for estimation of the system states with the covariance matrix of the state estimation error [158]. A large number of singular values in state covariance matrix indicates high uncertainty in the estimated state whereas less number singular values indicate more confidence [159]. KF deals with uncertainty in the estimation of internal battery states as the state equations are repeatedly evaluated during system operation. KF is the optimum state estimator which aims at linear Gaussian systems [160]. KF accuracy reduces or might suffer from divergence problem when it comes to strong nonlinear system and noise is non-Gaussian. The battery is a non-linear dynamic system hence nonlinear variants of KF have been extensively purposed for addressing the issues in the estimation of internal battery states. For instances, Plett et al. [30] introduces **Extended Kalman Filter (EKF)** to estimate internal states of battery using different battery models [53].

TABLE 1.6: Comparison of Internal States Estimation Techniques

Method	Benefits	Drawbacks	References
<b>AHM</b>	Easy to implement Less computational burden the current measurement and the efficiency is precise.	Incorrect initial SOC value results in cumulative error Accuracy effected with the presence of uncertain disturbances Demands high precision of current sensors.	[99, 174–176]
<b>OCV</b>	Convenient implementation More accurate Algorithm not required for implementation	Long resting period required to settle at operating equilibrium. Applicable for standing mode of the vehicle	[?, 64, 103, 117, 177]
<b>Resistance</b>	Simple and easy	SOC estimation accuracy is high only during the end period of discharge process Variation of resistance is high compared to SOC	[63, 120, 121]
<b>EIS</b>	Online implementation, Relatively cheap Better accuracy is realizable by normalizing impedance	To analyse aging and temperature effect demands large number of experimentation	[83, 125–127]
<b>ANN</b>	Battery model not required Effectively work for non-linear condition	Demand high quantity and quality of training data Uncertainty in measurement results in inaccuracy	[92, 131–134, 137, 138, 178]
<b>FL</b>	Effectively work for non-linear dynamic system	Demand large memory and efficient processing unit High computational burden	[130, 135, 136, 139]
<b>SVM</b>	Well-suited for non-linear and high dimension models	High computation burden. Time consuming trail and error procedure required to adjust model parameters	[140–142, 179–181]
<b>SMO</b>	Improved tracking control enables stable operation	Switching gain adjustment is complex	[148, 152–154]
<b>PIO</b>	Computationally powerful Robust to external perturbations	Improper designed controller results inaccurate results	[147, 155, 156]



Method	Benefits	Drawbacks	References
<b>KF</b>	Precise state estimation in uncertainties (such as Gaussian noise)	Not implemented for state estimation of non-linear system Demand complex mathematical calculation Divergence occurs due to inaccurate model	[49, 101, 157, 157, 159, 160]
<b>EKF</b>	Accurately estimates states for non-linear dynamic system.	Linearization of non-linear system results in divergence Calculation of Jacobian matrix is required	[90, 102, 162–164, 182]
<b>UKF</b>	Precise state estimation upto non-linear dynamic systems of $3^{rd}$ order. Calculation of Jacobian matrix not required	Lacks robustness to uncertainties.	[142, 165–168]
<b>CDKF</b>	Calculation of Jacobian matrix not required Improved robustness and accuracy	Heavy calculation	[183–185]
<b>PF</b>	Efficiently work with non-linear, Gaussian and non-Gaussian systems Fast Accurate.	Solution requires implementation of complex mathematical algorithms.	[169–173, 186]

EKF utilizes Taylor's series linearization process to approximate the non-linear system with Linear Time-Varying (LTV) system [161]. Taylor's series is approximated to first or second order term is depending upon computation time and accuracy required by battery management system designers [102]. Ignoring the higher order of Taylor series expansion influence estimation error and requirement of solving Jacobian matrix for second order results in instability of the filter [162]. This local linearization process results in degradation in the accuracy of estimation methods [163]. Thus, EKF based estimation results in moderate improvement as compared to commonly used KF [164]. To overcome this local linearization and high computational problem, Sigma-Point Kalman filters (SPKF) has developed. SPKF approximates statistical distribution characteristics of the nonlinear system by Gaussian Random Variables (GRV) [165]. Theoretically, SPKF captures higher order moments of distribution rather than linearization. The two common types of SPKF are the Unscented Kalman filter (UKF) and the Central Difference Kalman filter (CDKF). UKF utilizes the unscented transformation, and CDKF utilizes Sterling's polynomial interpolation methods for computing the approximate means and covariance for the states of the system [165]. The attractive feature of the SPKF is that there is no need for complex calculation of a Jacobian matrix [166]. As well SPKF predicts non-linear system states up to third order which increases its accuracy compare to EKF [167]. However, SPKF doesn't provide the true global approximation of the system because of the small set of trial points and demand more computation power due to the evaluation of Cholesky factorization on every step [168]. The main disadvantage associated with SPKF is that noise in systems is assumed to be Gaussian [142]. However, this assumption may not be true in real battery application. This assumption can lead to exacerbation of filters convergence [169]. In order to improve prediction accuracy, PF has been developed for estimation of internal battery states [170]. PF approximates the non-linear system's probability density function by applying based on the Bayesian techniques with the Monte Carlo simulation method [171]. PF uses a weighted set of samples (particles) for approximating the filtering distribution [172]. PF accurately estimate the states of the nonlinear system with Gaussian as well as non-Gaussian noise [173].

### 1.2.6 Power Management Strategies

The power management system defines efficient control schemes to increase the performance of the EVs at a lower cost by targeting multiple objectives simultaneously. The

power management has described as a set of rules or an algorithm regulating the operation of the EV based on measured input to achieve the predefined goals and the controlled outputs. The primary goals of the power management system include managing the power-sharing among the available power sources while satisfying the power demanded by drive-train of EVs. The power-sharing strategy can be determined either by the set of predefined rules or by optimization based algorithms. Hence, so far, power management strategies can be categorized as a rule-based and optimization-based approach for dealing with power management problem as shown in Figure. This section outlines the state-of-the-art for power management strategy in the various kinds of EVs and explains their advantages and disadvantages [187–193].

**Optimization-based approaches** mainly formulate power management as an optimization problem within feasible constraints. This method regulates the control variables based on the objective function that is minimizing the power consumption over the fixed driving cycle [194]. The optimization-based approaches further classified into global optimization and real-time optimization approach. Various global optimization-based approaches have been adopted to solve the power management problem as linear programming [195], quadratic programming [196], dynamic programming [197], mixed integer programming [198] and meta-heuristic optimization techniques [199]. Especially, dynamic programming based on the optimal control theory generates the most effective solutions while dealing with power management problem. However, global optimization techniques require prior and future knowledge about the overall driving power demand for the given driving cycle [197]. These approaches demands too much computational effort compared with rule-based approaches. Therefore, global optimization cannot be applied to real-time control due to its non-causal nature and heavy computational burden [187]. Moreover, global optimization approaches usually serve as good theoretical benchmarks and useful to tune design parameters for online control strategies [188]. Real-time optimization approach defines instantaneous objective function instead of global objective function. Instantaneous objective function depends only upon the current system parameters and should include equivalent power consumption. Hence, the obtained solution are not globally optimal but it can be implemented in real-time. Real-time optimization approaches are simple to implement with limited memory resources and computational cost. Real-time optimization approach can be categories as the equivalent consumption minimization strategy (ECMS) and model predictive control (MPC) [190]. ECMS is to formulate global optimization into local optimization problem by minimizing equivalent fuel consumption. The equivalent factor is proposed to convert electric energy to equivalent fuel energy [200]. The equivalence factor of ECMS is not known in advance hence, it is calculated based

on average of power flow for given driving cycle. The equivalence factor influences the performance power management system as proper estimation of equivalent factor depends on battery SOC, driving cycle and direction of current [200]. This approach finds near-optimal solution but it suffers from high sensitivity to statistical parameters hence the approach requires fine tuning of parameters for driving cycle separately. MPC deal with multivariate constrained control problems [189]. MPC is an optimization-based receding horizon control strategy, which has the potential to maintain the computational burden within an acceptable range and increase its adaptability for various driving cycles [191]. MPC is neither sensitive nor short-sighted due to its capability of solving optimization problem over the future prediction horizon [193]. However, knowledge about future driving cycle is required in advance by driving prediction methods [192]. Even MPC utilize the solution method of dynamic programming to find the optimal solution which provides sub-optimal solution.

TABLE 1.7: Comparative study of different energy management schemes.

Scheme type	Pros	Cons
Deterministic rule-based	Simple implementation; Computationally efficient	Intensive parameter calibration and tuning is needed; Optimal solution is not assured; Non-portability.
Fuzzy rule-based	Robust to noise in measurements; Requires less computations; Simple execution.	Optimal solution is not assured; Adjusting membership function and fuzzy rule is necessary; Non-portability.
Real-time optimization	Compatible for HEVs; Sub-optimal solutions are feasible.	Global optima unachievable; Complex integration in contemporary vehicle control.
Global optimization	Optimal solution attainable; Calibration not needed.	Advanced information of driving cycles is required; Complex computation; Direct integration not feasible.

**Rule-based approaches** is heuristic approaches which effectively control the flow of power between energy sources by defining a set of rules [201]. These rules are formulated based on human expertise, foreknowledge, operational limits and safety boundaries [202]. The main advantages of rule-based approaches are low computation requirement. The rule-based approaches are the most direct and widely used approaches due to its easy implementation, high computation efficiency and does not requires knowledge about the future driving cycle. Recently these approaches are used in Toyota Prius and Honda Insight [203]. The rule-based approach further classified into deterministic and fuzzy rule-based algorithms. A deterministic rule-based power management strategy formulated in term of

fixed rules defined using prior knowledge about the overall driving power demand [196]. Consequently, driving cycle prediction and recognition introduced to determine the driving power demand [204]. The deterministic rule-based method implemented based on state machine control logic, which has been composed by the number of states, transition and transition condition. The states define possible driving situations, i.e., operation modes and each state are connected to other by the transition. The transition condition depends on battery SOC, request torque and pedal angle. Due to fixed rules, deterministic rule-based approach lacks the flexibility to different driving cycles and ability to deal with uncertainty caused by the model error of drivetrain. Fuzzy-logic rule-based power management approach formulates a collection of fuzzy rules based on expert knowledge and reasoning [205]. These fuzzy rules offer a qualitative description of the controlled system but depend on long development duration. Utilizing the fuzzy logic rule-based approach removes the dependency of the control system on the precise mathematical model [206]. The main advantages of fuzzy logic rule-based approach are adaption as well as robustness to measurement noise and component variability [207]. Fuzzy-logic rule-based approach is suitable for the nonlinear, multi-domain and time-varying system [208]. However, it difficult to appropriately derive membership function and fuzzy rules when power control depends on more variables [209]. Based on the above analysis, rule-based approaches depends on employed rules which are difficult to define due to lacks any rigorous mathematical analysis and theoretical basis. Furthermore, any optimization or minimization is not involved, hence, the optimal solution cannot be guaranteed.

### 1.3 Research gaps

This research work mainly focuses on developing a battery monitoring system for effective battery management while driving. The primary function of the battery management system is to monitor and regulate the internal battery states for developing power management system of the dual battery-powered EVs. From the review of related research work, it could be concluded that the prerequisite for estimation of internal battery states is to build a battery model that could reflect the dynamic behavior of the battery. Throughout the years, the researchers have developed numerous types of battery models with different level of accuracy and complexity to predict the behavior of the Li-ion battery. Electrochemical battery models were based on electrochemical methodologies involving current densities at the electrodes, electrolyte concentration parameters and many other electro-chemistry parameters implementation for battery modeling. All the electrochemical mechanism inside the battery is represented by a spatial partial differential equation.

These equations require large computational power to solve them. Moreover, the data-driven battery model train the sample dataset to approximate electrochemical model. Data-driven models demands large amount of data analysis and more significant dataset for training and testing of the battery model. Hence, accuracy of these models relies on the quality training datasets. Equivalent circuit-based methods replace the chemical reaction by circuit components. Equivalent circuit based battery model has gained a lot of interest amongst battery management system designers for parameter estimation purpose because of it's simplified mathematical and numerical approach that minimizes the necessity for the computationally intensive procedure. Hence in this research work, a tradeoff is made over actual behavior and complexity in computations. The approach to be considered in this work shall be combined equivalent circuit based battery model which can model transient, DC response and runtime behavior of the battery model. Developing an accurate battery model requires the precise value of the parameters of battery model circuit components. The values of circuit components vary rapidly over the runtime of the battery and depend upon many operating conditions such as SOC, C-rate, temperature, number of cycle and hysteresis effect. However, various empirical non-linear equations utilized to describe the behavior of the battery in the literature were different. The authors have modeled components with a combination of exponential functions and  $2^{nd}$  to  $6^{th}$  order polynomial functions. Also, some authors have considered the influence of stress factors, such as hysteresis effect and temperature. Consequently, depending on which effect of the stress factor has to be taken into account, accuracy, and complexity of the model, empirical non-linear equations are obtained from measurements data. For battery parameter identification, a set of EIS or charge-discharge tests were performed and then error minimization algorithms were applied to fit with the measured data with tests results. In other words, these parameters are identified using curve fitting on the data collected using experimentation on hardware. These experimentations are time-consuming and require substantial financial investment. The focus of this work will be to develop a battery model based on data provided by manufactures without performing the expensive experiment. This battery model shall represent not only the static also the dynamic behavior of the battery. Model-based estimation methods such as variants of KF [210], and neural network-based methods analyze voltage responses in the time domain for varying operating conditions. Variants of KF require less computation power, but these methods assume model equation to be linear or slightly non-linear whereas battery parameter estimation problem is a high dimensional non-linear problem. Neural network based methods require a large amount of training data and high computational power to estimate model parameters accurately. Various tests have to be performed under different operating conditions

in a laboratory to obtain voltage responses for modeling battery using these methods. The battery parameter modeling is a high dimensional non-linear problem which requires intensive computation overhead for the solution using conventional methods. To avoid time-consuming experimentation which requires substantial financial investment, parameter estimation is formulated as an optimization problem to identify parameters of the battery using voltage characteristic data provided by manufactures. According to No Free Lunch (NFL) theorem [211], a single optimization approach could not be considered suitable for solving all optimization problems hence comparison is performed for six heuristic techniques for estimation of battery parameters. With the development of an accurate battery model with identified parameters battery management system demands to estimates the battery internal states for safe operation of battery. The review mentioned in Section 1.2.5 investigates the various estimation methods of internal states of the battery. The review identifies that internal battery states can be estimated by utilizing conventional, data-driven and model-based methods. The conventional methods are easy to implement, however, they are highly affected by external distributions. Data-driven methods perform well with non-linear and high dimensional models with an ability to predict the internal states accurately by using well computed training data for all possible operating condition. Generation of large amount of data is the main drawback of data-driven methods which demands large memory and complex computation. The nonlinear observer has enhanced robustness against the disturbances and improved performance in terms of accuracy, converge speed and computation cost. Nevertheless, the model could deliver inaccurate results if the controller is not properly designed. Adaptive filters are the most favored techniques since they can predict non-linear dynamics states with good precision, high efficiency and less computational cost. As battery model is developed to represent the dynamic behavior of the battery, hence, model-based adaptive filters are recognized as appropriate battery internal states estimation methods. Different variants of adaptive filters are utilized for estimation of battery internal states. In this research work, performance of different kinds of adaptive filters are compared for estimation of battery internal states.

In [14] author suggested the concept of dual-battery powered EVs which improves energy consumption and cost compared with EV with single battery pack. Utilization of dual battery demands power management between them for optimal power supply to the EVs. In the literature, various power management strategies have been developed for hybrid EVs. On the basis of thorough analysis of different power management strategies, it could be concluded that rule-based power management approach has been commercially adopted due to its east implementation and high computational efficiency. However, as any optimization is not involved, the optimal solution cannot be obtained. Optimization-based

approaches overcome inherent drawbacks of rule-based approach through the implementation of optimization control procedure. Optimization-based approaches demand high computation power for real-time application. Practically, the hybrid power management strategy should be developed which would not only have the optimal solution but also readily applicable to real-time control. All power management strategies were analysed for Hybrid EVs only, hence, it is required to develop a power management system for dual battery-powered EVs.

## 1.4 Research Objectives

Battery management system is a very exhaustive field with many research topics, so scope must be defined to limit the topics in the thesis. The research aim about this thesis work is to design and validate a novel battery management system for condition monitoring and power management system for Li-ion batteries to extend the lifetime, enhance the reliability, and optimize the performance of battery systems. For developing the battery management system and power management system following step by step, objectives have been formulated:

1. To develop high-fidelity battery model for online condition monitoring and power management of Li-ion battery by accurate measurements of model parameters.
2. To analyze model-based online condition monitoring algorithms for estimating of internal states of Li-ion batteries.
3. Modeling a dual battery powered EV and its power management by controlled DC/DC converter switching

## 1.5 Organization of the thesis

As mentioned in the earlier section, the prime focus of the thesis is to implement a battery management system which includes the development of battery monitoring and power management system. Figure 1.10 illustrates the flow of the thesis in the form of a block diagram highlighting the significant portions covered in each chapter. The thesis has been organized as follows:



**Chapter 1** The literature necessary to develop an insight of the topic, a brief outline of the development of battery technologies and battery monitoring system has been given. This chapter reviews the state-of-the-art and provides the reader with a background of the battery management system, battery modeling and various techniques that are responsible for the estimation of battery model parameters and internal states. Finally, different power management strategies have been discussed in details.

**Chapter 2** The primary objective of this research work is to develop a method which can determine the critical parameters of the battery from the manufacture catalogue data without conducting expensive and time-consuming experiments. The parameter estimation is considered as an optimization problem and solution is obtained by utilization of six different heuristic techniques. As a single optimization approach could not be regarded as suitable for solving all optimization problems, hence comparison is performed for six heuristic techniques for estimation of battery parameters. The efficacy of the proposed method has been validated by comparing the obtained results with battery parameters derived from standard Pulse-Current Charge-Discharge Test (PCDT). As well as the performance of all heuristic optimization approaches has been examined by the quality of the solution, the rate of convergence, computational error and statistical significance.

**Chapter 3** This chapter presents a state estimator that can reflect the internal states of the battery. Firstly battery SOC is estimated based on the state-space model from the battery model developed in Chapter 2. Model-based estimation methods have been compared regarding their robustness, accuracy and execution time. Then, the change in battery capacity under specific working conditions is related to the battery SOH. To determine the general model for capacity degradation empirical equations based models are developed by using curve fitting techniques. With the help of empirical capacity degradation model, the complexity of model tuning can be reduced notably. Finally, the information about battery current SOH and RUL has been determined by using different model-based estimation technique and the effectiveness of each method in estimation is analyzed.

**Chapter 4** This chapter presents the introduction to the proposed rule-based meta-heuristic power management system for dual battery-powered EVs. The power management problem includes the real-time optimal power-sharing between two batteries promoting the maximization of usage of batteries capacity while maintaining SOC of batteries at adequate levels. Starting from a brief description of the modeling approach adopted for computation of demanded power for a given driving cycle. Detailed description of the developed architecture for power management with defined problem formation is presented

in this chapter. The validation of the proposed power management system has been done for normalized ECE 15 driving cycle depending on different initial SOC conditions.

Finally, **Chapter 5** summaries the contributions of this thesis and highlights potential future research opportunities.

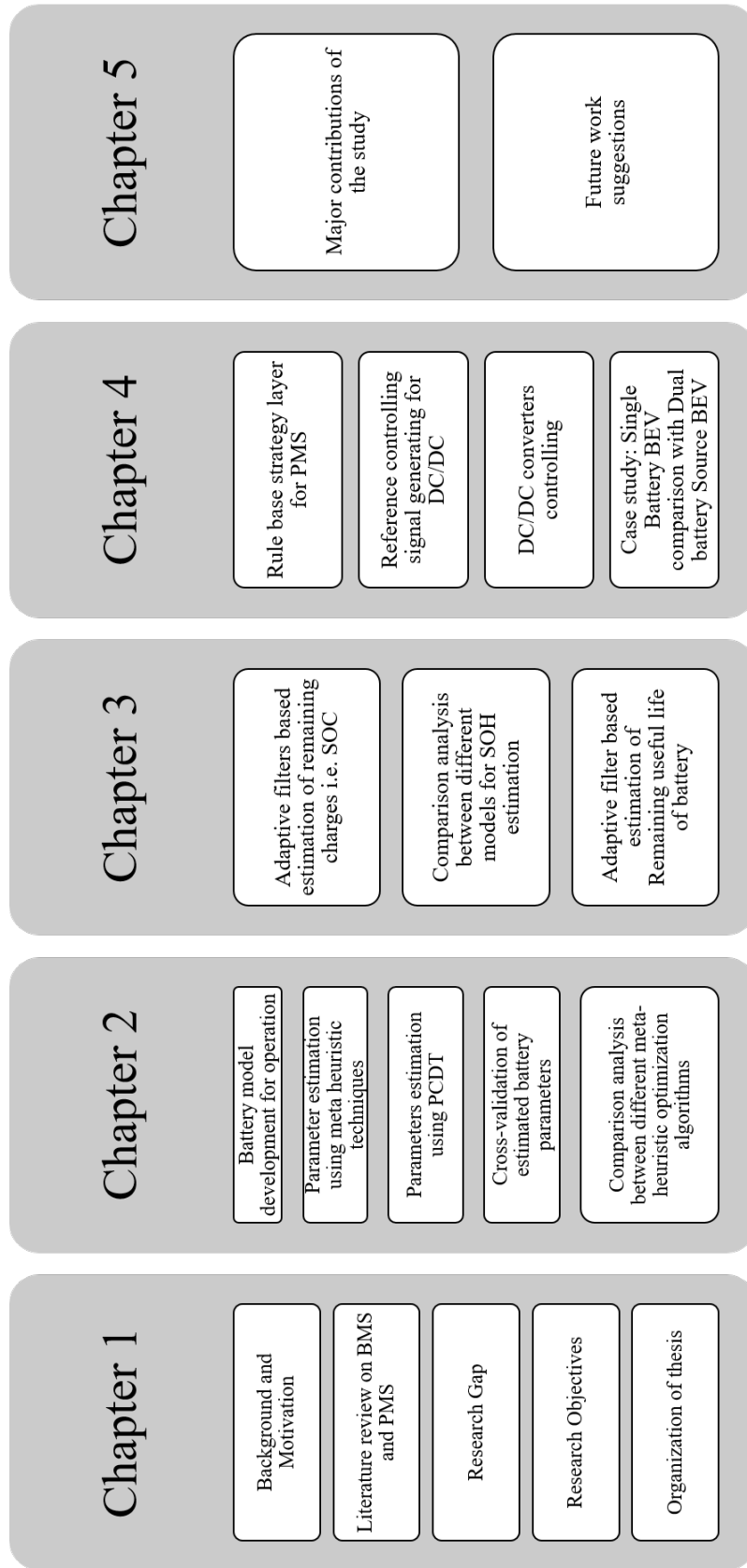


FIGURE 1.10: Block diagram of thesis organization



## Chapter 2

# Modeling and Parameter Estimation of Battery

### 2.1 Introduction

The battery management system requires an accurate model of the battery for estimation of its internal states such as State-of-Charge (SOC) and State-of-Health (SOH) in EVs. Developing a battery model requires the accurate values of the parameters of the battery. Since the parameters change with the variation in temperature, SOC and C-rate, it is necessary to analyze the effect of parameter change on battery model [212]. Especially in the applications of EVs, the change in parameters will be more significant than other applications because the C-rate and temperature changes are relatively higher [37]. The primary purpose of this chapter is to introduce a simple and efficient methodology for accurate battery modeling and the identification of the parameters of the battery. The combined equivalent circuit model incorporates the benefits of Thevenin-based, impedance-based and runtime-based model. Hence, it has been utilized to mimic the dynamic behavior of battery during various operating conditions. Voltage response circuit part of combined equivalent circuit is composed similarly to the Thevenin battery model which contain various active and passive circuit elements to represent the electrochemical process taking place inside the battery. Detailed modeling of voltage response circuit considering the dependency of the battery on SOC, C-rate and temperature have been discussed in the Section 2.2. Dependency of model circuit elements has been described with a combination of exponential functions and  $2^{nd}$  to  $6^{th}$  order polynomial functions [213, 214]. In the literature [89–91], parameters of the equations are identified using curve fitting on the data collected using

experimentation on hardware. These experiments are time-consuming and require substantial financial investment. The proposed method is an alternative way to identify the parameters of the battery using voltage characteristic data provided by the manufactures. The proposed parameter identification approach has been formulated as an optimization problem which has been discussed in detail in the Section 2.3. This optimization problem is a high-dimensional and non-linear problem which requires a intensive computation overhead for the solution using conventional methods. According to No Free Lunch (NFL) theorem [211], a single optimization approach could not be considered suitable for solving all optimization problems. Hence, the performance of six heuristic techniques for estimation of battery parameters has been compared under similar execution conditions. Out of these six heuristic techniques, Genetic Algorithm (GA) and Particle Swarm Optimization (PSO) are time-tested techniques for optimization problems while Different Evolution (DE), Teaching Learning Based Optimization (TLBO), Grey Wolf Optimization (GWO) and Ageist Spider Monkey Optimization (ASMO) are state-of-the-art algorithms. An overview of heuristic optimization algorithms utilized for the purpose of identification of parameters has been discussed in Section 2.4. Following this, simulation results using the proposed method for parameters estimation have been discussed in detail in the Section 2.5. The efficacy of the proposed method has been validated by comparing the obtained results with battery parameters derived from standard Pulse-Current Charge-Discharge Test (PCDT). Further, the performance of all heuristic optimization approaches have been examined by the quality of the solution, the rate of convergence, computational error and statistical significance using both parametric (*t-test*) and non-parametric tests (Wilcoxon test) in the Section 2.5.3. Finally, the concluding remarks on the work carried out in this chapter have been summarized in the Section 2.6.

## 2.2 Equivalent circuit model of Li-ion batteries

Equivalent circuit based battery model conceptualizes the electrochemical mechanism of the battery using the SOC dependent voltage source, resistors, capacitor and non-linear components like Warburg impedance and diodes to approximate the dynamics of the battery. A combined equivalent circuit model incorporates the energy balance circuit and voltage response circuit as shown in Figure 1.7 for representing the dynamic behaviour of the battery. The voltage response circuit represents the transient dynamics of the battery. It is similar to Thevenin-based battery model as shown in Figure 2.1. It consists of a voltage source  $V_{oc}$  which denotes the Open Circuit Voltage (OCV), ohmic resistance  $R_0$ , electrochemical diffusion process resistance and capacitance represented by  $R_n$  and  $C_n$

respectively. Energy balance circuit models battery runtime and DC response by utilizing capacitor  $C_{use}$ , resistance  $R_{dis}$  and current-controlled current source  $I_{BL}$ . The values of circuit components vary over a large range during the runtime time of the battery. These values depend upon many operating conditions such as SOC, C-rate (capacity normalized current), temperature, number of cycles and hysteresis effect.

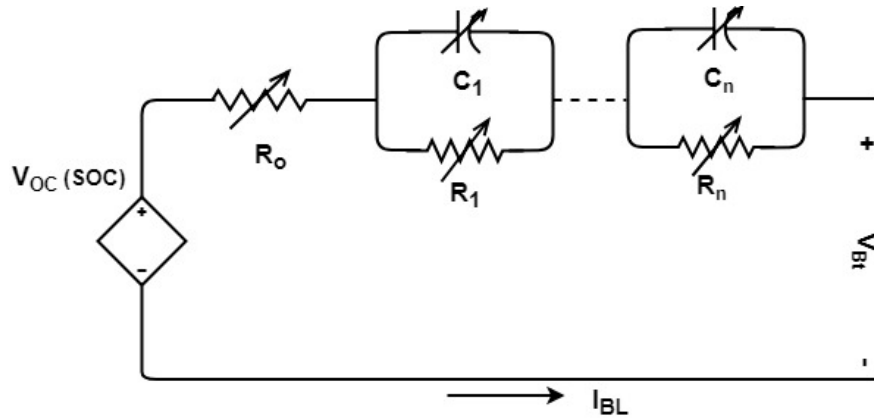


FIGURE 2.1: Voltage response part of the combined equivalent circuit based battery model with 1 RC network

Practical equivalent circuit modeling demands that the components of the voltage response circuit part should be related with the electrochemical process in the battery. In [66], the authors suggested that the relationship between the battery model parameters and the electrochemical process can be obtained by comparing given battery model with the impedance-based model. Internal impedance calculated using Electrochemical Impedance Spectroscopy (EIS) measurements were used to form  $2^{nd}$  order Randles circuit as shown in Figure 1.4. Here, bulk resistance represented by  $R_{bk}$  denotes the electric conductivity of the separator, electrodes, and the electrolyte. Surface film layer electrode resistance and capacitance are represented by  $R_{sei}$  and  $C_{sei}$  respectively. Charge transfer resistance is represented by  $R_{ct}$ , double layer capacitance is represented by  $C_{dl}$  and diffusion process of the battery is represented by Warburg impedance  $Z_W$ . In real-time EV application, the sampling rate of data acquisition should be at least 1 Hz, since most of the existing driving cycle also have 1 Hz speed-time signals [215]. However, the energy consumption of a EV is evaluated at high sampling rates (1 Hz-10 Hz) to achieve more accurate and reliable characterization of EV efficiency [216] as dynamics of the battery of the vehicles can be evaluated more accurately at the high sampling rate [66]. Hence, this sampling rate of the data acquisition system causes high frequency  $R_{sei}$  and  $C_{sei}$  indistinguishable from  $R_{bk}$ . In the voltage response circuit  $R_{bk}$  is represented by  $R_0$  [217]. Additionally,

the  $Z_W$  is approximated by the  $n$  number of parallel resistor-capacitor network where  $n$  defines the order of voltage response circuit.

Equivalent circuit based battery model has gained a lot of interest amongst battery management system designers for parameter estimation purpose because of its simplified mathematical and numerical approach that minimizes the necessity for the computationally intensive procedure. It gives a good trade-off between exactness, complexity, and usability depending upon different RC networks used for voltage response circuit part of the battery model. In the research literature, different forms of Thevenin's equivalent circuit based battery model depending on the number of RC pairs, the effect of hysteresis and impact of aging, have been developed by researchers [56, 68]. In [218], the author compared complexity versus modeling error for the Thevenin RC network circuit models, by varying the number of RC pairs and concluded that increasing the number of RC pairs decreases the error and increases the computation time. In [39, 68], the authors utilized multi-objective particle swarm optimization to compare the practicality of different equivalent circuit based model incorporating model accuracy and complexity. The comparison between different equivalent circuit based models concluded that the first-order RC model is most suitable for a Li-ion battery. The addition of more RC networks generally improves the model accuracy but increases the computational burden. Hence, the first-order RC model has been utilized for identification of battery model parameters.

The empirical non-linear equations utilized to describe the transient behavior of the battery were not alike. The researchers have modeled components with a combination of exponential functions and  $2^{nd}$  to  $6^{th}$  order polynomial functions [213, 214]. Some researchers also considered the influence of stress factors, such as hysteresis effect and temperature. Consequently, depending on effect of the stress factor, the accuracy, and complexity of the model change. Equivalent circuit model of a Li-ion battery is presented in [72, 219], consisting of empirical non-linear equations extracted from measurement data obtained from experimental analysis. The first-order RC model parameters which are dependent on state-of-charge, C-rate, and temperature are formulated using a polynomial equation as given in equations (2.1)-(2.4), to exhibit the dynamic electrical performance of the battery [66, 72].

$$R_0 = ((a_1 + a_2x + a_3x^2)e^{a_4y} + (a_5 + a_6x + a_7x^2))e^{a_{32}(\frac{1}{T_o} - \frac{1}{T_r})} \quad (2.1)$$

$$R_1 = ((a_8 + a_9x + a_{10}x^2)e^{a_{11}y} + (a_{12} + a_{13}x + a_{14}x^2))e^{a_{33}(\frac{1}{T_o} - \frac{1}{T_r})} \quad (2.2)$$

$$C_1 = -((a_{15} + a_{16}x + a_{17}x^2)e^{a_{18}y} + (a_{19} + a_{20}x + a_{21}x^2))e^{a_{34}(\frac{1}{T_o} - \frac{1}{T_r})} \quad (2.3)$$

$$V_{oc} = (a_{22} + a_{23}x + a_{24}x^2)e^{a_{25}y} + (a_{26} + a_{27} + a_{28}y^2 + a_{29}y^3) - a_{30}x + a_{31}x^2 \quad (2.4)$$



Here,  $a_1, a_2 \dots a_{34}$  represent the polynomial coefficients to be determined;  $T_0$  and  $T_r$  denote the instantaneous and reference temperature of the battery respectively. The transient behavior of the battery is different for charging and discharging process. Hence, for the charging process,  $x$  (C-rate) and  $y$  (current charge state in battery) are substituted by charging current rate  $C_r$  and  $SOC$  and for discharging process by discharge current rate  $D_r$  and  $1 - DOD$  respectively.  $DOD$  represents depth of discharge which decreases with increase in model terminal voltage  $V_{Bt}^M$ . The C-rate for charging process ( $C_r$ ) and discharging process ( $D_r$ ) can be expressed as [104]:

$$C_r = \frac{I_{BL,c}}{Q_{nom}}; \quad D_r = \frac{I_{BL,d}}{Q_{nom}}; \quad (2.5)$$

Here,  $Q_{nom}$  is the nominal battery capacity provided by the manufacturer;  $I_{BL,c}$  is current flowing through battery terminals during charging process and  $I_{BL,d}$  is current flowing through battery terminals during discharging process.

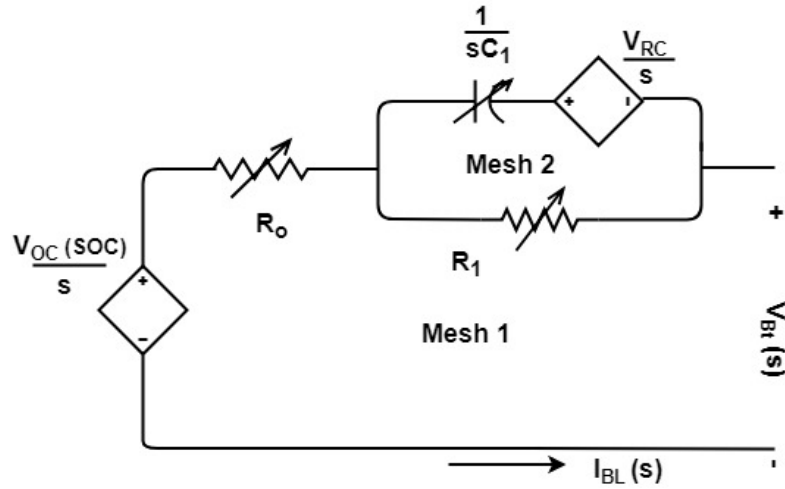


FIGURE 2.2: Battery Model with 1 RC network represented in s-domain

The equation for terminal voltage is derived using Laplace transform of the voltage response circuit. Figure 1.7 illustrates the s-domain representation of the voltage response circuit part of the battery model. Using Krichhoff's law, the dynamics of the circuit can be expressed as follows:

In the mesh 1:

$$-V_{Bt}^M(s) + \frac{V_{oc}}{s} - I_{BL}(s)R_0 - [I_{BL}(s) - I_{RC}(s)]R_1 = 0 \quad (2.6)$$

$$-V_{Bt}^M(s) + \frac{V_{oc}}{s} - I_{BL}(s)[R_0 + R_1] + I_{RC}(s)R_1 = 0$$

$$I_{RC}(s) = \frac{V_{Bt}^M(s)}{R_1} - \frac{V_{oc}}{R_1 s} + I_{BL}(s) \left[ \frac{R_0}{R_1} + 1 \right] \quad (2.7)$$

In the mesh 2:

$$-V_{Bt}^M(s) + \frac{V_{oc}}{s} - I_{BL}(s)R_0 - \frac{I_{RC}(s)}{C_1 s} - \frac{V_{RC}}{s} = 0 \quad (2.8)$$

substituting value of  $I_{RC}$

$$-V_{Bt}^M(s) + \frac{V_{oc}}{s} - I_{BL}(s)R_0 - \frac{V_{Bt}^M(s)}{R_1 C_1 s} + \frac{V_{oc}}{R_1 C_1 s^2} - \frac{I_{BL}(s)}{C_1 s} \left[ \frac{R_0}{R_1} + 1 \right] - \frac{V_{RC}}{s} = 0 \quad (2.9)$$

$$V_{Bt}^M(s) = \frac{V_{oc}}{s} - V_{RC} \left[ \frac{R_1 C_1}{1 + R_1 C_1 s} \right] - I_{BL}(s) \left[ R_0 + \frac{R_1}{1 + R_1 C_1 s} \right]$$

$$V_{Bt}^M(s) = \frac{V_{oc}}{s} - V_{RC} \left[ \frac{1}{s + \frac{1}{R_1 C_1}} \right] - I_{BL}(s) \left[ R_0 + \frac{1}{C_1} \left( \frac{1}{s + \frac{1}{R_1 C_1}} \right) \right]$$

using inverse Laplace transform:

$$V_{Bt}^M(t) = V_{oc} - V_{RC} e^{-\frac{t}{R_1 C_1}} - I_{BL}(t)R_0 - \frac{1}{C_1} \int_{\zeta=0}^{\zeta=t} I_{\zeta} e^{-\frac{(t-\zeta)}{R_1 C_1}} d\zeta \quad (2.10)$$

$$V_{Bt}^M(t) = V_{oc} - V_{RC} e^{-\frac{t}{R_1 C_1}} - I_{BL}R_0 - \frac{I_{BL}}{C_1} \left[ R_1 C_1 e^{-\frac{(t-\zeta)}{R_1 C_1}} \right]_{\zeta=0}^{\zeta=t} \quad (2.11)$$

$$V_{Bt}^M(t) = V_{oc} - V_{RC} e^{-\frac{t}{R_1 C_1}} - I_{BL}R_0 - I_{BL}R_1 \left[ 1 - e^{-\frac{t}{R_1 C_1}} \right] \quad (2.12)$$

For the constant current in the circuit, initial value of voltage across capacitor is represented by  $V_{RC} = \frac{Q(0)}{C_1}$  where  $Q(0)$  is the initial charge across the capacitor.

$$V_{Bt}^M(t) = V_{oc} - \frac{Q(0)}{C_1} e^{-\frac{t}{R_1 C_1}} - I_{BL}R_0 - I_{BL}R_1 \left[ 1 - e^{-\frac{t}{R_1 C_1}} \right] \quad (2.13)$$

Time-dependent nonlinear relation of the output terminal voltage  $V_{BL}^M$  for the constant current condition can be determined using equations (2.1)-(2.4). Output terminal voltage is obtained by rearranging equation (2.13) and it follows a polynomial equation as: [48] :

$$V_{Bt}^M = \left( \frac{Q(0)}{C_1} + I_{BL}R_1 \right) e^{-t/R_1 C_1} + V_{oc} - I_{BL}(R_0 + R_1) \quad (2.14)$$

Here  $t$  is sample time interval;  $I_{BL}$  is charging (-ve)/discharging(+ve) current.

The modeling of a battery is an offline problem. An accurate model mimics the behavior of the battery under different operating conditions. Once a model has been estimated, it is deployed in battery management system for online estimation of the states of the battery. With the help of empirical equation discussed in this section, battery model with describes the transient behavior of the battery at different SOC, C-rate and temperature values. However, to utilize this model for further estimation of battery internal states it is required to identify the parameter values of the empirical equation. The objective of parameter identification is achieved by minimizing the error between expected catalog voltage and the evaluated voltage from battery model at the different operating condition.

### 2.3 Objective function for optimization process

For battery modeling, one of the key challenges is to identify model parameters accurately. Battery parameters can be identified by experimentation on hardware-setup and analysis either in the frequency domain or in time domain [220]. The EIS testing method is performed by applying a small amplitude ac current of varying frequency to the battery and calculating impedance using voltage response [83]. The parameters of the battery are identified by impedance analysis in the frequency domain. Similarly, battery model parameters are identified using curve fitting on the data collected using experimentation on hardware using standard PCDT. These approaches are expensive and requires specialized electronic equipment to perform the experiment. The requirement of expertise and high computing power hinders the applicability of the approach [83]. Model-based estimation methods such as variants of Kalman filters [210], and neural network-based methods analyze voltage responses in the time domain for varying operating conditions. Variants of Kalman filters require less computation power, but these methods assume model equation to be linear (or slightly non-linear); whereas battery parameter estimation problem is a high dimensional non-linear problem. Neural network based methods require a large amount of training data and high computational power to properly estimate model parameters. Various tests have to be performed under various operating conditions in a laboratory to obtain voltage responses for modeling battery using these methods. To avoid time-consuming experimentation which requires substantial financial investment, parameter estimation is formulated as an optimization problem to identify parameters of battery using voltage characteristic data provided by manufactures. The battery parameter modeling is a high dimensional non-linear problem which require intensive computation overhead for solution using conventional methods. According to NFL theorem [211], a single optimization approach could not be considered suitable for solving all optimization problems, hence, the performance

comparison for six heuristic techniques has been examined. The motivation behind adopting mathematical optimization is to determine the coefficients of the polynomial equation that are used to describe the parameters of the first order RC model given in equations ((2.1)-(2.4)). The objective function evaluation was done in terms of minimizing the difference between the expected catalog voltage and the evaluated voltage curve at various temperatures. Thus this objective function was expressed as the Manhattan Euclidean distance between value of the output voltage obtained from described battery model and the voltage values given by the manufacturer at each sampling interval for both charging and discharging process. The objective function can be mathematically expressed as:

$$\min F(x) = \sum_{i=1}^n |V_{Bt,i}^M - V_{Bt,i}^C| \quad (2.15)$$

Here  $V_{Bt,i}^C$  denotes the catalog value given by the manufacturer and  $V_{Bt,i}^M$  denotes the output voltage value obtained from battery model at different SOC (or DOD) values.

The detailed description of various optimization algorithms utilized for identification of the optimal values of coefficients of the polynomial equation has been included in the following section. The concise information has been incorporated to familiarize with basics of heuristic algorithms, while the pseudo-codes assists in understanding similarities and differences in their implementation.

## 2.4 Meta-heuristic optimization algorithms for battery modeling

The battery parameter optimization is a high dimensional multimodal optimization problem, and different stochastic optimization algorithms yield different approximations of the optimal solution. Hence, six different meta-heuristic optimization techniques are utilized to determine the optimal values of polynomial coefficients  $a_1, a_2 \dots a_{34}$  for identification of parameters of the battery model. The objective function, described in the previous section, was modeled to incorporate the effect of various temperature levels, SOC and C-rate on the battery modeling. The generalized problem formulation of parameter estimation of the battery and its pseudo code has been added. A suitable meta-heuristic algorithm (2-7) can be incorporated in step 12 of algorithm 1 to update the population.

**Algorithm 1** Pseudocode to estimate battery parameters

- 
- 1: Read the battery data from manufacturer catalog for different temperature.
  - 2: Define the upper bound ( $u_{bd}$ ) and lower bounds ( $l_{bd}$ ) for each parameter coefficient ( $a_d$ ) for  $d = 1, 2, \dots, 34$ .
  - 3: Define Maximum iteration ( $maxiter$ ).
  - 4: Randomly initialize the population, represented by  $P$  solution sets, within the search space defined by upper and lower bounds i.e.  $x_p = [a_{p,1}, a_{p,2} \dots a_{p,34}]$ ,  $p = 1, 2, \dots, P$ . Here  $l_{bd} \leq a_{p,d} \leq u_{bd}$ ,  $d = 1, 2, 3, \dots, 34$ .
  - 5: **for**  $it = 0 : maxiter$  **do**
  - 6:     **for**  $p = 1 : P$  **do**
  - 7:         Calculate  $R_0, R_1, C_1, V_{oc}$  and  $V_{Bt}^M$  using eq. (2.1)-(2.4), for  $p^{th}$  solution ( $x_p$ ).
  - 8:         Calculate fitness  $f_p = F(x = x_p)$  for  $p^{th}$  solution ( $x_p$ ).
  - 9:     **end for**
  - 10:      $f^* = F(x = x^*)$
  - 11:     Update the population  $x_p$  ( $p = 1, 2, \dots, P$ ) using one of the optimizer algorithm: GA(Algorithm 2), PSO(Algorithm 3), DE(Algorithm 4), TLBO(Algorithm 5), GWO(Algorithm 6) or ASMO(Algorithm 7).
  - 12: **end for**
- 

**2.4.1 Genetic Algorithm (GA)**

GA was introduced by Holland et al. in 1988 [221] based on the principle of natural selection and genetics. The process of natural selection starts with the selection of fittest individuals from a population. In GA, a candidate solution to the optimization problem is represented in the form of strings referred as chromosomes. The process is launched by randomly initiating a set of chromosomes across the search space accompanied by creating offspring population using a set of genetic operators such as selection, crossover, and mutation to evaluate the fitness value over successive generations. The method of implementing the algorithm is described in Algorithm 2.

In the algorithm,  $P_s$  is the number of selected optimal population that are retained in the next iteration.  $r_1, r_2, r_c$  and  $r_m$  are random variables between 0 and 1.  $r_c$  and  $r_m$  used for selection of crossover and mutation process. The various parameters affecting the performance of GA were taken as follows: population size ( $P$ ) was taken as 1000,  $P_s$  was taken as 100, crossover rate ( $C_{prob}$ ) as 0.8 and mutation rate ( $M_{prob}$ ) was selected to be 0.2. GA was initially developed to solve combinatorial optimization problems. Although this makes it efficient in solving discrete optimization problems, but not that good for continuous problems. By encoding the chromosomes in binary form and using binary mutation and binary crossover, the GA can be used for discrete optimization problems. For example, in a generation two parent chromosome encoded as: 000000 and 111111 can result in offspring 000111 and 111000 in next generation through crossover after third

**Algorithm 2** Solution update using GA

---

```

1: Selection: Sort the population on the basis of fitness  $F(x_p)$ .
2: Crossover:
3: for  $p = P_s + 1 : P$  do
4:   Select 2 solutions randomly from optimal solutions ( $P_s$ ):  $a, b \in [1, P_s]$ .
5:   for  $d = 1 : D$  do
6:     if  $r_1 < C_{prob}$  then
7:        $x_p[d] = r_c \cdot x_a[d] + (1 - r_c) \cdot x_b[d]$ 
8:     else
9:        $x_p[d] = x_a[d]$ 
10:    end if
11:  end for
12: end for
13: Mutation:
14: for  $p = 1 : P$  do
15:  for  $d = 1 : D$  do
16:    if  $r_2 < M_{prob}$  then
17:       $x_p[d] = l_{bd} + r_m * (u_{bd} - l_{bd})$ 
18:    end if
19:  end for
20: end for

```

---

binary digit. Mutation can be implemented by swapping some of the digits from 0 to 1 and vice-versa.

### 2.4.2 Particle Swarm Optimization (PSO) Algorithm

PSO, introduced by Kennedy et al. in 1995 [222], is a swarm intelligence based method simulating the intelligent movement and information-sharing behavior among the population of different species throughout their food search. The optimization process comprises of a population of particles that operate collectively through velocity and position update influenced by personal best location and group past location to converge towards the optimal solution. The method of implementing the algorithm is described in Algorithm 3.

Here  $v_p$  is the velocity of the  $p^{th}$  solution;  $w$  is an inertia weight factor that linearly decreases from 0.9 to 0.1;  $c_1$  and  $c_2$  are acceleration constants with a value of 2 in this case;  $r_1$  and  $r_2$  are stochastic component of the optimization and are chosen randomly between 0 and 1 in each iteration;  $pb_p$  is the personal best position found by the  $p^{th}$  solution and  $gb$  is the global best position found so far. The population size ( $P$ ) was taken as 40. PSO algorithm is more suitable for continuous optimization problems and is easy to implement, but compared to GA, PSO lacks in solving discrete problems. Use of continuous values of

---

**Algorithm 3** Solution update using PSO

---

```

1: for  $p = 1 : P$  do
2:    $v_p = w.v_p + c_1.r_1.(pb_p - x_p) + c_2.r_2.(gb - x_p)$ 
3:    $x_p = x_p + v_p$ 
4:   if  $F(x_p) < F(pb_p)$  then
5:      $pb_p = x_p$ 
6:   end if
7:   if  $F(x_p) < F(gb)$  then
8:      $gb = x_p$ 
9:   end if
10: end for

```

---

inertia weight factor ( $w$ ) and acceleration constants ( $c_1$  and  $c_2$ ) makes it difficult to use velocity update equation for solution update in discrete optimization problems.

### 2.4.3 Differential Evolution (DE) Algorithm

DE was introduced by Storn et al. in 1997 [223] and is an evolutionary optimization algorithm. The candidate population moves in the search space iteratively by three evolutionary steps (Mutation, Crossover and Selection) given in equations (2.16), (2.17) and (2.18).

---

**Algorithm 4** Solution update using DE

---

```

1: for  $p = 1 : P$  do
2:   Randomly select  $a, b, c \in [1, P]$ .
3:    $v_{d,p} = x_a + M.(x_b - x_c)$ .
4:   if  $r_j \leq CR$  or  $j = I_r$  then
5:      $u_p = v_{d,p}$ 
6:   end if
7:   if  $r_j > CR$  or  $j \neq I_r$  then
8:      $u_p = x_p$ 
9:   end if
10:  if  $F(u_p) \leq F(x_p)$  then
11:     $x_p = u_p$ 
12:  end if
13: end for

```

---

$$v_{d,p} = x_a + M.(x_b - x_c) \quad (2.16)$$

$$u_p = \begin{cases} v_{d,p} & \text{if } r_j \leq CR \text{ or } j = I_r \\ x_p & \text{if } r_j > CR \text{ or } j \neq I_r \end{cases} \quad (2.17)$$

$$x_p = \begin{cases} u_p & \text{if } F(u_p) \leq F(x_p) \\ x_p & \text{if } F(u_p) > F(x_p) \end{cases} \quad (2.18)$$

Here  $x_a$ ,  $x_b$  and  $x_c$  are randomly chosen candidate solutions,  $M$  is the mutation factor (between 0 and 2) and  $v_d$  is a donor vector.  $u$  is the trail vector,  $r$  is a random variable between 0 and 1,  $I_r$  is random integer between 0 and  $T$ , and  $CR$  is crossover constant. The population size ( $P$ ) was taken as 40. The algorithm can be implemented as given in Algorithm 4. Compared to GA and PSO, DE is much more robust as it is good against both discrete and continuous optimization problems. Further, similar to PSO an iteration of DE is much faster than GA and other more complex algorithms described later on. But compared to more advanced algorithms it lacks any capability to avoid stagnation problems.

#### 2.4.4 Teaching Learning Based Optimization (TLBO) Algorithm

TLBO was introduced by Rao et al. in 2012 [224] as a population-based optimization algorithm inspired by the teaching-learning process in a class room. In this algorithm, the influence of a teacher on the output of the learners in a class is evaluated. The algorithm uses two modes of learning: (1) Teacher phase and (2) Learner phase. In this algorithm, a population is a group of learners, design variables of the optimization are the subjects offered and fitness value of optimization are the performance results of learners. The method of implementing the algorithm is described in Algorithm 5.

Here  $T_F$  is the randomly chosen teaching factor (its value is either 1 or 2);  $r$  and  $r_p$  are random variables within range of 0 and 1 and  $M_s$  is the mean solution value. The population size ( $P$ ) was taken as 40. Although TLBO is much harder to implement compared to PSO and DE, but due to implementation of hierarchical group based solution update strategies it is more efficient against complex optimization problems.



**Algorithm 5** Solution update using TLBO

---

```

1:  $M_s = \frac{1}{P} \cdot \sum_{p=1}^P x_p$ 
2: for  $p = 1 : P$  do
3:    $dM_s = r \cdot (x^* - T_F \cdot M_s)$ 
4:    $x'_p = x_p + dM$ 
5:   if  $F(x'_p) < F(x_p)$  then
6:      $x_p = x'_p$ 
7:   end if
8: end for
9: for  $p = 1 : P$  do
10:  Select  $q$  randomly between 1 and  $P$ .
11:   $X_p = \begin{cases} X_p + r_p(X_p - X_q) & \text{if } F(X_p) < F(X_q) \\ X_p + r_p(X_q - X_p) & \text{if } F(X_q) < F(X_p) \end{cases}$ 
12: end for

```

---

**2.4.5 Grey Wolf Optimization (GWO) Algorithm**

GWO was introduced by Mirjalili et al. in 2014 [225]. It is meta-heuristic algorithm based on social hierarchy, and hunting mechanism of grey wolves. For implementing social hierarchy, four kinds of grey wolves (alpha, beta, delta, and omega) are employed. Following steps are considered to simulate hunting behavior: searching, encircling and attacking prey. The method of implementing the algorithm is described in Algorithm 6.

$$A_p = 2 \cdot c_{v,p} \cdot r_1 - c_{v,p} \quad (2.19)$$

$$C_p = 2 \cdot r_2 \quad (2.20)$$

**Algorithm 6** Solution update using GWO

---

```

1: Update  $x_\alpha$ ,  $x_\beta$  and  $x_\delta$  to assign them the best three solution parameters from the population.
2: for  $p = 1 : P$  do
3:   Calculate  $A_\alpha$ ,  $A_\beta$  and  $A_\delta$  using (2.19).
4:   Calculate  $C_\alpha$ ,  $C_\beta$  and  $C_\delta$  using (2.20).
5:    $x_1 = x_\alpha - A_\alpha \cdot |C_\alpha \cdot x_\alpha - x_p|$ 
6:    $x_2 = x_\beta - A_\beta \cdot |C_\beta \cdot x_\beta - x_p|$ 
7:    $x_3 = x_\delta - A_\delta \cdot |C_\delta \cdot x_\delta - x_p|$ 
8:    $x = \frac{x_1 + x_2 + x_3}{3}$ 
9: end for

```

---

Here,  $c_v$  is the control variable that linearly decreased from 2 to 0;  $A$  and  $C$  are coefficient vectors;  $r_1$  and  $r_2$  are random variables within the range of 0 and 1. The population size

( $P$ ) was taken as 40. Compared to TLBO and ASMO, GWO is easier to implement. It is much faster to iterate over the solutions in case of GWO, but it is inefficient against complex optimization problems due to stagnation problems.

#### 2.4.6 Ageist Spider Monkey Optimization (ASMO) Algorithm

Spider monkey optimization was introduced by Bansal et al. in 2014 [226]. It is swarm intelligence-based method simulating foraging behavior of spider monkeys. In 2016, the lead author of the article Sharma et al. [227] proposed a modified version of spider monkey optimization which groups the population of spider monkey based on their ages. The algorithm works by dividing the population into groups. Each group is assigned (based on fitness value) a leader called Local Leader ( $LL$ ). The overall leader of the population (Global Leader or  $GL$ ) is the Local Leader with best fitness. All the solutions are updated

---

##### Algorithm 7 Solution update using ASMO

---

```

1:  $GL = x^*$ 
2: Update  $LL$  for each solution.
3: if  $LL$  is not changed for  $LL_{limit}$  then
4:   Reinitialize the solutions with that  $LL$ 
5: end if
6: if  $GL$  is not changed for  $GL_{limit}$  then
7:   Split one of the groups and reassign Local Leader( $LL$ ) for new groups
8: end if
9: for  $p = 1 : P$  do
10:  for  $d = 1 : D$  do
11:     $x'_p[d] = \begin{cases} x_p[d] + r_1 \cdot (LL_p[d] - x_p[d]) & \text{if } r_2 \geq pr_1 \\ + r_2 \cdot (x_r[d] - x_p[d]) & \\ x_p[d] & \text{if } r_2 < pr_1 \end{cases}$ 
12:  end for
13:  if  $F(x'_p) < F(x_p)$  then
14:     $x_p = x'_p$ 
15:  end if
16: end for
17: for  $p = 1 : P$  do
18:  for  $d = 1 : D$  do
19:     $x'_p[d] = \begin{cases} x_p[d] + r_3 \cdot (GL_p[d] - x_p[d]) & \text{if } r_4 \geq pr_2 \\ + r_4 \cdot (x_r[d] - x_p[d]) & \\ x_p[d] & \text{if } r_4 < pr_2 \end{cases}$ 
20:  end for
21:  if  $F(x'_p) < F(x_p)$  then
22:     $x_p = x'_p$ 
23:  end if
24: end for

```

---

in two steps based on the local leader and global leader positions. Further, to counter the problem of stagnation, there are two more steps that can be taken. If a particular  $LL$  does not move from its position for a particular number of iterations ( $LL_{limit}$ ), the solutions within it are reinitialized along with reassigning of the  $LL$  in that group. Further, if the  $GL$  does not move from its position for a particular number of iterations ( $GL_{limit}$ ), one of the group in the population is split into two parts and each is assigned a  $LL$ . In case the number of groups exceeds the limit, the algorithm combines the groups and reassign the local leaders. The method of implementing the algorithm is described in Algorithm 7.

$$pr_2 = 0.1 + 0.9 \cdot \frac{F(x^*)}{F(x_p)} \quad (2.21)$$

Here,  $r_1$  and  $r_3$  are random variables within the range of 0 and 1;  $r_2$  and  $r_4$  are random variables within the range of -1 and 1.  $pr_1$  (= 0.5) and  $pr_2$  are perturbation rates.  $pr_2$  is calculated as given by equation (2.21).

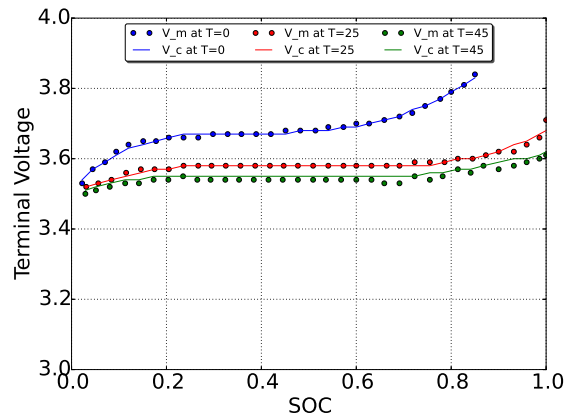
The ASMO algorithm has an inherent group breaking and merging behavior within it which prevents it from stagnating at a local optimum for a long time. In other words, ASMO performs well against complex optimization problems and in most cases it easily avoids stagnation problems due to its efficient multiple group fission-fusion solution update strategies. These group splitting and merger strategies helps the algorithm in finding the better solutions compared to other such algorithms and makes it more robust against complex multi-modal optimization problems. Further, the group based design enables easy parallel implementation of the algorithm to utilize multi-core systems effectively.

## 2.5 Results and Discussion

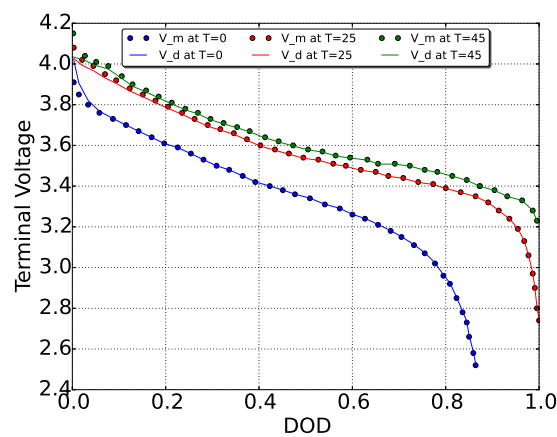
To evaluate the parameters of the battery model with the variation of temperature, a Panasonic 3.1Ah 18650 cylindrical battery was used and operated over a wide range of temperature ( $0^\circ C$  to  $45^\circ C$ ) in the simulation. Detail about the battery characteristics values is given in Appendix A. For identification of battery model parameters dependent on C-rate, SOC and temperature, six different meta-heuristic optimization techniques (GA, PSO, DE, TLBO, GWO, and ASMO), as described in last Section were utilized. The efficacy of the proposed method has been validated by comparing the obtained results with battery parameters derived from standard PCDT. Further, the performance of all heuristic optimization approaches have been examined and the conclusion obtained for the specified battery has been tabulated and compared in Section 2.5.3.

### 2.5.1 Estimated Parameters of the Battery Using Proposed Approach

For the purpose of evaluation, a particular algorithm is executed for ten identical trails on a specific model (charge or discharge) with an individual run consisting of 20,000 function evaluations. To reduce the effect of this randomness in comparing the results of different algorithms, we had to take multiple results with each algorithm. Further, the statistical tests like t-test work well on a sample size less than 30. Hence, considering the limited applicability of statistical tests and keeping reasonable computational time, we set the number of trials for each algorithm to 10. The battery model parameters corresponding to the most optimal solution, evaluated using the objective function value given in equation (2.15), are used for further model investigation. Figure 2.3 (a) and



(a)



(b)

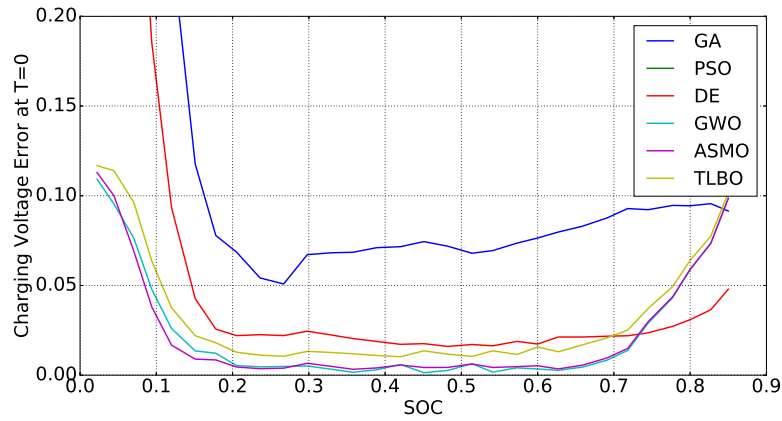
FIGURE 2.3: Predicted Characteristic Curve (a) For Charging (b) For Discharging (c) Error for Charging at 25°C (d) Error for Discharging at 25°C

TABLE 2.1: PC's  $a_1$  to  $a_{34}$  for charging and discharging

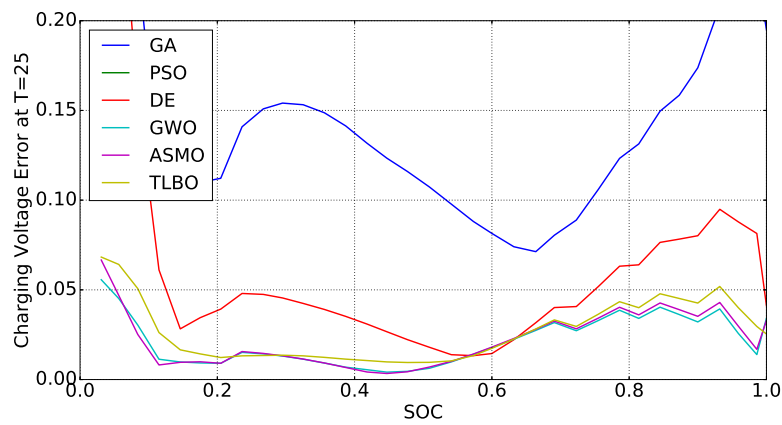
	Charging						Discharging					
	GA	PSO	DE	TLBO	GWO	ASMO	GA	PSO	DE	TLBO	GWO	ASMO
$a_1$	0.513	0.012	0.237	0.006	0.009	0.007	0.189	0.000	0.038	0.002	0.003	0.019
$a_2$	0.687	0.012	0.125	0.001	0.003	0.010	0.325	0.025	0.024	0.026	0.009	0.006
$a_3$	0.175	0.054	0.144	0.005	0.047	0.016	0.336	0.099	0.025	0.013	0.013	0.009
$a_4$	28.7	16.8	36.1	3.44	0.689	39.3	34.9	37.2	7.21	9.54	4.56	25.10
$a_5$	0.008	-0.115	0.069	0.233	0.018	0.024	0.066	0.032	0.400	0.018	0.012	0.059
$a_6$	0.110	-0.021	0.268	0.040	0.354	0.048	0.640	-0.074	0.094	0.027	0.005	0.027
$a_7$	0.216	0.125	0.017	0.050	0.008	0.008	0.084	0.056	0.167	0.010	0.069	0.015
$a_8$	0.336	0.468	0.276	0.003	0.033	0.028	0.122	0.096	0.064	0.316	0.000	0.060
$a_9$	0.493	0.043	0.268	0.009	0.024	0.000	0.553	-0.012	0.005	0.181	0.532	0.236
$a_{10}$	0.578	0.087	0.725	0.006	0.034	0.002	0.513	0.128	0.050	0.398	0.112	0.282
$a_{11}$	15.3	37.6	35.9	5.7	23.4	39.6	15	12	2.95	0.357	1.09	1.13
$a_{12}$	0.130	0.216	0.154	0.001	0.890	0.179	0.458	0.414	0.353	0.262	0.042	0.364
$a_{13}$	0.077	0.179	0.116	0.294	0.010	0.234	0.559	0.400	0.496	0.372	0.190	0.728
$a_{14}$	0.032	0.404	0.205	0.127	0.010	0.528	0.198	0.140	0.376	0.080	0.963	0.257
$a_{15}$	293	389	72	2.63	12	238	13.6	194	11.9	5.19	7.71	18.3
$a_{16}$	0.771	0.107	0.368	0.980	0.124	0.617	0.140	0.331	0.780	0.435	0.058	0.321
$a_{17}$	0.261	0.038	0.879	0.013	0.027	0.159	0.191	0.797	0.546	0.231	0.002	0.211
$a_{18}$	18.4	20.0	10.2	16.5	1.3	29.4	21.7	9.01	24.9	22.9	1.32	17.3
$a_{19}$	416	570	646	338	360	689	629	691	697	547	688	698
$a_{20}$	0.646	0.713	0.435	0.840	0.003	0.644	0.557	0.479	0.271	0.112	0.035	0.858
$a_{21}$	0.703	0.635	0.531	0.384	0.574	0.803	0.653	0.853	0.895	0.132	0.005	0.796
$a_{22}$	0.834	0.830	0.558	0.000	0.014	0.065	0.001	0.030	0.232	0.223	0.017	0.111
$a_{23}$	0.492	0.050	0.567	0.009	0.011	0.091	0.905	0.822	0.055	0.004	0.034	0.010
$a_{24}$	0.380	0.437	0.521	0.022	0.004	0.064	0.011	0.139	0.106	0.004	0.010	0.052
$a_{25}$	13.1	15.9	25.6	2.81	19.5	39.8	29.8	13.2	28	2.6	13.9	14.6
$a_{26}$	1.050	-0.166	0.408	0.125	0.018	0.143	0.783	1.200	0.086	0.000	0.006	0.182
$a_{27}$	0.379	-0.086	0.083	0.189	0.169	0.051	0.215	0.432	0.096	0.001	0.046	0.228
$a_{28}$	0.647	0.287	0.045	0.002	0.009	0.051	0.508	0.413	0.100	0.062	0.001	0.069
$a_{29}$	0.827	0.062	0.083	0.000	0.001	0.012	0.692	0.240	0.129	0.058	0.018	0.032
$a_{30}$	0.546	0.472	0.267	0.002	0.956	0.763	0.415	0.643	0.995	0.002	0.505	0.891
$a_{31}$	0.340	0.920	0.038	0.217	0.013	0.422	2.520	0.187	0.034	0.005	0.164	0.036
$a_{32}$	3.408	20.784	0.811	0.338	0.127	6.509	7.490	5.079	0.898	0.190	0.032	0.283
$a_{33}$	16.461	2.028	2.161	2.378	1.181	0.625	8.563	3.267	0.115	0.031	0.006	0.004
$a_{34}$	21.282	2.619	8.563	21.615	2.278	2.610	1.280	6.360	3.109	0.202	1.089	1.139

(b) correspond to closeness of the estimated voltage curve with expected catalog voltage at various temperatures ( $0^\circ C$ ,  $25^\circ C$  and  $45^\circ C$ ) for both charge and discharge processes respectively. Voltage-SOC characteristics have linear behavior in the middle SOC (0.2 to 0.8) values and hence require fewer sample points in that region. On the other hand, at higher and lower SOC values, they have exponential behavior that requires more sample points for accurate estimation of parameters. It can be observed from these curves that the voltage characteristic curves obtained from the model are following the catalog curves for all the measured temperatures. Due to the presence of non-linearity in the voltage characteristics for the low and high SOC values, most of the estimation errors occur in these region as represented by the small amount of deviations in the curves (Figure 2.3 (a) and (b)).

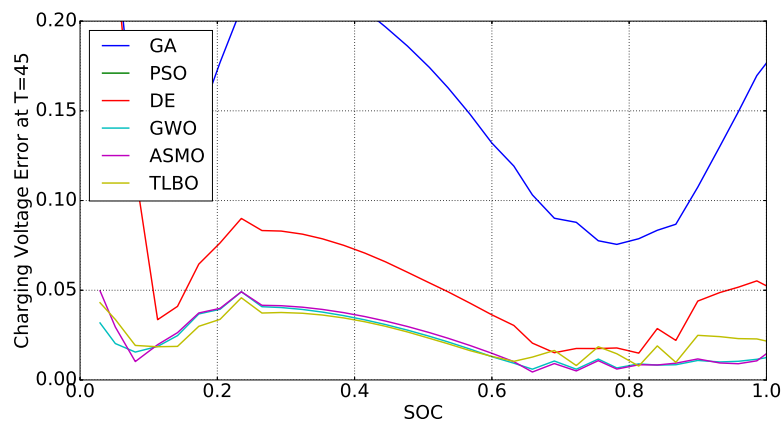
Error in the prediction of characteristic curves for battery terminal voltage at different



(a)

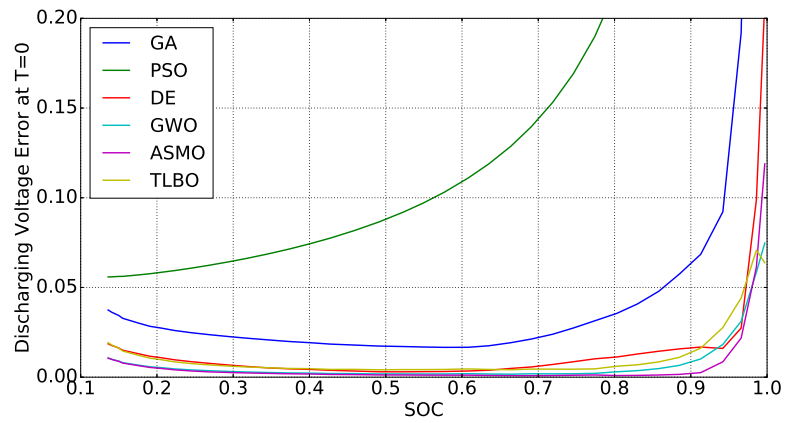


(b)

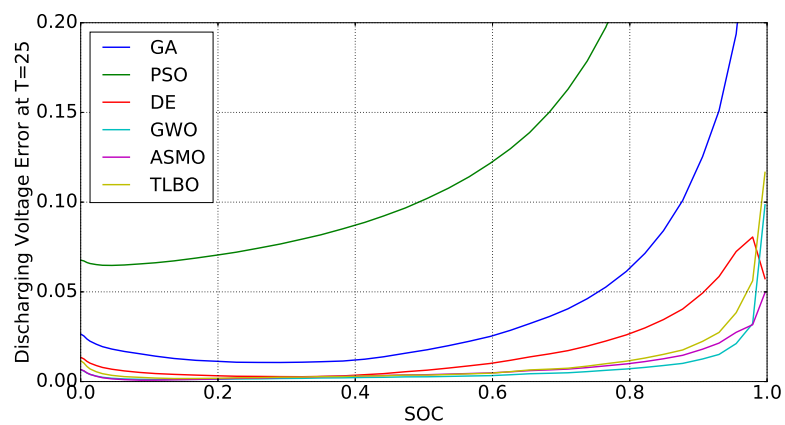


(c)

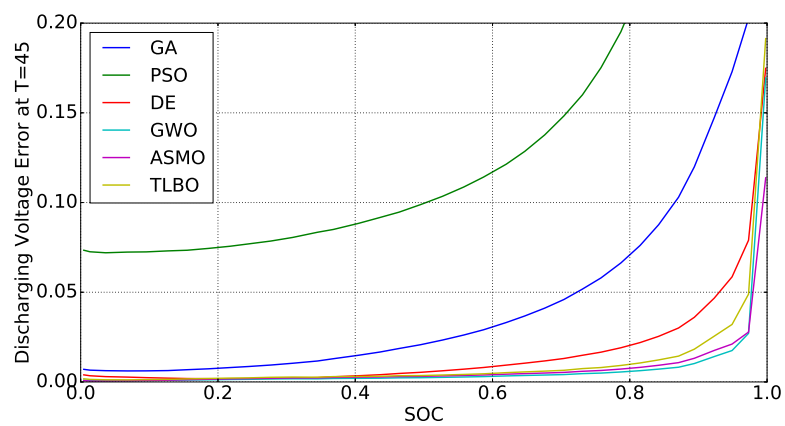
FIGURE 2.4: Predicted Characteristic Curve Error For charging at (a)  $0^{\circ}\text{C}$  (b)  $25^{\circ}\text{C}$  (c)  $45^{\circ}\text{C}$



(a)



(b)



(c)

FIGURE 2.5: Predicted Characteristic Curve Error For discharging at (a)  $0^{\circ}C$  (b)  $25^{\circ}C$  (c)  $45^{\circ}C$

temperature values ( $0^{\circ}C$ ,  $25^{\circ}C$ ,  $45^{\circ}C$ ) for both charge and discharge process utilizing different optimization techniques has been illustrated in Figure 2.4 and Figure 2.5 respectively. The predicted voltage error is computed corresponding to different SOC values within range 0 to 1 at different temperatures. The effect of non-linearity of voltage characteristics is apparent in these curves, as for all the optimization techniques, most of the error is present in the lower and higher SOC regions. The comparison between different optimization techniques has been made using different coloured lines. The high performance of ASMO and GWO algorithms are quite evident from these figures at all the measured temperatures for both charge and discharge processes. ASMO algorithm shows least error for most of the SOC values for all three temperature values compared to other optimization algorithms for both tasks.

The values of battery polynomial coefficients corresponding to best accuracy of the voltage characteristics obtained after optimization for both charging and discharging state have been tabulated in Table 2.1. The given battery parameter optimization problem belongs to a class of multimodal optimization problems. These problems, by nature, have a large number of local optima. Further, the high dimensionality (34 in this case) of the objective function, makes it almost impossible to find the global optima of the problem. In general, the solutions for these problems are approximate, and the given evolutionary optimization techniques are known to solve such problems by finding multiple approximate solutions of such problems and finally selecting the best approximation. Not all methods are capable of finding equally good approximations of the solution, thus resulting in different combinations of the parameter values for each solution. In general, each set of optimized parameter represents different local optima in the objective function solution surface.

### 2.5.2 Validation of estimated battery parameters

The estimated parameter values obtained with the proposed model are cross-validated by Constant-current Pulse Charge-Discharge Test (PCDT) in the present section. PCDT involves alternate cycles of charging/discharging and relaxing the battery for calculation of model parameters values. This test allows to observe the dynamic behavior of the battery at different temperatures. The procedure of PCDT is as follows [228]: firstly, the battery was fully charged using Constant-Current Constant-Voltage (CC-CV) charging technique. During CC-CV charging, the battery was charged at constant current with 1 C-rate until the terminal voltage of the battery reaches upper-threshold voltage 4.2 V. Thereafter, the voltage was held constant, and the current decays exponentially to 0.01 C as the battery begins to saturate [99]. Secondly, the battery was discharged by applying a positive pulse



current (C/2-rate) for 712 seconds followed by a relaxation period with zero current for 7126 seconds with 10% change of SOC. The foregoing process was repeatedly performed until the voltage reaches lower-threshold voltage 2.4 V. Finally, the battery was again charged by following the same routine with negative pulse current (C/2-rate) until the battery gets fully charged. The terminal voltage and current response of the battery for PCDT at room temperature ( $25^{\circ}\text{C}$ ) are shown in Figure 2.6 (a). In the same way, PCDT was carried out for temperature  $0^{\circ}\text{C}$  and  $45^{\circ}\text{C}$ .

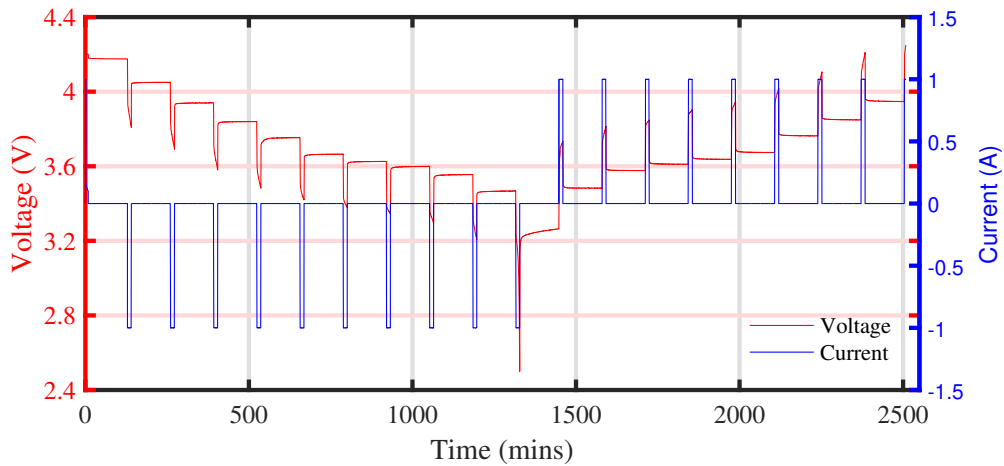


FIGURE 2.6: Voltage and current profile for Pulse Charge-Discharge Test at  $25^{\circ}\text{C}$

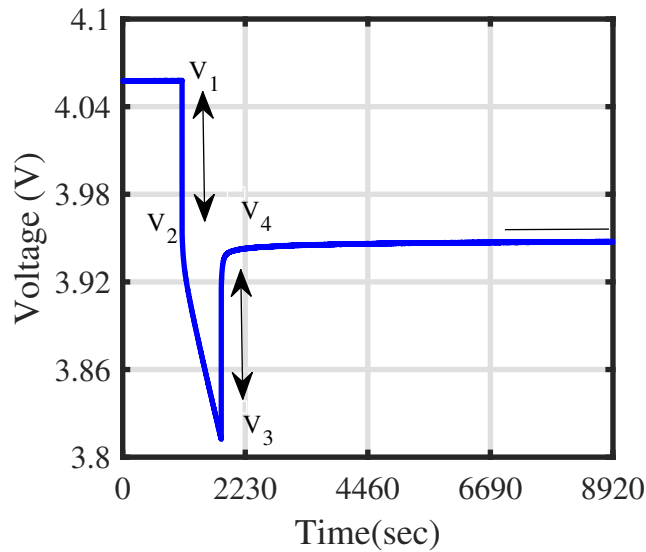


FIGURE 2.7: Voltage response to the pulse current

The terminal voltage of battery can be expressed as:

$$V_{Bt}^M(t) = V_{oc}(t) - I_{BL}(t)R_0 - V_{RC}(t) \quad (2.22)$$

$$V_{RC}(t) = \begin{cases} I_{BL}(t)R_1(1 - e^{-(t-t_0)/R_1C_1}) & \text{for } t_0 < t < t_d \\ \frac{Q(0)}{C_1}e^{-(t-t_d)/R_1C_1} & \text{for } t_d < t < t_r \end{cases} \quad (2.23)$$

Here,  $t_0$  and  $t_d$  denote time instant at the starting and end of the pulse respectively during charging and discharging scenario; whereas  $t_r$  denotes time instant at the end of relaxation;  $V_{RC}$  denotes voltage drop across  $R_1C_1$ .

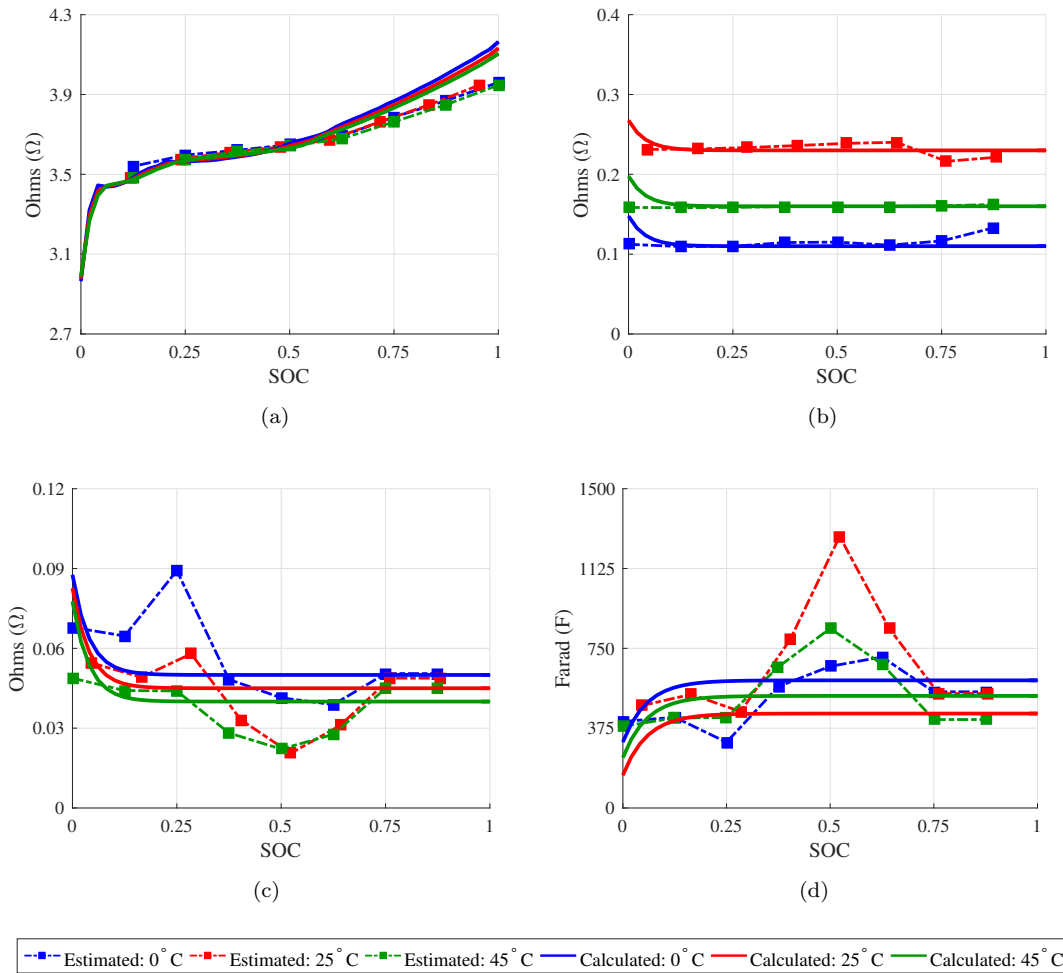


FIGURE 2.8: Plots for parameters estimated using proposed model and PCDT For Charging (a)  $V_{oc}$  (b)  $R_0$  (c)  $R_1$  (d)  $C_1$

The values of parameter identified for battery model at different temperatures and SOC/DOD during charging/discharging scenario are shown in Figure 2.8 and 2.9 respectively.  $V_{oc}$  is defined as the measured terminal voltage when the battery reaches steady-state.

An assumption is made that all transients have settled by the time instant  $t_r$ , and the terminal voltage of the battery at time instant  $t_r$  (i.e.  $V_1$  in Figure 2.7) is considered as OCV (i.e.  $V_{oc}$ ) value during charging/discharging scenario.

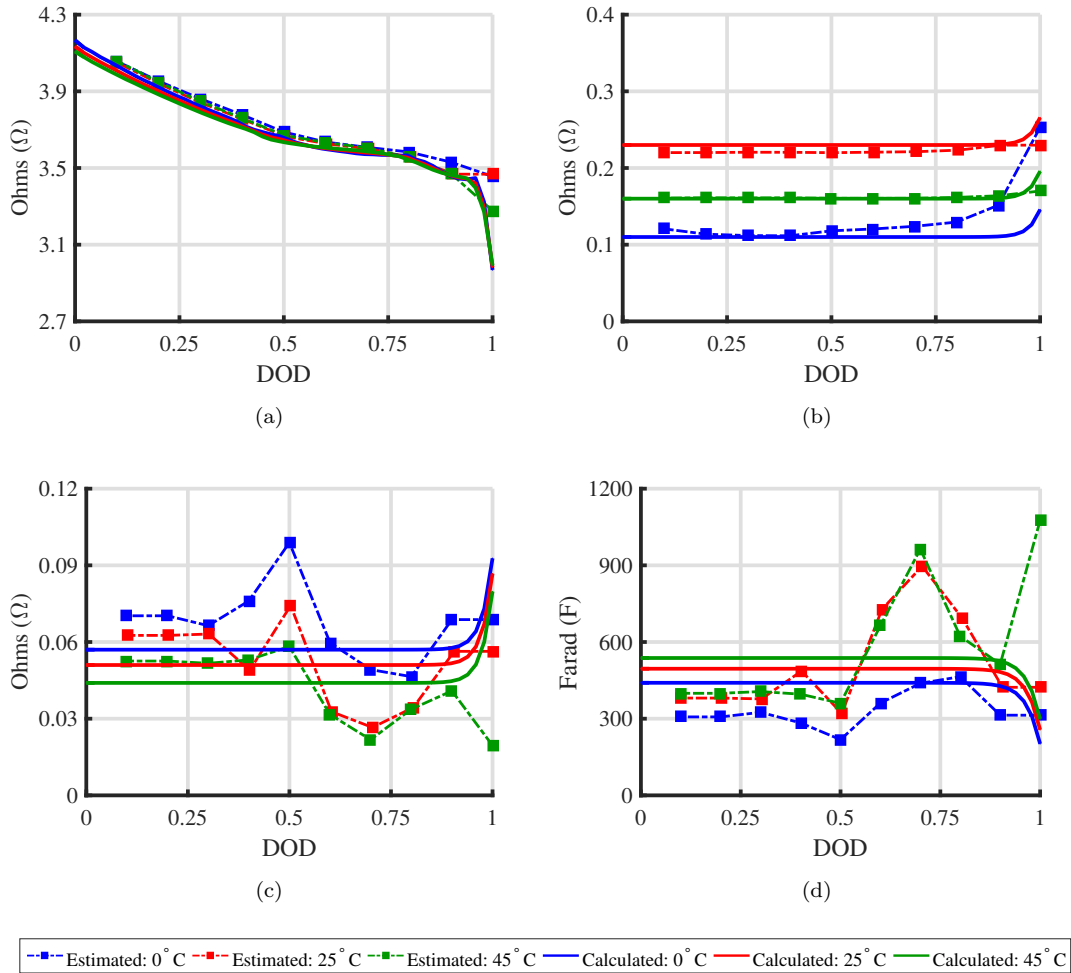


FIGURE 2.9: Plots for parameters estimated using proposed model and PCDT For Discharging (a)  $V_{oc}$  (b)  $R_0$  (c)  $R_1$  (d)  $C_1$

Figure 2.8 (a) and 2.9 (a) show the relationships between  $V_{oc}$  and SOC/DOD at different temperatures and illustrate an agreement between values obtained from proposed method and PCDT. The consistency of  $V_{oc}$  at various temperatures indicates the low sensitivity of  $V_{oc}$  to temperature.  $V_{oc}$  change rapidly with low values of SOC and high values of DOD. Otherwise, there is approximately linear variation between  $V_{oc}$  and SOC/DOD.

The values of  $R_0$ ,  $R_1$  and  $C_1$  were extracted from voltage drop obtained after subtracting terminal voltage from OCV. The voltage drop can be divided in two portions as shown in Figure 2.7 (b): firstly, the ohmic resistance voltage drop is the average of difference

$(V_1 - V_2)$  and  $(V_3 - V_4)$ . It is considered as the voltage drop across resistance  $R_0$  of the battery. The value of  $R_0$  can be calculated as the average of resistance obtained by dividing difference of voltages by difference of current at corresponding instant of time [74]. From Figure 2.8 (b) and 2.9 (b), it can be observed that  $R_0$  is sensitive to temperature but there is a small difference in the curves for different SOC and DOD indicating that  $R_0$  is approximately independent of SOC and DOD. Secondly, the transient voltage drop between  $(V_2 - V_3)$  followed by voltage rise after  $V_4$  depends on the  $R_1$  of the battery. It is difficult to experimentally measure the time constant for polarization.

From equation (2.23), it can be observed that during charging and discharging process,  $V_{RC}$  is represented by the exponential function. Non-linear Least Square Fitting (NLSF) method is used to fit PCDT data with simulated terminal voltage obtained using equation (2.23). NLSF approach minimizes the error and optimize the value of the parameters.

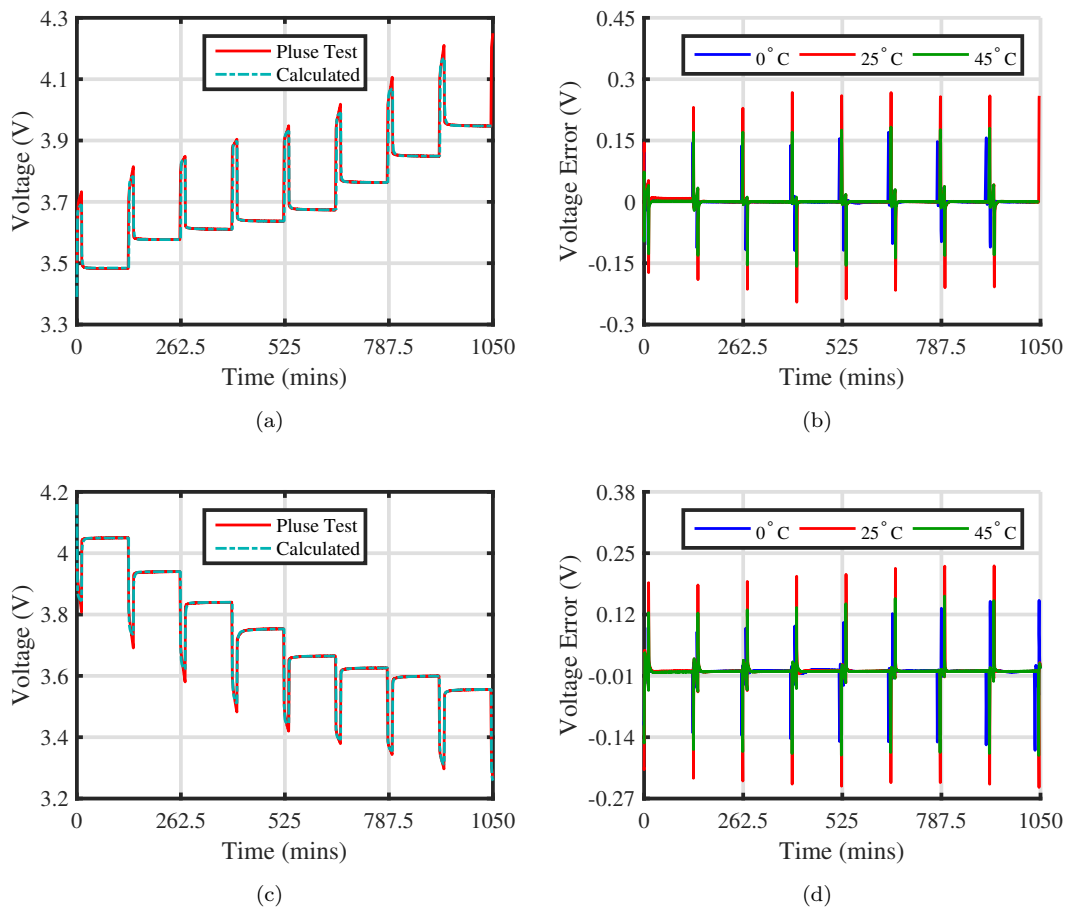


FIGURE 2.10: Plots for the PCDT voltages and calculated voltage from the extracted parameters For charging (a) Terminal voltage (b) Prediction error; For discharging (a) Terminal voltage (b) Prediction error

Through this approach, the value of  $R_1$  and  $C_1$  can be determined. The plots in Figure 2.8 (c) and 2.9 (c) indicate the value of  $R_1$  and Figure 2.8 (d) and 2.9 (d) indicate the value of  $C_1$  for charging and discharging scenario respectively estimated by NLSF approach and proposed method. The similarity between the values of parameters  $R_1$  and  $C_1$  obtained from the proposed method and PCDT indicates the effectiveness of the proposed work. As shown in Figures  $R_1$  tends to decrease slowly with increasing SOC. Similarly,  $R_1$  increases significantly with increase in DOD. High value of  $R_0$  and  $R_1$  at low temperature  $0^\circ C$  oppose the current flow in/form the battery which will limit the amount of extractable energy in battery.

To validate the estimated parameters of the battery model, the battery terminal voltage at  $25^\circ C$  obtained with the PCDT is compared with the terminal voltage obtained from equation (2.23) considering previously calculated value of the parameters. The plots of corresponding voltage at room temperature  $25^\circ C$  and predication error at various temperatures ( $0^\circ C, 25^\circ C, 45^\circ C$ ) for both charging and discharging scenarios are shown in Figure 2.10. The maximum error in predicted voltage is less than  $\pm 0.3$  at various temperatures.

### 2.5.3 Performance analysis of various optimization algorithms

For evaluation purpose, a particular algorithm was employed ten times on specific models (charge and discharge) with an individual run consisting of 20,000 function evaluations based on convergence analysis. The sample size considered for GA was 1000, 40 for ASMO and PSO, DE, TLBO, and GWO each were taken with a population of sample size 40. The objective function for optimization given in equation (2.15) was adopted for comparison of quality and accuracy of estimation of parameters through different optimization techniques. The proposed model of identification of battery parameters is evaluated with different optimization algorithms under similar execution conditions. Results are obtained at three different temperatures, and the solution quality, computation efficiency, and convergence characteristics of all algorithms are compared.

For comparing the computational burden of the algorithms, the average convergence plots of different algorithms in case of charging and discharging scenarios have been given in Figure 2.11. In both scenarios, TLBO, GWO and ASMO algorithms converged more quickly than PSO, GA and DE, thus proving themselves to be less computationally expensive.

The performance of the executed optimization approaches is analyzed in terms of best and worst fitness function value, standard deviation and mean of the fitness function. Each algorithm is executed for ten identical trails and the calculation of statistical performance

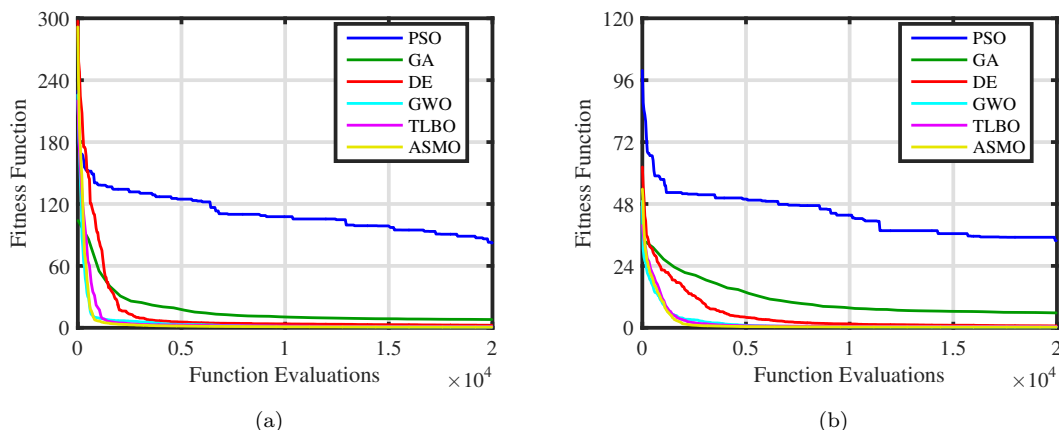


FIGURE 2.11: Convergence curves for (a) Charging (b) Discharging

indices in the case of charging and discharging is presented Table 2.2. Compared to GA, PSO, DE and TLBO algorithms, ASMO and GWO produced much lower mean error in both the charging and discharging scenarios. This shows the robustness of these algorithms in different scenarios (Charging and Discharging). Further, the much lower standard-deviation values show that algorithms performed consistently over all the runs justifying their reliability. ASMO marginally outperformed GWO algorithm in terms of mean error. This is due to fusion-fission based group formation in the ASMO algorithm which helps it to avoid the stagnation condition. The best fitness value obtained by ASMO is better than best fitness value obtained by other methods for both charging (0.572) and discharging (0.272) scenarios indicating the superiority of ASMO algorithm over other approaches. Further, in both scenarios, the best result was given by the ASMO algorithm which was used for plotting the predicted voltage characteristic curves (Figure 2.3 (a) and (b)).

TABLE 2.2: Error comparison for charge and discharge Model

	GA	PSO	DE	TLBO	GWO	ASMO
<b>Charging</b>						
<b>Mean</b>	7.9904	81.5254	2.4461	1.0541	0.7750	<b>0.6991</b>
<b>St.D</b>	2.9043	26.0813	0.1674	0.2775	<b>0.0594</b>	0.0950
<b>Worst</b>	12.1405	121.8897	2.7140	1.5447	<b>0.8868</b>	0.8932
<b>Best</b>	2.9802	39.9198	2.2520	0.7680	0.6862	<b>0.5724</b>
<b>Discharging</b>						
<b>Mean</b>	5.7681	23.3100	0.7406	0.4778	0.3269	<b>0.2983</b>
<b>St.D</b>	5.0248	1.8921	0.0848	0.0913	0.0287	<b>0.0191</b>
<b>Worst</b>	19.543	25.9502	0.8635	0.6658	0.3729	<b>0.3373</b>
<b>Best</b>	2.4044	21.2600	0.6060	0.3755	0.2869	<b>0.2718</b>

Although classical performance metrics such as mean, standard deviation, best and worst fitness value, convergence rate are suitable methods of comparing the algorithms, but they are not sufficient to find the difference in performance of the algorithms. This can be seen clearly in previous results that there is not much distinction between GWO and ASMO algorithms. To compare the performance and statistical significance of computationally intelligent algorithms, the popularity of parametric and nonparametric tests has increased

TABLE 2.3: T-test for charging scenario

		<b>GA</b>	<b>PSO</b>	<b>DE</b>	<b>TLBO</b>	<b>GWO</b>	<b>ASMO</b>
<b>GA</b>	t	0	-8.836	6.033	7.525	7.863	7.943
	h	0	1	1	1	1	1
	p	1	$5.79 \times 10^{-8}$	$1.05 \times 10^{-5}$	$5.79 \times 10^{-7}$	$3.13 \times 10^{-7}$	$2.71 \times 10^{-7}$
<b>PSO</b>	t	8.836	0	9.558	9.726	9.760	9.769
	h	1	0	1	1	1	1
	p	$5.79 \times 10^{-8}$	1	$1.78 \times 10^{-8}$	$1.37 \times 10^{-8}$	$1.3 \times 10^{-8}$	$1.28 \times 10^{-8}$
<b>DE</b>	t	-6.033	-9.558	0	13.59	29.80	28.75
	h	1	1	0	1	1	1
	p	$1.05 \times 10^{-5}$	$1.78 \times 10^{-8}$	1	$6.64 \times 10^{-11}$	$9.02 \times 10^{-17}$	$1.7 \times 10^{-16}$
<b>TLBO</b>	t	-7.525	-9.726	-13.59	0	3.118	3.837
	h	1	1	1	0	1	1
	p	$5.79 \times 10^{-7}$	$1.37 \times 10^{-8}$	$6.64 \times 10^{-11}$	1	$5.94 \times 10^{-3}$	$1.21 \times 10^{-3}$
<b>GWO</b>	t	-7.863	-9.760	-29.80	-3.118	0	2.145
	h	1	1	1	1	0	1
	p	$3.13 \times 10^{-7}$	$1.3 \times 10^{-8}$	$9.02 \times 10^{-17}$	$5.94 \times 10^{-3}$	1	$4.58 \times 10^{-2}$
<b>ASMO</b>	t	-7.943	-9.769	-28.75	-3.837	-2.145	0
	h	1	1	1	1	1	0
	p	$2.71 \times 10^{-7}$	$1.28 \times 10^{-8}$	$1.7 \times 10^{-16}$	$1.21 \times 10^{-3}$	$4.58 \times 10^{-2}$	1

TABLE 2.4: T-test for discharging scenario

		<b>GA</b>	<b>PSO</b>	<b>DE</b>	<b>TLBO</b>	<b>GWO</b>	<b>ASMO</b>
<b>GA</b>	t	0	-10.35	3.169	3.334	3.430	3.448
	h	0	1	1	1	1	1
	p	1	$5.21 \times 10^{-9}$	$5.32 \times 10^{-3}$	$3.69 \times 10^{-3}$	$2.99 \times 10^{-3}$	$2.87 \times 10^{-3}$
<b>PSO</b>	t	10.35	0	37.56	37.99	38.28	38.33
	h	1	0	1	1	1	1
	p	$5.21 \times 10^{-9}$	1	$1.49 \times 10^{-18}$	$1.22 \times 10^{-18}$	$1.06 \times 10^{-18}$	$1.04 \times 10^{-18}$
<b>DE</b>	t	-3.169	-37.56	0	6.660	14.59	16.07
	h	1	1	0	1	1	1
	p	$5.32 \times 10^{-3}$	$1.49 \times 10^{-18}$	1	$3 \times 10^{-6}$	$2.05 \times 10^{-11}$	$4.06 \times 10^{-12}$
<b>TLBO</b>	t	-3.334	-37.99	-6.660	0	4.987	6.087
	h	1	1	1	0	1	1
	p	$3.69 \times 10^{-3}$	$1.22 \times 10^{-18}$	$3 \times 10^{-6}$	1	$9.56 \times 10^{-5}$	$9.43 \times 10^{-6}$
<b>GWO</b>	t	-3.430	-38.28	-14.59	-4.987	0	2.622
	h	1	1	1	1	0	1
	p	$2.99 \times 10^{-3}$	$1.06 \times 10^{-18}$	$2.05 \times 10^{-11}$	$9.56 \times 10^{-5}$	1	$1.73 \times 10^{-2}$
<b>ASMO</b>	t	3.448	-38.33	-16.07	-6.087	-2.622	0
	h	1	1	1	1	1	0
	p	$2.87 \times 10^{-3}$	$1.04 \times 10^{-18}$	$4.06 \times 10^{-12}$	$9.43 \times 10^{-6}$	$1.73 \times 10^{-2}$	1

in last few years. T-test (Parametric) and Wilcoxon test (Non-Parametric) can be carried out for comparing different algorithms. The key performance metrics include p-value, h-value along with the corresponding t-value during statistical analysis that are calculated by executing at least ten identical trails for all the algorithms. Table 2.3 and 2.4 show the p-value, h-value along with the corresponding t-value of all algorithms in comparison to each other for charging and discharging scenarios. The algorithms in the first column are used as base algorithms in reference to which the algorithms in the first row have been compared. p-Value represents the probability of rejection of the null hypothesis. Its value lies in between 0 and 1. Lesser the p-value, more is the difference between the compared algorithms. Hypothesis test or h-value also indicates the rejection of the null hypothesis. h-value of 1 represents confirmation of the rejection of null hypothesis and thus indicates that the compared algorithms are different. For hypothesis testing, a significance level of 5% was taken. The t-test assesses whether the mean of two groups of results is statistically different from each other or not. For the purpose of testing, two-tailed t-test was adopted

TABLE 2.5: Wilcoxon-test for charging scenario

		<b>GA</b>	<b>PSO</b>	<b>DE</b>	<b>TLBO</b>	<b>GWO</b>	<b>ASMO</b>
<b>GA</b>	h	0	1	1	1	1	1
	p	1	$1.83 \times 10^{-4}$	$1.83 \times 10^{-4}$	$1.83 \times 10^{-4}$	$1.83 \times 10^{-4}$	$1.83 \times 10^{-4}$
<b>PSO</b>	h	1	0	1	1	1	1
	p	$1.83 \times 10^{-4}$	1	$1.83 \times 10^{-4}$	$1.83 \times 10^{-4}$	$1.83 \times 10^{-4}$	$1.83 \times 10^{-4}$
<b>DE</b>	h	1	1	0	1	1	1
	p	$1.83 \times 10^{-4}$	$1.83 \times 10^{-4}$	1	$1.83 \times 10^{-4}$	$1.83 \times 10^{-4}$	$1.83 \times 10^{-4}$
<b>TLBO</b>	h	1	1	1	0	1	1
	p	$1.83 \times 10^{-4}$	$1.83 \times 10^{-4}$	$1.83 \times 10^{-4}$	1	$3.61 \times 10^{-4}$	$8.77 \times 10^{-4}$
<b>GWO</b>	h	1	1	1	1	0	1
	p	$1.83 \times 10^{-4}$	$1.83 \times 10^{-4}$	$1.83 \times 10^{-4}$	$3.61 \times 10^{-4}$	1	$4.12 \times 10^{-4}$
<b>ASMO</b>	h	1	1	1	1	1	0
	p	$1.83 \times 10^{-4}$	$1.83 \times 10^{-4}$	$1.83 \times 10^{-4}$	$8.77 \times 10^{-4}$	$4.12 \times 10^{-4}$	1

TABLE 2.6: Wilcoxon-test for discharging scenario

		<b>GA</b>	<b>PSO</b>	<b>DE</b>	<b>TLBO</b>	<b>GWO</b>	<b>ASMO</b>
<b>GA</b>	h	0	1	1	1	1	1
	p	1	$1.81 \times 10^{-4}$	$1.83 \times 10^{-4}$	$1.83 \times 10^{-4}$	$1.82 \times 10^{-4}$	$1.82 \times 10^{-4}$
<b>PSO</b>	h	1	0	1	1	1	1
	p	$1.81 \times 10^{-4}$	1	$1.81 \times 10^{-4}$	$1.81 \times 10^{-4}$	$1.80 \times 10^{-4}$	$1.80 \times 10^{-4}$
<b>DE</b>	h	1	1	0	1	1	1
	p	$1.83 \times 10^{-4}$	$1.81 \times 10^{-4}$	1	$3.30 \times 10^{-4}$	$1.82 \times 10^{-4}$	$1.82 \times 10^{-4}$
<b>TLBO</b>	h	1	1	1	0	1	1
	p	$1.83 \times 10^{-4}$	$1.81 \times 10^{-4}$	$3.3 \times 10^{-4}$	1	$1.82 \times 10^{-4}$	$1.82 \times 10^{-4}$
<b>GWO</b>	h	1	1	1	1	0	1
	p	$1.82 \times 10^{-4}$	$1.8 \times 10^{-4}$	$1.82 \times 10^{-4}$	$1.82 \times 10^{-4}$	1	$2.1 \times 10^{-2}$
<b>ASMO</b>	h	1	1	1	1	1	0
	p	$1.82 \times 10^{-4}$	$1.80 \times 10^{-4}$	$1.82 \times 10^{-4}$	$1.82 \times 10^{-4}$	$2.1 \times 10^{-2}$	1



with 5% significance level. The negative t-value with ASMO as base algorithm along with low p-value and h-value of 1 with respect to all the other algorithms proves ASMO to be significantly better than other algorithms including GWO. A further comparison has been made in Table 2.5 and 2.6 using the Wilcoxon ranked sum test. For this test, the comparison data was taken in normalized form with a significance level of 5%. This test finds if there is a significant difference between the two compared algorithms. As evident from the h-value of 1, there is a significant difference in the performance of the ASMO algorithm and other algorithms including GWO.

T-test and Wilcoxon test clearly show that the ASMO algorithm performed significantly better than all other tested algorithms. The lower mean fitness value and standard deviation of the ASMO prove its superiority in the battery parameter estimation scenario. Further, the low computational requirements signify the robustness of the algorithm, thus making it a prime choice for the task of battery parameter estimation.

## 2.6 Chapter Summary

An accurate determination of the parameters of battery model plays an indispensable part in replicating the behavior of battery. In this chapter, a first-order RC battery model incorporating the effect of the temperature on the battery parameters with SOC and C-rate is utilized. The parameter estimation is modeled in optimization framework as minimization of the Manhattan distance between the voltage computed from the battery model and catalog voltages supplied by the manufacturer. Six different meta-heuristic optimization techniques (*viz.* GA, PSO, DE, TLBO, GWO, and ASMO) have been utilized to obtain optimal parameters of the model. The performance of applied optimization techniques is compared in terms of their ability and accuracy in the extraction of the battery model parameters with a lower convergence rate. For the model, GWO and ASMO optimization techniques proved to be more robust, reliable and gave an optimal solution in both charging and discharging scenarios. The lower mean fitness value (charging:0.699/discharging:0.298) and standard deviation (less than 1) of the Ageist Spider Monkey Optimization (ASMO) proved its superiority in battery parameter estimation. For precise statistical investigation of computational intelligence algorithms, parametric (T-test) and non-parametric tests (Wilcoxon test) have been performed. From performance index and test-based study, it was concluded that the ASMO algorithm functions more reliably than all other tested algorithms. Further, the low computational requirements signify the simplicity of the algorithm, thus presenting it as an appropriate option for the evaluation of battery model

parameters. The values of parameters extracted using ASMO are validated with values evaluated from PCDT. It is observed from the validation process that there is a similarity between parameters values obtained from both the methods. Therefore, the proposed technique can be used as an alternative for estimation of battery parameters.

## Chapter 3

# Online Assessment of Battery Performance

### 3.1 Introduction

Accurate estimation of the State-of-Charge (SOC) and State-of-Health (SOH) are of great significance in battery management system due to the requirement of ensuring safe and reliable operation of a Li-ion battery in EVs. For driving purpose, it is essential for the driver to have information about how long the driver can still drive with the present charge in the battery. If the driver does not have the precise information, it will create a lot of inconvenient if the charge gets finished before completion of the ride. Conventional internal combustion engine automobile has a dashboard for fuel gauge that shows the absolute level of fuel remaining in the tank. Similarly, battery SOC corresponds to the amount of energy left inside a battery to power the EVs. For EVs customers it is essential to determine the current remaining available capacity so that driver can recharge or change the battery for traveling. Moreover, another inevitable problem with the battery is that their performance (health) deteriorate gradually with cycling (usage) and calendar life (aging) due to irreversible chemical changes with load variations. With the determination of the current remaining available capacity of the battery, it is also vital to identify battery current maximum available capacity ahead of time so that decision for battery replacement could be made. In the combined equivalent circuit based battery model, the energy balance circuit represents battery degradation with charging and discharging with the help of  $R_{s,dis}$  and  $C_{use}$ . Battery SOC variation is given by  $V_{SOC}$  whose value changes between 0 to 1. The accuracy of SOC estimation depends mainly on the fidelity of the

battery model and the robustness of the estimation techniques. The review related to the estimation of internal battery states identify that estimation can be performed by utilizing conventional, data-driven and model-based methods. The conventional methods are easy to implement, however, they are highly affected by external distributions. Data-driven methods perform well with non-linear and high dimensional models with an ability to predict the internal states accurately by using well-computed training data for all possible operating condition. Generation of a large amount of data is the main drawback of data-driven methods which demands large memory and complex computation. The nonlinear observer has enhanced robustness against the disturbances and improved performance in terms of accuracy, converge speed and computation cost. Nevertheless, the model could deliver inaccurate results if the controller is not properly designed. Adaptive filters are the most favored techniques since they can predict non-linear dynamics states with good precision, high efficiency and less computational cost. As the battery model has been developed to represents the dynamic behavior of the battery, hence, model-based adaptive filters recognized as appropriate battery internal states estimation methods. Different variants of adaptive filters are utilized for estimation of internal battery states. In this work, comparison among the model-based estimation techniques such as Extended Kalman Filter (EKF), Sigma-point Kalman Filter (SPKF) and Particle Filter (PF) for estimation of battery SOC has been performed. The battery model developed in Chapter 2 has been used for analyzing the quality and execution time for the different variant of KF. Model-based estimation methods have been compared regarding their robustness, accuracy and computational time. The voltage response circuit of the combined equivalent battery model primary intended to capture the short-term behavior of the batteries in terms charging and discharging process. Whereas, battery capacity degradation is the much slower chemical reaction. To mismatch in the complexity and time-scale, most battery capacity degradation model are based on pattern analysis of measured data rather than the fundamental process modeling. To determine the general model for capacity degradation empirical equations based models are developed by using curve fitting techniques. With the help of empirical capacity degradation model, the complexity of model tuning can be reduced notably. In this work, two different empirical capacity degradation models have been developed and their effectiveness in analyzed for representing the degradation behavior of the battery. Empirical battery capacity degradation model was developed by curve fitting using capacity degradation data obtained from the life-cycle test. Information about battery current SOH and remaining useful life (RUL) has been determining by using different model-based estimation technique and effectiveness of each method in estimation is analyzed. This chapter deals with the estimation of internal

states of the battery using model-based estimation methods. Problem formulation using a state space model regarding the estimation of internal states of the battery has been defined in Section 3.2. The state space model for estimation of battery SOC is realized using the voltage response circuit developed in Chapter 2. Whereas the state space model for battery SOH estimation is accomplished using the empirical model developed using life-cycle test data. Detail description about process method and estimation techniques has discussed in Section 3.3. Estimation results under different operating conditions are shown in Section 3.4 to authenticate the validity of the proposed methods and conclusion obtained regarding the estimation of SOC and SOH is given in the Section 3.5.

## 3.2 Problem Formulation for Estimation of Battery Internal States

The model-based adaptive filter methods are designed to estimate internal states of the battery based on the state-space model. The diagnostic models have configured for one-step ahead prediction, which allow recursive estimation of battery states [157]. A general discrete-time state-space model that describes characteristics of the system governed by the non-linear stochastic difference equations are defined as follow [229]:

### State Equation

$$x_{k+1} = f(x_k, u_{k+1}, w_k) \quad (3.1)$$

with a measurement

### Measurement Equation

$$y_{k+1} = h(x_{k+1}, u_{k+1}, v_{k+1}) \quad (3.2)$$

Here,  $x \in \mathbb{R}^n$  represents the n-dimensional unobserved state vector of the system;  $y \in \mathbb{R}^m$  represents the m-dimensional output measurement vector ;  $u \in \mathbb{R}^{N_u}$  represents the known (measured/deterministic) one-dimensional input vector of the system; random variable  $w \sim \mathcal{N}(\bar{w}, \sum_w)$ ,  $\sum_w \in \mathbb{R}^{N_w \times N_w}$  and  $v \sim \mathcal{N}(\bar{v}, \sum_v)$ ,  $\sum_v \in \mathbb{R}^{N_v \times N_v}$  represents the Gaussian process-noise and the Gaussian measurement-noise (respectively), describing uncertainty in real system. Both process and measurement noise are assumed to be independent from each other hence they have zero mean value and variance represented by  $\sum_w$  and  $\sum_v$  respectively. Subscript  $k$  with variable indicates the value of that variable at the time  $t_k$  where  $t_k = t_0 + k\delta$  and  $\delta$  is the time step. Correspondingly, non-linear function  $f(\cdot)$  relates

the state at the previous time step  $k$  to the state at current time step  $k + 1$  and non-linear function  $h(\cdot)$  relates the state  $x_k$  to the measurement  $y_k$ . And the state  $x$  of the system has mean  $\bar{x}$  and covariance  $\Sigma_x$ .

### 3.2.1 SOC estimation model

A battery can be modeled as a nonlinear, time-varying system with state variables that describe states. The measurement are typically the voltage, current and temperature. In the previous chapter, the battery model has been expressed by continuous time ordinary differential equations. For the implementation of SoC estimation strategies, the discrete form of battery model has to be utilized. To represent battery model by discrete-time ordinary difference equations, assume sampling time  $\Delta t$  to be small enough such that current can be considered constant over sampling time. The battery model discrete state-space equations describing dynamic effect derived from equation (1.1) and (2.12) can be expressed as:

#### State Equation

$$\begin{bmatrix} SOC_{k_i+1} \\ V_{RC,k_i+1} \end{bmatrix} = \begin{bmatrix} 1 & 0 \\ 0 & \exp\left(\frac{-\Delta t}{R_{1,k_i} C_{1,k_i}}\right) \end{bmatrix} \begin{bmatrix} SOC_{k_i} \\ V_{RC,k_i} \end{bmatrix} + \begin{bmatrix} -\frac{\Delta t}{Q_n} \\ (1 - \exp\left(\frac{-\Delta t}{R_{1,k_i} C_{1,k_i}}\right)) R_1 \end{bmatrix} (I_{BL,k_i} + w_{k_i}) \quad (3.3)$$

#### Measurement Equation

$$V_{Bt,k_i+1} = V_{oc}(SOC_{k_i+1}) - I_{BL,k_i+1} R_{0,k_i+1} - V_{RC,k_i+1} + v_{k_i+1} \quad (3.4)$$

Here,  $k_i$  refers iteration number, the state vector is  $x = [SOC \ V_{RC}]^T$  and the current  $I_{BL}$  and terminal voltage  $V_{Bt}^M$  as the input and output variables respectively.

### 3.2.2 Capacity degradation model

Battery aging will reduce the maximum available battery capacity compared to the fresh battery. Battery capacity degradation occurs with repeated charging and discharging of the battery. Prognostic of battery failure can be performed by developing capacity degradation model from life-cycle test data. The capacity degradation model is developed by using life-cycle test datasets for 18650 commercialized (LFP) Li-ion batteries. Four different battery  $B_1 - B_4$  has been examined to collect the datasets. The battery

degradation datasets have been adopted from the Center for Advanced Life Cycle Engineering (CALCE) battery research group of the University of Maryland. The life-cycle test has been conducted sequentially by performing multiple charging-discharging cycles under room temperature and repeated until capacity degraded to 80 % of maximum capacity of the unused battery. Using the battery test equipment, firstly the batteries were fully charged at constant current with 1C charging rate (i.e., 1.1A) under standard constant current-constant voltage mode. The batteries have been charged until the battery voltage reaches to 4.2V then current has exponential drop till 0.05A while maintaining batteries voltage at 4.2V. Discharging was carried out at a 1C rate until the batteries voltage reaches 2.5V. The test was run at room temperature which was approximately  $25^{\circ}C$ . The discharge capacity was recorded after each full charge-discharge process. Data collection will terminate when battery full charge capacity reaches EUL point. The detail specification of the battery is listed in Appendix A. Figure 3.1 shows capacity degradation data obtained from the life-cycle test of four different battery.

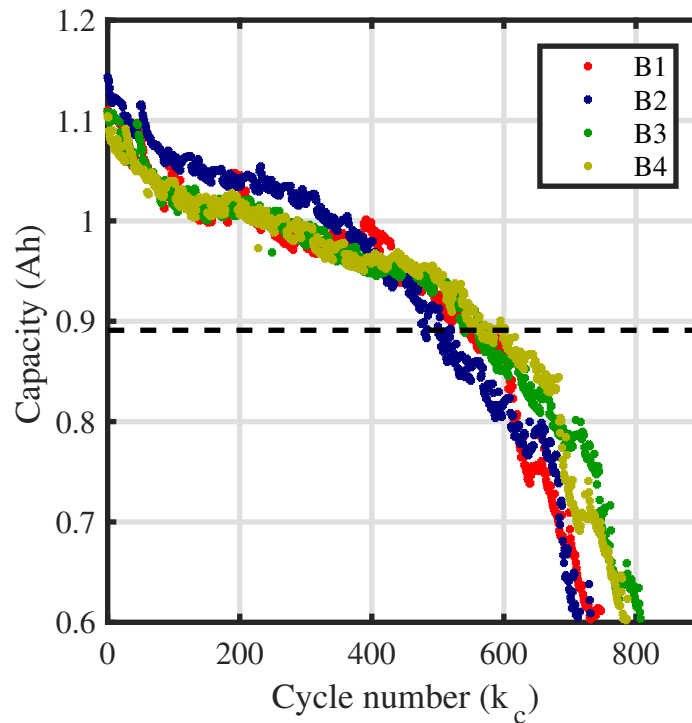


FIGURE 3.1: Capacity data set

Two empirical regression models have been considered to investigate the battery capacity degradation behavior through life-cycle test data. A polynomial and exponential model have been empirically established through fitting of battery degradation data using regression analysis.

### Polynomial model

$$Q_{pk_c} = p_1 * k_c^2 + p_2 * k_c + p_3 \quad (3.5)$$

### Exponential Model

$$Q_{ek_c} = e_1 * \exp(e_2 * k_c) + e_3 * \exp(e_4 * k_c) \quad (3.6)$$

Where  $k_c$  refers the cycle number, parameters of polynomial model and exponential model are represented through  $p_1, p_2, p_3$  and  $e_1, e_2, e_3, e_4$  respectively.

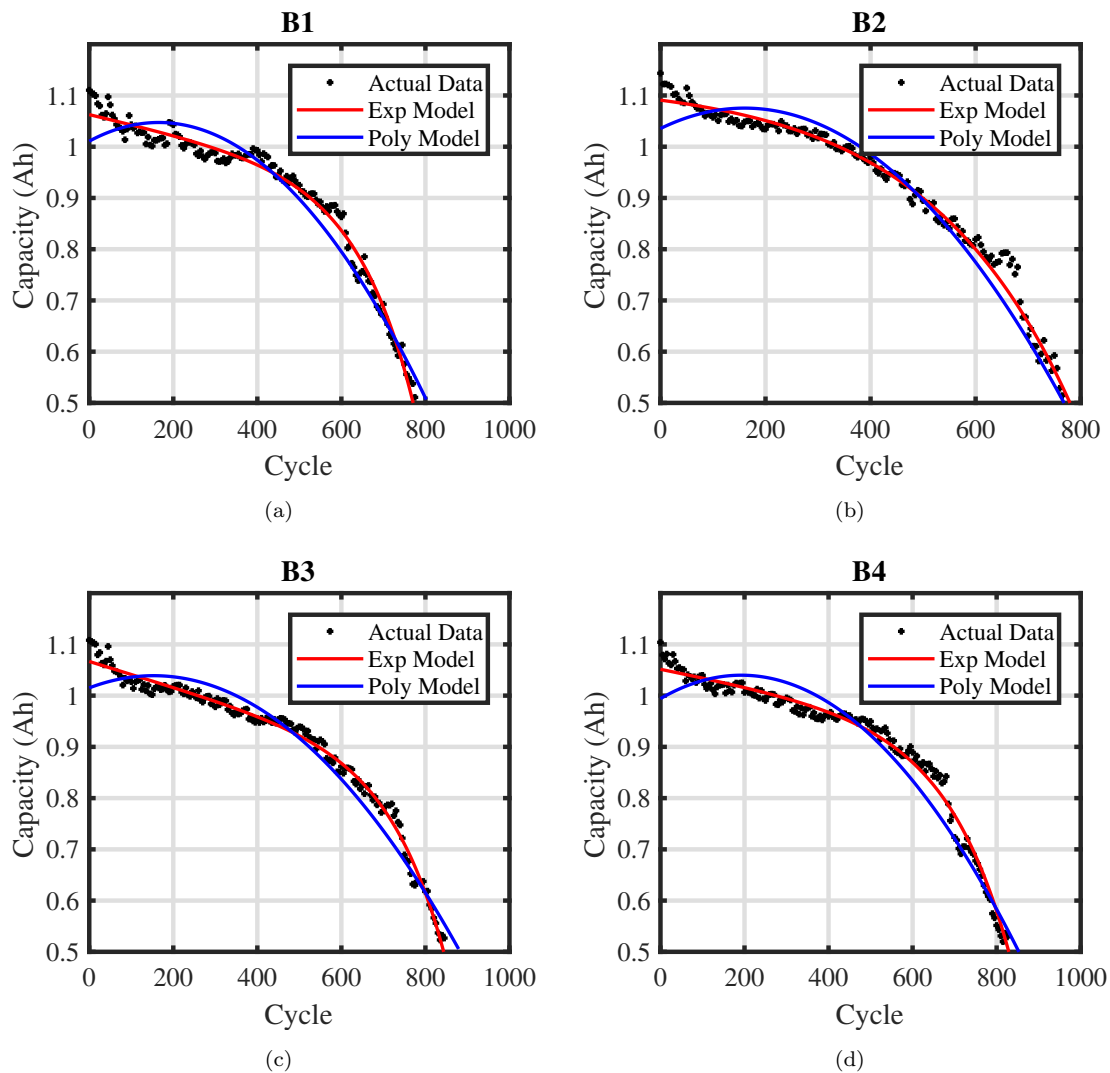


FIGURE 3.2: Curve fitting based on polynomial and exponential model.

To evaluate the goodness-of-fit of given models capacity data over the whole life (up to EUL) was used. Models fitting is performed in MATLAB environment using curve fitting tool. Based on the model's characteristics polynomial model was estimated using linear



least square method while the exponential model was determined using the nonlinear least square method. Aim of both the methods is to minimize the sum of the square of the errors. Figure 3.2 shows curve fitting for battery B1-B4 based on polynomial model and exponential model. Figure 3.2 shows that exponential model fits well with data as compared to polynomial model. Obtained mean parameters value for both polynomial model and exponential model with lower bound and upper bound are shown in Table 3.2. Fitted parameters are calculated with the bound of 95% confidence intervals. With help of lower and upper bound parameters value variance of parameter can also be calculated for further use.

The accuracy of prediction of battery performance and health depends upon the accuracy of the capacity model. Model accuracy and goodness-of-fit of regression can be validated by using two indices the adjusted R-square and RMSE.  $R_{adj}^2$  is modification of  $R_{square}$  to compensate for the extra variable included in the model. The best fit is indicated by “1” in  $R_{adj}^2$  and “0” in RMSE. Table 3.1 shows the value of adjusted R-square and RMSE for both exponential and polynomial model. From the table, it can be an analyze that for exponential model the adjusted  $R^2$  is more close to 1 and RMSE is near to 0 compared to the polynomial model. This shows that the exponential model has better global regression performance compare to the polynomial. Hence exponential model is suitable for analysis degradation of battery capacity and predicting RUL.

TABLE 3.1: Goodness-of-fit for polynomial and exponential model

Battery	$R^2$		RMSE		Adjust $R^2$	
	Polynomial	Exponential	Polynomial	Exponential	Polynomial	Exponential
<b>B1</b>	0.9430	0.9861	0.0392	0.0194	0.9428	0.9861
<b>B2</b>	0.9812	0.9926	0.0367	0.0232	0.9812	0.9925
<b>B3</b>	0.9493	0.9918	0.0367	0.0147	0.9492	0.9918
<b>B4</b>	0.9439	0.9891	0.0418	0.0184	0.9438	0.9890

Accurate state estimation and prediction not only rely on a precise model but also depend on the adjustments of model parameters to track the variation in the capacity fade. Gradually estimated parameters value converges to their respective actual values when more capacity data become available. Dynamic capacity fade characterization and estimation of current capacity for prediction of RUL are performed by using adaptive filter algorithm. Adaptive filter algorithm solves any estimation problem by minimizing the mean-square-error of discrete state space model.

The discrete state space model to describe the dynamic behavior of capacity fading, including the state transition and measurement equations can be expressed as follow:

TABLE 3.2: Parameters values for polynomial and exponential model

Battery	Parameter	Lower Bound	Mean	Upper Bound	Parameter	Lower Bound	Mean	Upper Bound
B1	$p_1$	-1.39E-06	-1.33E-06	-1.28E-06	$e_1$	-1.83E-03	-1.41E-03	-9.96E-04
	$p_2$	3.94E-04	4.41E-04	4.88E-04	$e_2$	7.07E-03	7.42E-03	7.77E-03
	$p_3$	1.00E+00	1.01E+00	1.02E+00	$e_3$	1.06E+00	1.06E+00	1.07E+00
					$e_4$	-1.97E-04	-1.76E-04	-1.56E-04
B2	$p_1$	-1.59E-06	-1.55E-06	-1.52E-06	$e_1$	-4.69E-02	-3.78E-02	-2.87E-02
	$p_2$	4.62E-04	4.98E-04	5.34E-04	$e_2$	3.39E-03	3.61E-03	3.82E-03
	$p_3$	1.03E+00	1.04E+00	1.04E+00	$e_3$	1.12E+00	1.13E+00	1.14E+00
B3					$e_4$	-4.71E-05	-2.99E-08	4.71E-05
	$p_1$	-1.05E-06	-1.01E-06	-9.71E-07	$e_1$	-7.59E-04	-6.15E-04	-4.71E-04
	$p_2$	2.72E-04	3.11E-04	3.49E-04	$e_2$	7.34E-03	7.60E-03	7.86E-03
	$p_3$	1.01E+00	1.02E+00	1.02E+00	$e_3$	1.06E+00	1.07E+00	1.07E+00
B4					$e_4$	-2.47E-04	-2.35E-04	-2.23E-04
	$p_1$	-1.28E-06	-1.24E-06	-1.19E-06	$e_1$	-2.08E-03	-1.68E-03	-1.27E-03
	$p_2$	4.32E-04	4.75E-04	5.19E-04	$e_2$	6.43E-03	6.69E-03	6.95E-03
	$p_3$	9.86E-01	9.94E-01	1.00E+00	$e_3$	1.05E+00	1.05E+00	1.06E+00
				$e_4$	-1.68E-04	-1.50E-04	-1.33E-04	

### State Equation

$$x_{k_c+1} = [e_{1,k_c+1}; e_{2,k_c+1}; e_{3,k_c+1}; e_{4,k_c+1}] \quad (3.7)$$

$$e_{1,k_c+1} = e_{1,k_c} + \omega_{e1,k_c}$$

$$e_{2,k_c+1} = e_{2,k_c} + \omega_{e2,k_c}$$

$$e_{3,k_c+1} = e_{3,k_c} + \omega_{e3,k_c}$$

$$e_{4,k_c+1} = e_{4,k_c} + \omega_{e4,k_c} \quad (3.8)$$

### Measurement Equation

$$Q_{k_c+1} = y_{k_c+1} = e_{1,k_c+1} * \exp(e_{2,k_c+1} * k) + e_{3,k_c} * \exp(e_{4,k_c+1} * k) + v_{k_c+1}$$

Where  $w_{ei} \sim \mathcal{N}(\bar{w}_{ei}, \sum_{w,ei})$ ,  $\sum_w, ei \in \mathbb{R}^{N_w,ei \times N_w,ei}$  and  $v \sim \mathcal{N}(\bar{v}, \sum_v)$ ,  $\sum_v \in \mathbb{R}^{N_v \times N_v}$  represents the process noise for each parameter and model measurement noise respectively.  $x_k$  refers parameters vector of capacity degradation model for cycle  $k$  and  $Q_k$  refers to measurement output which is battery capacity degradation data. With the measured capacity, the unscented Kalman filter is incorporated to adjust the parameters and update states value sequentially. In this process, predication of capacity is performed after the state value is updated. The RUL prediction is performed by the difference between predicated capacity cycle number and EUL cycle number:

$$RUL = k_{c,EUL} - k_{c,MC} \quad (3.9)$$

Where  $k_{c,EUL}$  is the cycle number at which predicated capacity hits the capacity value at EUL point and  $k_{c,MC}$  is the cycle number at which predication of RUL is performed.

## 3.3 Estimation Techniques

The adaptive filter algorithms estimate the needed state  $x_{k+1}$  based on the observations  $y_{0:k+1} = [y_1, y_2 \dots y_k]$  under the rule of minimizing mean squared error between observation and estimated output [229]. The current state  $x_{k+1}$  recursively updates through predicted value of the previous state  $x_k$ . and current value of the measured input  $u_{k+1}$ . The state of a system is a group of dynamic variables that evolve through time, and its evolution through time is governed by a dynamic system, perturbed by process noise [230]. The measurements are functions of the state and the measurement noise. The basic idea of the

adaptive filter based techniques is the state space model, the system and measured signal combined with white noise.

### 3.3.1 Extended Kalman filter (EKF)

For estimation purpose, Kalman Filter (KF) was developed in 1960 [158]. KF is a linear filter that estimates states of the system by utilizing the measured value with noise and uncertainty and produces the value that approaches closer to the true value [49]. KF recursively updates the current state of the system through predicted value of the previous state and current value of the measured input. Since the battery is a non-linear system, linear KF cannot be utilized for SOC estimation purposes [164]. Hence to improve the estimation accuracy, the nonlinear version called the EKF used for SOC estimation of the battery. The EKF uses Taylor-series to linearize the non-linear state equation and transform the nonlinear problem to linear problem.

To implement EKF, nonlinear state equation are linearized about the current mean and the covariance using first-order Taylor-series expansion at each time step. Here assumption is made that both  $f(\cdot)$  and  $h(\cdot)$  are differentiable at all operating points,

$$f(x_k, w_k, u_k) \approx f(x_k, w_k, u_k) \quad (3.10)$$

$$\begin{aligned} \hat{A}_k &= \left. \frac{df(\cdot)}{dx_k} \right|_{x_k=\hat{x}_k^+} & \hat{B}_k &= \left. \frac{df(\cdot)}{dw_k} \right|_{w_k=\bar{w}_k} \\ \hat{C}_k &= \left. \frac{dh(\cdot)}{dx_k} \right|_{x_k=\hat{x}_k^+} & \hat{D}_k &= \left. \frac{dh(\cdot)}{dv_k} \right|_{v_k=\bar{v}_k} \end{aligned} \quad (3.11)$$

Here,  $A_k$  represents  $n \times n$  system matrix;  $B_k$  represents  $n \times 1$  input matrix;  $C_k$  represent  $m \times n$  output matrix;  $D_k$  is  $m \times 1$  feed-forward matrix.

The detail computation process of EKF estimation strategies to develop an adaptive model-based internal states estimation is illustrated in Figure 3.3

Here,  $KG_k$  denotes the Kalman gain matrix,  $\hat{y}_k$  is the estimated measured output,  $\hat{x}_k^-$  and  $\hat{x}_k^+$  are for the prior estimate before the measurement and the posterior estimate after the measurement respectively,  $\Sigma_{x_k}^-$  and  $\Sigma_{x_k}^+$  are covariance matrix of state estimation error before and after measurement respectively. In the multi-dimensional Taylor-series expansion, EKF obtained only first order accuracy in prediction of posterior mean and covariance of states. EKF does not take into account inherent uncertainty in prior states during the linearization process. In fact linearization around current state omits the

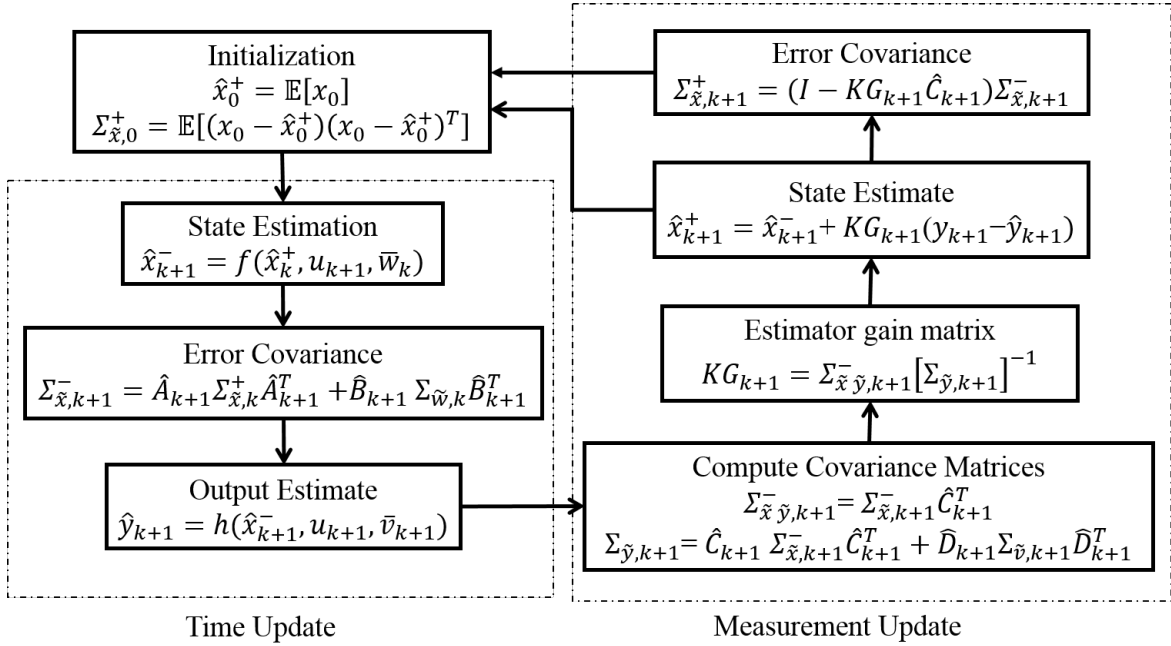


FIGURE 3.3: EKF algorithm based SOC estimation approach

crucial expectation operators. These approximations often introduce substantial error in evaluation of posterior mean and covariance of states which leads to divergence of the filter and suboptimal performance.

#### Disadvantages:

1. In the EKF, state distribution is propagated analytically through the first-order Taylor's series expansion. The first-order approximation introduces substantial errors in the prediction of posterior mean and covariance of states which leads to sub-optimal performance and sometimes divergence of the filter. Hence EKF is difficult to tune if model non-linearities are severe and leads to unreliable estimation of states.
2. EKF performance depends upon the accuracy of the system model and parameters. Even EKF performance will decrease or even diverge if the system and measurement noise don't satisfy the Gaussian distribution.

### 3.3.2 Sigma Points Kalman filter (SPKF)

EKF based estimation methods have some shortcomings which result in the decrease in accuracy and lead to unstable filters. To overcome EKF shortcomings, SPKF utilizes a small fixed group of functions (called sigma points) to linearize the nonlinear system [165].

These sigma points are deterministically calculated using the mean and square-root decomposition of the covariance matrix of the prior state. Based on characterizing method, SPKF can be categorized as follow: Unscented Kalman Filter (UKF) and Central Difference Kalman Filter (CDKF). UKF utilizes the unscented transformation and CDKF utilizes Sterling's polynomial interpolation methods for linearization of the nonlinear system [231]. Using these approaches, if the dimension of the state is  $N_x$  then to capture first and second order moments of the prior states,  $2N_x + 1$  sigma point  $\chi_k$  are required with corresponding weights. Higher order moments can be captured, if so desired, at the cost of using more sigma-points. SPKF will eliminate the computational burden of Jacobian matrices and approximates up to second order. Hence, the calculation of derivatives could be avoided which implies that original function need not to be differentiable. The detail computation process of SPKF algorithmic is illustrated in Algorithm 3.4.

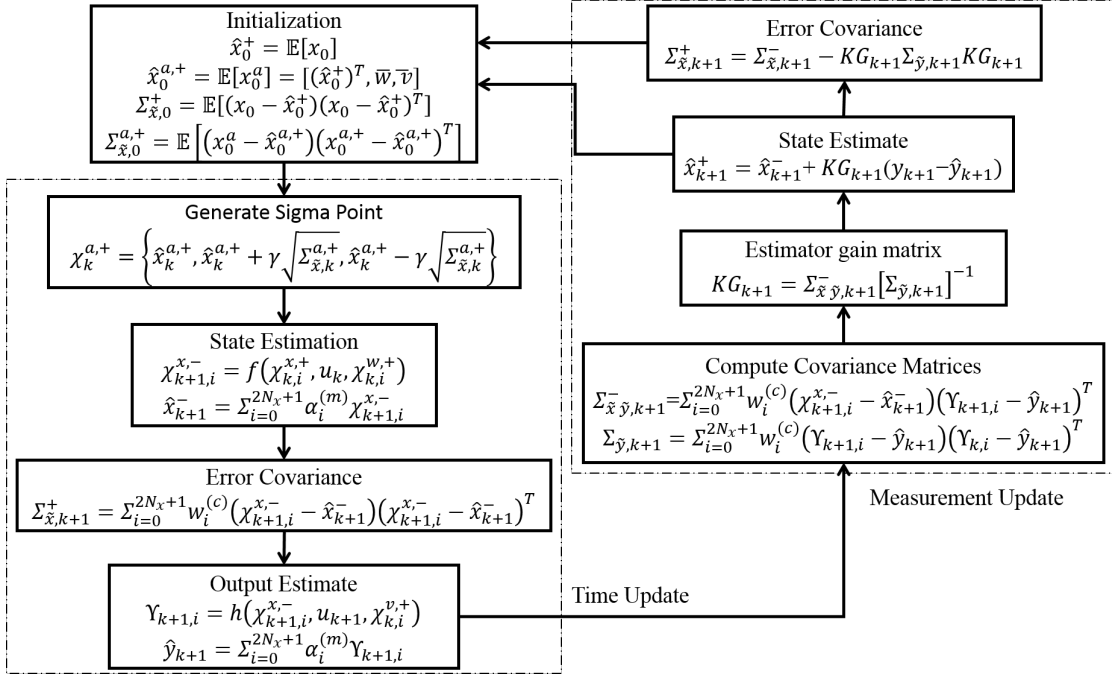


FIGURE 3.4: SPKF algorithm based SOC estimation approach

Here,  $\gamma$  is a scalar scaling factor that determines the spread of the sigma-points around the prior mean;  $x_k^a$  is the augmented random vector,  $\hat{x}_{k-1}^{a,+}$  is posteriori state estimate vector defined as  $\hat{x}_{k-1}^{a,+} = [(\hat{x}_{k-1}^+)^T, \bar{w}, \bar{v}]^T$ ,  $\Sigma_{\tilde{x},k-1}^{a,+}$  is posterior covariance defined as  $\Sigma_{\tilde{x},k-1}^{a,+} = \text{diag}(\Sigma_{\tilde{x},k-1}^{a,+}, \Sigma_{\bar{w}}, \Sigma_{\bar{v}})$ ,  $w_i^{(m)}$  and  $w_i^{(c)}$  are weighting constant. Both the filters follows same implementation procedure except the choice of sample points required more variable in case of UKF ( $\alpha, \beta, \kappa$ ) than CDKF ( $h$ ). Weights are determined for both the filters has been shown in Table 3.3.

TABLE 3.3: Parameters values for different SPKF filters

Method	$\gamma$	$w_0^{(m)}$	$w_i^{(m)}$	$w_0^{(c)}$	$w_i^{(c)}$
UKF	$\sqrt{L + \lambda}$	$\frac{\lambda}{L + \lambda}$	$\frac{\lambda}{2(L + \lambda)}$	$\frac{\lambda}{L + \lambda} + (1 - \alpha^2 + \beta)$	$\frac{1}{2(L + \lambda)}$
CDKF	h	$\frac{h^2 - L}{h^2}$	$\frac{1}{2h^2}$	$\frac{h^2 - L}{h^2}$	$\frac{1}{2h^2}$

Here,  $\lambda = \alpha^2(L + \kappa) - L$  with  $10^{-2} \geq \alpha \geq 1$  and value of  $\kappa$  is either between 0 and 3-L.  $\beta$  incorporates prior information. h may take any positive value but optimal value is consider as  $h = \sqrt{3}$  for Gaussian random variables.

### 3.3.3 Particle Filter (PF)

Accuracy of states estimation using EKF and SPKF depends on the accuracy of the model parameters. These filter also fails if used with nonlinear non Gaussian applications. Hence, to improve the robustness of estimation methods, Particle Filter (PF) was developed for dealing with complex distribution other Gaussian distribution. PF is a recursive statistical filter based on the Monte Carlo techniques and recursive Bayesian estimation. The Monte Carlo method is applied to approximate required state posterior probability distribution by a collection of random samples known as particles  $x_{k,i=1}^i$  with associated weight vector  $w_{k,i=1}^i$ . Its complicated to draw random particles directly from the true posteriori density function. Alternative and easy process to generate random particles is recursively update the posterior distribution using sequential importance sampling and re-sampling.

The PF algorithm is described as follows:

1. **Initialization:** Randomly draw  $N_p$  initial state particles  $x_0^i (i = 1, 2, \dots, N_p)$  from prior probability distribution  $p(x_0)$  having  $\mathcal{N}(\bar{x}, \sum_x)$  and initial weight for particular particles is assigned as  $w_0^i = 1/N_p$ . Large the  $N_p$  the better the estimation but more computation will be needed. Number of particles  $N_p$  depend upon type of system and computation cost. The threshold of re-sampling can be initialized as  $N_{th} = \frac{2}{3}N_p$ .  
**For k=1,2,...**

2. **Importance sampling:** Update the value of states using state equation and update the weight of the particle according to following equation:

$$w_{k+1}^i = w_k^i \frac{p(y_{k+1}|x_{k+1}^i)p(x_{k+1}^i|x_k^i)}{q(x_{k+1}^i|x_k^i,y_{1:k})} \quad (3.12)$$

3. **Weight normalization** update and normalize the important weights for each particle. calculate the  $i^{th}$  particle's likelihoods.

$$w_{k+1}^i = \frac{w_{k+1}^i}{\sum_{i=1}^{N_p} w_{k+1}^i} \quad (3.13)$$

4. **Resampling:** Each particle is reserved or abandoned selectively according to its weight and then new set of particles is obtained.

$$N_{eff} = \frac{1}{\sum_{i=1}^{N_p} (w_{k+1}^i)^2} \quad (3.14)$$

If the effective sample size  $N_{eff}$  is below the given threshold  $N_{th}$ , then resampling procedure is performed to get the new particles.

5. **State estimation:** Using new set of  $N_p$  particles and their associated weights, propagates the state particles  $x_{k+1}^i$  to the next step by the system process equation.

$$\hat{x}_{k+1} = \sum_{i=1}^{N_p} \bar{w}_{k+1}^i x_{k+1}^i \quad (3.15)$$

## 3.4 Results and discussions

The high power Li-ion batteries (*LFP*) with a nominal capacity of 3.3 Ah and nominal voltage 3.7 V of the 18650 cylinder type were used for evaluation of the accuracy of state estimation methods. Capacity and life-cycle tests were executed for collecting reference data for evaluating the efficiency of adaptive filters in the estimation of internal battery states such as SOC and SOH respectively.

### 3.4.1 SOC estimation

A proper SOC estimation technique should be applicable of functioning efficiently during different loading conditions. To simulate the dynamic performance of EVs battery for actual driving load, US Advanced Battery Consortium (USABC) designed standard load profiles. Driving cycles are standardized driving pattern defined as the test cycles applied for evaluation and comparison of different types of drivetrains regarding their efficiency and emissions. These are sequences of speed-time data points which represents the driving behavior and traffic conditions in a specific area. Dynamic stress test (DST) driving



cycle profile represents driving conditions for an urban city travel pattern. When battery discharges from being fully charged (at 3.6V) to fully discharged (at 2V), the process includes several cycles of the standard DST cycle. Figure 3.5 illustrates sequence cycles for current and voltage of conventional DST profile at room temperature ( $25^{\circ}\text{C}$ ). This sequential driving profile is utilized for performance analysis of state estimator

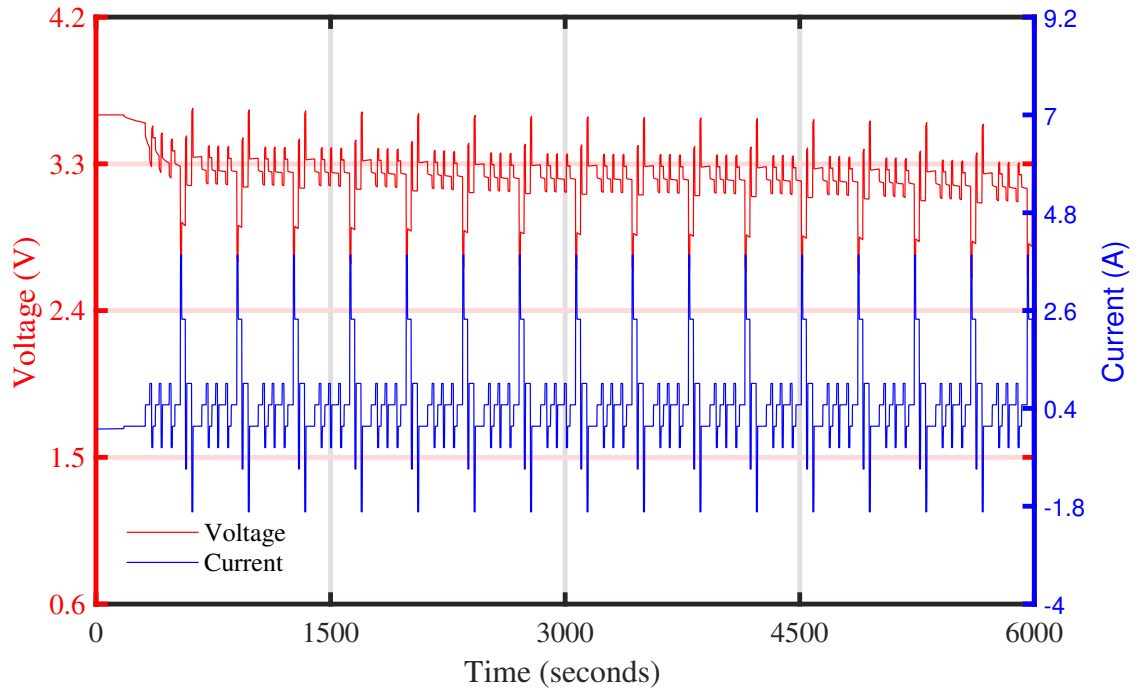


FIGURE 3.5: Voltage and current profile for DST driving cycles

Performance evaluation of different SOC estimation techniques is carried out with the different initial guess for the battery SOC. First, SOC estimation performed with assuming correct initial SOC value  $\hat{x}_0^+ = [100]^T$  then assuming wrong initial SOC value  $\hat{x}_0^+ = [90]^T$ . Covariance of error was assumed as  $\Sigma_{\hat{x},k,0}^+ = \text{diag}([1e^{-3}])$ . For the execution of estimation of SOC using EKF, UKF, CDKF, and PF, the value of the process  $\Sigma_p$  and observation  $\Sigma_m$  noise covariance were deliberately selected by using the trial-and-error method to assure convergence of the algorithms. For evaluation purpose white noise is assumed hence the mean value of process and measurement noise are set to be zero, and the value for the covariance of process noise  $\Sigma_p$  and measurement noise  $\Sigma_m$  are set to be 0.2. Particles for PF are assumed to be 200, and the threshold value for re-sampling is 0.5.

The required current value for the typical driving cycle is applied to the battery terminal in the laboratory, for simulating its dynamic discharge behavior during operation of EVs. In this dissertation, DST driving profiles are considered for evaluating the performance of adaptive filters methods for estimation of the battery SOC at different ambient

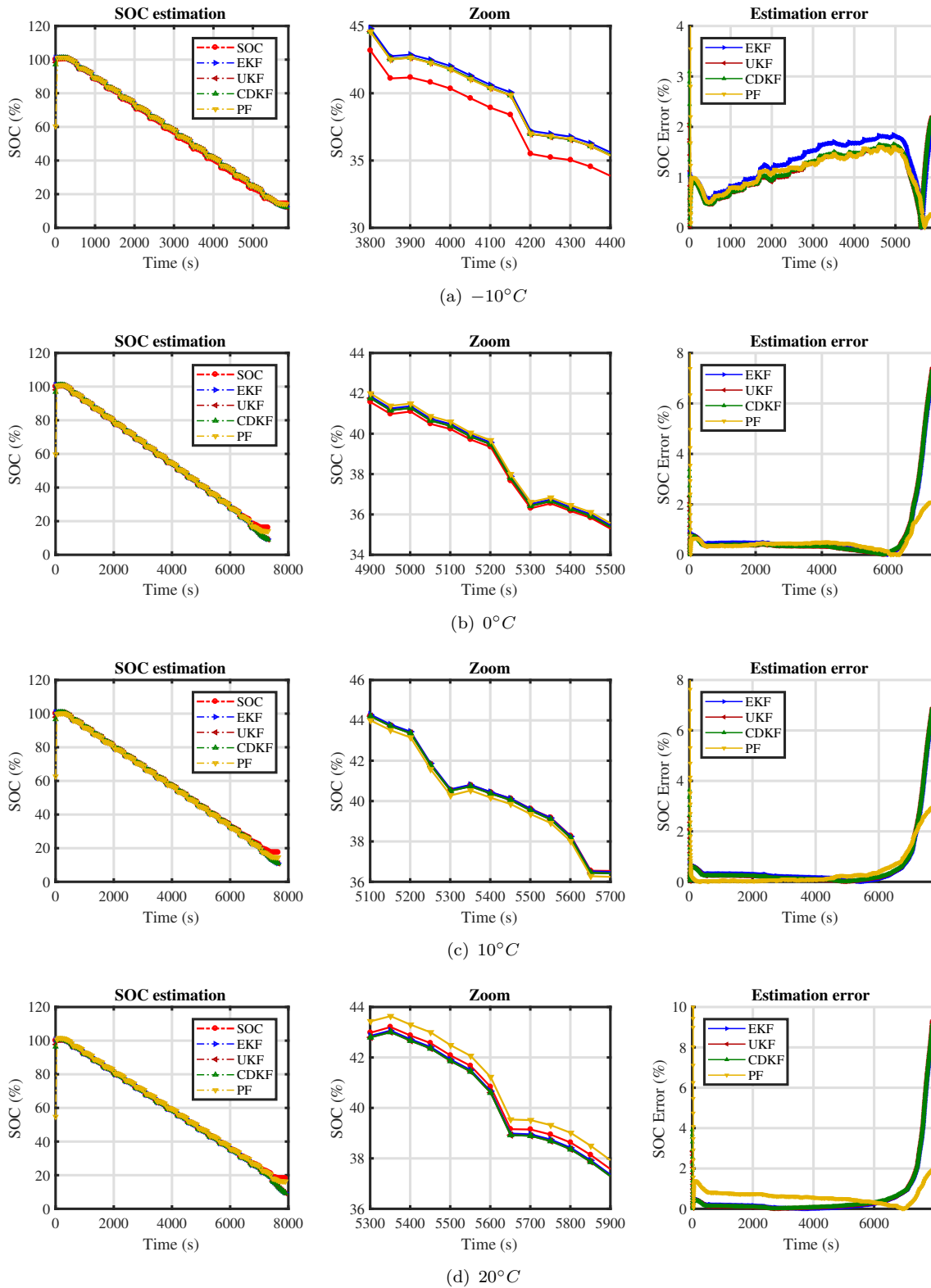


FIGURE 3.6: Estimation results of different adaptive KF assuming correct initial SOC value (a)  $-10^{\circ}\text{C}$  (b)  $0^{\circ}\text{C}$  (c)  $10^{\circ}\text{C}$  (d)  $20^{\circ}\text{C}$

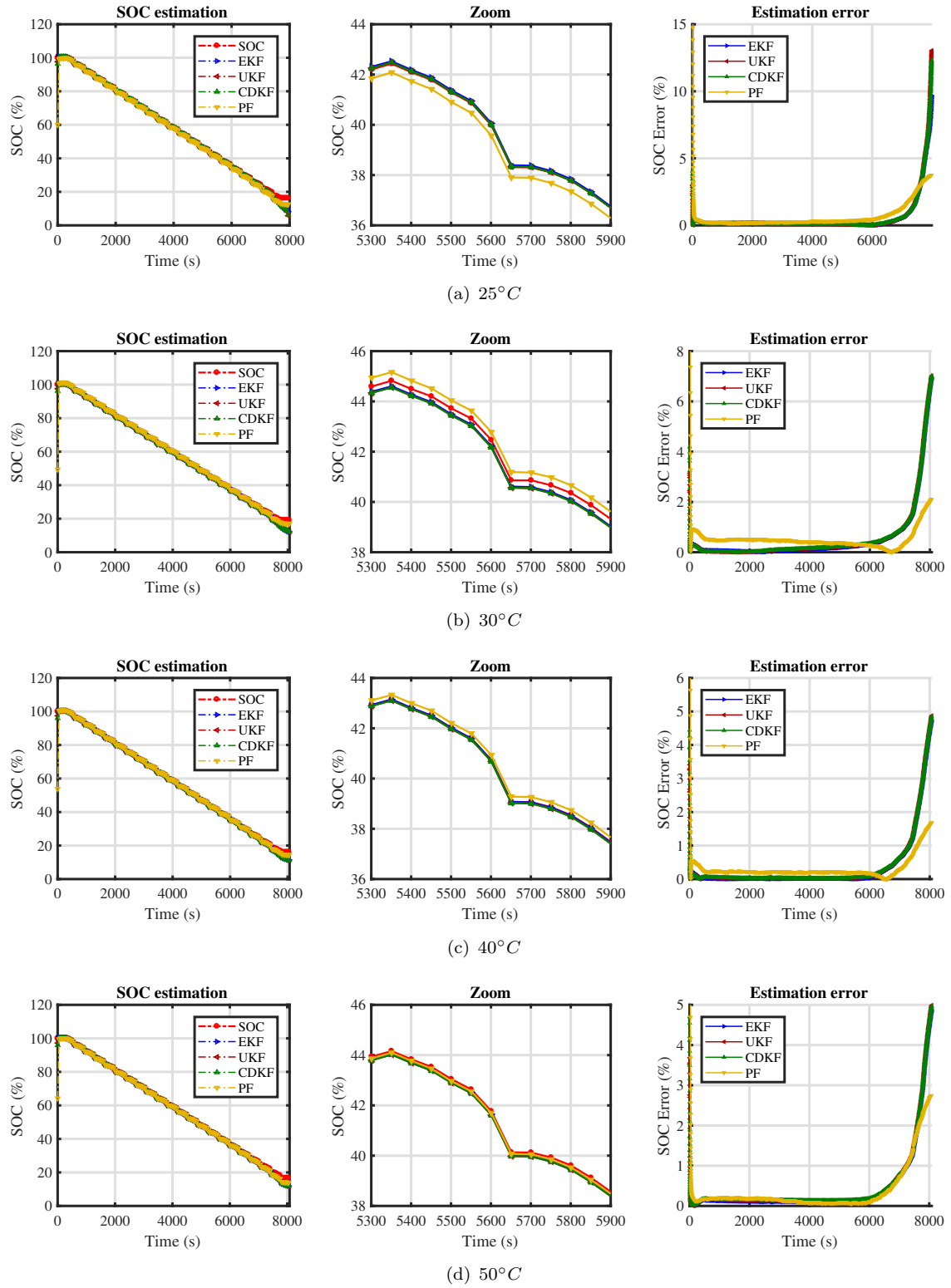


FIGURE 3.7: Estimation results of different adaptive KF assuming correct initial SOC value (a) 25°C (b) 30°C (c) 40°C (d) 50°C

temperatures. DST profile contains both processes discharging and charging with positive current defining discharge and negative current defining charge behavior of battery. Figure 3.6 and 3.7 illustrates recorded capacity test data using controlled ampere-hour method corresponding to the discharge of battery at different temperatures. In practical application usually, batteries are operated in between 20% to 90% SOC values only hence for estimation purpose data below 20% SOC is discarded.

Estimated SOC values with defining correct SOC initial value from adaptive filters at various temperatures is illustrated in Figure 3.6 and 3.7. The red color graph represents the true SOC value, while blue, brown, green and yellow graph represents the estimated SOC value using EKF, UKF, CDKF, and PF filters. Figure 3.6 and 3.7 contains SOC estimation values, zoom of SOC estimation graph and their errors in the estimated value for different temperatures. It can be observed from graphs that the estimated SOC value with correct initial SOC can track the true experimental SOC profiles more precisely with EKF and PF. Maximum absolute SOC error value is 2% , 8% , 8% , 10% , 15% , 8% , 6% and 5% ,and 5% corresponding to  $-10^{\circ}C$ ,  $0^{\circ}C$ ,  $10^{\circ}C$ ,  $20^{\circ}C$ ,  $25^{\circ}C$ ,  $30^{\circ}C$ ,  $40^{\circ}C$  and  $50^{\circ}C$  respectively for EKF, UKF and CDKF estimation methods. Whereas for all the temperature maximum absolute SOC error is approximately less 4% in case PF estimation. Hence, SOC estimation based on PF yields comparatively minor fluctuations. Error plots also indicate that corresponding to the low value of SOC estimated SOC slowly divergences away from reference SOC. The reason for large the difference between the values of SOC at the end of the graph is the error in the measurement of quantities using sensors and error due to Coulombic counting methods. Also, it's illustrated by figures that as the temperature value decreases battery discharges very fast compare to high-temperature value. Since SOC of the battery is less than 10% at  $-10^{\circ}C$  whereas for another case its approximately more than 20%. Hence, the performance of the battery decrease with a decrease in the value of temperature. Hence a more accurate model to capture the transient behavior of the battery at low temperature is worthy to investigate in the future study.

Further quantification of estimators performance can be executed by determining root-mean-square and mean absolute error between reference SOC value and estimated SOC values. Mathematical, the root- mean- square error can be expresses by following equation:

$$RMSE = \sqrt{\frac{\sum_{k=1}^n (SOC_k^M - SOC_k^E)^2}{n}} \quad (3.16)$$

Mathematically, mean absolute error can be expressed by the following equation:

$$MAE = \frac{1}{n} \sum_{k=1}^n |SOC_k^M - SOC_k^E| \quad (3.17)$$

Here,  $SOC_k^M$  stands for measured SOC value from Coulomb Counting method and  $SOC_k^E$  stands for estimated SOC values from EKF, UKF, CDKF, and PF.

TABLE 3.4: Prediction error statistics at different temperature assuming correct initial SOC value

	RMSE				MAE			
	EKF	UKF	CDKF	PF	EKF	UKF	CDKF	PF
$-10^\circ C$	1.3624	<b>1.1917</b>	1.2058	2.0506	1.2983	<b>1.1265</b>	1.1392	1.1957
$0^\circ C$	<b>1.3701</b>	1.4033	1.4014	1.5598	0.7186	0.6740	0.6747	<b>0.5744</b>
$10^\circ C$	<b>1.2276</b>	1.2569	1.2592	1.6133	0.5538	0.5299	0.5314	<b>0.4732</b>
$20^\circ C$	<b>1.4789</b>	1.5253	1.5227	1.8996	<b>0.5619</b>	0.5796	0.5805	0.7218
$25^\circ C$	<b>1.3627</b>	1.5524	1.5094	1.6596	0.5152	0.5196	<b>0.5132</b>	0.6946
$30^\circ C$	<b>1.2728</b>	1.2947	1.2983	1.9615	<b>0.5253</b>	0.5488	0.5508	0.5994
$40^\circ C$	<b>0.9012</b>	0.9267	0.9287	1.5579	<b>0.3243</b>	0.3530	0.3539	0.3828
$50^\circ C$	<b>0.9418</b>	0.9669	0.9693	1.5062	<b>0.4167</b>	0.4561	0.4575	0.4431

TABLE 3.5: Execution time analysis (in secs) assuming correct initial SOC value

	EKF	UKF	CDKF	PF
$-10^\circ C$	2.3757	2.2658	3.1938	<b>1.9929</b>
$0^\circ C$	2.4426	2.3230	2.9864	<b>2.0949</b>
$10^\circ C$	2.6293	2.8861	3.6077	<b>2.5205</b>
$20^\circ C$	2.8277	<b>2.5136</b>	3.2501	2.5311
$25^\circ C$	3.1270	<b>2.5391</b>	3.1446	2.6841
$30^\circ C$	2.6307	2.5017	3.1987	<b>2.2129</b>
$40^\circ C$	2.7071	3.1231	3.1356	<b>2.2897</b>
$50^\circ C$	3.1084	2.5453	3.1657	<b>2.2599</b>

The value of root-mean-square and mean absolute error for different estimator is given in Table 3.4. From the table, it can be concluded that maximum root-mean-square error among all temperature for EKF is 1.37%, UKF is 1.55%, CDKF is 1.52 %, and PF is 2.05%. Maximum mean absolute error among all temperature using EKF us 1.2 %, UKF is 1.2%, CDKF is 1.3%, and PF is 1.19 %. Hence, the precision of EKF based estimation algorithm is higher than other algorithms for estimation of SOC at different temperatures. The execution time of the estimation methods is determined using "tic-toc" command in MATLAB to evaluate calculation time required to run the script. The execution time for performing battery SOC estimation is shown in Table 3.5. From the table, it can be concluded that the maximum execution time taken by EKF is 3.12 sec, UKF is 3.1 sec,

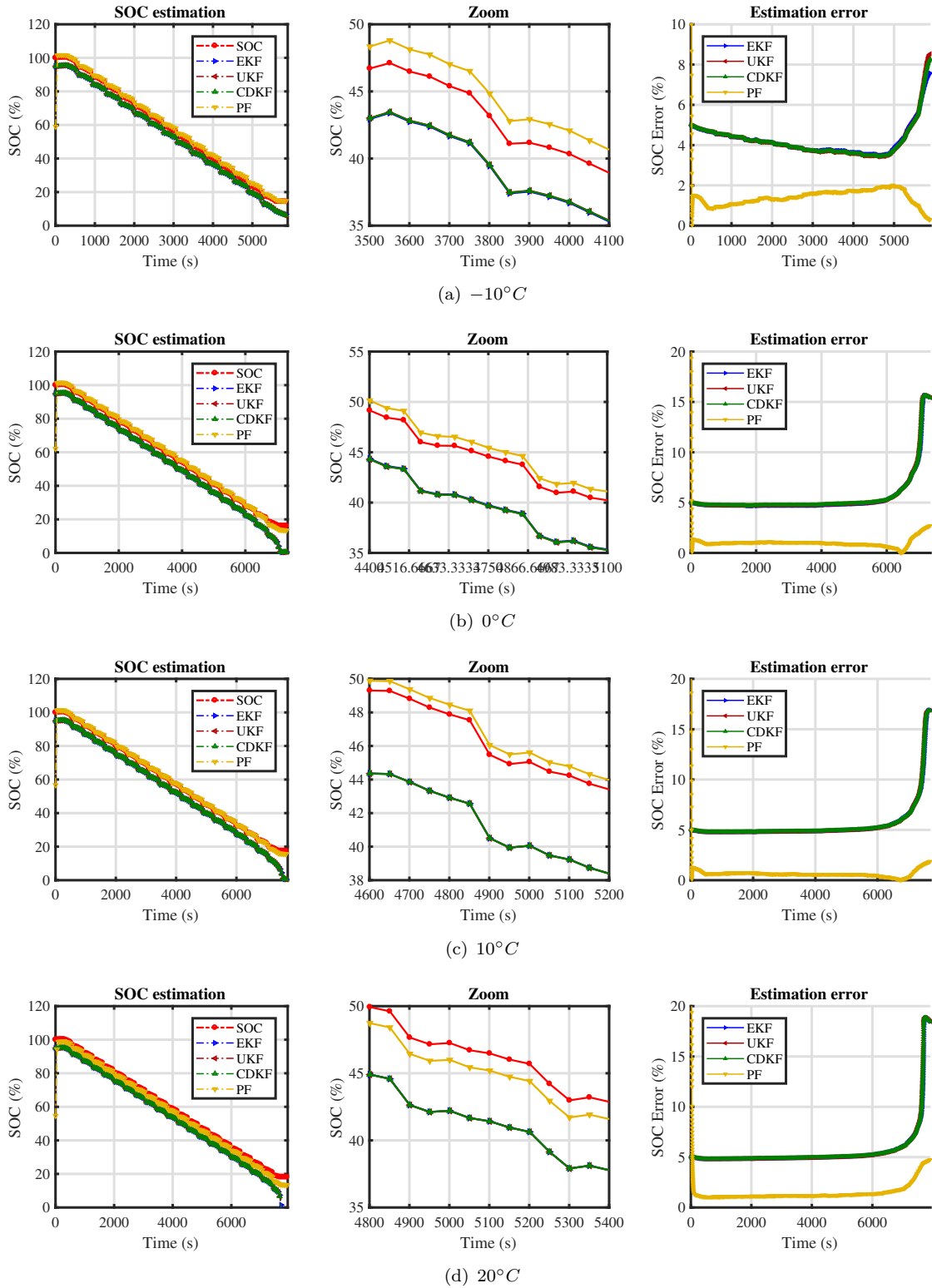


FIGURE 3.8: Estimation results of different adaptive KF assuming incorrect initial SOC value (a)  $-10^{\circ}C$  (b)  $0^{\circ}C$  (c)  $10^{\circ}C$  (d)  $20^{\circ}C$

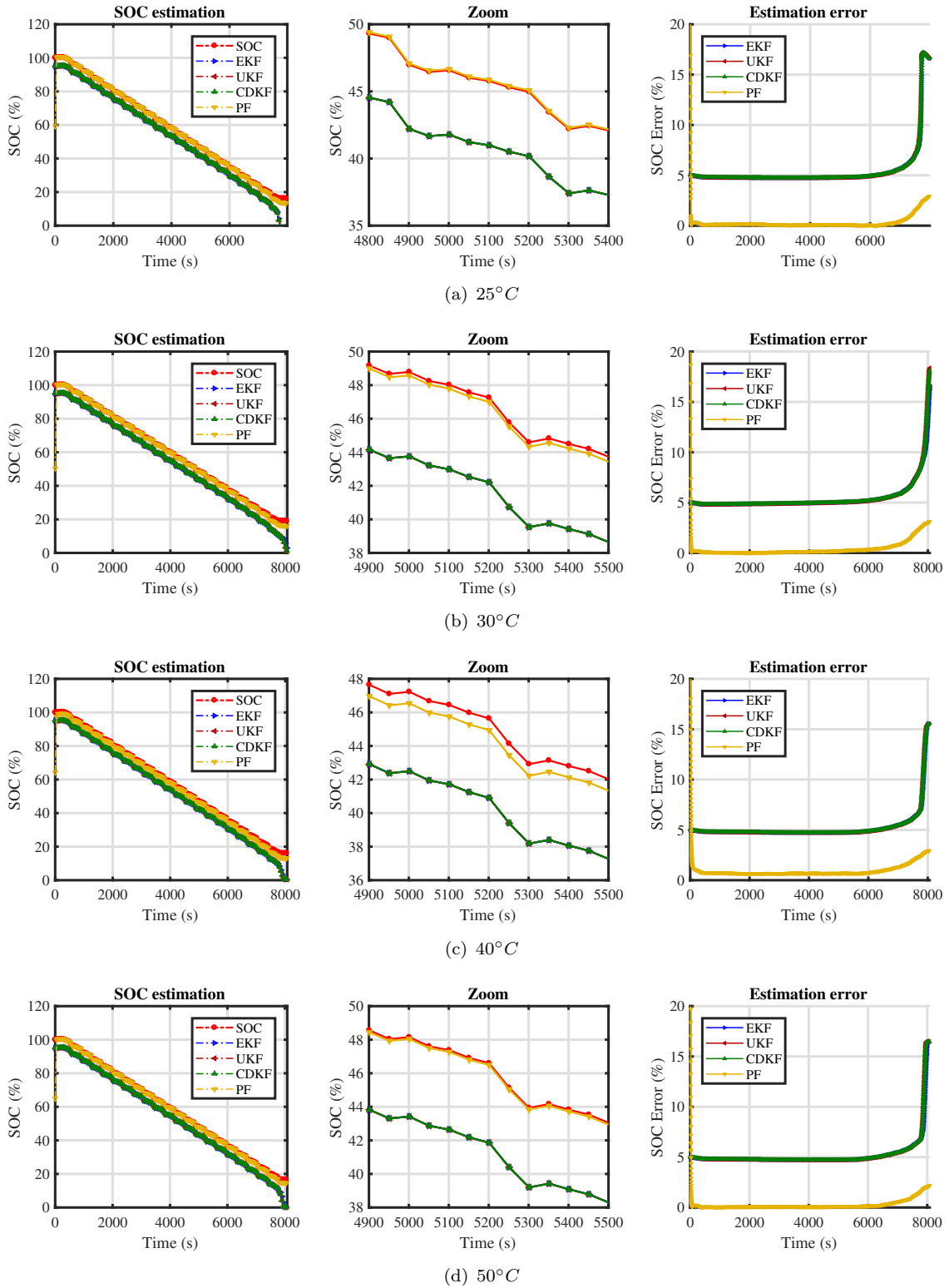


FIGURE 3.9: Estimation results of different adaptive KF assuming incorrect initial SOC value (a) 25°C (b) 30°C (c) 40°C (d) 50°C

SPKF is 3.6 sec and PF is 2.5 sec. Hence although the PF takes more computation cost, it is more robust than EKF to measure noise in the battery system.

The main drawback of Coulomb Counting method is that it depends upon initial SOC values in the estimation of current battery SOC value. If the initial values identification is not correct then estimated SOC values are not accurate. To identify the accuracy and efficiency of SOC estimation methods the effect of the incorrect initial SOC values is evaluated in this work. Estimated SOC values assuming incorrect SOC initial value from adaptive filters at various temperatures is illustrated in Figure 3.8 and 3.9. Similar to correct initial SOC values, the red color graph represents the true SOC value, while blue, brown, green and yellow graph represent the estimated SOC value using EKF, UKF, CDKF, and PF filters. Figure 3.8 and 3.9 contains SOC estimation values, zoom of SOC estimation graph and their errors in the estimated value for different temperatures. It can be observed from graphs that the estimated SOC value with incorrect initial SOC can track the true experimental SOC profiles more precisely PF. Maximum absolute SOC error value is 9% , 15% , 17% , 20% , 17% , 18% , 16% and 15% corresponding to  $-10^{\circ}C$ ,  $0^{\circ}C$ ,  $10^{\circ}C$ ,  $20^{\circ}C$ ,  $25^{\circ}C$ ,  $30^{\circ}C$ ,  $40^{\circ}C$  and  $50^{\circ}C$  respectively for EKF, UKF and CDKF estimation methods. Whereas for all the temperature maximum absolute SOC error is approximately less 4% in case PF estimation. Hence, SOC estimation based on PF yields accurate estimation of SOC for both correct and incorrect assumption of initial SOC values. The accuracy of other estimator decreases with the incorrect assumption of initial SOC values.

TABLE 3.6: Prediction error statistics at different temperature assuming incorrect initial SOC value

	RMSE				MAE			
	<b>EKF</b>	<b>UKF</b>	<b>CDKF</b>	<b>PF</b>	<b>EKF</b>	<b>UKF</b>	<b>CDKF</b>	<b>PF</b>
$-10^{\circ}C$	4.3076	4.3106	4.3058	<b>2.0533</b>	4.2392	4.2216	4.2238	<b>1.4838</b>
$0^{\circ}C$	5.9308	5.9890	5.9768	<b>1.7938</b>	5.5105	5.56106	5.5522	<b>1.0995</b>
$10^{\circ}C$	5.8593	5.8971	5.8864	<b>1.7136</b>	5.5108	5.5299	5.5248	<b>0.7214</b>
$20^{\circ}C$	6.1366	6.1799	6.1689	<b>2.6904</b>	5.6411	5.6630	5.6576	<b>1.6184</b>
$25^{\circ}C$	5.8978	5.9230	5.9154	<b>1.3986</b>	5.6411	5.6630	5.6576	<b>1.6184</b>
$30^{\circ}C$	5.5704	5.6820	5.6531	<b>1.8870</b>	5.4031	5.4492	5.4375	<b>0.5012</b>
$40^{\circ}C$	5.4584	5.4868	5.4786	<b>1.7253</b>	5.2189	5.2321	5.2281	<b>1.0051</b>
$50^{\circ}C$	5.4430	5.5418	5.5251	<b>1.3590</b>	5.2049	5.2504	5.2426	<b>0.3365</b>

The value of root-mean-square and mean absolute error for different estimator assuming incorrect initial SOC values are given in Table 3.6. From the table, it can be concluded that maximum root-mean-square error among all temperature for EKF is 6.13%, UKF is 6.17%,



CDKF is 6.16 %, and PF is 2.6%. Maximum mean absolute error among all temperature using EKF is 5.6 %, UKF is 5.66%, CDKF is 5.65%, and PF is 1.19 %. Hence, the precision of PF based estimation algorithm is higher than other algorithms as its execution doesn't depend on the initial values of SOC. The execution time for performing battery SOC estimation assuming incorrect initial SOC value is shown in Table 3.5. From the table, it can be concluded that the maximum execution time taken by EKF is 3.5 sec, UKF is 5.0 sec, SPKF is 3.9 sec and PF is 2.7 sec. This demonstrates that the PF can estimate the battery SOC with higher accuracy in less execution time with begin effect with initial values of the battery SOC.

TABLE 3.7: Execution time analysis (in secs) assuming incorrect initial SOC value

	<b>EKF</b>	<b>UKF</b>	<b>CDKF</b>	<b>PF</b>
$-10^{\circ}C$	2.3756	5.0729	3.1253	<b>1.9885</b>
$0^{\circ}C$	<b>2.5128</b>	2.8560	3.1434	2.8249
$10^{\circ}C$	3.4919	<b>2.4770</b>	3.0679	2.9406
$20^{\circ}C$	2.6106	2.5814	3.8407	<b>2.2680</b>
$25^{\circ}C$	2.6827	2.6363	3.8939	<b>2.5423</b>
$30^{\circ}C$	2.9738	<b>2.6230</b>	3.2060	2.7540
$40^{\circ}C$	2.6809	2.6483	3.9108	<b>2.3036</b>
$50^{\circ}C$	2.6404	3.3102	3.4300	<b>2.3752</b>

### 3.4.2 SOH estimation

Performance of the adaptive filters estimation techniques for prediction of RUL is discussed in this section. Four different batteries with same capacity has been utilize for analysis of capacity degradation behavior and effectiveness of the different estimation methods. Experimental data collected using lifespan test and exponential model of capacity degradation model is utilized for estimation process. Figures 3.10, 3.11, 3.12 and 3.13 visualizes predicted capacity using the exponential model utilizing different training data sets with different estimation techniques for batteries B1-B4 on different prediction cycles. In these graphs the green line indicates measured capacity data using life cycle test. The vertical line in each graph refers to the end of training samples after which capacity prediction performed using adaptive filters. The horizontal line in each graph refers the battery performance endpoint (EUL). To investigate the prediction performance of the models three different prediction points are used. Prediction points are defined as the cycle at which battery reaches 1/3, 1/2 and 2/3 of life cycle test data.

The prognostic results for battery B1 with 1/3 cycles ( $k_c = 187$ ), 1/2 cycles ( $k_c = 280$ ) and 2/3 cycles ( $k_c = 373$ ) data point of life-cycle datasets are used to update the model

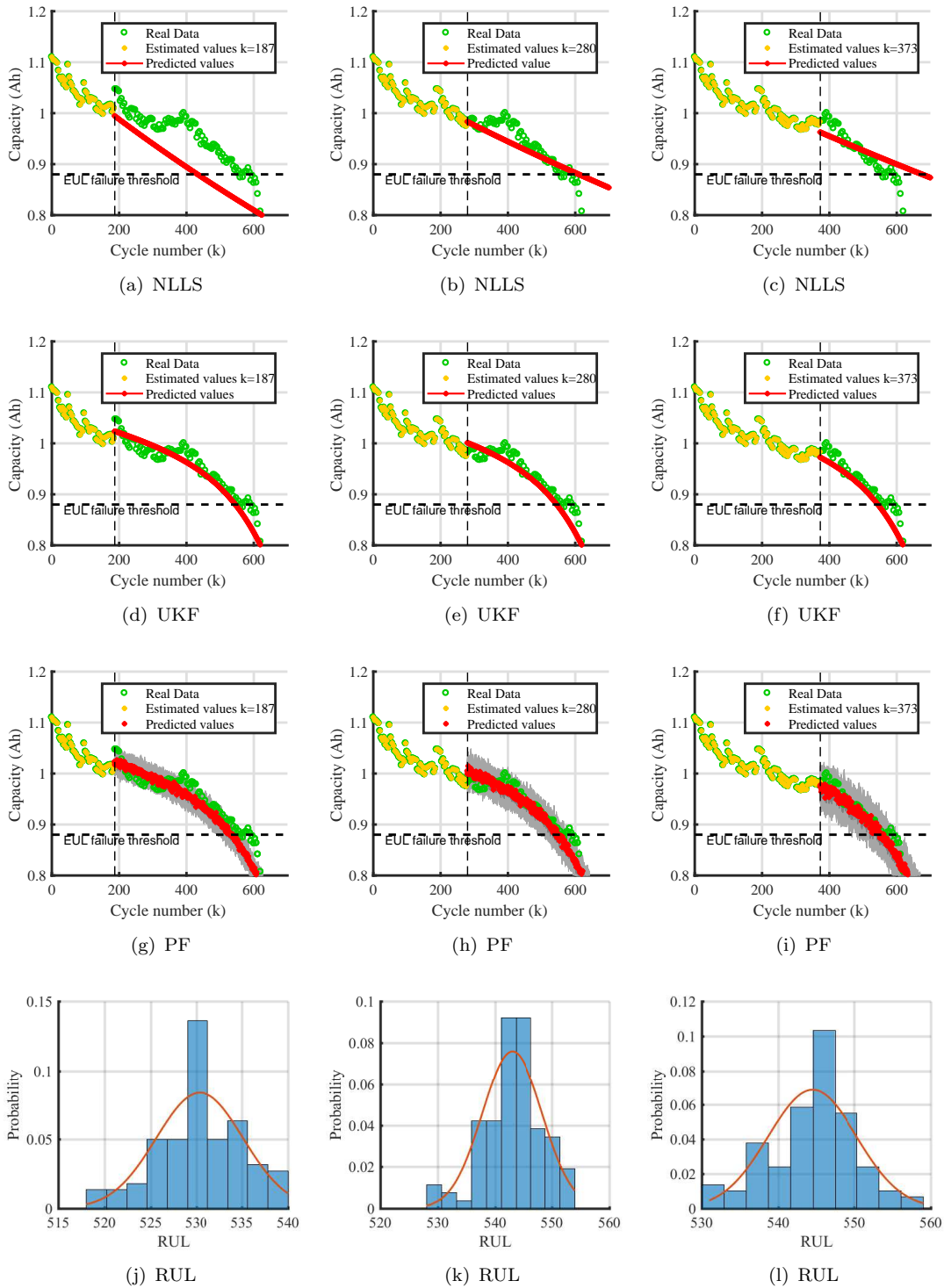


FIGURE 3.10: Comparison of RUL prediction results under different prediction point

using different estimation methods and probability distribution graph obtained from PF are shown in Figure 3.10 (a)-(d). Figure 3.10 (a) illustrate estimated capacity using NLLS

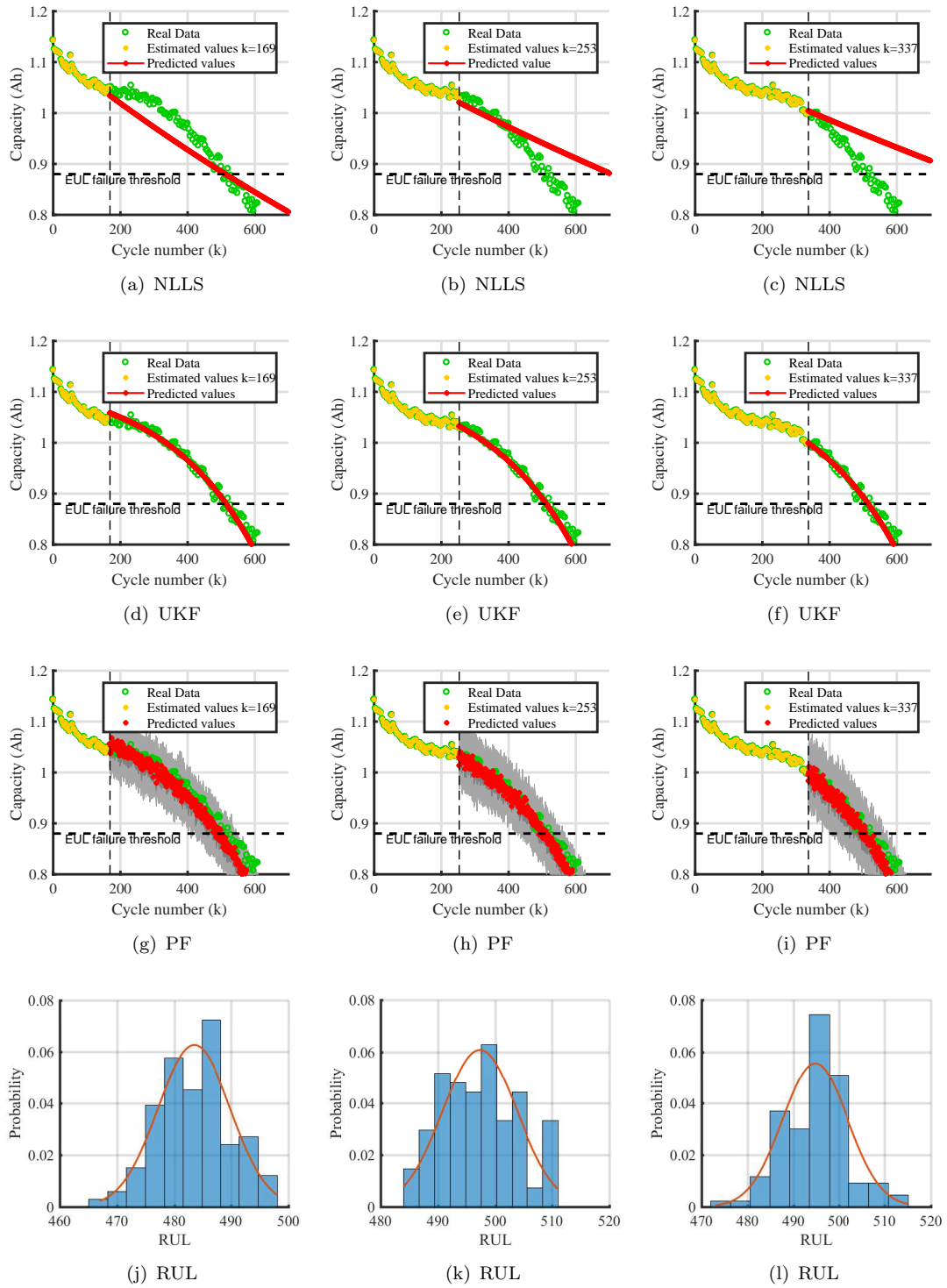


FIGURE 3.11: Comparison of RUL prediction results under different prediction point

with different training data sets. From graph it is concluded that with less training data sets NLLS provides very poor consistency in estimation. Where as with large training data

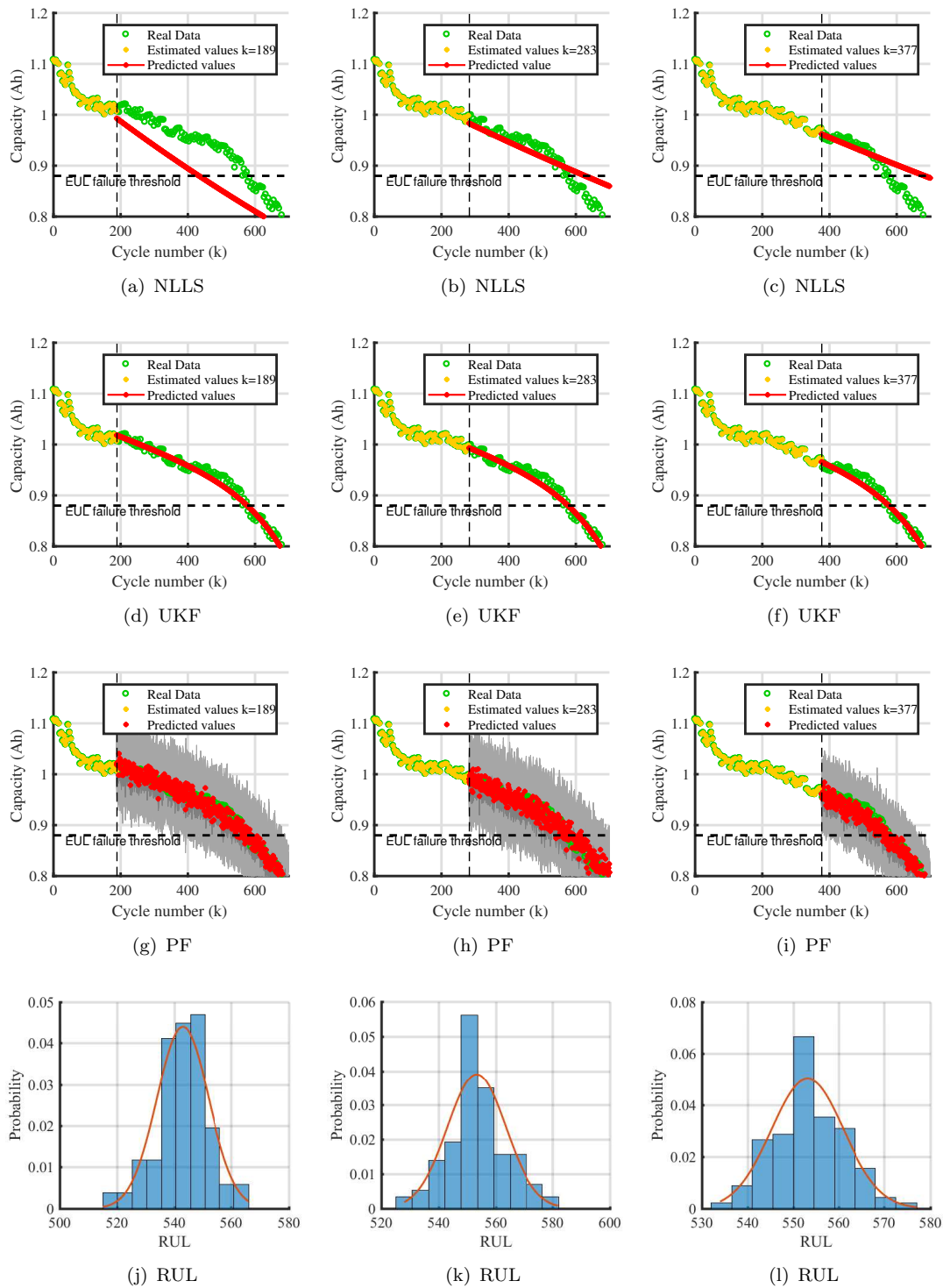


FIGURE 3.12: Comparison of RUL prediction results under different prediction point

also results are will poor as it can be seen through graphs that battery has been already reached to its EUL points where estimation still showing enough maximum capacity is

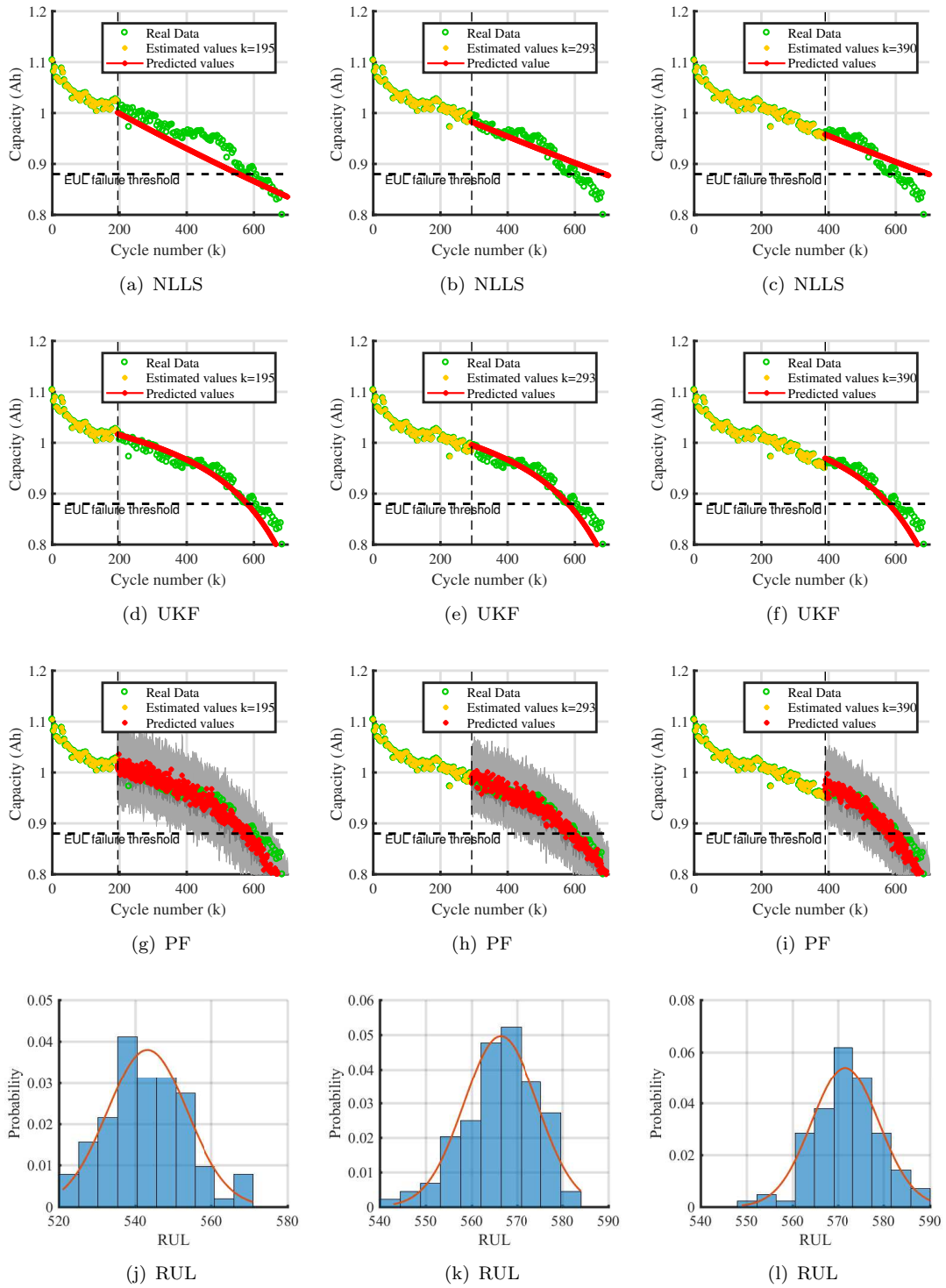


FIGURE 3.13: Comparison of RUL prediction results under different prediction point

available. Figure 3.10 (b) illustrate outcomes using UKF with different training data sets. From graph it is concluded UKF will provide approximately accurate estimation of

capacity. Similarly 3.10 (c) shows the distribution of particle for estimation of capacity and predicted capacity maximum capacity with each number of cycles with grey and red color respectively for different training data set. Advantage of particle filters is it provide more accurate estimation for all cycle values where as UKF diverted as from true capacity at some number of the cycles. Similarly Figure 3.11 shows prognostic results for the batteries B2 with the help of different data points of life-cycle test datasets for updating the model. Figure 3.11 (a) shows more clearly that NLLS is not appropriate for capacity estimation with all training data sets hence NLLS technique will be avoided for estimation of RUL of battery. Figure 3.11 (b) and (c) its clear that UKF and PF both are appropriate for estimation of battery maximum capacity with the variation of number of cycles. Figure 3.12 shows prognostic results for the batteries B3 with the help of different data points of life-cycle test datasets for updating the model. Different estimation methods are used are respective outcomes are shown in the graphs. Similarly prognostic results for B4 with different training datasets using NLLS , UKF and PF are shown in Figure 3.13. From all the analysis for capacity estimation for different batteries is concluded that UKF and PF provides accurate battery capacity estimation with the variations of number of cycles.

For analysis effectiveness of NLLS, UKF and PF in estimation of battery RUL comparison is shown in summarized in Table 3.8. Table contain information about actual failure cycle from datasets, prediction cycle, estimated failure cycle and prediction error. Actual failure cycle is the value of maximum battery capacity at EUL point for the capacity degradation data obtained from life-cycle test. Table show actual failure life for four batteries having same capacity and it can be seen that no two batteries will have same failure cycle number even they are manufactured identically because of variation in environmental conditions. Hence to identify SOH and RUL different of estimation are used. Prediction cycle is

TABLE 3.8: Performance comparison for RUL prediction using defined estimation methods

Battery ID	Real Failure cycle time	Prediction cycle (% cycle)	NLLS		UKF		PF	
			Cycle Number	Error	Cycle Number	Error	Cycle Number	Error
B1	560	187 (1/3)	434	126	546	14	533	27
		280 (1/2)	612	-52	546	14	546	14
		373 (2/3)	677	-117	545	15	551	9
B2	506	169 (1/3)	514	-8	516	-10	486	20
		253 (1/2)	708	-202	514	-8	492	14
		377 (2/3)	807	-301	516	-10	497	9
B3	566	189 (1/3)	435	131	578	-12	548	18
		283 (1/2)	629	-63	578	-12	542	24
		377 (2/3)	685	-119	578	-12	560	6
B4	585	195 (1/3)	556	29	581	4	568	17
		293 (1/2)	691	-106	581	4	574	11
		390 (2/3)	699	-114	580	5	574	11

value of cycle number at which estimation process for RUL is performed. Cycle at which battery reaches 1/3, 1/2 and 2/3 of life cycle test data are considered for calculating RUL at different cycle number. Prediction cycle values for different batteries are shown in the Table 3.8. Predicted RUL can be visualized as the cycle life from the end of the training sample till corresponding cycle at which battery capacity hits EUL line. Predication error is different between capacity values obtained from lifespan test and estimated capacity value at the EUL point. Predication error is shown in Table 3.8 having both value positive and negatives values. The positive error was showing that prediction on for battery EUL is before the actual occurrence of EUL whereas negative error showing that the prediction for EUL is after the actual EUL value. Early prediction of EUL will not affect battery, but prediction after EUL will cause catastrophic failures. It is concluded from Table 3.8 that predication error in case of NLLS and UKF are negative for most of cases hence NLLS and UKF are not suitable estimation techniques for prediction of RUL and SOH of the battery. Where as PF is having all positive value for predication error which shows that PF estimation battery failure way ahead hence replacement of battery can be performed by actually occurrence of it. PF particles probability distribution for prediction of RUL is assumed as Gaussian whose variance shown in Figure 3.10 (d), 3.11 (d), 3.12 (d) and 3.13 (d). This distribution is obtained from estimated values using by different particles in PF. For battery B1 estimation variance is 23 for 1/3 cycle , 24 for 1/2 cycle and 30 for 2/3 cycle data sets used for prediction. For battery B2 variances are 31 , 25 and 41 for training data set containing 1/3 cycle, 1/2 cycle and 2/3 cycle data points. Graph for probability distribution for battery B2 using PF is shown in Figure 3.11. Similarly of battery B3 and B4 probability distribution in prediction of RUL is shown in Figure 3.12 and 3.13 respectively for different training data points.

### 3.5 Chapter Summary

SOC estimation is the most significant function in battery management system which signifies residual range for recharge of battery and overcharge/overdischarge limit to enhance the life of battery. The contribution of this chapter is to systemically compare SOC based estimation strategies (EKF, UKF, CDKF and PF) in terms of SOC accuracy and individual advantages. Battery SOC for different operational conditions are identified and validated under DST driving cycle current profile. The comparison results confirmed at PF can be robust in practice as it provide the high estimation and prediction accuracy with the wrong initialized SOC values as well as correct initialized SOC. The results show that the PF can maintain simultaneously small errors and relatively fast computation time for real-time

applications compare to other non-linear filters. In addition, SOC estimation perform better at high temperatures than at low, hence a more accurate model to capture dynamics of battery at low temperature is worthy to investigate in future study. Battery aging leads to gradually deteriorates in battery capacity due to irreversible chemical changes while charging and discharging process. Degradation of battery capacity after threshold points causes insulation damage or catastrophic failures such as explosion and spontaneous combustion. In this chapter, two empirical model has been analyses for modeling battery capacity degradation over life-span of the battery. The exponential model inherently demonstrates the superiority in representing capacity degradation behavior compared to the polynomial model. Subsequently, the model has employed with NLLS, UKF and PF to deal with prediction of RUL of the battery. Three different datasets (1/3, 2/3 and 2/3 of the life cycle) are utilized for training, and remaining cycle datasets are utilized for prediction purpose. To address the uncertainties, a NLLS, UKF and PF approach was considered to adjust the model parameters and, hence, PF determined to be more accurate method to track the capacity fade. PF used state estimates from training data creating a diversity of particles. Adjustments were made to the weights of the particles, which affected the prediction PDF, but the state estimates were not changed from data available for predictions. The final RUL prediction can be obtained in the form of a probability density function so that the confidence level of the prediction can be assessed. Thus, the results demonstrate that PF provides the considerably accurate prediction of SOH and RUL with the less absolute error for different training datasets of all the batteries.







## Chapter 4

# Power management for EV Powered by Dual Battery System

### 4.1 Introduction

The use of clean energy in the transportation industry has gained substantial attention in the last two decades with the increase in fuel price and harmful gases emitted by burning fossil fuels in conventional vehicles. EVs emit no greenhouse gas, and hence they are a potential alternative to the internal combustion engine (ICEs) automobiles. However, the automobile industry had been limited to EVs with short range because of small battery capacity, long charging time, and lack of charging infrastructure. Nowadays, the advent of Li-ion batteries has reinforced the automobile sector to develop long-range EVs. Brands such as Mercedes Benz, Nissan, Tesla, Toyota, and others are developing EVs with the single sizeable Li-ion battery which leads to an oversizing of the battery and high initial cost. However, in [14] author suggested the concept of EV having two different size battery sources. Small size battery pack is fixed, and big size battery pack can be swape according to requirement. For short range, fixed small size battery is used which will reduce the mass of the EV and improve the energy consumption per unit distance. For more extended range, small size battery with swappable large size battery pack is utilized to power the drive train in the EV. The author has analyzed and evaluated the performance of proposed EV concept in comparison with single larger pack EVs and proved that there is a significant improvement in energy consumption ( up to 17 %), and economic benefits are achievable by distributing the cost of the large battery pack over the lifetime of the

vehicle. Benefits of using different size batteries encourage further studies in the development of power management systems for the dual battery-powered EVs. The core concerns of power management systems are to effectively provide energy from each battery source to match the power demanded and stored energy in the battery sources during regenerative braking. In this chapter, requested power computation for a given driving cycle has been performed with detail modeling of dual battery power EVs is presented in Section 4.2. In the literature, various power management strategies have been developed for hybrid EVs. On the basis of thorough analysis about different power management strategies, it could be concluded that rule-based power management approach has been commercially adopted due to its easy implementation and high computational efficiency. However, as any optimization is not involved, the optimal solution cannot be obtained. Optimization-based approaches overcome inherent drawbacks of rule-based approach through the implementation of optimization control procedure. Optimization-based approaches demand high computation power for real-time application. Practically, the hybrid power management strategy should be utilized which would not only have the optimal solution but also readily applicable to real-time control. In this chapter advanced and simple control rule-based meta-heuristic optimization power management strategies are developed to achieve optimal power distribution between dual battery sources while keeping the operation of battery in the defined safety region. The transition between the vehicle's operation modes has determined with the help of predefined rules based on the current operating condition. Whereas, the power-sharing between the two batteries determined by utilizing optimization based techniques. Problem formulation and architecture of the power management system for dual battery powered EV are presented in Section 4.3. Discussion on outcomes of the power management system is present in Section 4.4. The main conclusion and summary of the chapter has been given in Section 4.5.

## 4.2 Test bed system modeling

A small dimension EV based on Toyota S model 85D is considered as test-bed to investigate the power management strategies developed for the dual battery-powered EVs. The architecture of the power management system for dual battery powered EV is presented in Figure 4.1. In this test-bed modeling, the main components are two batteries for power supply, two bidirectional DC-DC converters for controlling each battery source, one power management system, propulsion motor drive and drivetrain of the EV. The calculation of power demanded from energy sources is evaluated using detail modeling of vehicle drivetrain in the present section.

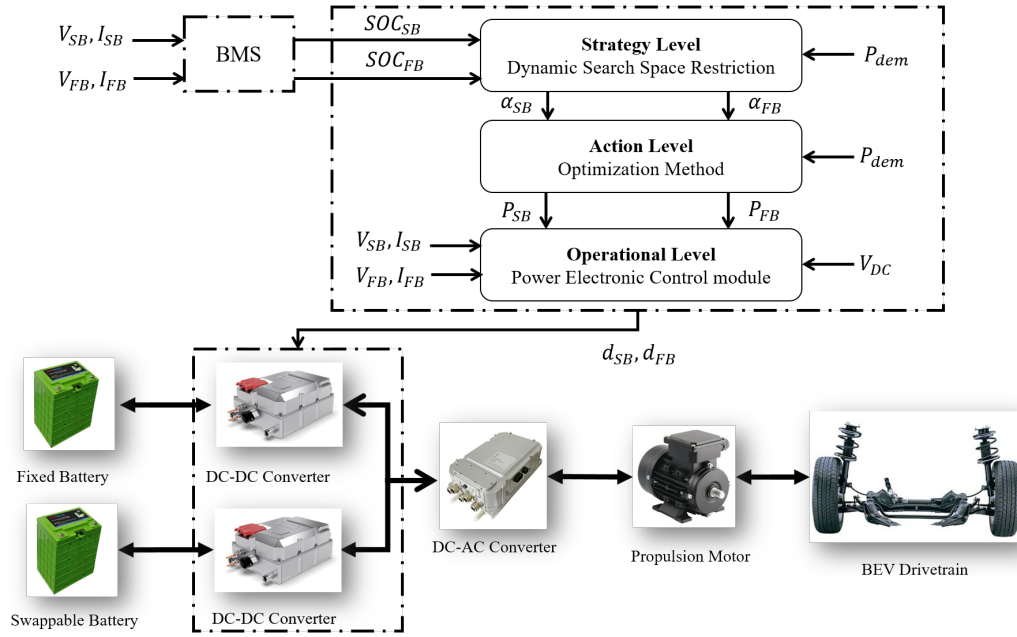


FIGURE 4.1: Architecture of the power management system for a dual battery powered EV platform

### 4.2.1 Drivetrain modeling

The EV dynamics work on the fundamental principle of physics, i.e., Newton's second law of motion. Newton's second law of motion states that the acceleration of an object produced by a net force is directly proportional to the magnitude of the net force. The first step in EV modeling to determine the value of resultant tractive effort applied by drivetrain to overcome the resistive forces which try to retard the motion of the EV. The tractive force ( $F_{te}$ ) produces enough momentum in the contact area between the tires and the road surface to drive the EV in the forward direction. The resistive forces that are influencing the movement of the EV along a slope shown in Figure 4.2. The resistive forces can be classified as follow: rolling resistance force ( $F_{rr}$ ), aerodynamic drag force ( $F_{ad}$ ), hill climbing force ( $F_{he}$ ), linear acceleration force ( $F_{la}$ ) and rotational acceleration force ( $F_{wa}$ ).

#### Rolling Resistance Force ( $F_{rr}$ )

The rolling resistance forces are the friction forces that arise when the tires of the EV rolls on the surface of the road. It is directly proportional to the weight of the EV hence its is approximately constant and does not depends on upon the speed of the EV. The equation for rolling resistance force can express as :

$$F_{rr} = \mu_{rr} g M_{ev} \quad (4.1)$$

Here  $M_{ev}$  represents the mass of EV which include curb and cargo weight [kg];  $g$  represents standard gravity constant [9.81 m/s<sup>2</sup>];  $\mu_{rr}$  refers to rolling resistance coefficient of the tires. The value of  $\mu_{rr}$  depends upon the type of tires and pressure exerted on the tires.

### Aerodynamic Drag Force ( $F_{ad}$ )

The aerodynamic drag forces are the friction forces that arise due to motion of EV through the air. It defined as the function of air density, shape, the frontal area of the EV and air passages. The equation for the aerodynamic drag force can be expressed as:

$$F_{ad} = \frac{1}{2} \times \rho_{air} \times A_{front} \times C_{drag} \times (\nu_{ev})^2 \quad (4.2)$$

Here  $A_{front}$  represents the cross-sectional area of the EV [m<sup>2</sup>];  $\nu_{ev}$  is the speed of EV [m/s];  $C_{drag}$  is a constant called the aerodynamic drag coefficient;  $\rho_{air}$  refers the density of the air [kg/m<sup>3</sup>] and air density depends on the variations of temperature, humidity and attitude. This thesis considers the value of air density to be 1.225 kg/m<sup>3</sup> which has been reported in the literature.

### Hill Climbing Force ( $F_{hc}$ )

The hill climbing force arises when EV drives upon slope. This force includes EV weight component acting along the direction of the slope. The equation for the hill climbing force can be expressed as:

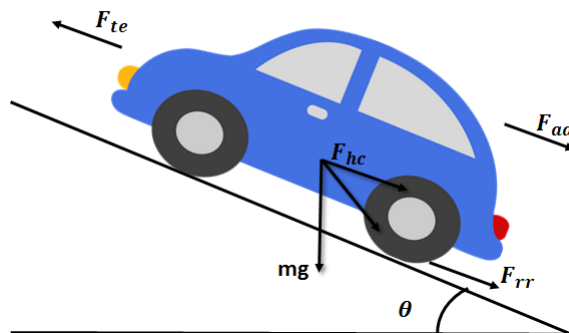


FIGURE 4.2: The resistive forces applied on a EV moving along a slope

$$F_{hc} = g \times \sin(\alpha_{gra}) \times M_{ev} \quad (4.3)$$

Here  $\alpha_{gra}$  refers the gradient of the road and all the other variables are same as defined in Section 4.2.

#### Linear Acceleration Force ( $F_{la}$ )

According to Newton's second law, if the vehicle velocity is changing, then it will generate a force in addition to the forces illustrated in Figure 4.2. This additional force will cause the linear acceleration of the vehicle. The equation for the linear acceleration force can be expressed as:

$$F_{la} = M_{ev} \times \frac{dv_{ev}}{dt} \quad (4.4)$$

#### Rotational Acceleration Force ( $F_{\omega a}$ )

In addition to linear acceleration in the EV, rotational acceleration is also required to be considered. Rotational acceleration force is applied for the faster angular rotation of the wheels. The equation for the rotational acceleration force can be expressed as:

$$F_{\omega a} = J \frac{G^2}{r_{wh}^2 \eta_g} \frac{dv_{ev}}{dt} \quad (4.5)$$

Here  $G$  refers the gear ratio of transmission system;  $r_{wh}$  refers the radius of wheel [m];  $\eta_g$  is efficiency of gear system and  $J$  refers propulsion motor rotor inertia.

#### Tractive Effort ( $F_{te}$ )

The Vehicle propulsion system must generate a tractive force ( $F_{te}$ ) to overcome rolling resistance force, aerodynamic drag force, hill climbing force, linear acceleration force and rotational acceleration force to accelerate the vehicle. The total tractive effort is the sum of all these forces:

$$F_{te} = F_{rr} + F_{ad} + F_{hc} + F_{la} + F_{\omega a} \quad (4.6)$$

When EV slows down then linear acceleration force and rotational acceleration force will consider as negative, and when the vehicle is coming down a slope, then hill climbing force will be considered as negative.

To accelerate the vehicle the required traction torque ( $\tau_{te}$ ) [ $Nm$ ] at wheels and angular speed ( $\omega_{wh}$ ) [ $rpm$ ] of the wheels can be intuitively computed as follow:

$$\tau_{te} = F_{te} \times r_{wh} \quad (4.7)$$

$$\omega_{wh} = \frac{60 \times \nu_{ev}}{2\pi r_{wh}} \quad (4.8)$$

If desired speed values are defined, then the torque values can be compute using vehicle dimensions and parameters data as listed in Appendix A.

#### **Traction power** $P_{te}$ [ $W$ ]

To estimate the total power requirement by drivetrain can be calculated by using the traction torque and angular speed (obtained from drive cycle)

$$P_{te} = F_{te} \times \nu_{ev} \quad (4.9)$$

A gear-box is placed in between the propulsion motor and the wheels to reduce the shaft torque  $\omega_s$  [ $rpm$ ] and to amplify the shaft torque  $\tau_{st}$  [ $Nm$ ]. The gear ratio is fixed during the operation; thus, shaft torque, shaft angular velocity, and power  $P_m$  [ $W$ ] of the propulsion motor can be expressed as:

$$\tau_{sh} = \begin{cases} \frac{\tau_{te}}{\eta_g \times G} & \text{if } P_{te} \geq 0 \\ \frac{\tau_{te} \times \eta_g}{G} & \text{if } P_{te} < 0 \end{cases} \quad (4.10)$$

$$\omega_{sh} = \omega_{wh} \times G \quad (4.11)$$

$$P_m = \frac{\pi}{30} \times \tau_{sh} \times \omega_{sh} \quad (4.12)$$

Here  $G$  represents transmission ratio of gear-box.

The electrical power demanded from sources can be computed from drivetrain mechanical power with taking into consideration the efficiencies of the propulsion motor ( $\eta_m$ ), the inverter ( $\eta_{VFD}$ ), and the dc/dc converter ( $\eta_{con}$ ). The requested power from energy sources



can be expressed as:

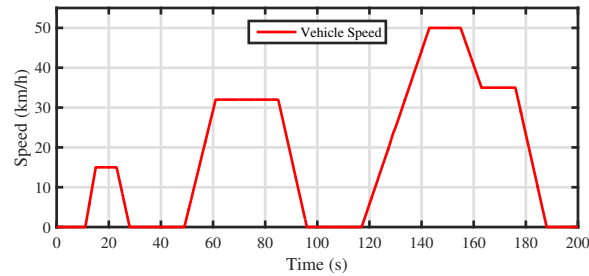
$$P_{dem}(t) = \frac{P_m(t)}{\eta_m(t) \cdot \eta_{VFD}(t) \cdot \eta_{con}(t)} \quad (4.13)$$

## 4.2.2 Driving cycle

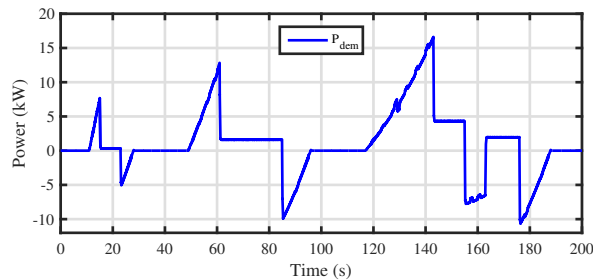
Power demanded by a drivetrain or power requested from the source as a function of time for ECE 15 urban driving cycles can be calculated using equation (4.9) and (4.13) respectively. The detailed specification about vehicle body, transmission units, dynamic and aerodynamics vehicle characteristics are given in Appendix A. In this work ECE 15 driving cycle speed profile  $\nu_{ev}(t)$ ,  $t \in [0, T_{dc}]$  with specified vehicle data are utilized to determine the power demanded  $P_{dem}$  by the considered EV. Vehicle speed profile and total power demanded from battery sources are shown in Figure 4.3. Detail parameters of ECE 15 driving cycles are given in Table 4.1.

TABLE 4.1: Driving cycles main parameters

Driving Cycle	Standing [%]	Driving [%]	Acceleration Speed [km/h]	Maximum Speed [km/h]	Total Distance [km]	Time [min]
ECE 15 [0 195]	23.08	76.92	18.4	50.07	5.968	19.5



(a)



(b)

FIGURE 4.3: The speed and power demand for EV for ECE 15

### 4.3 Power management system architecture

The primary objective of the power management system is to minimize the difference between power demanded and power supplied by the batteries while keeping the operation of batteries in a defined safety region and without degradation of their lifespan. The power management problem includes the real-time optimal power-sharing between two batteries promoting to the maximization of usage of batteries capacity while maintaining SOC of batteries at adequate levels. Another objective of power management problem is regulating the DC link voltage at desired values. These two problems can not be decoupled entirely and should be jointly tackled. To solve these problem power management system is proposed for the dual battery powered EVs. The hierarchy structure of the subsystems of integrated rule-based metaheuristic optimization power management approach is presented in Figure 4.1. The proposed power management system architecture consists of three management levels: strategic level, action planning level, and operation level. Initially, in strategic level the search space is recursively constraints based on a set of rules. These set of rules are developed on the basis of power demanded by EVs and present value of SOC in the batteries. Action layer is formulated to address real-time power-sharing optimization problems using metaheuristic techniques. The differential evolution metaheuristic is used to define an optimized power share without prior knowledge of power demand. In the operational level, strategies for development of duty cycle for DC-DC converters are presented. The reference power signal values for the controllers are obtained by optimizing the power management problem in action planning level. Before discussing the operation of each level in detail, problem formation for the power management system is done in the next subsection.

#### 4.3.1 Problem formulation

Batteries are the primary sources of power in proposed EV concept hence the overall objective of power management system is to know how to optimally split the required power between batteries in such a way that it leads to the maximization of usage of batteries capacity while maintaining SOC of batteries at adequate levels. The instantaneous power demanded by drivetrain is a linear combination of the instantaneously available power acquired from both the batteries. In the proposed power management system the equation for the fundamental power balancing equation can be expressed as:

$$P_{dem}(t) = \sum_{j \in SB,FB} P_j(t) \quad (4.14)$$

Here  $P_{dem}(t)$  refers to the power demanded by the drivetrain of the EV and  $P_j(t)$  refers to the power supplied from each of the battery where  $j$  is the specified battery.

The optimal quantity of the power supplied by each of the battery source for the given demanded power by drivetrain can be obtained by identifying optimal solution for equation (4.14). To limit the instantaneous power retrieves or supplied from each battery, a set of constraints is defined based upon the specification and characteristics of each battery. The set of constraints can be defined as:

$$P_j^{min} \leq P_j(t) \leq P_j^{max} \text{ with } j \in SB, FB \quad (4.15)$$

The power  $P_j(t)$  of each battery can be represented in terms of a power assignment factor  $\alpha_j(t)$

$$P_j(t) = \alpha_j(t) \cdot P_j^{max}; \alpha_j(t) \in [LB_j, HB_j] \quad (4.16)$$

Here,  $\alpha_j(t)$  power assignment factors are control variable in the power management optimization problem which applies constraints on the power supplied by the batteries.  $\alpha_j(t)$  varies between the lower and upper bound for the power sharing by the batteries.  $\alpha_j \in [-1, 0]$  means that the battery  $j$  will absorb power and  $\alpha_j \in [0, 1]$  means that the battery  $j$  will supply power.

### Objective function

The fundamental objective of the power management system is to optimally share the power demanded by the drivetrain of the EV. This objective can obtain by minimizing the difference between power demanded and power provided by each the battery source at each instant of time subjected to the constraints which establish the operation range defined by the practical limits of each battery. Mathematically it can be expressed as:

$$\text{minimize } |P_{dem}(t) - [\alpha_{SB}(t)P_{SB}(t) + \alpha_{FB}(t)P_{FB}(t)]| \quad (4.17)$$

$$\text{subject to : } \alpha_j \in [LB_j, UB_j]$$

$$P_j^{min} \leq P_j(t) \leq P_j^{max}$$

$$SOC_j^{min} \leq SOC_j(t) \leq SOC_j^{max} \text{ with } j \in SB, FB \quad (4.18)$$

For an online implementation of the power management problem, the constraints set  $\alpha_j$  must redefine in each iteration depending upon  $P_{dem}$  and current SOC of each battery. These set of constraints will restrict the search space to obtain the optimal solution for

the power management optimization problem. Then, optimization techniques are used to achieve optimal power-sharing by each battery to define the reference power signal values for controlling of DC-DC converters. Thereby, the power management problem has been subdivided into three levels, and each level is thoroughly discussed in next sections.

### 4.3.2 Strategy Level

The strategy level is related to restrict the search space by defining some sets of rules which are determined mainly by experience and expert knowledge. These sets of rules are designed to restrict the solution search space according to demanded power and the SOC values for the batteries at every instant of time by mapping of SOC into search space. The search space is restricted to help the optimization technique to determine a battery solution quickly by narrowing down the search space to the regions of interests. The solution search space is restricted by imposing lower and upper bound to power assignment factor  $\alpha_j(t)$ .

Displacement of the vehicle can be divided into the following phases: standing phase, an acceleration phase (light or high) and a deceleration phase. The sets of rules implemented with if-then operation rules as a function of demanded power  $P_{dem}$  and  $SOC_j$  using thresholds values defined by a fine-tuning process with complete knowledge of the characteristics and efficiency of the batteries are shown in Algorithm 8.

---

#### Algorithm 8 Set of rules for search space restriction scheme

---

- 1: **Rule 1 : Standing**
  - 2: **if**  $P_{dem} = 0$  **then**  $\alpha_{SB} \in [0, 0]$ ,  $\alpha_{FB} \in [0, 0] \Rightarrow$  **CASE A**
  - 3: **if**  $P_{dem} = 0 \cap SOC_{SB} > \tau_{SOC_{SB}}^{min} \cap SOC_{FB} < \tau_{SOC_{FB}}^{min}$  **then**  $\alpha_{SB} \in [0, 1]$ ,  $\alpha_{FB} \in [-1, 0] \Rightarrow$  **CASE B**
  - 4: **if**  $P_{dem} = 0 \cap SOC_{SB} < \tau_{SOC_{SB}}^{min} \cap SOC_{FB} > \tau_{SOC_{FB}}^{min}$  **then**  $\alpha_{SB} \in [-1, 0]$ ,  $\alpha_{FB} \in [0, 1] \Rightarrow$  **CASE C**
  - 5: **Rule 2: Light Acceleration**
  - 6: **if**  $P_{dem} > 0$  **then**  $\alpha_{SB} \in [0, 1]$ ,  $\alpha_{FB} \in [0, 1] \Rightarrow$  **CASE D**
  - 7: **if**  $P_{dem} > 0 \cap SOC_{SB} > \tau_{SOC_{SB}}^{min} \cap SOC_{FB} < \tau_{SOC_{FB}}^{min}$  **then**  $\alpha_{SB} \in [0, 1]$ ,  $\alpha_{FB} \in [-1, 0] \Rightarrow$  **CASE E**
  - 8: **if**  $P_{dem} > 0 \cap SOC_{SB} < \tau_{SOC_{SB}}^{min} \cap SOC_{FB} > \tau_{SOC_{FB}}^{min}$  **then**  $\alpha_{SB} \in [-1, 0]$ ,  $\alpha_{FB} \in [0, 1] \Rightarrow$  **CASE F**
  - 9: **Rule 3: Deceleration or Braking**
  - 10: **if**  $P_{dem} < 0$  **then**  $\alpha_{SB} \in [-1, 0]$ ,  $\alpha_{FB} \in [-1, 0] \Rightarrow$  **CASE G**
  - 11: **if**  $P_{dem} < 0 \cap SOC_{FB} < \tau_{SOC_{FB}}^{min}$  **then**  $\alpha_{SB} \in [0, 1]$ ,  $\alpha_{FB} \in [-1, 0] \Rightarrow$  **CASE H**
  - 12: **if**  $P_{dem} < 0 \cap SOC_{SB} < \tau_{SOC_{SB}}^{min}$  **then**  $\alpha_{SB} \in [-1, 0]$ ,  $\alpha_{FB} \in [0, 1] \Rightarrow$  **CASE I**
- 

To understand the underlying rationale for the each given set of rules based on expert knowledge corresponding power flow, SOC map and constrained search space are shown

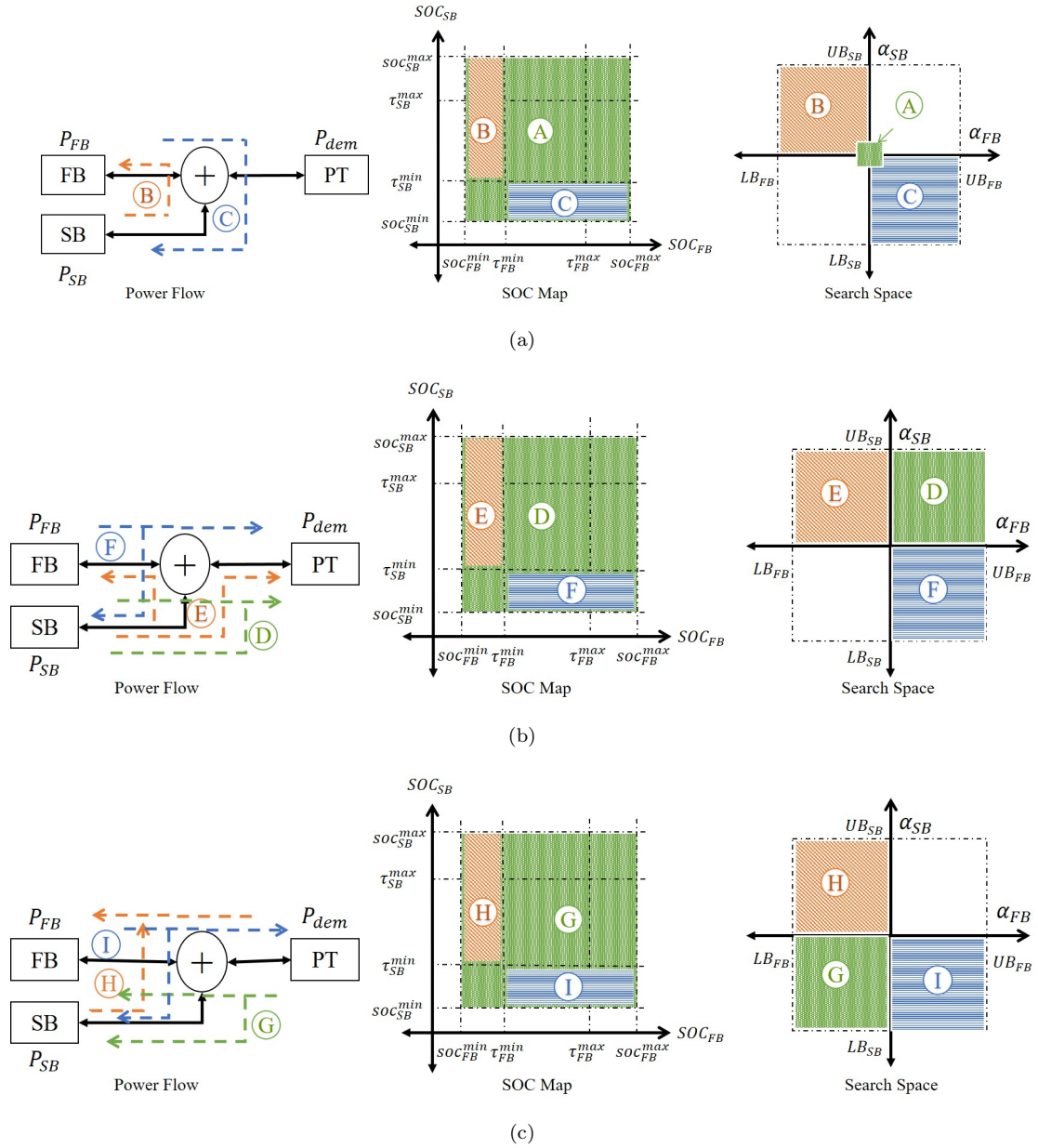


FIGURE 4.4: Rules for strategy planning level

in Figure 4.4. Figure 4.4(a) presented power flow direction, SOC map and constrained search space corresponding to rule 1 for the standing mode of EV. According to rule 1, three cases (A,B,C) are considered depending upon  $P_{dem}$  and SOC values of batteries. Case A states that when there is no power demand  $P_{dem} = 0$ , and both the batteries have high SOC value, then the search space will be reduced to  $\alpha_j \in [0, 0]$ . Hence, nothing will happen if both the batteries are well charged, and there is no power required by the drivetrain. Whereas for the same power demand if the SOC value for the fixed battery

$SOC_{FB}$  is below the threshold value  $\tau_{SOC_{FB}}^{min}$  while swappable battery is still have enough energy i.e. ( $SOC_{SB} \geq \tau_{SOC_{SB}}^{min}$ ) then the search space is defined to  $\alpha_{SB} \in [0, 1]$  and  $\alpha_{FB} \in [-1, 0]$  (see Case B). This means the swappable battery will charge the fixed battery to enable future acceleration requiring power peak to be supplied by the fixed battery. Inversely, when the fixed battery have high SOC value  $SOC_{FB}$  then the search space is restricted to  $\alpha_{SB} \in [-1, 0]$  and  $\alpha_{FB} \in [0, 1]$ . Hence, the fixed battery will discharge to the swappable battery for leveling the SOC values so that it could charge during braking model of operation of the EV. Figure 4.4(b) presented power flow direction, SOC map and constrained search space corresponding to rule 2 for the light acceleration mode of EV. According to rule 2, three cases (D, E, F) are considered depending upon  $P_{dem}$  and SOC values of batteries. Case D states that when there is power demand  $P_{dem} > 0$ , then the search space will be reduced to  $\alpha_j \in [0, 1]$ . Hence, both batteries will be utilized to supply the demanded power. Whereas for the same power demand if the SOC value for the fixed battery  $SOC_{FB}$  is below the threshold value  $\tau_{SOC_{FB}}^{min}$  while swappable battery is still have enough energy i.e. ( $SOC_{SB} \geq \tau_{SOC_{SB}}^{min}$ ) then the search space is defined to  $\alpha_{SB} \in [0, 1]$  and  $\alpha_{FB} \in [-1, 0]$  (see Case E). This means the swappable battery will supply the demanded power by charging the fixed battery to enable future acceleration requiring power peak to be supplied by the fixed battery. Inversely, when the fixed battery have high SOC value  $SOC_{FB}$  then the search space is restricted to  $\alpha_{SB} \in [-1, 0]$  and  $\alpha_{FB} \in [0, 1]$ . Hence, the fixed battery will supply the demanded power by charging the swappable battery. Figure 4.4(c) presented power flow direction, SOC map and constrained search space corresponding to rule 3 for the declaration or braking mode of EV. According to rule 3, three cases (G, H, I) are considered depending upon  $P_{dem}$  and SOC values of batteries. Case E states that when there is regenerative power  $P_{dem} < 0$  due to braking, then the search space will be reduced to  $\alpha_j \in [-1, 0]$ . Hence, both batteries will be utilized to store the power generated from braking. Whereas for the same generated power if the SOC value for the fixed battery  $SOC_{FB}$  is below the threshold value  $\tau_{SOC_{FB}}^{min}$  then the search space is defined to  $\alpha_{SB} \in [0, 1]$  and  $\alpha_{FB} \in [-1, 0]$  (see Case E). This means the fixed battery will be charged from regenerative braking and swappable battery. Inversely, when the swappable battery is below the threshold value  $SOC_{SB}$  then the search space is restricted to  $\alpha_{SB} \in [-1, 0]$  and  $\alpha_{FB} \in [0, 1]$ . Hence, the swappable battery will be charged from regenerative power.

### 4.3.3 Action Planning Level

The primary objective of action planning level of global power management system is to feed the power request of EV with available energy continuously.

This level can be implemented by using optimization techniques having objective function defines as the online power-sharing between both the batteries under the strict guidelines developed by the power management system in strategy level. The aim of the action planning level is to supply the demanded power without any interruption and reduced degradation of batteries lifespan. Action planning level produces a set of the decisions within the operation region constrained by strategy level depending upon power demanded and SOC values of batteries. Therefore, action planning level determines the references power signals to control the converters operations in the operational level of the power management system. In this research work, the DE optimization approach has been implemented to obtain the optimal solution for the formulated problem. Pseudo-code for implementation of DE optimization technique is presented in Algorithm 4 of Chapter 2. The objective function for power sharing is defined using equation (4.17). The initial solution considered for implementation of optimization is  $\alpha_{SB}(t) = \alpha_{FB}(t) = 0$ . Depending on the demanded power and SOC of each battery the power management systems reduce the search space for optimization technique. The process of reducing search space will increase the speed of optimization techniques. When the solution is converged to the optimal solution optimization techniques will stop and provides reference power signals of operational level.

### 4.3.4 Operation Level

The operational level of power management system deals with dynamics and operations of power electronics converters used in the dual battery powered EV. Power flow of each battery sources is controlled by the individual bi-directional DC-DC converter for each of them. The function of converters is to step up the input voltage and control the power flow from each battery. The proposed control management for each DC-DC converters is shown in Figure 4.5. The reference signals for controlling the converters are the set points for the DC-link voltage and the swappable battery pack current. The controller for the fixed battery is composed by a double loop controller with the combination of current and voltage controllers, and for swappable battery, only current controller is used. The double loop controller having a voltage controller as the outer loop will maintain constant DC link voltage depending upon nature of the loads, i.e., voltage fed drive for the electric

motor. Hence, voltage controller regulates the DC link voltage ( $V_{DC}$ ) to a constant voltage reference value ( $V_{DC}^{REF}$ ). Current controllers in both the controlling blocks control the current flow in the battery by means of proportional integral controllers which develop pulses for triggering of the gates with duty-cycles ( $d_{SB}$ ) and ( $d_{FB}$ ) for swappable and fixed battery respectively.

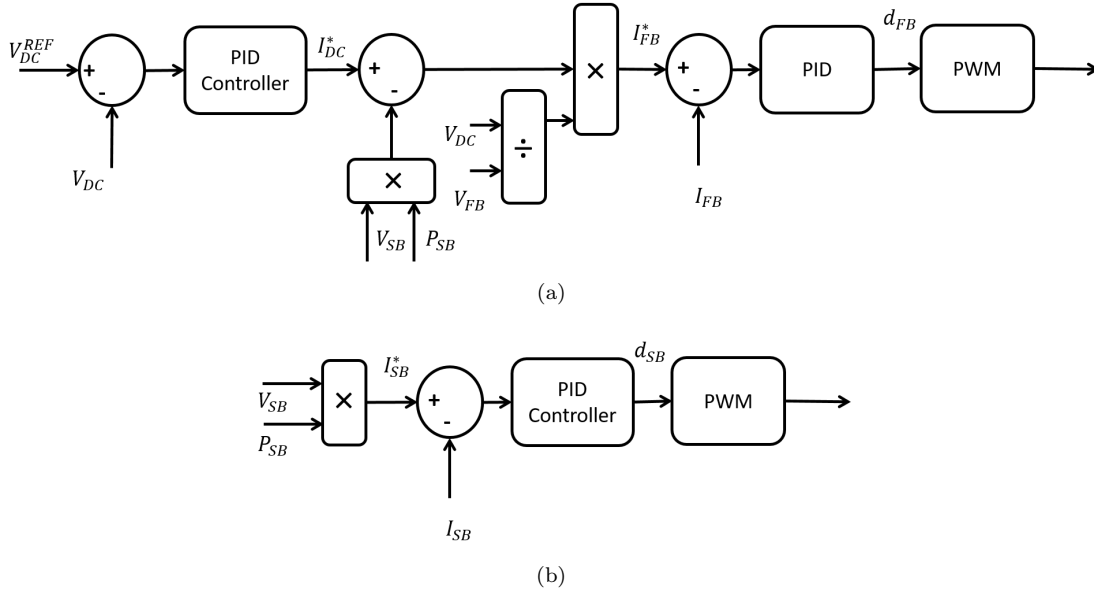


FIGURE 4.5: Controlling strategies for DC-DC converter (a) Fixed battery (b) Swappable battery

## 4.4 Results and Discussion

Dual battery powered EV testbed system based on the specification of Tesla Model S with the Power management system has been implemented in MATLAB/Simulink as shown in Figure 4.6. Simulink model contains three main blocks: one block for power management systems, one for electrical components and one for mechanical components of considered EV. The detail specification for vehicle model and both the batteries are given in Appendix A. The reference load for simulated EV is defined by an ECE 15 driving cycle. Proposed dual battery power management algorithm is validated by obtaining simulation outcomes for the ECE 15 driving cycle with different initial SOC values of the batteries. Three different initial values of SOC's considered for testing and validation purpose are

- **Case I:** When SOC of both battery are same
- **Case II:** When  $SOC_{SB} > \tau_{SOC_{SB}}^{min}$  and  $SOC_{FB} < \tau_{SOC_{FB}}^{min}$

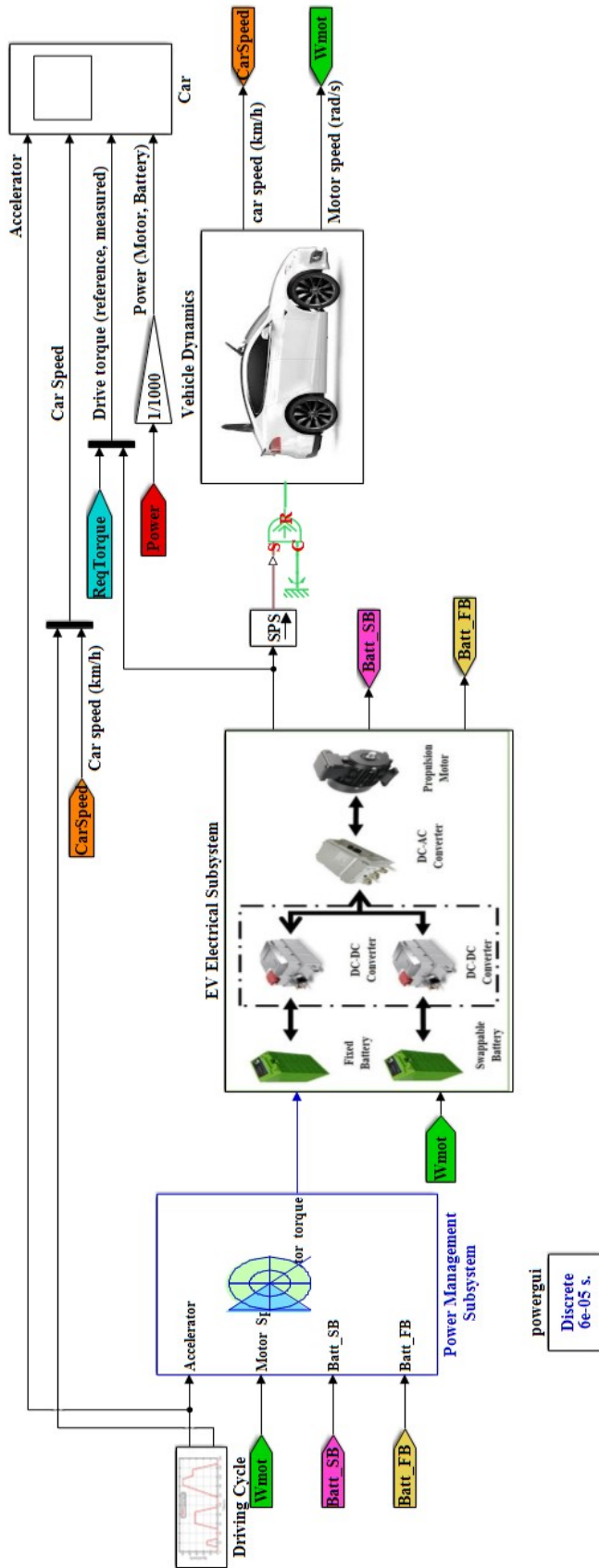


- **Case III:** When  $SOC_{SB} < \tau_{SOC_{SB}}^{min}$  and  $SOC_{FB} > \tau_{SOC_{FB}}^{min}$

The SOC threshold values were set as:  $\tau_{SOC_{FB}}^{max} = 0.85$ ;  $\tau_{SOC_{FB}}^{min} = 0.35$ ;  $\tau_{SOC_{SB}}^{max} = 0.85$ ;  $\tau_{SOC_{SB}}^{min} = 0.35$ . Power management for dual battery powered EV is performed with unknown demanded power until the end of the cycle. In all simulations, the DE algorithm was parameterized with  $N_{cycles}=30$ . The control parameters of DE optimization techniques have been tuned after extensive experimentation. For tuning purpose, present SOC of each battery is considered. Figures 4.7 , 4.8 and 4.9 represents the results for ECE 15 cycle with different initial SOC values. These figures present the results for powers sharing, SOC's evaluation, strategy level cases histogram, and power assignment factors.

### Case I: When SOC of both battery are same

The ECE 15 driving cycle power-sharing decompositions between dual battery sources when the initial SOC's values are equal i.e.  $SOC_{SB} = SOC_{FB} = 60\%$  is presented in Figure 4.7 (a). Simulation of ECE 15 driving cycle begins with  $P_{dem} = 0$ , and as both the batteries are above the specified minimum threshold, then strategy level defines these conditions as CASE A. Accordingly, the DE optimization techniques restricted the search space where the solutions correspond to no power flow through the drivetrain. This aspect is clear in the first part of the power-sharing graph. Hence when there is no demand power and both the batteries SOC are above the specified minimum threshold, there will be no change in SOC values also. The next EV operations are acceleration; now the strategy level defines search space for DE optimization techniques referring to CASE D. Power demanded by drivetrain is supplied by both the battery sources as above are having sufficient SOC's. When there is power demanded and both batteries are having sufficient SOC's then power is supplied by both of them with the same discharging rates. The objective of using both battery source for supply demanded power is to avoid the burden on single battery source because if the single battery is used to supply the power, it will discharge at the high current rate compared with when both the batteries are used. The low discharging rate will increase the battery lifespan. It is clear from Figure 4.7 (b) that both the batteries sources are discharging with approximately same discharge rate hence one single battery is overburdened. After acceleration, EV will operate in deceleration mode for the given driving cycle. During deceleration, the strategy level restricts search space for DE optimization techniques referring to CASE G. During regenerative braking, both batteries are charged at same rate. The previously defined case will repeat in the next displacement for given driving cycles since the battery SOC will remain above the threshold. The



The 'Ts' parameter used in this model is set to 6e-5 by the Model Properties Callbacks

FIGURE 4.6: Dual battery powered EV in MATLAB/Simulink

variation of operation cases depending on power demanded by the drive train and SOC values of each source are shown in Figure 4.7 (c). The graphical representation of the power assignment factor depending on restricted search space computed by the power management system is presented in 4.7(d).

**Case II: When  $SOC_{SB} > \tau_{SOC_{SB}}^{\min}$  and  $SOC_{FB} < \tau_{SOC_{FB}}^{\min}$**

The ECE 15 driving cycle power-sharing decompositions between dual battery sources when the initial SOC values for sizeable swappable battery is higher than minimum threshold value, i.e.,  $SOC_{SB} = 80\%$  and initial SOC values for fixed small battery is less than minimum threshold value, i.e.,  $SOC_{FB} = 30\%$  is presented in Figure 4.8 (a). At the beginning of the ECE 15 driving cycle, the assumption that the fixed battery SOC will be below minimum threshold leads the strategy level to guide the DE optimization technique differently from the previous cases simulations. For this case, strategy level reduces the search space for implementation of DE optimization to the region designated as CASE B in Figure 4.4. At standing mode, when there is no power demand swappable battery will charge the fixed battery pack so that both of them can be utilized when power demanded by EV to maintain the low discharging rate. Whereas in Case I for the standing condition of the EV strategy level define CASE A depending on the SOC condition of the batteries. The DE optimization technique decides to charge fixed battery using swappable battery such that  $SOC_{SB}$  reduces and allows storing of the power in the next regenerative braking mode. In the cruising phases strategy level reduces the search space to the region defined by CASE E in Figure 4.4 where as for Case I it was CASE D in the simulation for the same time interval. The DE optimization technique decides to supply demanded power using swappable battery because it is having sufficient SOC values to maintain the power flow. In the regenerative braking compared to last Case I strategy level to restrict the search space to the region defined by CASE H. In this mode, fixed battery is charged using regenerative braking power because its SOC level is less than the minimum threshold value. For the ECE 15 driving cycle in the given time interval same cases will repeat for all next standing, acceleration and regenerative braking mode. The variation of operation cases depending on power demanded by the drive train and SOC values of each source are shown in Figure 4.8 (c). The graphical representation of the power assignment factor depending on restricted search space computed by the power management system is presented in 4.8(d).

### Case III: When $SOC_{SB} < \tau_{SOC_{SB}}^{\min}$ and $SOC_{FB} > \tau_{SOC_{FB}}^{\min}$

In this case, the ECE 15 driving cycle power-sharing decompositions between dual battery sources is different with the last section. In this section, the initial SOC values for swappable battery is lower than minimum threshold value, i.e.,  $SOC_{SB} = 30\%$  and initial SOC values for fixed small battery is higher than minimum threshold value, i.e.,  $SOC_{FB} = 80\%$ . Simulation results for powers sharing, SOC evaluation, strategy level cases histogram, and power assignment factors for this CASE are presented in Figure 4.9. In this case, for standing mode strategy level restrict the search space to the region designated as CASE C in Figure 4.4. Since the SOC of swappable battery is less than the minimum threshold value, it will get charge from small battery to supply the demanded power in acceleration mode with low discharging rate. Otherwise full power demand by drivetrain will be supplied by small battery at high discharging rate. Discharging with high current rate will decrease the life of the battery. Other reason is for reducing fixed battery SOC level is to allowing storing of the excess power in the regenerative braking mode. In the cruising phases, strategy level reduces the search space to the region defined by CASE F in Figure 4.4 bases of which the DE optimization technique decides to supply demanded power using fixed battery because of higher SOC level to maintain the power flow. In the regenerative braking strategy level restrict the search space to the region defined by CASE I. In this mode, swappable battery is charged using regenerative braking power because its SOC level is less than the minimum threshold value. For the ECE 15 driving cycle in the given time interval same cases will repeat for all next standing, acceleration and regenerative braking mode. The variation of operation cases depending on power demanded by the drive train and SOC values of each source are shown in Figure 4.9 (c). The graphical representation of the power assignment factor depending on restricted search space computed by the power management system is presented in 4.9 (d).

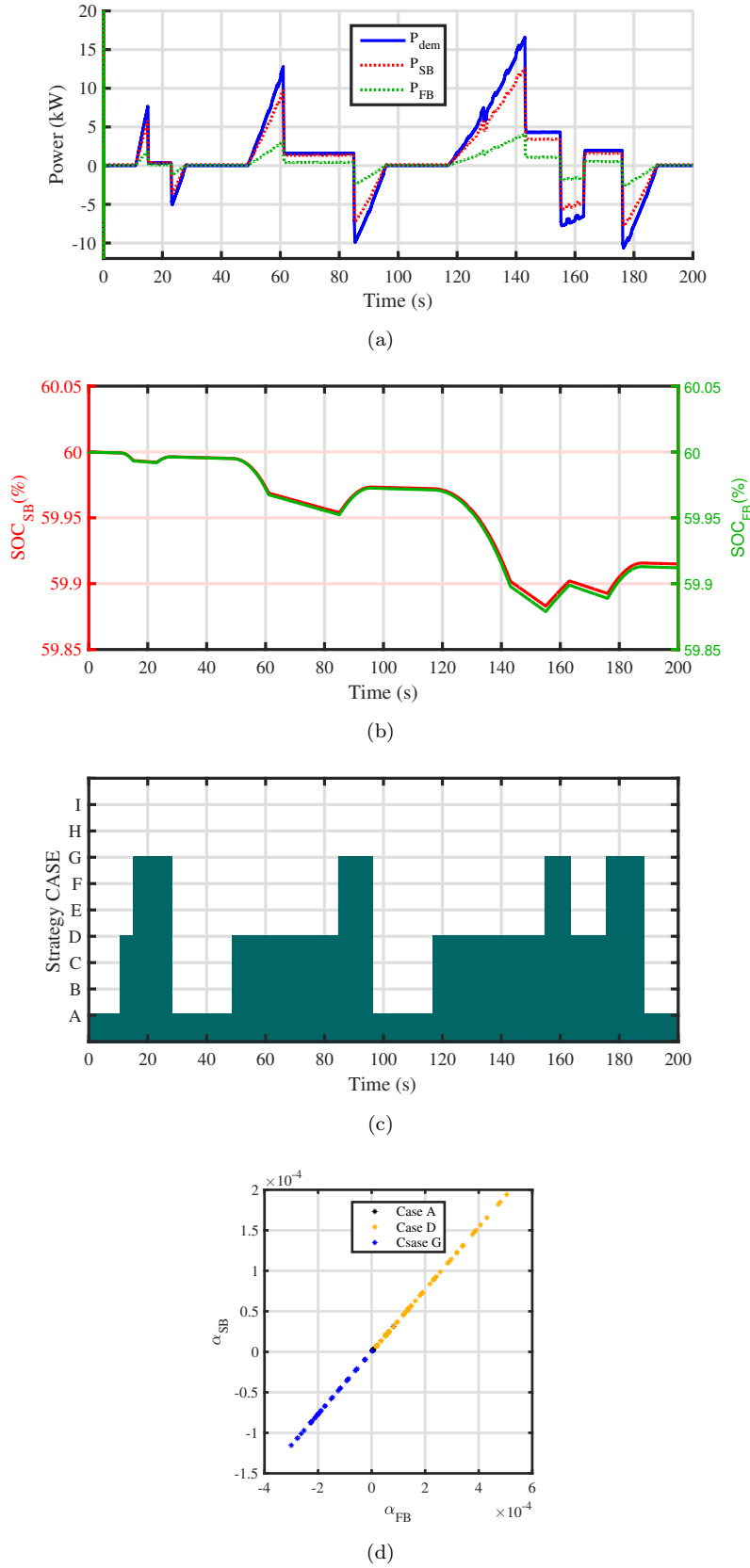
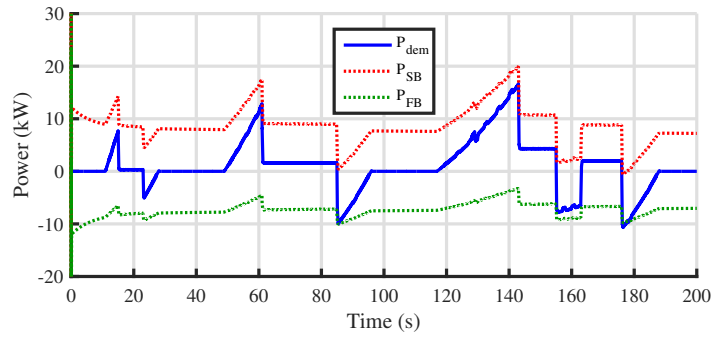
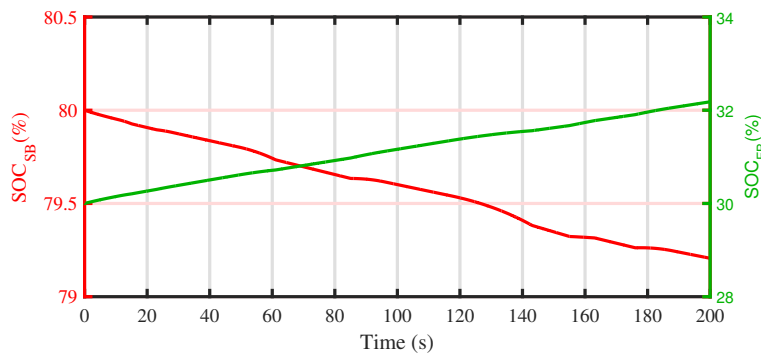


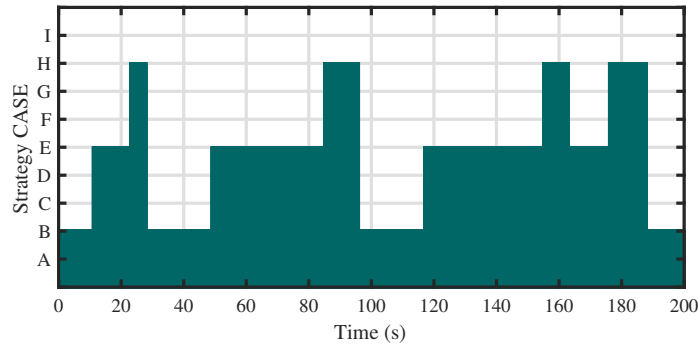
FIGURE 4.7: ECE 15 driving cycles results for initial SOC values  $SOC_{SB} = 60\%$  and  $SOC_{FB} = 60\%$



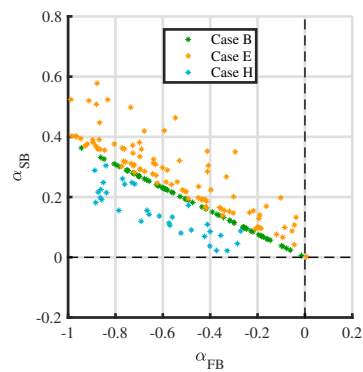
(a)



(b)



(c)



(d)

FIGURE 4.8: ECE 15 driving cycles results for initial SOC values  $SOC_{SB} = 80\%$  and  $SOC_{FB} = 30\%$

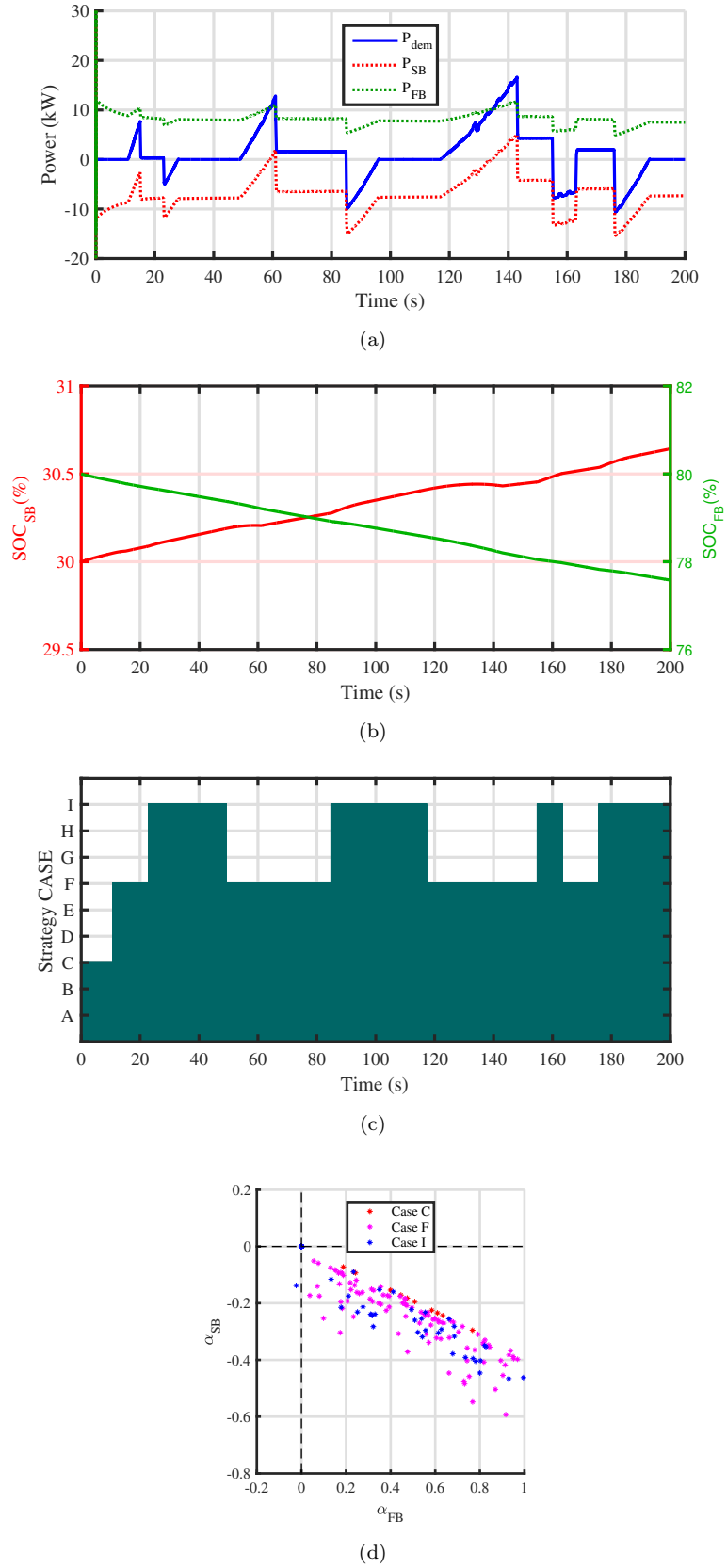


FIGURE 4.9: ECE 15 driving cycles results for initial SOC values  $SOC_{SB} = 30\%$  and  $SOC_{FB} = 80\%$

## 4.5 Chapter Summary

This chapter proposes a rule-based heuristic optimization power management system for optimally sharing demanded power between the batteries in the dual battery powered EVs. In this approach, three level power management scheme has been formulated based on strategy, action planning and operational levels. Firstly, strategy level restricted the search space using a sets of rules and in action level this search space is utilized to identify the reference power signals for controlling bidirectional converters used for given power sources. In operational level, DC-DC converters are used to control the power supply from each batteries depending on the demanded power. Validation of proposed power management system tested for normalized ECE 15 driving cycle depending on different initial SOC conditions. The simulation results prove the effectiveness of the proposed power management system with allowing to fulfill the demanded power requirement among the both the batteries. The power management system avoid the burden on single battery for long distance, it share load among both the batteries with equal charging and discharging rates. Low charging rate and discharge rate compared to single battery will increase the life of batteries. Development of effective power management system help in increasing range of batteries for extended range and increase the probability of using dual battery powered EVs. Since Dual battery powered EVs have less weight for short range which will also increase their battery life and long range covered compared to single large size battery.



## Chapter 5

# Conclusions and Future Scope

### 5.1 Major Contributions of this Study

1. For enhancement of the functionality of battery management system, key issues such as parameter estimation, SOC estimation, RUL prediction and health assessment were analyzed.
2. Estimation of unknown battery parameters can be performed by utilizing the terminal voltage data provided by manufacturers considering parameter estimation as an optimization problem. Effects of C-rate, SOC and temperature were considered to develop a practical and accurate model of battery.
3. The performances of applied optimization techniques are compared in terms of their ability and accuracy in the extraction of the battery model parameters with a lower convergence rate. For the model, GWO and ASMO optimization techniques proved to be more robust, reliable and gave an optimal solution in both charging and discharging scenarios. The lower mean fitness value (charging: 0.699/discharging: 0.298) and standard deviation (less than 1) of the ASMO proved its superiority in battery parameter estimation. For precise statistical investigation of computational intelligence algorithms, parametric (T-test) and non-parametric tests (Wilcoxon test) have been performed. From performance index and test-based study, it was concluded that the ASMO algorithm functions reliably than all other tested algorithms. Further, the low computational requirements signify the robustness of the algorithm, thus presenting it as an appropriate option for the evaluation of battery model parameters.

4. The parameters values extracted using ASMO are validated with parameters values evaluated from PCDT. It is observed from validation process that there is a similarity between parameters values obtained from both the methods. Therefore, the proposed technique can be used as an alternative for estimation of battery parameters.
5. Fast computation, high estimation and prediction accuracy even with incorrect initial SOC values shows that the PF is practically robust for real-time applications compared to other non-linear filters. It is also noted from the results that the PF offers good accuracy and shorter running time in online applications in comparison to other non-linear filters.
6. Exponential model is considerably accurate for representing capacity degradation trends in a battery.
7. NLLS, UKF, PF were tested for estimation of SOH of the battery using different quantity of training data. PF shows superior performance by appropriately adapting the weights of its particles. PF utilized estimates of system states derived from training data generating a diversified pool of particles. The prediction PDF was observed to be influenced by adjusting the weights of the particles. However, the state estimates remained unchanged from data available for predictions.
8. The probability density function was used to assess confidence level in final RUL prediction.
9. A rule-based power management system is developed for effective control of power sharing between two batteries in a dual-battery powered EV. The proposed scheme was implemented for standard driving cycles. The results of the complete management system offer promising solution to the power sharing between the two sources.

## 5.2 Suggestions for Future Works in this Research Domain

1. The effectiveness of battery management system can be enhanced by incorporating estimation of internal power of battery with varying operational conditions.
2. The model of battery can be upgraded by integrating the effect of degradation, hysteresis and self-discharge. Different objective functions can be evaluated for battery parameter estimation.
3. SOC estimation perform better at high temperatures than at low, hence a more accurate model to capture dynamics of battery at low temperature is worthy to

investigate in future study. Even effect of capacity degradation trend on the estimation of battery SOC needs to be investigated for that focus will on joint estimation approach for together prediction of SOC and SOH.

4. SOH estimation may be even more enhanced by considering the effect of resistance on the capacity.
5. An equivalent circuit model can be considered for assessment of remaining useful life for further analysis of SOH.



# Appendix A

## Data Specification

Vehicle dimensions and parameters data for Tesla 85D cars is given as follow:

Parameters	Unit	Symbols	85D
<b>Vehicle</b>			
Mass	[ <i>kg</i> ]	<i>M<sub>ev</sub></i>	2108+482
Vehicle frontal area	[ <i>m</i> <sup>2</sup> ]	<i>A<sub>front</sub></i>	2.34
Rolling resistance coefficient		<i>μ<sub>rr</sub></i>	0.0084
Aerodynamic drag coefficient		<i>C<sub>drag</sub></i>	0.24
Air Density	[ <i>kg/m</i> <sup>3</sup> ]	<i>ρ<sub>air</sub></i>	1.225
Auxiliary Power	[ <i>W</i> ]	<i>P<sub>aux</sub></i>	200
Wheel Radius	[ <i>m</i> ]	<i>r<sub>wh</sub></i>	0.35
Gear Ratio		<i>G</i>	9.73
Gear Inertia	[ <i>kg/m</i> <sup>2</sup> ]		0.05
Gear efficiency		<i>η<sub>g</sub></i>	0.96
Maximum velocity	[ <i>km/h</i> ]		224
Acceleration [0-60mph]			5.4
<b>Motor</b>			
Rated torque	[ <i>Nm</i> ]		440
Rated power	[ <i>kW</i> ]		270
Rated speed	[ <i>rpm</i> ]		5600
Maximum speed	[ <i>rpm</i> ]		18400
Efficiency			0.95
Inertia	[ <i>kg/m</i> <sup>2</sup> ]		0.2
<b>Battery</b>			
Minimum Pack voltage	[ <i>V</i> ]		240
Nominal Pack voltage	[ <i>V</i> ]		345
Maximum Pack voltage	[ <i>V</i> ]		403
Pack Energy	[ <i>kWh</i> ]		85
Pack Specific Energy	[ <i>Wh/kg</i> ]		156

A Panasonic 3.1Ah NCR18650A cylindrical battery is utilized for analysis purpose. The detail about characteristics of the battery is given as follow:

Parameter	Unit	Value
Nominal capacity	[Ah]	3.1
Nominal voltage	[V]	3.6
Maximum voltage	[V]	4.2
Minimum voltage	[V]	2.5
Nominal charging current	[A]	1.65
Nominal discharging current	[A]	0.62
Capacity at nominal voltage	[Ah]	2.95
Temperature operation range	$^{\circ}C$	-20 to +60
Weight Approx.	<i>g</i>	40.7
Nominal dimension	<i>mm</i>	68.9mm $\times$ 18.50mm

Dual-battery powered EVs requires two different size battery packs. Details characteristics for both the batteries is given as follow:

Parameter	Unit	Fixed Battery	Swappable battery
Energy	[kWh]	21	64
Number of modules		16	16
Number of series battery		6	6
Number of parallel battery		18	56
Nominal capacity	[Ah]	55	172
Nominal voltage	[V]	345	345
Maximum voltage	[V]	403	403
Minimum voltage	[V]	240	240

# Bibliography

- [1] Y.-J. Zhang, H.-R. Peng, Z. Liu, and W. Tan, “Direct energy rebound effect for road passenger transport in china: a dynamic panel quantile regression approach,” *Energy Policy*, vol. 87, pp. 303–313, 2015.
- [2] I. P. on Climate Change, *Climate change 2014: mitigation of climate change*. Cambridge University Press, 2015, vol. 3.
- [3] V. Gulati, “National electric mobility mission plan 2020,” *Department of Heavy Industry, Ministry of Heavy Industries & Public Enterprises, Government of India*, 2012.
- [4] P. Commission *et al.*, “Interim report of the expert group on low carbon strategies for inclusive growth,” *Planning Commission, Government of India, New Delhi, India*. Available online at [http://planningcommission.nic.in/reports/genrep/Inter\\_Exp.pdf](http://planningcommission.nic.in/reports/genrep/Inter_Exp.pdf), 2011.
- [5] W. Li, R. Long, H. Chen, and J. Geng, “A review of factors influencing consumer intentions to adopt battery electric vehicles,” *Renewable and Sustainable Energy Reviews*, vol. 78, pp. 318–328, 2017.
- [6] A. internationale pour l’évaluation du rendement scolaire, *Global EV outlook 2016: Beyond one million electric cars*. OECD Publishing, 2016.
- [7] A. M. Andwari, A. Pesiridis, S. Rajoo, R. Martinez-Botas, and V. Esfahanian, “A review of battery electric vehicle technology and readiness levels,” *Renewable and Sustainable Energy Reviews*, vol. 78, pp. 414–430, 2017.
- [8] S. Manzetti and F. Mariasiu, “Electric vehicle battery technologies: From present state to future systems,” *Renewable and Sustainable Energy Reviews*, vol. 51, pp. 1004–1012, 2015.
- [9] N. Nitta, F. Wu, J. T. Lee, and G. Yushin, “Li-ion battery materials: present and future,” *Materials today*, vol. 18, no. 5, pp. 252–264, 2015.
- [10] O. Egbue and S. Long, “Barriers to widespread adoption of electric vehicles: An analysis of consumer attitudes and perceptions,” *Energy policy*, vol. 48, pp. 717–729, 2012.
- [11] S. Abada, G. Marlair, A. Lecocq, M. Petit, V. Sauvart-Moynot, and F. Huet, “Safety focused modeling of lithium-ion batteries: A review,” *Journal of Power Sources*, vol. 306, pp. 178–192, 2016.

- 
- [12] D. Andrea, *Battery management systems for large lithium ion battery packs*. Artech house, 2010.
- [13] L. Lu, X. Han, J. Li, J. Hua, and M. Ouyang, "A review on the key issues for lithium-ion battery management in electric vehicles," *Journal of power sources*, vol. 226, pp. 272–288, 2013.
- [14] J. V. Barreras, C. Pinto, R. de Castro, E. Schaltz, S. J. Andreasen, P. O. Rasmussen, and R. E. Araújo, "Evaluation of a novel bev concept based on fixed and swappable li-ion battery packs," *IEEE Transactions on Industry Applications*, vol. 52, no. 6, pp. 5073–5085, 2016.
- [15] A. Khaligh, Z. Li *et al.*, "Battery, ultracapacitor, fuel cell, and hybrid energy storage systems for electric, hybrid electric, fuel cell, and plug-in hybrid electric vehicles: State of the art," *IEEE transactions on Vehicular Technology*, vol. 59, no. 6, pp. 2806–2814, 2010.
- [16] A. Burke, B. Jungers, C. Yang, and J. Ogden, "Battery electric vehicles: An assessment of the technology and factors influencing market readiness, advanced energy pathways (aep) project, task 4.1 technology assessments of vehicle fuels and technologies public interest energy research (pier) program california energy commission," *Davis (CA): UC Davis, Institute of Transportation Studies*, 2007.
- [17] X. Hu, C. Zou, C. Zhang, and Y. Li, "Technological developments in batteries: a survey of principal roles, types, and management needs," *IEEE Power and Energy Magazine*, vol. 15, no. 5, pp. 20–31, 2017.
- [18] K. Liu, K. Li, Q. Peng, and C. Zhang, "A brief review on key technologies in the battery management system of electric vehicles," *Frontiers of Mechanical Engineering*, pp. 1–18, 2018.
- [19] J. Dixon, "Energy storage for electric vehicles," in *Industrial Technology (ICIT), 2010 IEEE International Conference on*. IEEE, 2010, pp. 20–26.
- [20] J. M. Miller, "Energy storage system technology challenges facing strong hybrid, plug-in and battery electric vehicles," in *Vehicle Power and Propulsion Conference, 2009. VPPC'09. IEEE*. IEEE, 2009, pp. 4–10.
- [21] B. Scrosati and J. Garche, "Lithium batteries: Status, prospects and future," *Journal of power sources*, vol. 195, no. 9, pp. 2419–2430, 2010.
- [22] S. Kukkonen, "Current trends in battery technology," in *ECV national seminar, Sept*, 2014.
- [23] Z. Yang, J. Zhang, M. C. Kintner-Meyer, X. Lu, D. Choi, J. P. Lemmon, and J. Liu, "Electrochemical energy storage for green grid," *Chemical reviews*, vol. 111, no. 5, pp. 3577–3613, 2011.
- [24] W. Lu, C. M. López, N. Liu, J. T. Vaughey, A. Jansen *et al.*, "Overcharge effect on morphology and structure of carbon electrodes for lithium-ion batteries," *Journal of The Electrochemical Society*, vol. 159, no. 5, pp. A566–A570, 2012.



- [25] Y. Yang, X. Hu, D. Qing, and F. Chen, "Arrhenius equation-based cell-health assessment: application to thermal energy management design of a hev nimh battery pack," *Energies*, vol. 6, no. 5, pp. 2709–2725, 2013.
- [26] Q. Wang, J. Sun, and C. Chen, "Enhancing the thermal stability of licoo<sub>2</sub> electrode by 4-isopropyl phenyl diphenyl phosphate in lithium ion batteries," *Journal of power sources*, vol. 162, no. 2, pp. 1363–1366, 2006.
- [27] Q. Wang and J. Sun, "Enhancing the safety of lithium ion batteries by 4-isopropyl phenyl diphenyl phosphate," *Materials Letters*, vol. 61, no. 16, pp. 3338–3340, 2007.
- [28] Q. Wang, P. Ping, X. Zhao, G. Chu, J. Sun, and C. Chen, "Thermal runaway caused fire and explosion of lithium ion battery," *Journal of power sources*, vol. 208, pp. 210–224, 2012.
- [29] S. Zhou, *Advances in battery manufacturing, service, and management systems*. John Wiley & Sons, 2016.
- [30] G. L. Plett, "Extended kalman filtering for battery management systems of lipb-based hev battery packs: Part 1. introduction," *Journal of power sources*, vol. 134, no. 2, pp. 252–261, 2004.
- [31] E. Meissner and G. Richter, "Battery monitoring and electrical energy management: Precondition for future vehicle electric power systems," *Journal of power sources*, vol. 116, no. 1-2, pp. 79–98, 2003.
- [32] F. Conte, "Battery and battery management for hybrid electric vehicles: a review," *e & i Elektrotechnik und Informationstechnik*, vol. 123, no. 10, pp. 424–431, 2006.
- [33] A. Szumanowski and Y. Chang, "Battery management system based on battery nonlinear dynamics modeling," *IEEE transactions on vehicular technology*, vol. 57, no. 3, pp. 1425–1432, 2008.
- [34] W. Waag, C. Fleischer, and D. U. Sauer, "Critical review of the methods for monitoring of lithium-ion batteries in electric and hybrid vehicles," *Journal of Power Sources*, vol. 258, pp. 321–339, 2014.
- [35] K. W. E. Cheng, B. Divakar, H. Wu, K. Ding, and H. F. Ho, "Battery-management system (bms) and soc development for electrical vehicles," *IEEE transactions on vehicular technology*, vol. 60, no. 1, pp. 76–88, 2011.
- [36] S. F. Tie and C. W. Tan, "A review of energy sources and energy management system in electric vehicles," *Renewable and Sustainable Energy Reviews*, vol. 20, pp. 82–102, 2013.
- [37] S. Bhide and T. Shim, "Novel predictive electric li-ion battery model incorporating thermal and rate factor effects," *IEEE Transactions on vehicular technology*, vol. 60, no. 3, pp. 819–829, 2011.
- [38] A. Seaman, T.-S. Dao, and J. McPhee, "A survey of mathematics-based equivalent-circuit and electrochemical battery models for hybrid and electric vehicle simulation," *Journal of Power Sources*, vol. 256, pp. 410–423, 2014.

- [39] S. Nejad, D. Gladwin, and D. Stone, "A systematic review of lumped-parameter equivalent circuit models for real-time estimation of lithium-ion battery states," *Journal of Power Sources*, vol. 316, pp. 183–196, 2016.
- [40] J. Meng, G. Luo, M. Ricco, M. Swierczynski, D.-I. Stroe, and R. Teodorescu, "Overview of lithium-ion battery modeling methods for state-of-charge estimation in electrical vehicles," *Applied Sciences*, vol. 8, no. 5, p. 659, 2018.
- [41] D. W. Dees, V. S. Battaglia, and A. Bélanger, "Electrochemical modeling of lithium polymer batteries," *Journal of power sources*, vol. 110, no. 2, pp. 310–320, 2002.
- [42] B. Liu, S. Yin, and J. Xu, "Integrated computation model of lithium-ion battery subject to nail penetration," *Applied energy*, vol. 183, pp. 278–289, 2016.
- [43] C. Zou, C. Manzie, and D. Nešić, "A framework for simplification of pde-based lithium-ion battery models," *IEEE Transactions on Control Systems Technology*, vol. 24, no. 5, pp. 1594–1609, 2016.
- [44] S. Santhanagopalan, Q. Guo, P. Ramadass, and R. E. White, "Review of models for predicting the cycling performance of lithium ion batteries," *Journal of Power Sources*, vol. 156, no. 2, pp. 620–628, 2006.
- [45] K. A. Smith, C. D. Rahn, and C.-Y. Wang, "Control oriented 1d electrochemical model of lithium ion battery," *Energy Conversion and management*, vol. 48, no. 9, pp. 2565–2578, 2007.
- [46] A. P. Schmidt, M. Bitzer, Á. W. Imre, and L. Guzzella, "Experiment-driven electrochemical modeling and systematic parameterization for a lithium-ion battery cell," *Journal of Power Sources*, vol. 195, no. 15, pp. 5071–5080, 2010.
- [47] X. Han, M. Ouyang, L. Lu, and J. Li, "Simplification of physics-based electrochemical model for lithium ion battery on electric vehicle. part ii: Pseudo-two-dimensional model simplification and state of charge estimation," *Journal of Power Sources*, vol. 278, pp. 814–825, 2015.
- [48] M. W. Verbrugge and R. S. Conell, "Electrochemical and thermal characterization of battery modules commensurate with electric vehicle integration," *Journal of the Electrochemical Society*, vol. 149, no. 1, pp. A45–A53, 2002.
- [49] D. D. Domenico, G. Fiengo, and A. Stefanopoulou, "Lithium-ion battery state of charge estimation with a kalman filter based on a electrochemical model," in *Control Applications, 2008. CCA 2008. IEEE International Conference on*. Ieee, 2008, pp. 702–707.
- [50] C. Hu, G. Jain, P. Zhang, C. Schmidt, P. Gomadam, and T. Gorka, "Data-driven method based on particle swarm optimization and k-nearest neighbor regression for estimating capacity of lithium-ion battery," *Applied Energy*, vol. 129, pp. 49–55, 2014.
- [51] Y. Z. Zhang, H. W. He, and R. Xiong, "A data-driven based state of energy estimator of lithium-ion batteries used to supply electric vehicles," *Energy Procedia*, vol. 75, pp. 1944–1949, 2015.

- [52] R. Xiong, F. Sun, Z. Chen, and H. He, "A data-driven multi-scale extended kalman filtering based parameter and state estimation approach of lithium-ion polymer battery in electric vehicles," *Applied Energy*, vol. 113, pp. 463–476, 2014.
- [53] R. Xiong, F. Sun, X. Gong, and C. Gao, "A data-driven based adaptive state of charge estimator of lithium-ion polymer battery used in electric vehicles," *Applied Energy*, vol. 113, pp. 1421–1433, 2014.
- [54] A. Nuhic, T. Terzimehic, T. Soczka-Guth, M. Buchholz, and K. Dietmayer, "Health diagnosis and remaining useful life prognostics of lithium-ion batteries using data-driven methods," *Journal of power sources*, vol. 239, pp. 680–688, 2013.
- [55] O. Tremblay, L.-A. Dessaint, and A.-I. Dekkiche, "A generic battery model for the dynamic simulation of hybrid electric vehicles," in *Vehicle power and propulsion conference, 2007. VPPC 2007. IEEE*. IEEE, 2007, pp. 284–289.
- [56] M. Nikdel *et al.*, "Various battery models for various simulation studies and applications," *Renewable and Sustainable Energy Reviews*, vol. 32, pp. 477–485, 2014.
- [57] Y.-H. Kim and H.-D. Ha, "Design of interface circuits with electrical battery models," *IEEE Transactions on Industrial Electronics*, vol. 44, no. 1, pp. 81–86, 1997.
- [58] B. Y. Liaw, G. Nagasubramanian, R. G. Jungst, and D. H. Doughty, "Modeling of lithium ion cells—a simple equivalent-circuit model approach," *Solid state ionics*, vol. 175, no. 1, pp. 835–839, 2004.
- [59] H. Chan, "A new battery model for use with battery energy storage systems and electric vehicles power systems," in *Power Engineering Society Winter Meeting, 2000. IEEE*, vol. 1. IEEE, 2000, pp. 470–475.
- [60] V. Johnson, "Battery performance models in advisor," *Journal of power sources*, vol. 110, no. 2, pp. 321–329, 2002.
- [61] M. Dürr, A. Cruden, S. Gair, and J. McDonald, "Dynamic model of a lead acid battery for use in a domestic fuel cell system," *Journal of power sources*, vol. 161, no. 2, pp. 1400–1411, 2006.
- [62] J. P. Cun, J. N. Fiorina, M. Fraise, and H. Mabboux, "The experience of a ups company in advanced battery monitoring," in *Telecommunications Energy Conference, 1996. INT-ELEC'96., 18th International*. IEEE, 1996, pp. 646–653.
- [63] S. Zhang, K. Xu, and T. Jow, "Electrochemical impedance study on the low temperature of li-ion batteries," *Electrochimica acta*, vol. 49, no. 7, pp. 1057–1061, 2004.
- [64] J. Xu, C. C. Mi, B. Cao, and J. Cao, "A new method to estimate the state of charge of lithium-ion batteries based on the battery impedance model," *Journal of power sources*, vol. 233, pp. 277–284, 2013.
- [65] R. Xiong, J. Cao, Q. Yu, H. He, and F. Sun, "Critical review on the battery state of charge estimation methods for electric vehicles," *IEEE Access*, vol. 6, pp. 1832–1843, 2018.

- [66] L. Lam, "A practical circuit-based model for state of health estimation of li-ion battery cells in electric vehicles," *Master of Science Thesis, University of Technology Delft. doi*, vol. 10, 2011.
- [67] M. Dubarry and B. Y. Liaw, "Development of a universal modeling tool for rechargeable lithium batteries," *Journal of Power Sources*, vol. 174, no. 2, pp. 856–860, 2007.
- [68] X. Hu, S. Li, and H. Peng, "A comparative study of equivalent circuit models for li-ion batteries," *Journal of Power Sources*, vol. 198, pp. 359–367, 2012.
- [69] Z. Chen, R. Xiong, J. Tian, X. Shang, and J. Lu, "Model-based fault diagnosis approach on external short circuit of lithium-ion battery used in electric vehicles," *Applied energy*, vol. 184, pp. 365–374, 2016.
- [70] T. Kim, Y. Wang, H. Fang, Z. Sahinoglu, T. Wada, S. Hara, and W. Qiao, "Model-based condition monitoring for lithium-ion batteries," *Journal of Power Sources*, vol. 295, pp. 16–27, 2015.
- [71] B. Payyappilly and V. John, "Run-time simulation model for li-ion battery using in-circuit extracted mass transport parameters," in *Transportation Electrification Conference (ITEC-India), 2017 IEEE*. IEEE, 2017, pp. 1–6.
- [72] M. Chen and G. A. Rincon-Mora, "Accurate electrical battery model capable of predicting runtime and iv performance," *IEEE transactions on energy conversion*, vol. 21, no. 2, pp. 504–511, 2006.
- [73] O. Erdinc, B. Vural, and M. Uzunoglu, "A dynamic lithium-ion battery model considering the effects of temperature and capacity fading," in *Clean Electrical Power, 2009 International Conference on*. IEEE, 2009, pp. 383–386.
- [74] R. Jackey, M. Saginaw, P. Sanghvi, J. Gazzarri, T. Huria, and M. Ceraolo, "Battery model parameter estimation using a layered technique: an example using a lithium iron phosphate cell," SAE Technical Paper, Tech. Rep., 2013.
- [75] C. Zhang, K. Li, S. Mcloone, and Z. Yang, "Battery modelling methods for electric vehicles-a review," in *Control Conference (ECC), 2014 European*. IEEE, 2014, pp. 2673–2678.
- [76] A. Fotouhi, D. J. Auger, K. Propp, S. Longo, and M. Wild, "A review on electric vehicle battery modelling: From lithium-ion toward lithium–sulphur," *Renewable and Sustainable Energy Reviews*, vol. 56, pp. 1008–1021, 2016.
- [77] S. Barcellona and L. Piegari, "Lithium ion battery models and parameter identification techniques," *Energies*, vol. 10, no. 12, p. 2007, 2017.
- [78] Y.-H. Chiang, W.-Y. Sean, and J.-C. Ke, "Online estimation of internal resistance and open-circuit voltage of lithium-ion batteries in electric vehicles," *Journal of Power Sources*, vol. 196, no. 8, pp. 3921–3932, 2011.

- [79] H. Rahimi-Eichi, F. Baronti, and M.-Y. Chow, "Modeling and online parameter identification of li-polymer battery cells for soc estimation," in *Industrial Electronics (ISIE), 2012 IEEE International Symposium on*. IEEE, 2012, pp. 1336–1341.
- [80] —, "Online adaptive parameter identification and state-of-charge coestimation for lithium-polymer battery cells," *IEEE Transactions on Industrial Electronics*, vol. 61, no. 4, pp. 2053–2061, 2014.
- [81] H. Pang, F. Zhang *et al.*, "Experimental data-driven parameter identification and state of charge estimation for a li-ion battery equivalent circuit model," *Energies*, vol. 11, no. 5, pp. 1–14, 2018.
- [82] X. Lin, H. E. Perez, S. Mohan, J. B. Siegel, A. G. Stefanopoulou, Y. Ding, and M. P. Castanier, "A lumped-parameter electro-thermal model for cylindrical batteries," *Journal of Power Sources*, vol. 257, pp. 1–11, 2014.
- [83] M. Hess, T. Sasaki, C. Villeveille, and P. Novák, "Combined operando x-ray diffraction-electrochemical impedance spectroscopy detecting solid solution reactions of lifepo4 in batteries," *Nature communications*, vol. 6, 2015.
- [84] M. Coleman, W. G. Hurley, and C. K. Lee, "An improved battery characterization method using a two-pulse load test," *IEEE Transactions on energy conversion*, vol. 23, no. 2, pp. 708–713, 2008.
- [85] B. Pattipati, C. Sankavaram, and K. Pattipati, "System identification and estimation framework for pivotal automotive battery management system characteristics," *IEEE Transactions on Systems, Man, and Cybernetics, Part C (Applications and Reviews)*, vol. 41, no. 6, pp. 869–884, 2011.
- [86] H. R. Eichi and M. Chow, "Adaptive parameter identification and state-of-charge estimation of lithium-ion batteries," in *Proc. 38th Annual Conference of the IEEE Industrial Electronics Society*. Citeseer, 2012, pp. 4012–4017.
- [87] X. Cheng, L. Yao, Y. Xing, and M. Pecht, "Novel parametric circuit modeling for li-ion batteries," *Energies*, vol. 9, no. 7, p. 539, 2016.
- [88] C. Fleischer, W. Waag, H.-M. Heyn, and D. U. Sauer, "On-line adaptive battery impedance parameter and state estimation considering physical principles in reduced order equivalent circuit battery models: Part 1. requirements, critical review of methods and modeling," *Journal of Power Sources*, vol. 260, pp. 276–291, 2014.
- [89] G. L. Plett, "Extended kalman filtering for battery management systems of lipb-based hev battery packs: Part 2. modeling and identification," *Journal of power sources*, vol. 134, no. 2, pp. 262–276, 2004.
- [90] C. Hu, B. D. Youn, and J. Chung, "A multiscale framework with extended kalman filter for lithium-ion battery soc and capacity estimation," *Applied Energy*, vol. 92, pp. 694–704, 2012.

- [91] W.-J. Yang, D.-H. Yu, and Y.-B. Kim, "Parameter estimation of lithium-ion batteries and noise reduction using an  $h_\infty$  filter," *Journal of Mechanical Science and Technology*, vol. 27, no. 1, pp. 247–256, 2013.
- [92] J. Kim, I. Lee, Y. Tak, and B. Cho, "State-of-health diagnosis based on hamming neural network using output voltage pattern recognition for a pem fuel cell," *international journal of hydrogen energy*, vol. 37, no. 5, pp. 4280–4289, 2012.
- [93] T. Feng, L. Yang, X. Zhao, H. Zhang, and J. Qiang, "Online identification of lithium-ion battery parameters based on an improved equivalent-circuit model and its implementation on battery state-of-power prediction," *Journal of Power Sources*, vol. 281, pp. 192–203, 2015.
- [94] M. Sitterly, L. Y. Wang, G. G. Yin, and C. Wang, "Enhanced identification of battery models for real-time battery management," *IEEE Transactions on Sustainable Energy*, vol. 2, no. 3, pp. 300–308, 2011.
- [95] X. Hu, F. Sun, Y. Zou, and H. Peng, "Online estimation of an electric vehicle lithium-ion battery using recursive least squares with forgetting," in *American Control Conference (ACC), 2011*. IEEE, 2011, pp. 935–940.
- [96] G. L. Plett, "Recursive approximate weighted total least squares estimation of battery cell total capacity," *Journal of Power Sources*, vol. 196, no. 4, pp. 2319–2331, 2011.
- [97] Y. Boujoudar, H. Hemi, H. El Moussaoui, H. El Markhi, and T. Lamhamdi, "Li-ion battery parameters estimation using neural networks," in *Wireless Technologies, Embedded and Intelligent Systems (WITS), 2017 International Conference on*. IEEE, 2017, pp. 1–4.
- [98] G. Capizzi, F. Bonanno, and G. M. Tina, "Recurrent neural network-based modeling and simulation of lead-acid batteries charge–discharge," *IEEE Transactions on Energy Conversion*, vol. 26, no. 2, pp. 435–443, 2011.
- [99] K. S. Ng, C.-S. Moo, Y.-P. Chen, and Y.-C. Hsieh, "Enhanced coulomb counting method for estimating state-of-charge and state-of-health of lithium-ion batteries," *Applied energy*, vol. 86, no. 9, pp. 1506–1511, 2009.
- [100] I. Baccouche, S. Jemmali, B. Manai, N. Omar, and N. E. B. Amara, "Improved ocv model of a li-ion nmc battery for online soc estimation using the extended kalman filter," *Energies*, vol. 10, no. 6, p. 764, 2017.
- [101] G. L. Plett, "Kalman-filter soc estimation for lipb hev cells," in *Proceedings of the 19th International Battery, Hybrid and Fuel Cell Electric Vehicle Symposium & Exhibition (EVS19). Busan, Korea, 2002*, pp. 527–538.
- [102] J. Lee, O. Nam, and B. Cho, "Li-ion battery soc estimation method based on the reduced order extended kalman filtering," *Journal of power sources*, vol. 174, no. 1, pp. 9–15, 2007.
- [103] N. A. Windarko and J.-H. Choi, "Soc estimation based on ocv for nimh batteries using an improved takacs model," *Journal of Power Electronics*, vol. 10, no. 2, pp. 181–186, 2010.

- [104] K. Thirugnanam, E. Reena, T. Joy, M. Singh, and P. Kumar, "Mathematical modeling of li-ion battery using genetic algorithm approach for v2g applications," *Energy Conversion, IEEE Transactions on*, vol. 29, no. 2, pp. 332–343, 2014.
- [105] M. Dubarry, V. Svoboda, R. Hwu, and B. Y. Liaw, "Capacity loss in rechargeable lithium cells during cycle life testing: The importance of determining state-of-charge," *Journal of Power Sources*, vol. 174, no. 2, pp. 1121–1125, 2007.
- [106] R. L. Hartmann *et al.*, "An aging model for lithium-ion cells," Ph.D. dissertation, University of Akron, 2008.
- [107] D. Liu, W. Xie, H. Liao, and Y. Peng, "An integrated probabilistic approach to lithium-ion battery remaining useful life estimation," *IEEE Transactions on Instrumentation and Measurement*, vol. 64, no. 3, pp. 660–670, 2015.
- [108] D. Wang, F. Yang, K.-L. Tsui, Q. Zhou, and S. J. Bae, "Remaining useful life prediction of lithium-ion batteries based on spherical cubature particle filter," *IEEE Transactions on Instrumentation and Measurement*, vol. 65, no. 6, pp. 1282–1291, 2016.
- [109] J. Zhang and J. Lee, "A review on prognostics and health monitoring of li-ion battery," *Journal of Power Sources*, vol. 196, no. 15, pp. 6007–6014, 2011.
- [110] Y. Xing, W. He, M. Pecht, and K. L. Tsui, "State of charge estimation of lithium-ion batteries using the open-circuit voltage at various ambient temperatures," *Applied Energy*, vol. 113, pp. 106–115, 2014.
- [111] M. U. Cuma and T. Koroglu, "A comprehensive review on estimation strategies used in hybrid and battery electric vehicles," *Renewable and Sustainable Energy Reviews*, vol. 42, pp. 517–531, 2015.
- [112] H. He, R. Xiong, and J. Fan, "Evaluation of lithium-ion battery equivalent circuit models for state of charge estimation by an experimental approach," *Energies*, vol. 4, no. 4, pp. 582–598, 2011.
- [113] B. Saha, K. Goebel, and J. Christophersen, "Comparison of prognostic algorithms for estimating remaining useful life of batteries," *Transactions of the Institute of Measurement and Control*, vol. 31, no. 3-4, pp. 293–308, 2009.
- [114] Y.-M. Jeong, Y.-K. Cho, J.-H. Ahn, S.-H. Ryu, and B.-K. Lee, "Enhanced coulomb counting method with adaptive soc reset time for estimating ocv," in *Energy Conversion Congress and Exposition (ECCE), 2014 IEEE*. IEEE, 2014, pp. 1313–1318.
- [115] I. Baccouche, A. Mlayah, S. Jemmali, B. Manai, and N. E. B. Amara, "Implementation of a coulomb counting algorithm for soc estimation of li-ion battery for multimedia applications," in *Systems, Signals & Devices (SSD), 2015 12th International Multi-Conference on*. IEEE, 2015, pp. 1–6.
- [116] J. Xie, J. Ma, and K. Bai, "Enhanced coulomb counting method for state-of-charge estimation of lithium-ion batteries based on peukert's law and coulombic efficiency," *Journal of Power Electronics*, vol. 18, no. 3, pp. 910–922, 2018.

- [117] S. Lee, J. Kim, J. Lee, and B. H. Cho, "State-of-charge and capacity estimation of lithium-ion battery using a new open-circuit voltage versus state-of-charge," *Journal of power sources*, vol. 185, no. 2, pp. 1367–1373, 2008.
- [118] C. Lin, Q. Yu, R. Xiong, and L. Y. Wang, "A study on the impact of open circuit voltage tests on state of charge estimation for lithium-ion batteries," *Applied Energy*, vol. 205, pp. 892–902, 2017.
- [119] G. Dong, J. Wei, C. Zhang, and Z. Chen, "Online state of charge estimation and open circuit voltage hysteresis modeling of lifepo4 battery using invariant imbedding method," *Applied energy*, vol. 162, pp. 163–171, 2016.
- [120] J. Remmlinger, M. Buchholz, M. Meiler, P. Bernreuter, and K. Dietmayer, "State-of-health monitoring of lithium-ion batteries in electric vehicles by on-board internal resistance estimation," *Journal of Power Sources*, vol. 196, no. 12, pp. 5357–5363, 2011.
- [121] X. Wei, B. Zhu, and W. Xu, "Internal resistance identification in vehicle power lithium-ion battery and application in lifetime evaluation," in *Measuring Technology and Mechatronics Automation, 2009. ICMTMA'09. International Conference on*, vol. 3. IEEE, 2009, pp. 388–392.
- [122] D. Haifeng, W. Xuezhe, and S. Zechang, "A new soh prediction concept for the power lithium-ion battery used on hevs," in *Vehicle Power and Propulsion Conference, 2009. VPPC'09. IEEE*. IEEE, 2009, pp. 1649–1653.
- [123] J. Remmlinger, M. Buchholz, T. Soczka-Guth, and K. Dietmayer, "On-board state-of-health monitoring of lithium-ion batteries using linear parameter-varying models," *Journal of Power Sources*, vol. 239, pp. 689–695, 2013.
- [124] K.-H. Tseng, J.-W. Liang, W. Chang, and S.-C. Huang, "Regression models using fully discharged voltage and internal resistance for state of health estimation of lithium-ion batteries," *energies*, vol. 8, no. 4, pp. 2889–2907, 2015.
- [125] J. Zhu, Z. Sun, X. Wei, and H. Dai, "A new lithium-ion battery internal temperature on-line estimate method based on electrochemical impedance spectroscopy measurement," *Journal of Power Sources*, vol. 274, pp. 990–1004, 2015.
- [126] M. Galeotti, L. Cinà, C. Giammanco, S. Cordiner, and A. Di Carlo, "Performance analysis and soh (state of health) evaluation of lithium polymer batteries through electrochemical impedance spectroscopy," *Energy*, vol. 89, pp. 678–686, 2015.
- [127] D. Andre, M. Meiler, K. Steiner, H. Walz, T. Soczka-Guth, and D. Sauer, "Characterization of high-power lithium-ion batteries by electrochemical impedance spectroscopy. ii: Modelling," *Journal of Power Sources*, vol. 196, no. 12, pp. 5349–5356, 2011.
- [128] X. Dang, L. Yan, K. Xu, X. Wu, H. Jiang, and H. Sun, "Open-circuit voltage-based state of charge estimation of lithium-ion battery using dual neural network fusion battery model," *Electrochimica Acta*, vol. 188, pp. 356–366, 2016.



- [129] P. Singh, C. Fennie, and D. Reisner, "Fuzzy logic modelling of state-of-charge and available capacity of nickel/metal hydride batteries," *Journal of Power Sources*, vol. 136, no. 2, pp. 322–333, 2004.
- [130] H. Sheng and J. Xiao, "Electric vehicle state of charge estimation: Nonlinear correlation and fuzzy support vector machine," *Journal of Power sources*, vol. 281, pp. 131–137, 2015.
- [131] W. He, N. Williard, C. Chen, and M. Pecht, "State of charge estimation for li-ion batteries using neural network modeling and unscented kalman filter-based error cancellation," *International Journal of Electrical Power & Energy Systems*, vol. 62, pp. 783–791, 2014.
- [132] M. Charkhgard and M. Farrokhi, "State-of-charge estimation for lithium-ion batteries using neural networks and ekf," *IEEE transactions on industrial electronics*, vol. 57, no. 12, pp. 4178–4187, 2010.
- [133] J. Liu, A. Saxena, K. Goebel, B. Saha, and W. Wang, "An adaptive recurrent neural network for remaining useful life prediction of lithium-ion batteries," NATIONAL AERONAUTICS AND SPACE ADMINISTRATION MOFFETT FIELD CA AMES RESEARCH CENTER, Tech. Rep., 2010.
- [134] W. Shen, K. Chau, C. C. Chan, and E. W. Lo, "Neural network-based residual capacity indicator for nickel-metal hydride batteries in electric vehicles," *IEEE Transactions on Vehicular Technology*, vol. 54, no. 5, pp. 1705–1712, 2005.
- [135] A. Zenati, P. Desprez, H. Razik, and S. Rael, "A methodology to assess the state of health of lithium-ion batteries based on the battery's parameters and a fuzzy logic system," in *Electric Vehicle Conference (IEVC), 2012 IEEE International*. IEEE, 2012, pp. 1–6.
- [136] C. Hametner and S. Jakubek, "State of charge estimation for lithium ion cells: Design of experiments, nonlinear identification and fuzzy observer design," *Journal of Power Sources*, vol. 238, pp. 413–421, 2013.
- [137] W. Shen, C. C. Chan, E. W. Lo, and K. Chau, "Adaptive neuro-fuzzy modeling of battery residual capacity for electric vehicles," *IEEE Transactions on Industrial Electronics*, vol. 49, no. 3, pp. 677–684, 2002.
- [138] B. Sun, L. Wang, and C. Liao, "Soc estimation of nimh battery for hev based on adaptive neuro-fuzzy inference system." in *Vehicle Power and Propulsion Conference, 2008. VPPC'08*. IEEE. IEEE, 2008, pp. 1–4.
- [139] X. Hu and F. Sun, "Fuzzy clustering based multi-model support vector regression state of charge estimator for lithium-ion battery of electric vehicle," in *Intelligent Human-Machine Systems and Cybernetics, 2009. IHMSC'09. International Conference on*, vol. 1. IEEE, 2009, pp. 392–396.
- [140] J. C. A. Anton, P. J. G. Nieto, C. B. Viejo, and J. A. V. Vilán, "Support vector machines used to estimate the battery state of charge," *IEEE Transactions on power electronics*, vol. 28, no. 12, pp. 5919–5926, 2013.

- 
- [141] V. Klass, M. Behm, and G. Lindbergh, "A support vector machine-based state-of-health estimation method for lithium-ion batteries under electric vehicle operation," *Journal of Power Sources*, vol. 270, pp. 262–272, 2014.
- [142] J. Meng, G. Luo, and F. Gao, "Lithium polymer battery state-of-charge estimation based on adaptive unscented kalman filter and support vector machine," *IEEE Trans. Power Electron.*, vol. 31, no. 3, pp. 2226–2238, 2016.
- [143] T. Kim and W. Qiao, "A hybrid battery model capable of capturing dynamic circuit characteristics and nonlinear capacity effects," *IEEE Transactions on Energy Conversion*, vol. 26, no. 4, pp. 1172–1180, 2011.
- [144] Q. Yu, R. Xiong, C. Lin, W. Shen, and J. Deng, "Lithium-ion battery parameters and state-of-charge joint estimation based on h infinity and unscented kalman filters," *IEEE Transactions on Vehicular Technology*, 2017.
- [145] M. Ye, H. Guo, and B. Cao, "A model-based adaptive state of charge estimator for a lithium-ion battery using an improved adaptive particle filter," *Applied Energy*, vol. 190, pp. 740–748, 2017.
- [146] X. Hu, F. Sun, and Y. Zou, "Estimation of state of charge of a lithium-ion battery pack for electric vehicles using an adaptive luenberger observer," *Energies*, vol. 3, no. 9, pp. 1586–1603, 2010.
- [147] J. Xu, C. C. Mi, B. Cao, J. Deng, Z. Chen, and S. Li, "The state of charge estimation of lithium-ion batteries based on a proportional-integral observer," *IEEE Transactions on Vehicular Technology*, vol. 63, no. 4, pp. 1614–1621, 2014.
- [148] I.-S. Kim, "The novel state of charge estimation method for lithium battery using sliding mode observer," *Journal of Power Sources*, vol. 163, no. 1, pp. 584–590, 2006.
- [149] —, "Nonlinear state of charge estimator for hybrid electric vehicle battery," *IEEE Transactions on Power Electronics*, vol. 23, no. 4, pp. 2027–2034, 2008.
- [150] B. S. Bhangu, P. Bentley, D. A. Stone, and C. M. Bingham, "Nonlinear observers for predicting state-of-charge and state-of-health of lead-acid batteries for hybrid-electric vehicles," *IEEE Transactions on Vehicular Technology*, vol. 54, no. 3, pp. 783–794, 2005.
- [151] X. Tang, Y. Wang, and Z. Chen, "A method for state-of-charge estimation of lifepo4 batteries based on a dual-circuit state observer," *Journal of Power Sources*, vol. 296, pp. 23–29, 2015.
- [152] F. Zhong, H. Li, S. Zhong, Q. Zhong, and C. Yin, "An soc estimation approach based on adaptive sliding mode observer and fractional order equivalent circuit model for lithium-ion batteries," *Communications in Nonlinear Science and Numerical Simulation*, vol. 24, no. 1-3, pp. 127–144, 2015.
- [153] C. R. Gould, C. M. Bingham, D. A. Stone, and P. Bentley, "New battery model and state-of-health determination through subspace parameter estimation and state-observer techniques," *IEEE Transactions on Vehicular Technology*, vol. 58, no. 8, pp. 3905–3916, 2009.

- [154] X. Chen, W. Shen, Z. Cao, and A. Kapoor, "A novel approach for state of charge estimation based on adaptive switching gain sliding mode observer in electric vehicles," *Journal of Power Sources*, vol. 246, pp. 667–678, 2014.
- [155] L. Zheng, L. Zhang, J. Zhu, G. Wang, and J. Jiang, "Co-estimation of state-of-charge, capacity and resistance for lithium-ion batteries based on a high-fidelity electrochemical model," *Applied Energy*, vol. 180, pp. 424–434, 2016.
- [156] R. Orjuela, B. Marx, J. Ragot, and D. Maquin, "Proportional-integral observer design for nonlinear uncertain systems modelled by a multiple model approach," in *Decision and Control, 2008. CDC 2008. 47th IEEE Conference on*. IEEE, 2008, pp. 3577–3582.
- [157] W. Junping, G. Jingang, and D. Lei, "An adaptive kalman filtering based state of charge combined estimator for electric vehicle battery pack," *Energy Conversion and Management*, vol. 50, no. 12, pp. 3182–3186, 2009.
- [158] J. Le Roux, "An introduction to kalman filtering: Probabilistic and deterministic approaches," *ASME J. Basic Engineering*, vol. 82, pp. 34–45, 1960.
- [159] J. Kim and B.-H. Cho, "State-of-charge estimation and state-of-health prediction of a li-ion degraded battery based on an ekf combined with a per-unit system," *IEEE Transactions on Vehicular Technology*, vol. 60, no. 9, pp. 4249–4260, 2011.
- [160] H. Dai, X. Wei, Z. Sun, J. Wang, and W. Gu, "Online cell soc estimation of li-ion battery packs using a dual time-scale kalman filtering for ev applications," *Applied Energy*, vol. 95, pp. 227–237, 2012.
- [161] L. Zhi, Z. Peng, W. Zhifu, S. Qiang, and R. Yinan, "State of charge estimation for li-ion battery based on extended kalman filter," *Energy Procedia*, vol. 105, pp. 3515–3520, 2017.
- [162] J. Han, D. Kim, and M. Sunwoo, "State-of-charge estimation of lead-acid batteries using an adaptive extended kalman filter," *Journal of Power Sources*, vol. 188, no. 2, pp. 606–612, 2009.
- [163] X. Liu, Y. He, and Z. Chen, "State-of-charge estimation for power li-ion battery pack using v min-ekf," in *Software Engineering and Data Mining (SEDM), 2010 2nd International Conference on*. IEEE, 2010, pp. 27–31.
- [164] X.-s. Hu, F.-c. Sun, and X.-m. Cheng, "Recursive calibration for a lithium iron phosphate battery for electric vehicles using extended kalman filtering," *Journal of Zhejiang University-Science A*, vol. 12, no. 11, pp. 818–825, 2011.
- [165] G. L. Plett, "Sigma-point kalman filtering for battery management systems of lipb-based hev battery packs: Part 2: Simultaneous state and parameter estimation," *Journal of power sources*, vol. 161, no. 2, pp. 1369–1384, 2006.
- [166] S. Santhanagopalan and R. E. White, "State of charge estimation using an unscented filter for high power lithium ion cells," *International Journal of Energy Research*, vol. 34, no. 2, pp. 152–163, 2010.

- [167] Z. He, M. Gao, C. Wang, L. Wang, and Y. Liu, "Adaptive state of charge estimation for li-ion batteries based on an unscented kalman filter with an enhanced battery model," *Energies*, vol. 6, no. 8, pp. 4134–4151, 2013.
- [168] Y. Tian, B. Xia, W. Sun, Z. Xu, and W. Zheng, "A modified model based state of charge estimation of power lithium-ion batteries using unscented kalman filter," *Journal of power sources*, vol. 270, pp. 619–626, 2014.
- [169] X. Liu, Z. Chen, C. Zhang, and J. Wu, "A novel temperature-compensated model for power li-ion batteries with dual-particle-filter state of charge estimation," *Applied Energy*, vol. 123, pp. 263–272, 2014.
- [170] M. Dalal, J. Ma, and D. He, "Lithium-ion battery life prognostic health management system using particle filtering framework," *Proceedings of the Institution of Mechanical Engineers, Part O: Journal of Risk and Reliability*, vol. 225, no. 1, pp. 81–90, 2011.
- [171] Y. Xing, E. W. Ma, K.-L. Tsui, and M. Pecht, "An ensemble model for predicting the remaining useful performance of lithium-ion batteries," *Microelectronics Reliability*, vol. 53, no. 6, pp. 811–820, 2013.
- [172] W. He, N. Williard, M. Osterman, and M. Pecht, "Prognostics of lithium-ion batteries based on dempster-shafer theory and the bayesian monte carlo method," *Journal of Power Sources*, vol. 196, no. 23, pp. 10 314–10 321, 2011.
- [173] D. Zhou, K. Zhang, A. Ravey, F. Gao, and A. Miraoui, "Online estimation of lithium polymer batteries state-of-charge using particle filter-based data fusion with multimodels approach," *IEEE Transactions on Industry Applications*, vol. 52, no. 3, pp. 2582–2595, 2016.
- [174] G. Wu, R. Lu, C. Zhu, and C. Chan, "An improved ampere-hour method for battery state of charge estimation based on temperature, coulomb efficiency model and capacity loss model," in *Vehicle Power and Propulsion Conference (VPPC), 2010 IEEE*. IEEE, 2010, pp. 1–4.
- [175] Y. Zhang, W. Song, S. Lin, and Z. Feng, "A novel model of the initial state of charge estimation for lifepo4 batteries," *Journal of Power Sources*, vol. 248, pp. 1028–1033, 2014.
- [176] F. Leng, C. M. Tan, R. Yazami, and M. D. Le, "A practical framework of electrical based online state-of-charge estimation of lithium ion batteries," *Journal of Power Sources*, vol. 255, pp. 423–430, 2014.
- [177] H. He, X. Zhang, R. Xiong, Y. Xu, and H. Guo, "Online model-based estimation of state-of-charge and open-circuit voltage of lithium-ion batteries in electric vehicles," *Energy*, vol. 39, no. 1, pp. 310–318, 2012.
- [178] Y.-S. Lee, W.-Y. Wang, and T.-Y. Kuo, "Soft computing for battery state-of-charge (bsoc) estimation in battery string systems," *IEEE Transactions on Industrial Electronics*, vol. 55, no. 1, pp. 229–239, 2008.
- [179] T. Hansen and C.-J. Wang, "Support vector based battery state of charge estimator," *Journal of Power Sources*, vol. 141, no. 2, pp. 351–358, 2005.

- [180] Q.-S. Shi, C.-H. Zhang, and N.-X. Cui, "Estimation of battery state-of-charge using  $\nu$ -support vector regression algorithm," *International Journal of Automotive Technology*, vol. 9, no. 6, pp. 759–764, 2008.
- [181] X. Chen, J. Yu, D. Tang, and Y. Wang, "Probabilistic residual life prediction for lithium-ion batteries based on bayesian ls-svr," *Acta Aeronautica et Astronautica Sinica*, vol. 34, no. 9, pp. 2219–2229, 2013.
- [182] R. Xiong, F. Sun, Z. Chen, and H. He, "A data-driven multi-scale extended kalman filtering based parameter and state estimation approach of lithium-ion olymer battery in electric vehicles," *Applied Energy*, vol. 113, pp. 463–476, 2014.
- [183] X. Hu, S. Li, H. Peng, and F. Sun, "Robustness analysis of state-of-charge estimation methods for twos of li-ion batteries," *Journal of power sources*, vol. 217, pp. 209–219, 2012.
- [184] L. Wang, L. Wang, C. Liao, and J. Liu, "Sigma-point kalman filter application on estimating battery soc," in *Vehicle Power and Propulsion Conference, 2009. VPPC'09. IEEE*. IEEE, 2009, pp. 1592–1595.
- [185] F. Sun, X. Hu, Y. Zou, and S. Li, "Adaptive unscented kalman filtering for state of charge estimation of a lithium-ion battery for electric vehicles," *Energy*, vol. 36, no. 5, pp. 3531–3540, 2011.
- [186] F. Li and J. Xu, "A new prognostics method for state of health estimation of lithium-ion batteries based on a mixture of gaussian process models and particle filter," *Microelectronics Reliability*, vol. 55, no. 7, pp. 1035–1045, 2015.
- [187] Y. Gurkaynak, A. Khaligh, and A. Emadi, "State of the art power management algorithms for hybrid electric vehicles," in *Vehicle Power and Propulsion Conference, 2009. VPPC'09. IEEE*. IEEE, 2009, pp. 388–394.
- [188] S. G. Wirasingha and A. Emadi, "Classification and review of control strategies for plug-in hybrid electric vehicles," *IEEE Transactions on vehicular technology*, vol. 60, no. 1, pp. 111–122, 2011.
- [189] S. F. Tie and C. W. Tan, "A review of power and energy management strategies in electric vehicles," in *Intelligent and Advanced Systems (ICIAS), 2012 4th International Conference on*, vol. 1. IEEE, 2012, pp. 412–417.
- [190] P. Zhang, F. Yan, and C. Du, "A comprehensive analysis of energy management strategies for hybrid electric vehicles based on bibliometrics," *Renewable and Sustainable Energy Reviews*, vol. 48, pp. 88–104, 2015.
- [191] M. Sabri, K. Danapalasingam, and M. Rahmat, "A review on hybrid electric vehicles architecture and energy management strategies," *Renewable and Sustainable Energy Reviews*, vol. 53, pp. 1433–1442, 2016.
- [192] E. Silvas, T. Hofman, N. Murgovski, L. P. Etman, and M. Steinbuch, "Review of optimization strategies for system-level design in hybrid electric vehicles," *IEEE Transactions on Vehicular Technology*, vol. 66, no. 1, pp. 57–70, 2017.

- [193] A. Ali and D. Söffker, “Towards optimal power management of hybrid electric vehicles in real-time: A review on methods, challenges, and state-of-the-art solutions,” *Energies*, vol. 11, no. 3, p. 476, 2018.
- [194] S. Zhang, R. Xiong, and F. Sun, “Model predictive control for power management in a plug-in hybrid electric vehicle with a hybrid energy storage system,” *Applied Energy*, vol. 185, pp. 1654–1662, 2017.
- [195] H. Morais, P. Kádár, P. Faria, Z. A. Vale, and H. Khodr, “Optimal scheduling of a renewable micro-grid in an isolated load area using mixed-integer linear programming,” *Renewable Energy*, vol. 35, no. 1, pp. 151–156, 2010.
- [196] S. Zhang and R. Xiong, “Adaptive energy management of a plug-in hybrid electric vehicle based on driving pattern recognition and dynamic programming,” *Applied Energy*, vol. 155, pp. 68–78, 2015.
- [197] X. Wang, H. He, F. Sun, and J. Zhang, “Application study on the dynamic programming algorithm for energy management of plug-in hybrid electric vehicles,” *Energies*, vol. 8, no. 4, pp. 3225–3244, 2015.
- [198] A. C. Luna, N. L. Diaz, M. Graells, J. C. Vasquez, and J. M. Guerrero, “Mixed-integer-linear-programming-based energy management system for hybrid pv-wind-battery micro-grids: Modeling, design, and experimental verification,” *IEEE Transactions on Power Electronics*, vol. 32, no. 4, pp. 2769–2783, 2017.
- [199] B. Sakhdari and N. Azad, “An optimal energy management system for battery electric vehicles,” *IFAC-PapersOnLine*, vol. 48, no. 15, pp. 86–92, 2015.
- [200] J. Gao, G. G. Zhu, E. G. Strangas, and F. Sun, “Equivalent fuel consumption optimal control of a series hybrid electric vehicle,” *Proceedings of the Institution of Mechanical Engineers, Part D: Journal of Automobile Engineering*, vol. 223, no. 8, pp. 1003–1018, 2009.
- [201] J. Peng, H. He, and R. Xiong, “Rule based energy management strategy for a series-parallel plug-in hybrid electric bus optimized by dynamic programming,” *Applied Energy*, vol. 185, pp. 1633–1643, 2017.
- [202] V. Herrera, A. Milo, H. Gaztañaga, I. Etxeberria-Otadui, I. Villarreal, and H. Camb-long, “Adaptive energy management strategy and optimal sizing applied on a battery-supercapacitor based tramway,” *Applied Energy*, vol. 169, pp. 831–845, 2016.
- [203] Z. Song, H. Hofmann, J. Li, X. Han, X. Zhang, and M. Ouyang, “A comparison study of different semi-active hybrid energy storage system topologies for electric vehicles,” *Journal of Power Sources*, vol. 274, pp. 400–411, 2015.
- [204] B. Wang, J. Xu, B. Cao, and B. Ning, “Adaptive mode switch strategy based on simulated annealing optimization of a multi-mode hybrid energy storage system for electric vehicles,” *Applied energy*, vol. 194, pp. 596–608, 2017.

- [205] H. He, R. Xiong, K. Zhao, and Z. Liu, "Energy management strategy research on a hybrid power system by hardware-in-loop experiments," *Applied Energy*, vol. 112, pp. 1311–1317, 2013.
- [206] Y. Eren, O. Erdinc, H. Gorgun, M. Uzunoglu, and B. Vural, "A fuzzy logic based supervisory controller for an fc/uc hybrid vehicular power system," *international journal of hydrogen energy*, vol. 34, no. 20, pp. 8681–8694, 2009.
- [207] S. Caux, W. Hankache, M. Fadel, and D. Hissel, "On-line fuzzy energy management for hybrid fuel cell systems," *International journal of hydrogen energy*, vol. 35, no. 5, pp. 2134–2143, 2010.
- [208] M. Zandi, A. Payman, J.-P. Martin, S. Pierfederici, B. Davat, and F. Meibody-Tabar, "Energy management of a fuel cell/supercapacitor/battery power source for electric vehicular applications," *IEEE transactions on vehicular technology*, vol. 60, no. 2, pp. 433–443, 2011.
- [209] M. Montazeri-Gh and M. Mahmoodi-k, "Development a new power management strategy for power split hybrid electric vehicles," *Transportation Research Part D: Transport and Environment*, vol. 37, pp. 79–96, 2015.
- [210] Y. Diab, F. Auger, E. Schaeffer, and M. Wahbeh, "Estimating lithium-ion battery state of charge and parameters using a continuous-discrete extended kalman filter," *Energies*, vol. 10, no. 8, p. 1075, 2017.
- [211] D. H. Wolpert and W. G. Macready, "No free lunch theorems for optimization," *Evolutionary Computation, IEEE Transactions on*, vol. 1, no. 1, pp. 67–82, 1997.
- [212] Y. Zhang, Y. Shang, N. Cui, and C. Zhang, "Parameters identification and sensitive characteristics analysis for lithium-ion batteries of electric vehicles," *Energies*, vol. 11, no. 1, p. 19, 2017.
- [213] R. C. Kroeze and P. T. Krein, "Electrical battery model for use in dynamic electric vehicle simulations," in *Power Electronics Specialists Conference, 2008. PESC 2008. IEEE*. IEEE, 2008, pp. 1336–1342.
- [214] Y. Hu, S. Yurkovich, Y. Guezennec, and B. Yurkovich, "Electro-thermal battery model identification for automotive applications," *Journal of Power Sources*, vol. 196, no. 1, pp. 449–457, 2011.
- [215] L. Berzi, M. Delogu, and M. Pierini, "Development of driving cycles for electric vehicles in the context of the city of florence," *Transportation Research Part D: Transport and Environment*, vol. 47, pp. 299–322, 2016.
- [216] A. Corti, V. Manzoni, and S. M. Savaresi, "Vehicle's energy estimation using low frequency speed signal," in *Intelligent Transportation Systems (ITSC), 2012 15th International IEEE Conference on*. IEEE, 2012, pp. 626–631.
- [217] E. Kuhn, C. Forgez, P. Lagonotte, and G. Friedrich, "Modelling ni-mh battery using cauer and foster structures," *Journal of power sources*, vol. 158, no. 2, pp. 1490–1497, 2006.

- [218] H. Zhang and M.-Y. Chow, "Comprehensive dynamic battery modeling for phev applications," in *IEEE PES General Meeting*. IEEE, 2010, pp. 1–6.
- [219] P. Bauer, L. Lam, S. Bhattacharya, A. Rojko, and P. van Duijsen, *A Practical Circuit-based Model for State of Health Estimation of Li-ion Battery Cells in Electric Vehicles: Report*. University of Technology, 2012.
- [220] J. Yang, B. Xia, Y. Shang, W. Huang, and C. Mi, "Improved battery parameter estimation method considering operating scenarios for hev/ev applications," *Energies*, vol. 10, no. 1, p. 5, 2016.
- [221] D. E. Goldberg and J. H. Holland, "Genetic algorithms and machine learning," *Machine learning*, vol. 3, no. 2, pp. 95–99, 1988.
- [222] R. C. Eberhart and J. Kennedy, "A new optimizer using particle swarm theory," in *Proceedings of the sixth international symposium on micro machine and human science*, vol. 1. New York, NY, 1995, pp. 39–43.
- [223] R. Storn and K. Price, "Differential evolution—a simple and efficient heuristic for global optimization over continuous spaces," *Journal of global optimization*, vol. 11, no. 4, pp. 341–359, 1997.
- [224] R. Rao, V. Savsani, and J. Balic, "Teaching–learning–based optimization algorithm for unconstrained and constrained real-parameter optimization problems," *Engineering Optimization*, vol. 44, no. 12, pp. 1447–1462, 2012.
- [225] S. Mirjalili, S. M. Mirjalili, and A. Lewis, "Grey wolf optimizer," *Advances in Engineering Software*, vol. 69, pp. 46–61, 2014.
- [226] J. C. Bansal, H. Sharma, S. S. Jadon, and M. Clerc, "Spider monkey optimization algorithm for numerical optimization," *Memetic Computing*, vol. 6, no. 1, pp. 31–47, 2014.
- [227] A. Sharma, A. Sharma, B. Panigrahi, D. Kiran, and R. Kumar, "Ageist spider monkey optimization algorithm," *Swarm and Evolutionary Computation*, vol. 28, pp. 58–77, 2016.
- [228] F. Zheng, Y. Xing, J. Jiang, B. Sun, J. Kim, and M. Pecht, "Influence of different open circuit voltage tests on state of charge online estimation for lithium-ion batteries," *Applied energy*, vol. 183, pp. 513–525, 2016.
- [229] S. Haykin, *Kalman filtering and neural networks*. John Wiley & Sons, 2004, vol. 47.
- [230] A. M. Bizeray, S. Zhao, S. R. Duncan, and D. A. Howey, "Lithium-ion battery thermal-electrochemical model-based state estimation using orthogonal collocation and a modified extended kalman filter," *Journal of Power Sources*, vol. 296, pp. 400–412, 2015.
- [231] E. A. Wan and R. Van Der Merwe, "The unscented kalman filter for nonlinear estimation," in *Adaptive Systems for Signal Processing, Communications, and Control Symposium 2000. AS-SPCC. The IEEE 2000*. Ieee, 2000, pp. 153–158.



# Publications

Following papers have been published/accepted out of this thesis work.

## International Journals

1. **Venu Sangwan**, Avinash Sharma, Rajesh Kumar and Akshay Kumar Rathore “ Model-based optimal parameter identification incorporating C-rate, state of charge and temperature effect for advance battery management system in electric vehicles”. IET Electrical Systems in Transportation 2018. IET Electrical Systems in Transportation, Volume 8, Issue 4, pp. 240-250, December 2018, DOI: 10.1049/iet-est.2018.0003.
2. **Venu Sangwan**, Avinash Sharma, Rajesh Kumar, Akshay Kumar Rathore, “High Fidelity Equivalent Circuit Model Parameter Extraction for Characterization and Simulation of Li-ion Cells in Battery Electric Vehicles”, In Electric power components and systems, (EPCS) , Volume 46, Issue 14-15, pp. 1672-1685, December 2018, <https://doi.org/10.1080/15325008.2018.1510443>.
3. **Venu Sangwan**, Rajesh Kumar and Akshay K Rathore, “State-of-Charge Estimation of Li-ion Battery at Different Temperatures using Particle Filter”, Journal of Electrical Engineering, <https://doi.org/10.1049/joe.2018.9234>.

## International Conferences

1. **Venu Sangwan**, Rajesh Kumar and Akshay K Rathore, “An Empirical Capacity Degradation Modeling and Prognostics of Remaining Useful Life of Li-ion Battery using Unscented Kalman Filter”, Proceeding of the 8th IEEE India International Conference on Power Electronics (IICPE-2018) at MNIT Jaipur from 13/12/2018 to 15/12/2018, DOI: 10.1109/IICPE.2018.8709470.
2. **Venu Sangwan**, Venkata R. Vakacharla, Rajesh Kumar and Akshay K Rathore, “Estimation of State of Charge for Li-ion Battery Using Model Adaptive Extended Kalman Filter”, Proceeding of the 7th IEEE International Conference on Power Systems at Pune from 21/12/2017 to 23/12/2017, DOI: 10.1109/ICPES.2017.8387385.

3. **Venu Sangwan**, Rajesh Kumar and Akshay K Rathore, “ Estimation of model parameters and state-of-charge for battery management system of Li-ion battery in EVs ”, Proceeding of the IEEE International Transportation Electrification Conference-India (ITEC) at Pune from 13/12/2017 to 15/12/2017, DOI: 10.1109/ITEC-India.2017.8333889.
4. **Venu Sangwan**, Rajesh Kumar and Akshay K Rathore, “State-of-Charge Estimation for Li-Ion battery using Extended Kalman Filter (EKF) and Central Difference Kalman Filter (CDKF) ”, Proceeding of the IEEE Industry Applications Society Annual Meeting (IAS), at Cincinnati, OH, USA from 01/10/2017 to 05/10/2017, DOI: 10.1109/IAS.2017.8101722.
5. **Venu Sangwan**, Avinash Sharma, Rajesh Kumar and Akshay K Rathore, “Optimal Parameter Estimation of Battery Model for Pivotal Automotive Battery Management System ”, Proceeding of the IEEE International Conference on Environment and Electrical Engineering and 2017 IEEE Industrial and Commercial Power Systems Europe (EEEIC / I&CPS Europe) at Milan, Italy from 06/06/2017 to 09/06/2017, DOI: 10.1109/EEEIC.2017.7977705.
6. **Venu Sangwan**, Avinash Sharma, Rajesh Kumar and Akshay K Rathore, “Equivalent circuit model parameters estimation of Li-ion battery: C-rate, SOC and Temperature effects”, in IEEE International conference on Power Electronics, Drives and Energy Systems (PEDES-2016) at Mar Baselios College of Engineering Trivandrum from 14/12/2016 to 17/12/2016, DOI: 10.1109/PEDES.2016.7914369.
7. **Venu Sangwan**, Avinash Sharma, Rajesh Kumar and Akshay K Rathore, “Estimation of Optimal Li-ion Battery Parameters considering c-rate, SOC and Temperature”, In 7th IEEE India International Conference on Power Electronics (IICPE 2016) at Thapar University Punjab from 17/10/2016 to 19/10/2016; DOI: 10.1109/IICPE.2016.8079484.
8. **Venu Sangwan**, Avinash Sharma, Rajesh Kumar and Akshay K Rathore, “Estimation of Battery Parameters of the Equivalent Circuit Models using Meta-Heuristic Techniques”, In IEEE International Conference on Power Electronics, Intelligent Control and Energy Systems (ICPEICES-2016) at DTU Delhi from 04/07/2016 to 06/07/2016, DOI: 10.1109/ICPEICES.2016.7853240.
9. **Venu Sangwan**, Rajesh Kumar and Akshay K Rathore, “Estimation of Battery Parameters of the Equivalent Circuit Model with Effect of SoC and Temperature using Grey Wolf Optimization”, In IEEE 6th International Conference on Power Systems (ICPS), 2016 at IIT Delhi from 04/03/2016 to 06/03/2016, DOI: 10.1109/ICPES.2016.7584086.

## Brief bio-data of the Author

Ms. Venu Sangwan received his B.Tech. degree in Electrical Engineering from Chaudhary Devi Lal Memorial Univeristy, Sirsa , Haryana, India in 2011, and M.Tech. degree in Electrical Engineering (Power Electronics) from Punjab Engineering College University of Technology Chandigarh, India in 2014. She completed her PhD in Electrical Engineering from Malaviya National Institute of Technology Jaipur, Rajasthan, India in July 2019. Her research interests includes Battery Management System, Electric Vehicle, Aritifcal Intelligence and Machine Learning Technqiues. She is Graduate Student Member of IEEE, USA.

